

**DEGENERATION AND MECHANICS OF THE SEGMENT ADJACENT TO A
LUMBAR SPINE FUSION:
A BIOMECHANICAL ANALYSIS**

By

Masoud Malakoutian

B.A.Sc., The University of Tehran, 2011

A THESIS SUBMITTED IN PARTIAL FULFILLMENT OF
THE REQUIREMENTS FOR THE DEGREE OF

MASTER OF APPLIED SCIENCE

in

The Faculty of Graduate and Postdoctoral Studies

(Mechanical Engineering)

THE UNIVERSITY OF BRITISH COLUMBIA

(Vancouver)

August 2014

© Masoud Malakoutian, 2014

Abstract

Introduction: The development of adjacent segment degeneration (ASD) as a common complication of spinal fusion is believed by some clinicians and researchers to have roots in kinematic changes and altered loading at the intervertebral levels beside the fusion (i.e. adjacent). Dynamic spinal implants and minimally invasive surgeries were introduced to minimize such kinematic changes and load alterations in attempts to prevent ASD. However, little is known whether the kinematic changes at the adjacent level to a fusion are common *in vivo* occurrences. Further, the role of iatrogenic muscle damage on loading at the adjacent levels has not been investigated previously.

Objectives: (1) To assess the current clinical evidence of *in vivo* kinematic changes at the levels adjacent to a lumbar spinal fusion. (2) To investigate the role of iatrogenic muscle damage on loading at the adjacent levels.

Methods: (1) A systematic search in the PubMed database was performed for studies that addressed kinematics of the segment adjacent to a lumbar spine fusion or any other spinal implant. (2) A musculoskeletal model of the lumbar spine with 210 muscles was developed. Muscle damage was simulated by detaching the muscles from the posterior elements of the operated vertebrae and its effect on spinal loads at the adjacent levels was assessed during upright standing.

Results: (1) The search identified 39 articles, among which 29 studied fusion. None of the studies observed any increase in range of motion (ROM) of the caudal adjacent segment, while for the rostral adjacent level the ROM was reported to increase in 10-30% of the patients. (2) The

axial forces at the adjacent levels increased with muscle damage, with the largest increases being at the rostral adjacent level (73%) in comparison to the caudal level (32%).

Discussion: The results of both studies imply higher susceptibility of the rostral adjacent level to disc degeneration, which is in harmony with the clinical prevalence of ASD occurring in 70 to 100% of the cases at the rostral level. The findings suggest that muscle damage secondary to spine surgery may play a key role in adjacent segment changes, independent of the spinal instrumentation.

Preface

This thesis was written in its entirety by Masoud Malakoutian. Dr. Thomas Oxland provided the original ideas, guidance for the direction of the project, and editing of the thesis. Drs. Sidney Fels and John Lloyd provided guidance and facilitated using of ArtiSynth software package for development of the model. Drs. John Street and Marcel Dvorak provided the clinical perspective.

A version of Chapter 2 has been submitted as:

- **Malakoutian M**, Volkheimer D, Street J, Dvorak MF, Wilke HJ, Oxland TR. *Do in vivo Kinematic Studies Provide Insight into Adjacent Segment Degeneration? – A Qualitative Systematic Literature Review.*

The author was responsible for reviewing all of the articles, creation of the tables, and writing of the chapter. Drs. Thomas Oxland, John Street, Marcel Dvorak, and Hans-Joachim Wilke helped with their valuable guidance. David Volkheimer assisted with the creation of the sole figure of this chapter. All co-authors contributed to the editing of the manuscript.

A version of Chapter 3 is being prepared for submission as:

- **Malakoutian M**, Lloyd J, Street J, Wilke HJ, Fels S, Oxland TR. *Role of Iatrogenic Muscle Damage on Loading at the Level Adjacent to a Lumbar Spine Fusion – A Biomechanical Analysis.*

The development of the model using ArtiSynth, all simulations, and post processing were performed by the author. The original idea and the overall direction were given by Dr. Thomas Oxland. The bone and muscle geometries were taken from the model developed by Christophy *et*

al. [1]. Drs. Sidney Fels and John Lloyd provided guidance for using ArtiSynth. Dr. John Lloyd further assisted with the derivation and implementation of the formulations presented in sections A.3, A.4, and A.5. Dr. John Street provided the clinical perspective. Drs. Thomas Oxland and Hans-Joachim Wilke assisted with the editing of this chapter.

Table of Contents

Abstract.....	ii
Preface.....	iv
Table of Contents.....	vi
List of Tables.....	ix
List of Figures.....	x
Acknowledgments.....	xv
Chapter 1 Introduction.....	1
1.1 Overview.....	1
1.2 Spine Anatomy.....	3
1.2.1 Vertebrae.....	3
1.2.2 Intervertebral Discs.....	5
1.2.3 Ligaments.....	6
1.2.4 Facet Joints.....	8
1.2.5 Spinal Musculature.....	9
1.3 Low Back Pain and Disc Degeneration.....	14
1.3.1 Low Back Pain.....	14
1.3.2 Intervertebral Disc Degeneration.....	14
1.3.3 Low Back Pain due to Disc Degeneration.....	15
1.3.4 Surgical Treatments.....	17
1.3.4.1 Fusion.....	17
1.3.4.2 Total Disc Replacement (TDR).....	25
1.3.4.3 Dynamic Implants.....	26
1.4 Adjacent Segment Disease (ASD).....	27
1.4.1 Adjacent Segment Hypermobility.....	30
1.4.2 Iatrogenic Muscle Damage.....	31
1.5 Musculoskeletal Modeling.....	33
1.5.1 Muscles.....	33
1.5.1.1 Morphology and Physiology.....	33
1.5.1.2 Mechanical Properties.....	35
1.5.1.3 Muscle Parameters.....	38
1.5.2 Solution Methods for Determining Muscle Forces.....	41
1.5.2.1 Forward Dynamics versus Inverse Dynamics.....	41

1.5.2.2 Tackling Muscle Redundancy through Optimization	43
1.5.3 Intra-Abdominal Pressure (IAP).....	47
1.5.4 Musculoskeletal Models of the Lumbar Spine	48
1.6 Objectives.....	51
1.7 Scope	52
Chapter 2 Do <i>in vivo</i> Kinematic Studies Provide Insight into Adjacent Segment Degeneration? – A Qualitative Systematic Literature Review	55
2.1 Introduction	55
2.2 Methodology	57
2.3 Results	61
2.4 Discussion	75
Chapter 3 Role of Iatrogenic Muscle Damage on Loading at the Level Adjacent to a Lumbar Spine Fusion – A Biomechanical Analysis.....	81
3.1 Introduction	81
3.2 Methodology	83
3.2.1 Geometrical Model	83
3.2.1.1 Bone	83
3.2.1.2 Functional Spinal Unit (FSU)	85
3.2.1.3 Muscles	90
3.2.1.4 Intra-abdominal Pressure (IAP).....	104
3.2.2 Solution Method	106
3.2.3 Validation	109
3.2.3.1 Calibration Procedure	111
3.2.4 Study Design	114
3.3 Results	117
3.3.1 Results for Scenarios of the Study Design	117
3.3.2 Further Results for scenario 1.....	119
3.4 Discussion	126
3.4.1 Limitations.....	131
3.4.1.1 Solution Method	131
3.4.1.2 Geometrical Model /Mechanical Properties	134
3.4.1.3 Study Design.....	136
Chapter 4 Discussion and Conclusion	137
4.1 Summary of Thesis Results.....	138

4.2 Evidence for Association of ASD and Iatrogenic Muscle Damage: Comparison between the Outcomes of Different Surgical Approaches	139
4.2.1 Minimally Invasive (MI) surgeries.....	139
4.2.2 Open vs. MI Surgeries	140
4.2.3 ALIF vs. PLIF.....	141
4.3 Evidence for Association of ASD and Adjacent Segment Kinematics: Comparison between Fusion and Motion Preserving Implants	141
4.3.1 Fusion vs. TDR.....	141
4.3.2 Fusion vs. Dynamic Implants	142
4.4 Fusion and Loss of Disc Height	143
4.5 Study Strengths and Limitations	145
4.5.1 Strengths	145
4.5.2 Limitations.....	147
4.5.2.1 Review Study.....	147
4.5.2.2 Musculoskeletal Modeling.....	148
4.6 Future Work and Conclusions.....	151
4.6.1 Future Work.....	151
4.6.2 Conclusions	152
Bibliography	154
Appendix A Introduction to Mathematical Background in ArtiSynth.....	177
A.1 Frames	177
A.2 Variation of Rotation Matrix.....	179
A.3 Frame Springs.....	182
A.4 Calculation of Frame Spring Jacobians.....	183
A.5 Linear Frame Spring.....	186
A.6 OffsetFrameSpring	189
A.7 Verification of “HeuerOffsetFrameSpring”	189
Appendix B Formulation for l^F	192
Appendix C Spinal Loads and Muscle Forces During Upright Standing.....	195
C.1 Spinal Loads	195
C.2 Muscle Forces.....	198

List of Tables

Table 1-1: Studies that support or do not support ASD risk factors.....	29
Table 2-1: Summary of the clinical articles addressing kinematics of the segments adjacent to a spinal fusion.....	62
Table 2-2: Summary of the clinical articles addressing kinematics of the segments adjacent to a TDR.....	65
Table 2-3: Summary of the clinical articles addressing kinematics of the segments adjacent to a dynamic implant.....	67
Table 2-4: How do the absolute values for sagittal ROM change after a spinal fusion?.....	70
Table 2-5: How do the absolute values for sagittal ROM change after a TDR?	70
Table 2-6: How do the absolute values for sagittal ROM change after a dynamic implant?	71
Table 2-7: Incidence of instability after a spinal fusion	71
Table 3-1: Masses and mass moments of inertia of the thorax, pelvis and sacrum, and transverse slices of the body at each lumbar vertebral level.....	84
Table 3-2: Correlation between the moments and rotations of the FSU.....	89
Table 3-3: Muscle parameters for the abdominal and spinal muscles.....	101
Table 3-4: Average of the maximum extension moment, IAP, and diaphragm area at different positions for the subjects of Daggfeldt <i>et al.</i> 's study.....	110
Table 3-5: Maximum extension moment and the equivalent maximum horizontal force measured for 10° extension and 10° flexion in the study by Daggfeldt <i>et al.</i>	110
Table 3-6: Minimum achievable errors for different optimization terms (w_1) when simulating neutral standing and holding crate far from the chest.....	112
Table 3-7: Maximum resistible force at 10° flexion ($\theta = -10^\circ$) and 10° extension ($\theta = 10^\circ$) for different muscle strength factors.....	113
Table 3-8: Comparison between the axial forces predicted by the model and the <i>in vivo</i> intradiscal pressure (IDP) measured in Wilke <i>et al.</i> 's study.....	114
Table 3-9: The ratios of muscle forces and their axial components between case 1 and case 2 for three different values of θ_2	130

List of Figures

Figure 1-1: Regions of the spine.....	3
Figure 1-2: Typical Lumbar Vertebrae.....	5
Figure 1-3. Structure of the intervertebral disc.....	6
Figure 1-4 Ligaments of the lumbar spine.....	7
Figure 1-5: Cross section of a facet joint.	9
Figure 1-6: A compendium of spinal muscles based on the description of Gray’s anatomy [10] and Clinically oriented anatomy [9].	10
Figure 1-7: The extrinsic back muscles.	11
Figure 1-8: The intrinsic back muscles.	13
Figure 1-9: Intervertebral Disc (IVD) Degeneration.	16
Figure 1-10: Various forms and consequences of disc degeneration.	17
Figure 1-11: Spinal Instrumentations.....	18
Figure 1-12: Instrumented posterolateral fusion.....	19
Figure 1-13: Retroperitoneal approach for ALIF.....	22
Figure 1-14: Lateral approach for lumbar interbody fusion..	23
Figure 1-15: Number of fusion surgeries performed for the 10 most common spinal problems..	24
Figure 1-16: Charité artificial disc.....	25
Figure 1-17: Dynesys.....	27
Figure 1-18: Loss of disc height over time indicating radiographic but not symptomatic ASD..	28
Figure 1-19: Symptomatic ASD with stenosis but without radiographic changes.....	28
Figure 1-20: Adjacent segment hypermobility..	30
Figure 1-21: Same postoperative ROM at the adjacent level when applying the same preoperative load.....	31
Figure 1-22: Muscle morphology.	34
Figure 1-23: Hill-type musculotendon actuator.....	35
Figure 1-24: Muscle force-length and force-velocity curves.....	36
Figure 1-25: Normalized force-length curve for Tendon..	37
Figure 1-26: Musculotendon contraction dynamics.	38

Figure 1-27: Muscle parameters including the pennation angle α , musculotendon length l^{MT} , and fiber length l^F	39
Figure 1-28: Forward Dynamics.....	42
Figure 1-29: Inverse Dynamics.....	43
Figure 1-30: Forward-dynamics assisted data tracking.	46
Figure 1-31: Parachute-like shape of the diaphragm.	47
Figure 2-1: Schematic demonstration of the difference between absolute ROM and relative ROM..	79
Figure 3-1: Schematic representation of an experiment for obtaining the stiffness of the FSU with the load cell located at the center of the upper segment..	87
Figure 3-2: Limitation of the bushing element for modeling the FSU.	87
Figure 3-3: The coordinate system used for the results of current study.....	89
Figure 3-4: Moment-rotation relation for flexion, extension, lateral bending, and the axial rotation of the FSU.....	90
Figure 3-5: Iliocostalis lumborum anatomy and its incorporation in our model..	92
Figure 3-6: Longissimus thoracis anatomy and its incorporation in our model..	93
Figure 3-7: Multifidus anatomy and its incorporation in our model..	93
Figure 3-8: Quadratus Lumborum anatomy and its incorporation in our model.....	95
Figure 3-9: Psoas major anatomy and its incorporation in our model.....	95
Figure 3-10: External oblique anatomy and its incorporation in our model.....	97
Figure 3-11: Internal oblique anatomy and its incorporation in our model.....	97
Figure 3-12: Rectus abdominis anatomy and its incorporation in our model.....	98
Figure 3-13: Modeling of a multi segmental muscle with seven attachment sites using MultiPointMuscle in ArtiSynth.	98
Figure 3-14: Rectus sheath modeled as a massless rigid body connected to the sacrum through a revolute joint.	99
Figure 3-15: The mechanical effect of the intra-abdominal pressure modeled as an upward force applied on the thorax.....	104
Figure 3-16: Symmetric target points specified for tracking the motion of the thorax.	108
Figure 3-17: The position of the subjects of Daggfeldt <i>et al.</i> 's study for measurement of the maximum extension moment about the L5-S1 joint.....	109

Figure 3-18: <i>In vivo</i> measured intradiscal pressure for three activities of Wilke <i>et al.</i> 's study..	111
Figure 3-19: Scenario 1 of the study design: comparing the spinal loads between a healthy subject and a patient undergoing sham surgery.	115
Figure 3-20: Scenario 2 of the study design: comparing the spinal loads between a patient receiving percutaneous pedicle screw fixation and a patient undergoing open fusion surgery.	115
Figure 3-21: Simulation of iatrogenic muscle damage to the longissimus thoracis pars thoracis.	116
Figure 3-22: Predicted spinal loads at the adjacent levels for scenario 1..	117
Figure 3-23: Predicted spinal loads at the adjacent levels for scenario 2..	118
Figure 3-24: Limitation of our method for calculation of muscle cross sectional areas at L4-L5 and L5-S1 levels.	120
Figure 3-25: Predicted spinal loads at all lumbar intervertebral levels for scenario 1..	120
Figure 3-26: Physiological cross sectional area (PCSA) and force of each muscle group crossing L1-L2 level for scenario 1.....	121
Figure 3-27: Physiological cross sectional area (PCSA) and force of each muscle group crossing L3-L4 level for scenario 1.....	122
Figure 3-28: Force in each internal oblique fascicle for scenario 1.....	123
Figure 3-29: Force in each external oblique fascicle for scenario 1.....	124
Figure 3-30: Muscle excitations during upright standing.....	125
Figure 3-31: A simple mathematical model of the spine.....	127
Figure 3-32: Importance of the position of point P to the analytical solution..	128
Figure 3-33 The ratios of muscle forces and their axial components between case 1 and case 2 as a function of θ_2	129
Figure A-1: Use of chain rule for obtaining the transformation matrix between two arbitrary frames.....	179
Figure A-2: Variation in frame configuration represented by an infinitesimal rotation angle. ..	180
Figure A-3: Verification of the HeuerOffsetFrameSpring performance under a sinusoidal shear force.	190
Figure A-4: Verification of the HeuerOffsetFrameSpring performance under a sinusoidal pure moment.	191

Figure C-1: Axial forces at all vertebral level during upright standing.....	195
Figure C-2: Shear forces at all vertebral level during upright standing.....	196
Figure C-3: Extension moments at all vertebral level during upright standing.....	197
Figure C-4: Forces in each muscle group during upright standing.....	198
Figure C-5: Normalized fiber length of each external oblique fascicle during upright standing..	
.....	200
Figure C-6: Active and passive forces in external oblique muscle group during upright standing.	
.....	200
Figure C-7: Normalized fiber length of each internal oblique fascicle during upright standing.	201
Figure C-8: Active and passive forces in internal oblique muscle group during upright standing.	
.....	201
Figure C-9: Normalized fiber length of each rectus abdominis fascicle during upright standing.	
.....	202
Figure C-10: Active and passive forces in rectus abdominis muscle group during upright	
standing.....	202
Figure C-11: Normalized fiber length of each psoas major fascicle during upright standing....	203
Figure C-12: Active and passive forces in psoas major muscle group during upright standing.	203
Figure C-13: Normalized fiber length of each quadratus lumborum fascicle during upright	
standing.....	204
Figure C-14: Active and passive forces in quadratus lumborum muscle group during upright	
standing.....	204
Figure C-15: Normalized fiber length of each multifidus fascicle during upright standing.....	205
Figure C-16: Active and passive forces in multifidus muscle group during upright standing. ..	205
Figure C-17: Normalized fiber length of each two-point iliocostalis lumborum fascicle during	
upright standing..	206
Figure C-18: Active and passive forces in two-point iliocostalis lumborum muscle group during	
upright standing.	206
Figure C-19: Normalized fiber length of each iliocostalis lumborum multi-point fascicle during	
upright standing..	207
Figure C-20: Active and passive forces in multi-point iliocostalis lumborum muscle group during	
upright standing.	207

Figure C-21: Normalized fiber length of each two-point longissimus thoracis fascicle during upright standing..	208
Figure C-22: Active and passive forces in two-point longissimus thoracis muscle group during upright standing.	208
Figure C-23: Normalized fiber length of each multi-point longissimus thoracis fascicle during upright standing..	209
Figure C-24: Active and passive forces in multi-point longissimus thoracis muscle group during upright standing.	209

Acknowledgments

I would like to first thank Dr. Thomas Oxland for providing me with the opportunity of working on this project. His continuous support, motivation, and optimistic views encouraged me to work hard and overcome the obstacles. Also his emphasis on the clinical aspect of the project taught me how to ask the right question and find my way in the field of biomechanics. I also would like to thank Drs. Sidney Fels and John Lloyd for facilitating using of ArtiSynth and Dr. John Street for providing the clinical perspective for this project.

Many thanks to my friends and lab mates, who were always there for help and support, specially: Hannah Gustafson, Angela Melnyk, Robyn Newell, Antonio Sanchez, Tim Bhatnagar, Steve Mattucci, and Kurt McInnes. Special thanks to my roommate Mohammad Honarvar, whose helping disposition and expertise in technical software packages made my graduate life way easier!

My deepest gratitude goes to my parents and my dear brother, Taha, for their unconditional love and unwavering support throughout my life.

Dedication

To whom I hope one day I can dedicate my entire life to

Chapter 1 Introduction

1.1 Overview

Fusion is the gold standard treatment for various spinal disorders. The number of fusion surgeries has increased at a 2.4 fold rate over the past decade [2]. One of the major complications of fusion is adjacent segment disease (ASD), which involves degeneration at the intervertebral levels beside the fused levels. While symptomatic ASD is prevalent in 0% to 30.3% of patients [3][4][5], up to 100% of patients have been reported to have developed radiographic ASD [6]. Various risk factors are counted for ASD; however, the exact pathogenesis of ASD still remains unclear. In contrast to some researchers who believe ASD is a natural progression of pre-existing degeneration, many believe ASD is the result of altered loading or changes in kinematics of the adjacent level.

Many changes are made to the structure of the spine during open fusion surgeries. The changes include laminectomy, facetectomy, removal of ligaments, resection of muscles, and addition of rigid fixation. Each of these factors can contribute to alteration of the loading at the adjacent level and may play a role in degeneration of the adjacent segment, but their extent of contribution is not fully known. Recently minimally invasive surgeries and various flexible instrumentations are growing as alternatives to open fusion surgeries and rigid fixations with the purpose of reducing morbidities and giving more flexibility to the operated levels so as to prevent or decelerate ASD. To what extent each of the aforementioned parameters can affect the loading on the spine and whether the proposed alternatives for fusion are proper solutions are not known.

In the following sections, an overview of spine anatomy and disc degeneration will be presented, followed by relevant findings on ASD, current surgical approaches for fusion, alternative spinal implants, and musculoskeletal modeling. The conclusions from these sections lead to my research questions and the objectives of my thesis.

1.2 Spine Anatomy

1.2.1 Vertebrae

The spine consists of 24 vertebrae plus the sacrum and coccyx, and is divided into five regions: cervical, thoracic, lumbar, sacral, and coccygeal (Figure 1-1). The cervical spine consists of seven vertebrae (C1 to C7). Twelve vertebrae comprise the thoracic spine (T1 to T12), which are attached to the ribs, and together form the thorax. Five vertebrae are in the lumbar spine (L1 to L5), while the sacrum and the coccyx can each be considered as one single bone. Note that each of the sacrum and the coccyx consist of four to five individual vertebrae that during adolescence fuse together and form one bone.

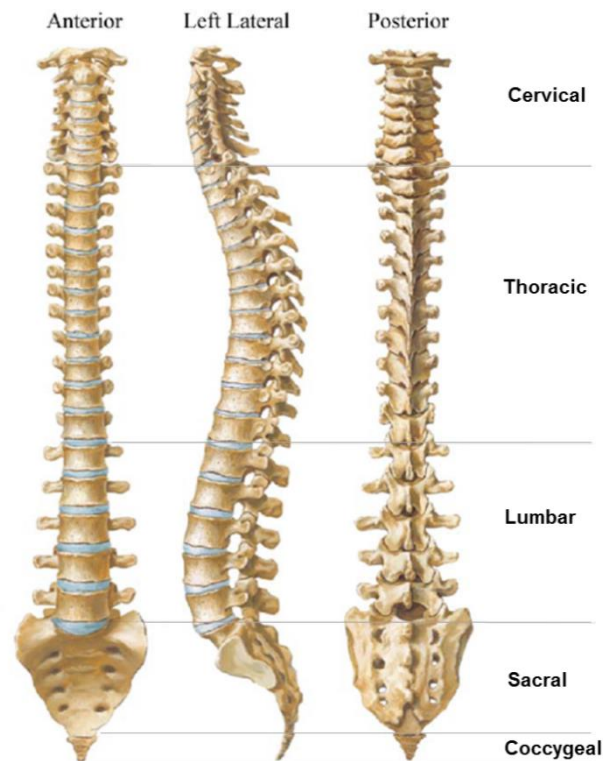


Figure 1-1: Regions of the spine. Adapted from [7] with permission from Elsevier Health Sciences.

A typical vertebra consists of an anterior segment, called “vertebral body”, and a posterior bony structure known as “neural arch”. These two parts surround a triangular foramen called “vertebral foramen”. When all spinal vertebrae are mounted on each other, their vertebral foramen form a canal, where the spinal cord and cauda equina are protected (see Figure 1-2).

The neural arch consists of two pedicles, two laminae, and some bony protrusions from the lumbar vertebra called processes. The pedicle is a short and thick bony protrusion that is projected through the posterior at upper part of the junction of the lateral and posterior surfaces of the lumbar vertebral body. The lamina is a broad strong bony plate that begins after the pedicle and through a posteromedial direction fuses to another lamina in the posterior midline. Other bony protrusions include spinous process, articular processes, transverse processes, mammillary processes, and accessory processes. The spinous process lies at the most posterior part of the lumbar vertebra. The superior and inferior articular processes project from the junction of the pedicle and the lamina and with superior and inferior articular processes of the adjacent vertebrae form the facet joints. The transverse processes in three upper vertebrae of the lumbar spine project at the junction of the pedicle and the lamina but in the other two vertebrae project from the pedicle and posterior part of the vertebral body.

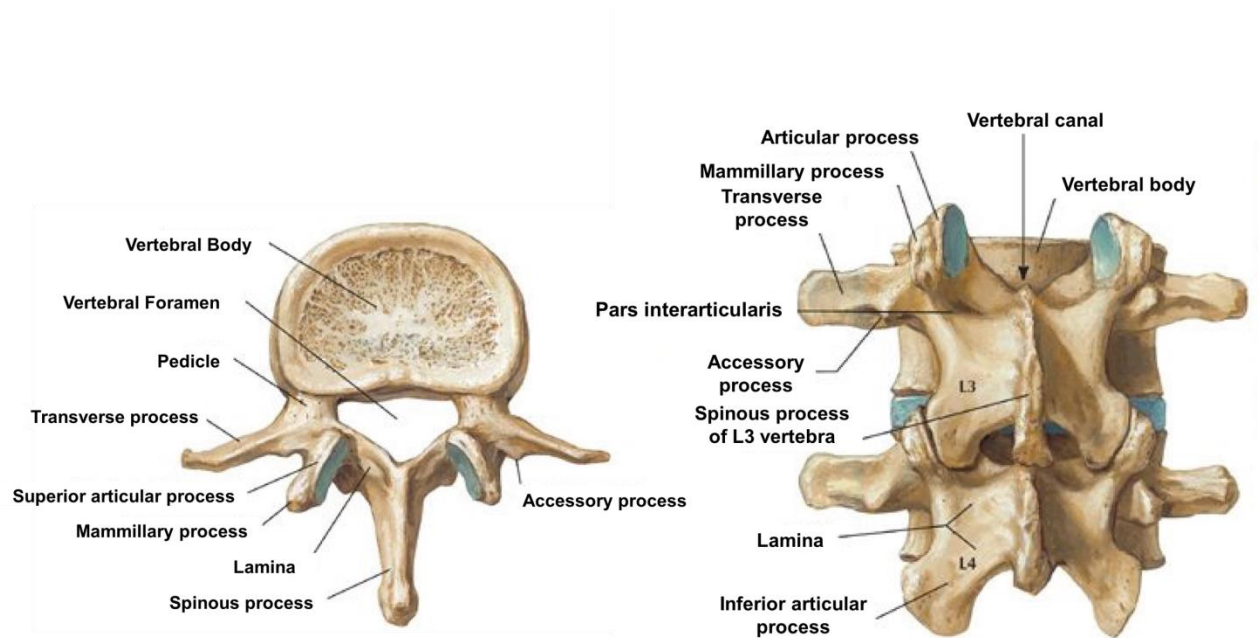


Figure 1-2: Typical Lumbar Vertebrae. Adapted from [7] with permission from Elsevier Health Sciences.

1.2.2 Intervertebral Discs

The vertebral bodies are connected together through intervertebral discs. Each disc consists of three components: nucleus pulposus, annulus fibrosus, and cartilaginous endplates. With a water content of 70-90%, the nucleus pulposus is the fluid-like substance located at the center of the disc and it comprises between 30-50% of the disc area. The nucleus is surrounded by the annulus fibrosus. The annulus fibrosus is comprised of concentric laminated bands of collagen fibers, with the fibers arranged in parallel to one another within each band. The fibers of each band are oriented at an angle of either 30 or -30 degrees with the transverse plane and at an opposite orientation with respect to the fibers of the adjacent bands (Figure 1-3). The top and bottom of each disc is covered by cartilaginous layers, also known as cartilaginous end-plates, which connect the inner zone of the discs to the vertebral bodies – the peripheral zone of the disc is directly attached to the adjacent vertebrae through fibers of the annulus fibrosus [8].

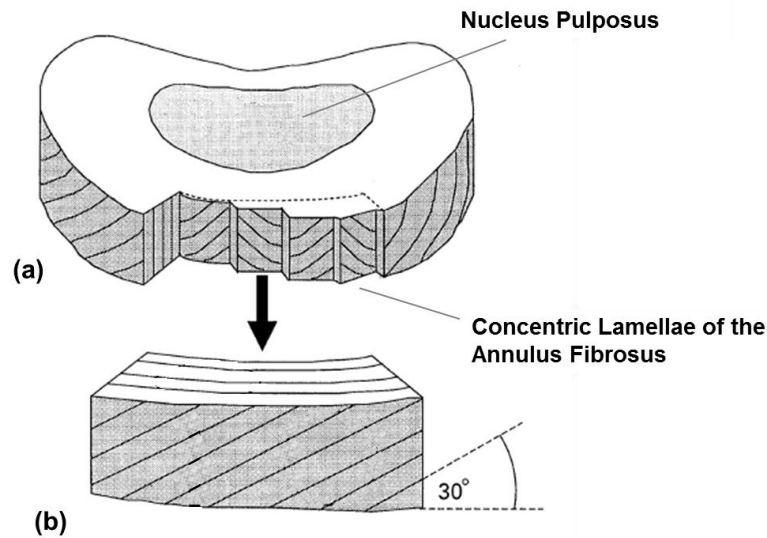


Figure 1-3: Structure of the intervertebral disc. (a) The lamellae of the annulus surrounding the nucleus and (b) orientation of the annulus fibers at $\pm 30^\circ$ from the vertebral end plates. Adapted from [263] with permission from Elsevier.

1.2.3 Ligaments

The ligaments of the lumbar spine can be classified into four major groups: ligaments of the vertebral bodies (which connect the vertebral bodies together), ligaments of the posterior elements, iliolumbar ligaments, and false ligaments.

Two well-known ligaments that interconnect the vertebral bodies are anterior longitudinal ligament (ALL) and posterior longitudinal ligament (PLL) (Figure 1-4). Starting from the sacrum and continuing into cervical region, ALL covers the anterior surface of the spinal column, while PLL is attached to posterior of the vertebral bodies. Both ALL and PLL connect the margins of the vertebral bodies together, therefore their primary function is to prevent separation of the anterior and posterior edges of the vertebral bodies in extension and flexion respectively. In addition to ALL and PLL, the outer layer of annulus fibrosus that is directly connected to the

vertebral bodies is also considered as a ligament, whose function is to restrict intervertebral motions in distraction, bending, and twisting [9].

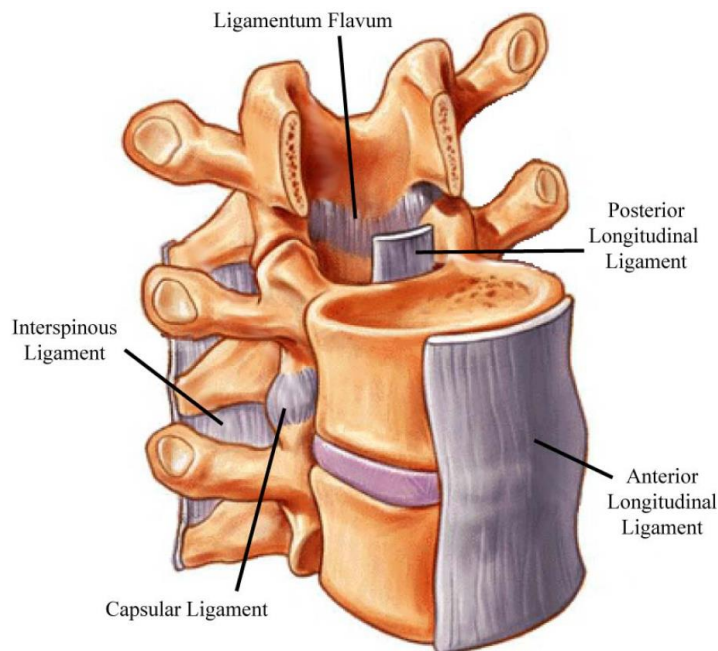


Figure 1-4: Ligaments of the lumbar spine. Adapted from <http://www.spineuniverse.com/anatomy/ligaments> with permission from © SpineUniverse.com, a Vertical Health, LLC property.

Ligamentum flavum, interspinous ligaments, and supraspinous ligaments are the ligaments that connect the posterior elements of the spine. Ligamentum flavum is a short and thick ligament that interconnects the laminae of the adjacent vertebrae. Contrary to other ligaments of the lumbar spine, ligamentum flavum mainly consists of elastin (80%), which gives it a special feature that fits well with its location, i.e. immediately behind the spinal canal.

Interspinous ligaments run over the top and bottom edges of the spinous processes and join them together, while supraspinous ligaments cover the posterior edges of the spinous processes and are mainly available at upper lumbar spine, in most of individuals ending at L4.

Iliolumbar ligaments connect the tips of the transverse processes of L5 to different areas on the anterior surface of the ilium and their role is to prevent L5 from sliding on the sacrum anteriorly and also to restrict L5 motion in flexion-extension, axial rotation, and lateral bending [9].

According to the classical classification, there are some other ligaments in the lumbar spine including intertransverse ligaments, transforaminal ligaments, and mamillo-accessory ligaments. However, they are not considered as true ligaments as those tissues do not connect two different bones together, or have irregular fiber orientations, or their collagen fibers are not as dense as ligaments. Therefore, they are structurally considered as bands of fascia that separates their surrounding compartments [9].

1.2.4 Facet Joints

The superior and inferior articular facets of adjacent vertebrae form facet joints, which are also known as zygapophysial joints. Like in other synovial joints, in facet joints the articulating surfaces are covered by articular cartilage. The joint is encompassed by a synovial membrane containing synovial fluid, and is supported by a capsular ligament surrounding that membrane (Figure 1-5).

In general, the role of the facet joints in the lumbar spine is to resist forward displacement and axial rotation of adjacent vertebrae with respect to each other. Depending on their curvature, orientation, and shape, the extent of that resistance varies between facet joints.

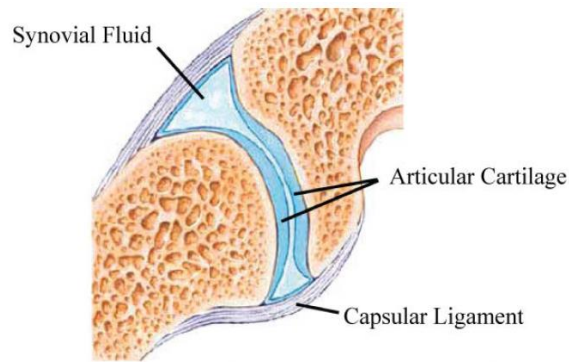


Figure 1-5: Cross section of a facet joint. Adapted from <http://umm.edu/programs/spine/health/guides/anatomy-and-function> with permission from the University of Maryland Medical Center.

1.2.5 Spinal Musculature

Back muscles consist of two major groups: the extrinsic and intrinsic muscle groups. While the intrinsic back muscles are responsible for production of spinal movement and controlling its posture, the extrinsic muscles are more involved in control and production of limb and respiratory movements [10] (see Figure 1-6 for a compendium of intrinsic and extrinsic spinal muscle groups).

The extrinsic back muscles consist of trapezius, latissimus dorsi, levator scapulae, and rhomboids at the superficial layer, and serratus posterior at the intermediate layer (Figure 1-7). The muscles at the superficial layer control limb movements. The trapezius, rhomboids, and levator scapulae contribute to stabilization, rotation, elevation, and retraction of the scapula while latissimus dorsi aids in extension, adduction, and internal rotation of the arm. Serratus posterior assists respiratory muscles in inspiration and expiration, by elevating the ribs in inspiration, and drawing them back and down in expiration [11].



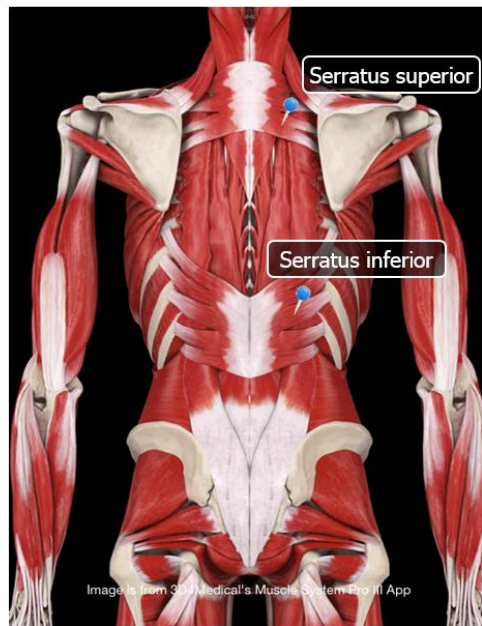
Figure 1-6: A compendium of spinal muscles based on the description of Gray’s anatomy [11] and Clinically Oriented Anatomy [10].



(a)



(b)



(c)

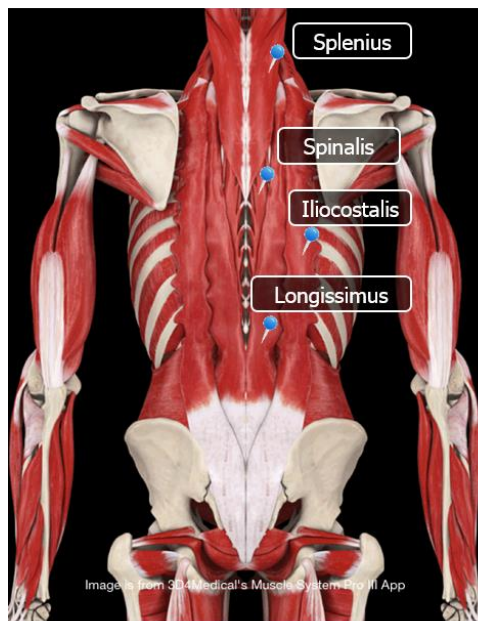
Figure 1-7: The extrinsic back muscles consisting of (a) trapezius, latissimus dorsi, (b) levator scapulae, and rhomboids at the superficial layer; and (c) serratus inferior and posterior at the intermediate layer. Reprinted from Muscle System Pro III app with permission from 3D4Medical company.

The intrinsic spinal muscles are divided into superficial, intermediate, and deep layers. At the superficial layer lies splenius muscles that are located at the cervical level of the spine and act as head and neck extensors (Figure 1-8.a).

At the intermediate level, erector spinae exists. It consists of three long columns of muscles, which from the most medial to the most lateral side are named as spinalis, longissimus, and iliocostalis, respectively (Figure 1-8a). According to their superior insertion points, each one of these muscles is divided into three further levels. For example, longissimus consists of longissimus capitis, longissimus cervicis, and longissimus thoracis. Longissimus thoracis has two parts: pars thoracis and pars lumborum. The fascicles of longissimus thoracis pars thoracis originate from the thoracic spine, whereas longissimus thoracis pars lumborum originates from lumbar vertebrae. The same is true for iliocostalis lumborum pars thoracis and pars lumborum.

Transversospinalis is the muscle group lying at the deep layer of intrinsic spinal muscles and consists of semispinalis, multifidus, and rotatores (Figure 1-8 b-d). While multifidus spans the entire vertebral column including the lumbar spine, neither rotatores nor semispinalis are found at the lumbar spine.

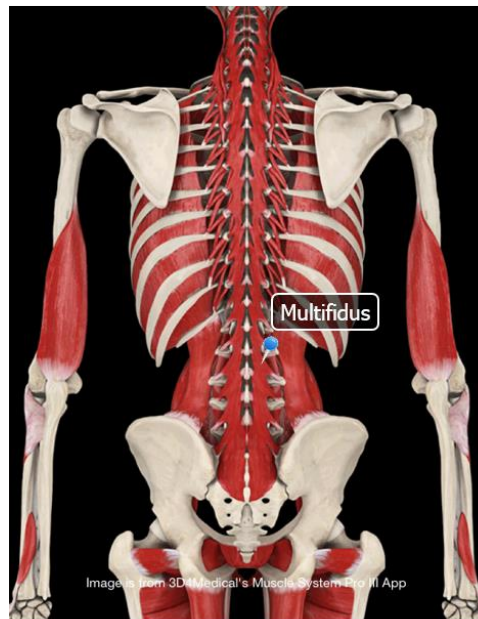
There are some minor deep muscles including interspinalis, intertransversarii, and levatores costarum but these muscles are deemed not to have much contribution to spinal loading [12][10]. In fact, due to their small size and having high density of muscle spindles, these muscles are assumed to have proprioceptive function in precise positioning of the vertebral column [10].



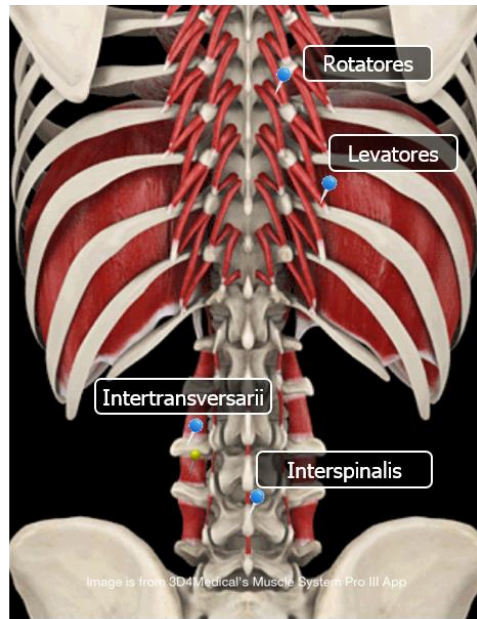
(a)



(b)



(c)



(d)

Figure 1-8: The intrinsic back muscles consisting of (a) splenius at the superficial layer; spinalis, longissimus, and iliocostalis at the intermediate layer; (b) semispinalis and (c) multifidus at the deep layer; and (d) rotatores, interspinalis, intertransversarii, and levatores as the minor deep muscles. Reprinted from Muscle System Pro III app with permission from 3D4Medical company.

1.3 Low Back Pain and Disc Degeneration

1.3.1 Low Back Pain

Low back pain is the second most common reason for visiting a physician in the United States and has an annual cost of more than \$100 billion [13][14], two-thirds of which are because of lost wages and reduced productivity [15]. About 90% of the patients with low back pain are treated with conservative treatments or medications [16]. However, the remainder that suffer from chronic low back pain undergo surgery and their costs account for more than 75% of total cost of low back pain [14]. The exact mechanism for initiation of low back pain remains unknown, but its association with degenerative disc disease is well recognized [17]. According to Kallewaard *et al.* [18], more than 40% of low back pain has origin in intervertebral disc degeneration.

1.3.2 Intervertebral Disc Degeneration

Disc degeneration is a process of biochemical, compositional, and mechanical change in the intervertebral disc that gradually leads to its structural failure. When accompanied with pain, it is called degenerative disc disease. The exact pathogenesis of disc degeneration is not known, however, age, genetic [19], and mechanical loading history [20] are believed to be important risk factors.

With aging and degeneration, the concentration of proteoglycan in the nucleus pulposus decreases and this alters the loading mechanism of the disc. Proteoglycan is the protein responsible for pressurizing the disc under compression. The molecular branches of proteoglycans have fixed negative charges, which attract positive ions into the nucleus pulposus to neutralize it. Absorption of positive ions, which increases the density of nucleus ions with

respect to the surrounding tissues, creates an osmotic pressure within the nucleus which absorbs water to equilibrate nucleus ion density with respect to its surrounding tissues. In an intact intervertebral disc, the superior and inferior end plates and lateral annulus fibers prevent the nucleus from expansion, increasing its pressure to as high as 3 MPa in some cases [21]. This hydraulic mechanism transmits spinal loads through intervertebral discs in a healthy subject. However, for degenerated discs this is not the case.

In a degenerated disc, a low density of aggregating proteoglycans decreases the ability of the nucleus to sufficiently absorb water and pressurize the disc [22]. Therefore, in the absence of enough hydrostatic pressure, the solid tissues have to carry the compressive load. On one hand, the annulus that in a healthy disc would contribute to transmission of spinal loads by bulging out and undergoing tension, in a degenerated disc bulges inward and is loaded in compression [23]; this fibrillates the lamellae of annulus over time and develops clefts and fissures in them [24]. In addition, the tissue structure in the nucleus changes into a more solid-like material to adapt itself to the altered mechanical loading [25]. As can be seen in Figure 1-9, in a severely degenerated disc, in contrast to a healthy disc, the nucleus and annulus cannot be differentiated from each other anymore. Apparently, reduction of proteoglycan is involved with these changes, but what stimulates, accelerates, or can decelerate its reduction is unknown.

1.3.3 Low Back Pain due to Disc Degeneration

Disc degeneration can lead to low back pain in different ways. Loss of disc height, which is a common outcome of disc degeneration can impose excessive compression load on facet joints and cause arthritis, which can be associated with pain. Degeneration-induced alterations in mechanical properties of the annulus can also lead to back pain through different mechanisms.

The decreased radial strength of the annulus contributes to disc bulging. Its fibrillation, cracks, and fissures, facilitate nucleus protrusion, known as disc herniation [26] (Figure 1-10). Both disc bulging and herniation can impinge nerve roots and be sources of pain. However, it is not known how much each of these mechanisms may contribute to generation of low back pain.

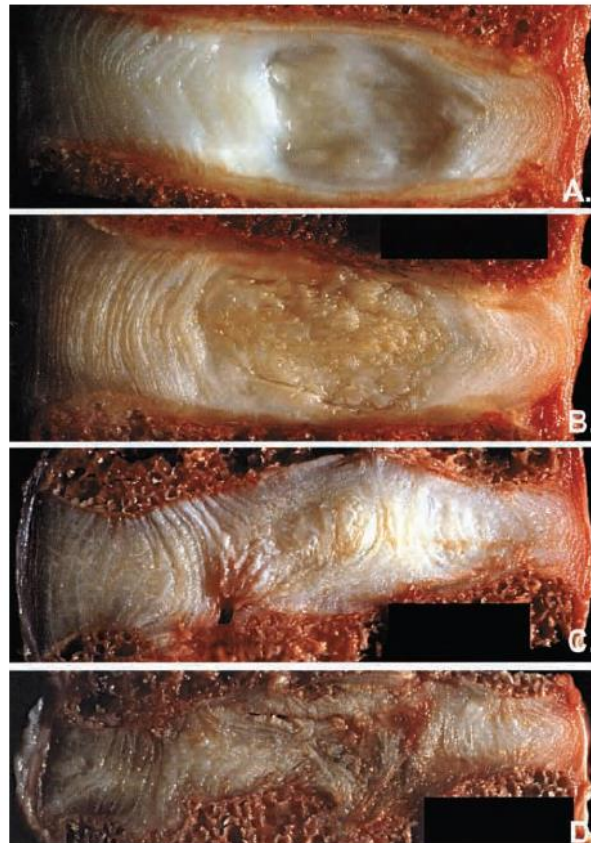


Figure 1-9: Intervertebral Disc (IVD) Degeneration. (A) Healthy IVD, (B) Moderately degenerated IVD, (C) Degenerated IVD, (D) Severely degenerated IVD. Reprinted from [27] with permission from Churchill Livingstone.

Both invasive and noninvasive methods are used for diagnosing disc degeneration. Loss of disc height and degenerative changes in end plates can be observed in plain radiographs. Other degenerative parameters such as disc bulging, annulus tears, osteophytes, and nucleus hydration can be identified through MRI [28]. However, none of these radiographic changes are

necessarily associated with pain. Conversely, a patient with low back pain may not have any of the degeneration signs. In those patients, to assess whether the patient is a candidate for surgery, discography is used. In this method a contrast agent is injected into the disc to see whether the same pain is sensed by the patient or not.

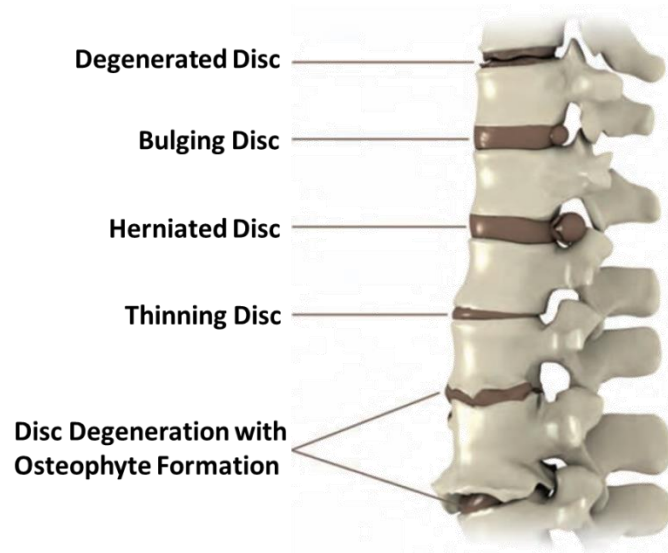


Figure 1-10: Various forms and consequences of disc degeneration. Reprinted from [22] with permission from Academic Press.

1.3.4 Surgical Treatments

1.3.4.1 Fusion

Fusion is the gold standard for treatment of various spinal disorders, with degenerative disc disease (DDD) being one main indication [29][2]. According to a recent study of surgical trends in United States, 28% of single-level fusion surgeries are due to DDD and after that, herniated nucleus pulposus (20%), stenosis (19%), and acquired spondylolisthesis (13%) are the most common indications [30].

In fusion surgery, a bone graft is placed between the vertebrae, so that the graft incorporates and makes a rigid connection between them. The main goal of spinal fusion is to stabilize the spine by restricting the motion of unstable segments. Various instrumentation devices have evolved to supplement spine fusion and thereby improve bone growth by preventing involved vertebrae from moving too much [31]. The first versions of instrumentation included rods and hooks, plates and screws, and most commonly rods and pedicle screws. (Figure 1-11)

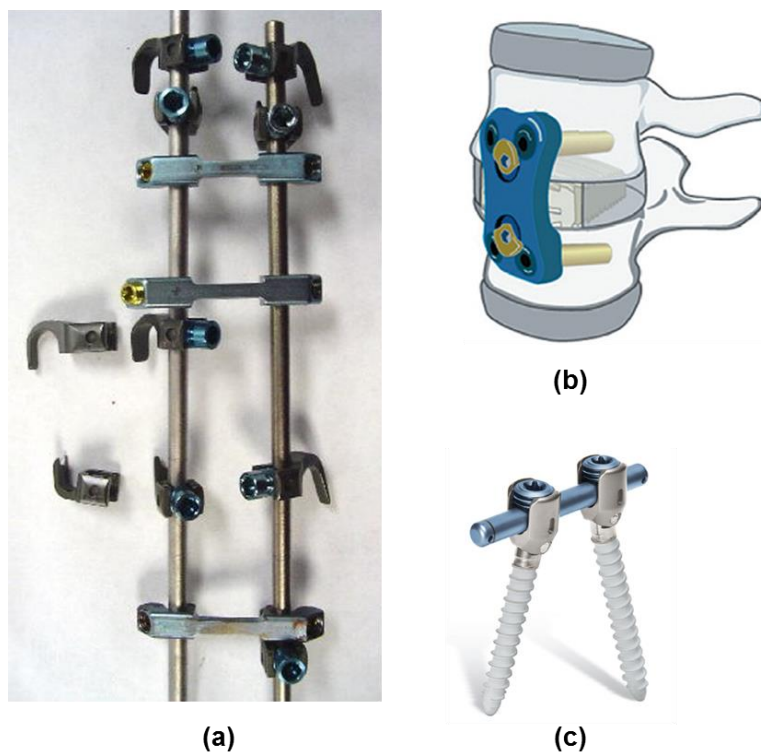


Figure 1-11: Spinal Instrumentations in forms of Harrington rods and hooks (a), plates and screws (b), and pedicle screws and rods (c). Figures are reprinted from http://www.med.wayne.edu/diagradiology/rsna2003/thoracic_rods_and_screws.htm, [32], and [33] with permission from Dr. Wilbur Smith¹, Wiley Publishing Asia Pty Ltd, and Hindawi Publishing Corporation, respectively.

¹ Chairman of the department of radiology, Wayne State University.

Various techniques for spinal fusion are available. The techniques include posterior lumbar interbody fusion (PLIF), transforaminal lumbar interbody fusion (TLIF), posterolateral fusion (PLF), anterior lumbar interbody fusion (ALIF), and direct lateral interbody fusion (DLIF). The main differences between these techniques are the places of bone grafts and the surgical approaches.

In all aforementioned interbody fusion surgeries, all or some portion of the intervertebral disc is removed and then bone grafts are placed between the vertebral bodies, while in posterolateral fusion the bone graft is placed only between posterior elements of the spine, including transverse processes and/or spinous processes of adjacent vertebrae (Figure 1-12). Interbody fusion can be combined by a posterolateral fusion to form a 360° fusion, also known as circumferential fusion. Circumferential fusion and PLF have the most (91%) and the least (85%) fusion rates, respectively, while the rate of fusion for PLIF and ALIF has been reported to be about 89% [31][34].

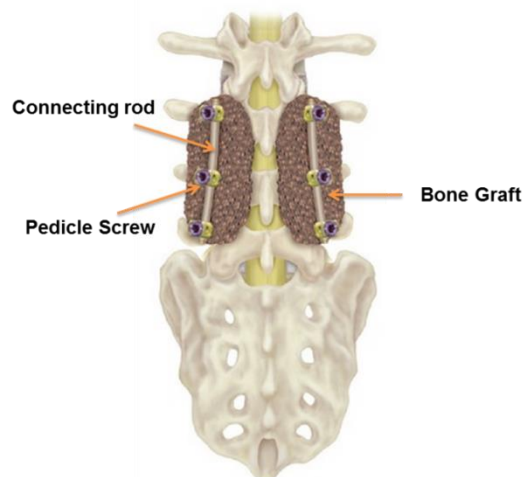


Figure 1-12: Instrumented posterolateral fusion. Adapted from <http://nw-mc.com/posterolateral-lumbar-fusion/>.

- *Surgical Approaches for Fusion*

Posterior Approach

Spinal fusion was first performed posteriorly. In the posterior approach, first, a midline skin incision is made over the involved vertebrae; the incision is continued then to the tips of the spinous processes. By using self-retaining retractors the soft tissues are held laterally and the muscles are detached from spinous processes to the tips of the transverse processes, exposing the posterior elements of the spine. While this amount of excision is enough for posterolateral fusion, in PLIF, part of the lower and upper edges of the lamina are cut and the dura is retracted toward the midline to provide room for exposure and removal of the disc [35].

Both PLIF and PLF involve stripping off the dorsal muscles. In order to decrease soft tissue morbidity, in 1998, Harms popularized transforaminal lumbar interbody fusion, where the spine is approached unilaterally [36]. In his method, in contrast to PLIF, instead of a full laminectomy, facetectomy is performed which leaves more bony elements for posterior fusion. Moreover, since the interspace is approached unilaterally, less retraction of the dural sac is needed. However, paraspinal muscle damage is substantial in this method too, though it is only on one side.

Recently, in favor of minimizing soft tissue injury and with the help of muscle-sparing tubular retractor systems, minimally invasive surgeries are growing. Instead of detaching muscles off their attachment sites, tubular dilators split the muscles making a way toward the disc. Subsequently, a tubular retractor is inserted serving as the corridor for both performing the operation and insertion of bone grafts and instruments. Both minimally invasive PLIF (MI PLIF) and MI TLIF are performed using tubular technique systems. The same tubes are used for insertion of percutaneous pedicle screws. Once the pedicle screws are inserted, a rod delivery

system such as SEXTANT (Medtronic Sofamor Danek) is used, especially in cases of long instrumentation, for insertion of the rods into the skin and guiding them through the heads of the screws. In addition to less morbidity, less blood loss and improving cosmetics are other advantages of minimally invasive methods. However, longer operation time [37], increased radiation exposure [38], and steeper learning curve [34] are the main disadvantages of MI surgeries.

Anterior Approach

The first interbody fusion was performed through ALIF [35]. In comparison to posterior approach, the anterior approach for fusion surgeries has the advantage of placing larger bone grafts between vertebral bodies, restoring the lordosis, and sparing posterior spinal muscles [34]. However, through an anterior approach the posterior elements of the spine cannot be accessed; therefore, for a circumferential fusion, the patient must be rotated during the surgery for an additional posterior incision.

ALIF can be performed via transperitoneal or retroperitoneal approaches. In transperitoneal approach, after a midline incision and bilateral retraction of the rectus muscles, the peritoneum is opened and all visceral tissues are pushed to the sides to open a corridor for exposure of the spinal column; whereas in retroperitoneal approach, after an oblique incision of the abdominal muscle, the peritoneum is left intact and retracted to one side (Figure 1-13). Through both approaches, once the spine is accessed, anteromedial attachments of psoas muscles and some portions of anterior ligaments are dissected to expose the disc for discectomy and consequently placing the bone grafts [39]. Due to attachment of hypogastric plexus and aorta to the anterior surface of the spinal column (Figure 1-13), high vascular injury and retrograde ejaculation are

the major complications of ALIF. It is noteworthy that the rate of retrograde ejaculation in transperitoneal approach (10%) has been reported to be ten times more than retroperitoneal approach (0.86%)[40].

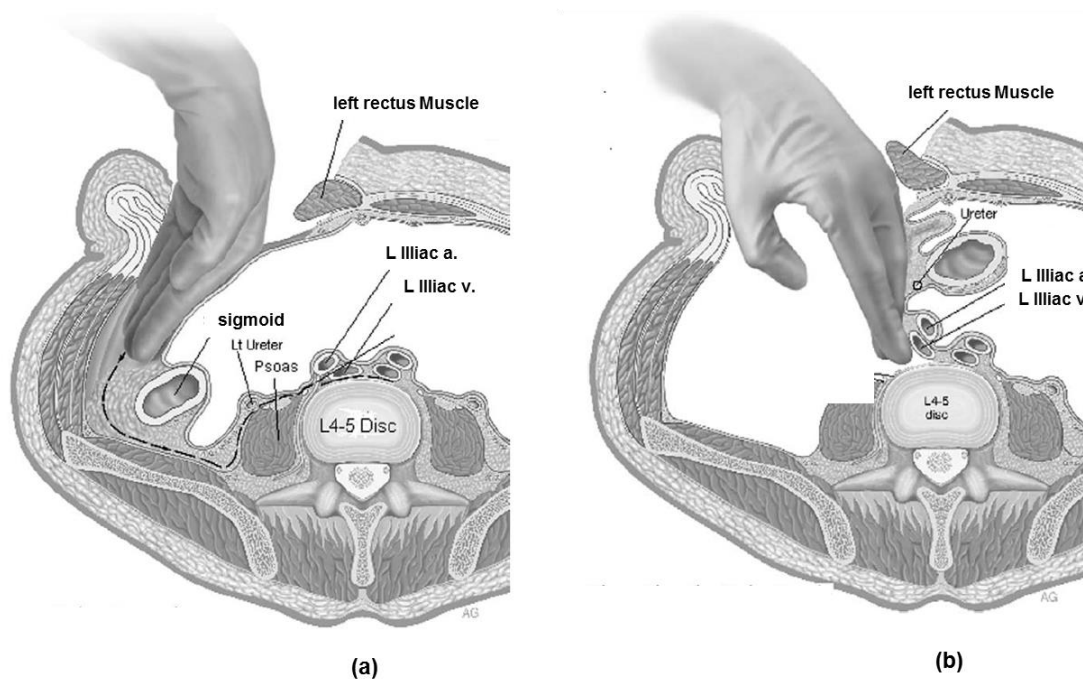


Figure 1-13: Retroperitoneal approach for ALIF. After incision of abdominal muscles and reaching the fatty region around the peritoneum, the retroperitoneum path is followed to access the spine (a). Following the resection of the psoas major from the operation levels, the iliac veins and arteries are gently detached from the anterior of the vertebrae and together with the peritoneum are pushed to one side so that the anterior column of the spine is exposed for the operation (b). Reprinted from [41] with permission from Elsevier.

Lateral Approach

Another approach for accessing the spine is direct lateral interbody fusion (DLIF), which is a modification of retroperitoneal ALIF [42]. In this method, two lateral incisions are made: one for probe insertion and the other for guiding the instruments (Figure 1-14). Instead of sharp detachment of muscles, tubular dilators are serially inserted in this method to split the psoas muscles and make a corridor for the operation. Moreover, percutaneous pedicle screw fixation is used for instrumentation, thereby minimizing soft tissue injury. However, similar to other

minimally invasive surgeries the learning curve for this approach is very steep. Also, similar to anterior approach, there is a high risk of injury to the lumbar plexus in this method, which necessitates continuous neural monitoring during the surgery.

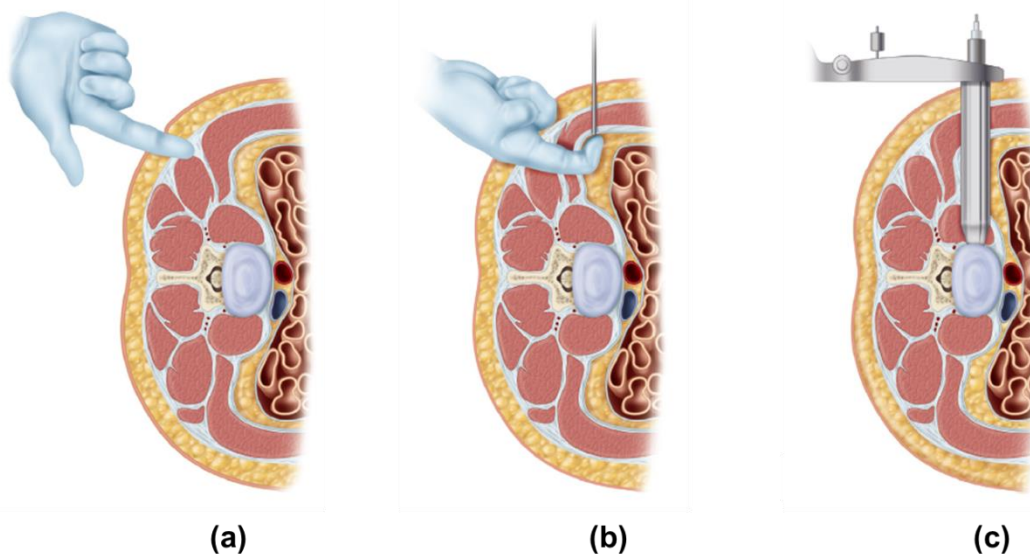


Figure 1-14: Lateral approach for lumbar interbody fusion. In this approach, two lateral incisions are made. The first incision is for accessing the fatty region behind the peritoneum (a) and guiding the tubular dilators that are serially inserted from the second incision (b). The dilators which are followed by a retractor split the psoas muscles and make a corridor to the spine for the operation (c). Reprinted from [42] with permission from Elsevier.

Although superiority of none of the aforementioned surgical approaches over others has been proven [43], it is interesting to note that posterior circumferential fusion ranks first in the treatment of degenerative disc disease. Recently, Pannel *et al.* [30] reviewed the database of a private insurance company that covers 25 million population of the United States. All patients receiving instrumented single-level lumbar fusion between 2004 to 2009 were identified and put into one of the five fusion groups: PLF, PLIF, PLIF with PLF, ALIF, or ALIF with PLF. In the 23,986 identified patients, posterior circumferential fusion (PLIF with PLF) was the most frequent method of fusion for the treatment of all the ten most common diagnoses (Figure 1-15).

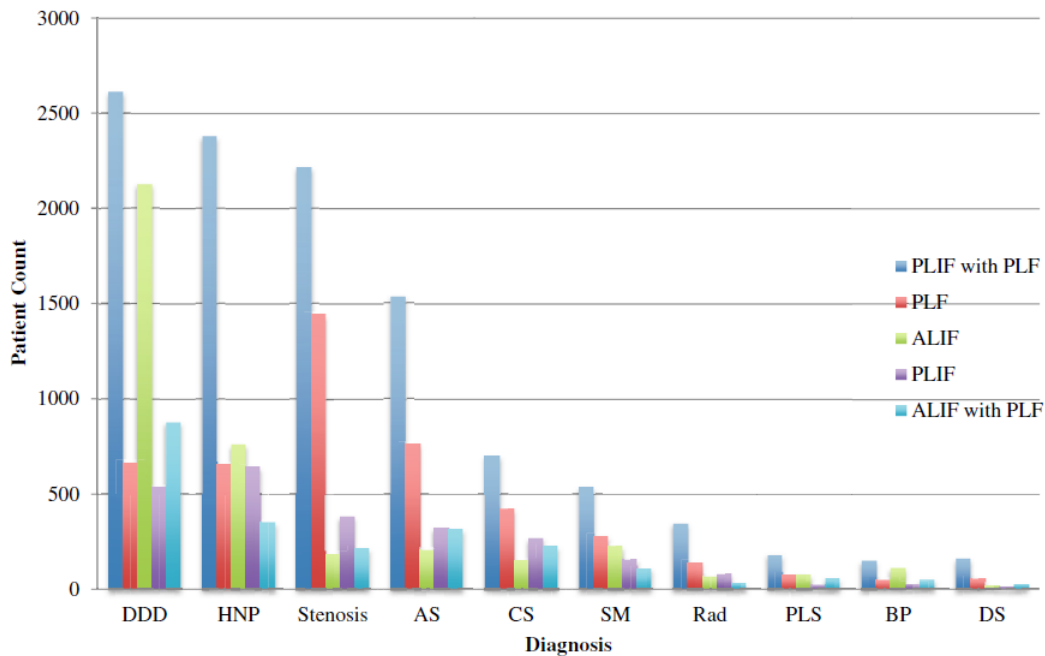


Figure 1-15: Number of fusion surgeries performed for the 10 most common spinal problems. AS, acquired spondylolisthesis, CS, congenital spondylolisthesis; DDD, degenerative disc disease; DS, disorders of the sacrum; HNP, herniated nucleus pulposus; PLS, postlaminectomy syndrome; Rad, radiculopathy; SM, spondylolysis without myelopathy. Reprinted from [30] with permission from Elsevier.

○ ***Fusion Complications***

Depending on surgical approaches, fusion-associated complications vary. This can include, infection, pseudoarthrosis, nonunion, failure of the instrumentation such as screw pull-out, and even vertebral fracture. One major complication of fusion surgeries is degeneration of the disc adjacent to the fusion leading to a disease known as adjacent segment disease (ASD), which is further discussed in section 1.4. Although the exact pathogenesis of ASD is not known, many believe the hypermobility of adjacent segments that compensate for motion loss of index levels alters the loading at the adjacent level and causes, or at least accelerates, progression of the disease. Based on this notion, both total disc replacement (TDR) and dynamic implants were

developed to provide mobility at the index level and therefore to decelerate development of ASD [44][45].

1.3.4.2 Total Disc Replacement (TDR)

The ideal purpose of total disc replacement is to replace the painful degenerated disc by a prosthesis that preserves the physiological motion of the treated level. The first version of intervertebral prostheses was simply a stainless steel sphere which was placed between the vertebral bodies. This concept was later replaced by ball and socket type artificial discs that continue until now. Recently, various forms of artificial discs such as Charité, ProDisc, Maverick, Activ-L, Mobidisc, SlideDisc, Physio-L, etc. are available, which mainly differ in number of pieces, biomaterials, and motion constraints (Figure 1-16). Among the aforementioned artificial discs, Charité, ProDisc, and Maverick have received FDA approval and have the longest follow ups.



Figure 1-16: Charité artificial disc. It consists of two end plates that are fixed to adjacent vertebral bodies and a core in between them that is domed on both sides, so that to articulate against the concave surfaces of the end plates. Reprinted from [46] with permission from lippincott williams & wilkins.

Depending on their types, complications of the artificial discs vary; however, the general complications of TDR can be divided into those related to the surgical approach (e.g. vascular injury, nerve damage, retrograde ejaculation, etc.), which ranges between 2.1% and 18.7%, and

those that are prosthetic related. Prosthetic related complications include osteolysis due to wear particles, subsidence, plate fracture, and implant failure, which range between 2% to 39.3% in the literature [47]. Although the few RCT studies contrasting TDR to fusion did not find it inferior to fusion, a consensus exists in the literature that more randomized studies and longer follow-ups are needed to evaluate the long term effects of TDR before its widespread usage[47].

1.3.4.3 Dynamic Implants

Dynamic stabilizers can be divided into two categories: interspinous distraction devices (ISDD) and pedicle-screw-based dynamic stabilizers (PSDS). As implied by their names, ISDDs are placed between the spinous processes of adjacent vertebrae. By distracting the two vertebrae, ISDDs can prevent narrowing of the intervertebral foramina in extension and are used in treatment of spinal stenosis, lumbar disc disease, and lumbar segmental instability. Some ISDDs such as X-STOP Spacer (Medtronic Spine and Biologics) and the Wallis implant (Zimmer Spine) act as non-compressible spacers; while other ISDDs such as Coflex device (Paradigm Spine) and DIAM are compressible and thus allow motion between the vertebrae.

PSDSs were introduced as alternatives to rigid instrumentations so as to provide mobility at the treated levels. In Dynesys, as one type of PSDSs, the pedicle screws are connected by polyethylene-terephthalate cords within polycarbonate urethane spacers. The cords and spacers are flexible but resist too much motion in flexion and extension, respectively (Figure 1-17). Other types of PSDSs include TOPS (Total Posterior System, Premia Spine), SSCS (Segmental Spinal Correction System, Osteotech), and BioFlex (Bio-Spine).

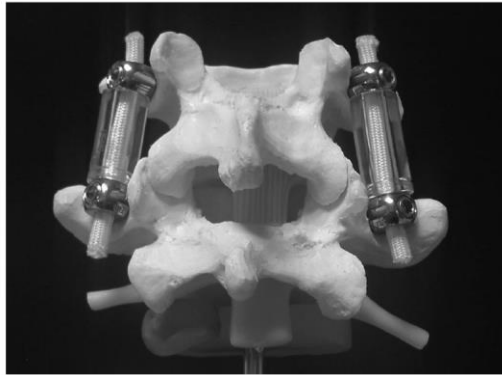


Figure 1-17: Dynesys. Reprinted from [48] with permission from Lippincott Williams & Wilkins.

1.4 Adjacent Segment Disease (ASD)

As noted by Park *et al.* [49] “adjacent segment disease (ASD) is a term with broad meaning, since it can describe nearly any abnormal process that develops in the mobile segment next to a spinal fusion”. Disc degeneration is a common form of ASD, as are listhesis, instability, stenosis, herniated nucleus pulposus, hypertrophic facet joint arthritis, and less commonly noted vertebral compression fracture [49][50][51][52]. A patient with asymptomatic ASD, only manifests radiographic degeneration and is pain-free (Figure 1-18), whereas with a symptomatic ASD, the patient suffers from pain, though they may not show any radiographic change at the adjacent disc (Figure 1-19). While the rate of symptomatic ASD ranges between 0 to 30.3% in the literature, the rate of radiographic ASD has been reported to range from 5.2 to 100% [6] [Park 2004].

The exact pathogenesis of ASD remains unclear; however, some risk factors have been identified. These include age, genetics, preexisting degeneration, sagittal misalignment, laminectomy, PLIF, number of fusion levels, and rigid instrumentation. Among these factors,

while age seems to be a major risk factor, the rest of the parameters are debatable. The studies that support or do not support each of these factors are provided in Table 1-1.

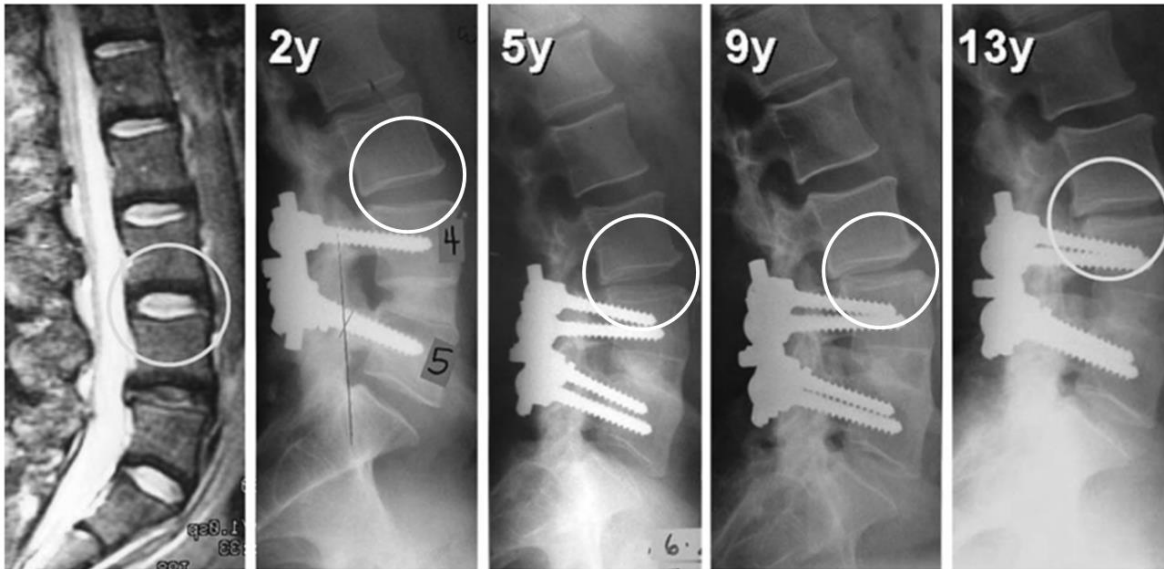


Figure 1-18: Loss of disc height over time indicating radiographic but not symptomatic ASD. Reprinted from [4] with permission from Lippincott Williams & Wilkins.

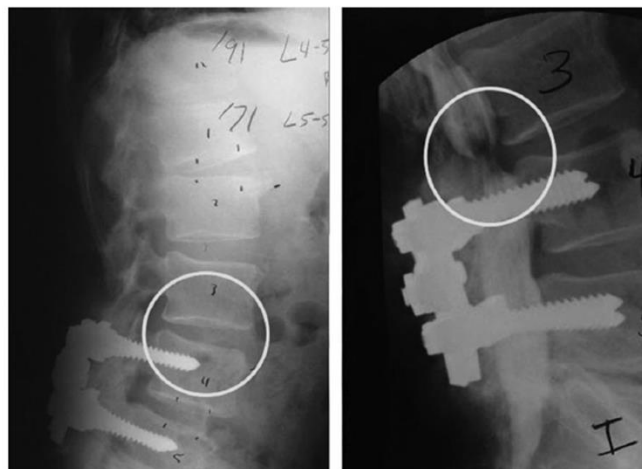


Figure 1-19: Symptomatic ASD with stenosis but without radiographic changes. Reprinted from [4] with permission from Lippincott Williams & Wilkins.

Table 1-1: Studies that support or do not support ASD risk factors.

Risk Factors	Supporting Studies	Not supporting Studies
Age	[4][53][54][55][56] [57] [58]	[59]
Pre-existing Degeneration	[60][61]	[62][63]
Method of Fusion	[58][64]	[65][45]
Sagittal alignment	[66][65] [56]	[58]
Number of fusion levels	[54][62] [56]	[65]
Rigid Instrumentation	[66][67]	[68]
Lordosis	[69]	[4]
Fusion Levels	[54] [62] [56]	
Laminectomy	[54]	

There is controversy on the nature of ASD in the literature. While some believe ASD is merely a natural progression of an underlying degeneration [70][50][71][72][73], others believe it is an abnormal accelerated degeneration that may have roots in altered biomechanics of the adjacent level [49][51][74][45]. As mentioned by Lund and Oxland [75], advocates of each of these two hypotheses can find supporting evidence in the literature.

Those who support the abnormal nature of ASD attribute its acceleration to altered loading or kinematic changes at the adjacent level. Measurement of disc load and correlating it to disc degeneration in human subjects is not feasible with current technology; however, both murine and bovine animal studies have shown that overloading in the form of static compressive or shear force accelerates disc degeneration [76][20][77][78][79]. Moreover, the level of the degeneration has been shown to correlate with time, frequency, and magnitude of the loading. Applying the same principle to human intervertebral disc implies that ASD may be due to overloading of the adjacent disc. Such an overloading of the disc can be the result of many factors including hypermobility of the remaining mobile segments, iatrogenic muscle damage, stiffness of the instrumentation, and any other change to the structure of the spine. Association of adjacent segment hypermobility and iatrogenic muscle damage with development of ASD are the focus of the current study and are further discussed in the following sections.

1.4.1 Adjacent Segment Hypermobility

One mechanism that can alter the loading at the adjacent level is possible adjacent segment hypermobility. As schematically demonstrated in Figure 1-20, assume preoperatively four of the lumbar vertebrae would flex to an amount 30° . That 30° would be almost evenly distributed between the three vertebral levels. But postoperatively, when three of the vertebrae are fused together, if patients would like to replicate the same range of motion, the adjacent segment needs to compensate for motion loss of the fused vertebrae. This requires application of higher bending moments, which is associated with higher strains and stresses in the disc and therefore, may accelerate disc degeneration. However, is this assumption correct? i.e., do patients postoperatively load their adjacent segments more to maintain their preoperative total lumbar ROM?

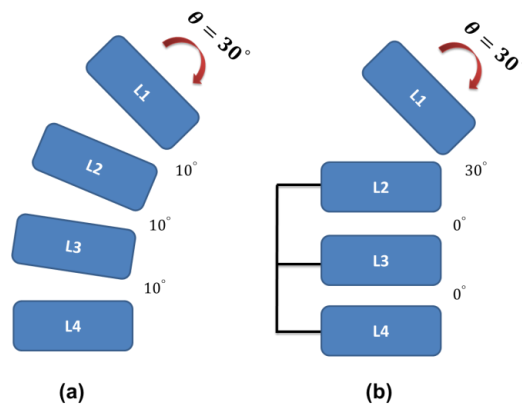


Figure 1-20: Adjacent segment hypermobility. If preoperatively four of the lumbar vertebrae would flex to an amount 30° , that 30° would be almost evenly distributed between the three vertebral levels (a). But postoperatively, when three of the vertebrae are rigidly fixated, if patients would like to replicate the same preoperative range of motion, all motion would be imposed on the adjacent segment.

An alternative assumption is that postoperatively patients are content with less mobility of their lumbar spine and do not let their adjacent segments get loaded more than it would preoperatively. In this case, with the assumption of applying the same amount of load on the

adjacent level, the motion of the adjacent segment should not change postoperatively (Figure 1-21).

Whether patients postoperatively follow the first scenario or the second, or a combination of both is not known [80]; but is an important question, the answer to which can determine whether adjacent segment hypermobility is a common occurrence to be linked with the degeneration of the adjacent disc.

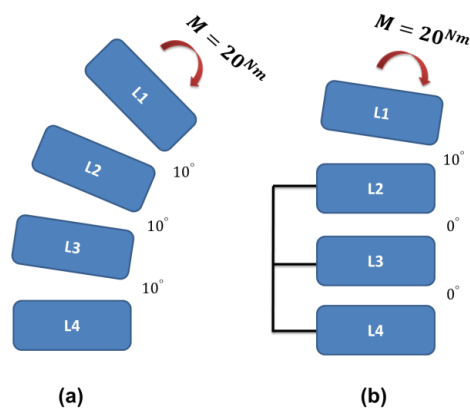


Figure 1-21: Same postoperative ROM at the adjacent level when applying the same preoperative load. If preoperatively a pure moment is applied on the spine each segment would rotate accordingly (a). If the same load is applied postoperatively when three of the vertebrae are rigidly fixated, although the total lumbar ROM would decrease, the ROM of the adjacent segment should not change (b).

1.4.2 Iatrogenic Muscle Damage

One parameter that may alter the loading at the adjacent level is the intraoperative injury to the paraspinal muscles. As described in section 1.3.4 under “Surgical Approaches for Fusion”, during open fusion surgeries, depending on the surgical approach, paraspinal muscles are resected from the posterior or anterior elements of the spine to provide exposure to the bony surfaces either for performing laminectomy/facetectomy or placement of the bone grafts. The resected muscles are then sutured and left there to heal, but will not reattach to the vertebrae.

Therefore, they will not be able to directly apply any load on the operated segments. Retraction of paraspinal muscles to the side, which is done for keeping the operation area open during the surgery, can also damage the muscles. Many studies have shown that the amount of muscle damage is correlated with retraction time [81][82][83], pressure [84], and extent of exposure [84].

Muscle damage after posterior fusion surgeries has been manifest in forms of loss of cross sectional area (CSA) [85], atrophy [86][87], altered EMG [88][89], and reduced muscle strength [90][91] [81] [86]. In a RCT study by Keller *et al.* [86], patients with chronic low back pain were randomized to instrumented posterolateral fusion or conservative treatments. The density of paraspinal muscles decreased only in the group receiving fusion. Kim *et al.* 2004 [90], measured multifidus CSA and trunk extension muscle strength of the patients who underwent open pedicle screw fixation (OPF) versus those who received percutaneous pedicle screw fixation (PPF). At 21 months follow-up multifidus CSA decreased significantly only in the group with OPF. Moreover, while extension muscle strength improved in PPF group, it remained unchanged for OPF group. Kramer *et al.* [89] noted that in comparison to a paired matched control group, the 20 patients of their study showed a 25% lower and 28% higher activation in multifidus and iliocostalis muscles, respectively, when lifting their trunk from a downward tilted to a straight prone position. Wang *et al.* [88] observed that the average amplitude and frequency of multifidus EMG at three months post-op was significantly higher in patients with MI TLIF in comparison to those with Open TLIF.

These consequences of iatrogenic muscle damage may lead to alterations in spinal loading after surgery, especially at the adjacent levels, and may affect or contribute to degeneration of the

adjacent disc. To the author's knowledge, the effect of iatrogenic muscle damage on spinal loading has not been investigated in the literature.

1.5 Musculoskeletal Modeling

1.5.1 Muscles

1.5.1.1 Morphology and Physiology

Muscle is an organized material with several structural levels. Each muscle consists of a number of fascicles that are separated from each other by perimysium (See Figure 1-22). These muscle fascicles each contain a set of muscle fibers surrounded by a connective tissue sheath known as endomysium that binds fibers together. Within each muscle fiber a large number of myofibrils lie parallel to one another in a way that gives the muscle its striated pattern. The functional contractile unit of muscles are sarcomeres that when connected together in series form a myofibril. Each sarcomere consists of thin and thick myofilaments that are mainly made up of the proteins actin and myosin.

The central nervous system controls the muscle force generation through the control of individual motor units. A motor unit consists of a motor neuron and a set of muscle fibers that are innervated by that motor neuron. Once a neural signal, or more precisely an action potential, reaches a muscle fiber, it causes a series of chemical actions that lead to release of Ca^{2+} ions into the sarcoplasm surrounding myofibrils. The released Ca^{2+} ions initiate the process of cross-

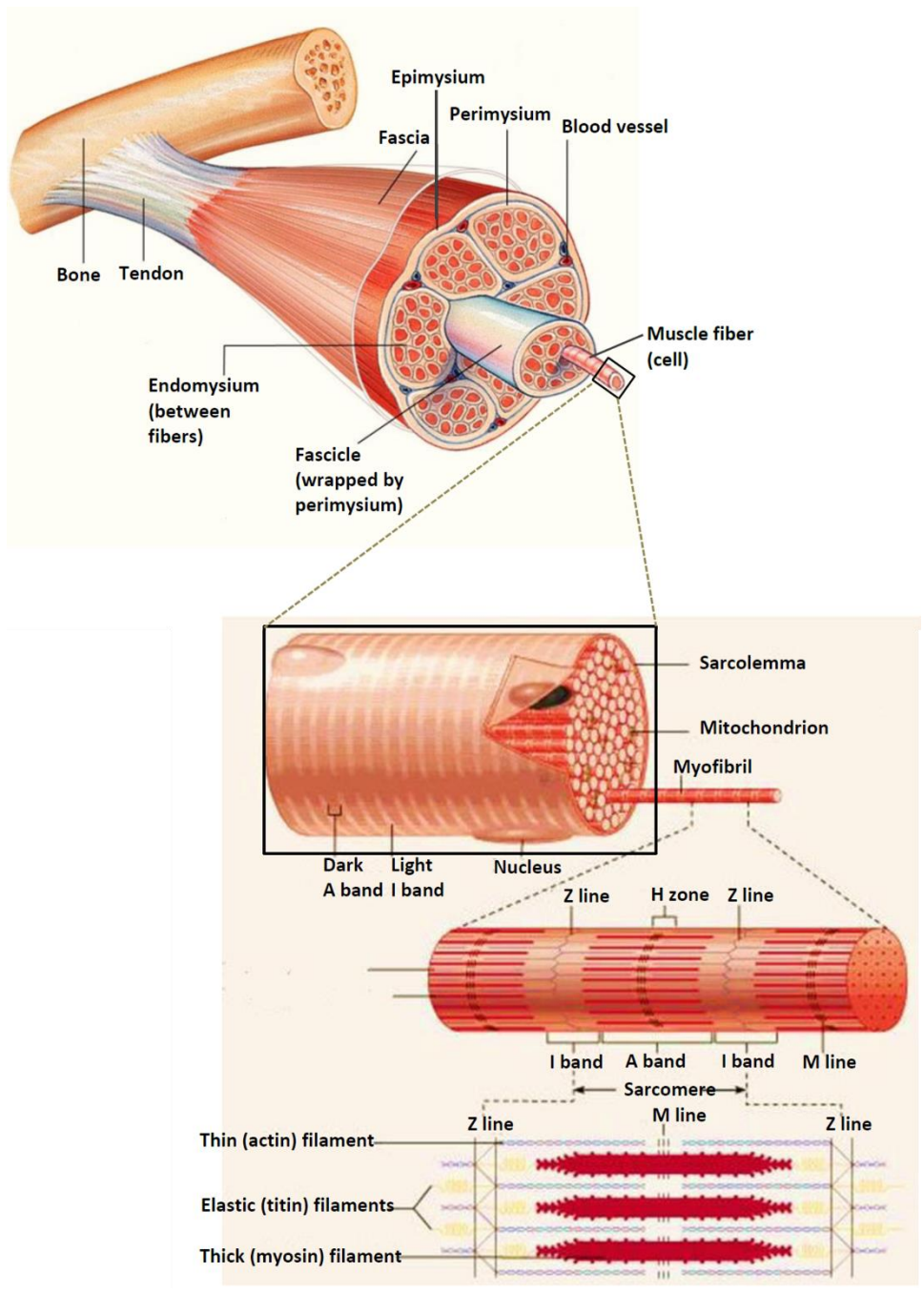


Figure 1-22: Muscle morphology. Adapted from Fig. 11.2 of [264] with permission from Pearson Education, Inc.

-bridge forming between myosin and actin, during which the myosin grabs the thin (actin) filament and slides it toward the center of the sarcomere and thus muscle contraction occurs. As soon as that neural signal disconnects, Ca^{2+} ions get retracted into the sarcoplasmic reticulum (a sac-like reservoir for Ca^{2+} ions inside fibers) and the muscle relaxes.

1.5.1.2 Mechanical Properties

In order to model the mechanical function of an entire muscle-tendon, each muscle fiber can be considered as a contractile element and a parallel passive spring, together in series with a nonlinear spring representing the tendon (Figure 1-23). This type of model, which is well-known as the Hill-type muscle model, is the mainstay of the majority of muscle-tendon models in the literature. This mechanically modeled muscle-tendon element is sometimes referred to as a musculotendon actuator.

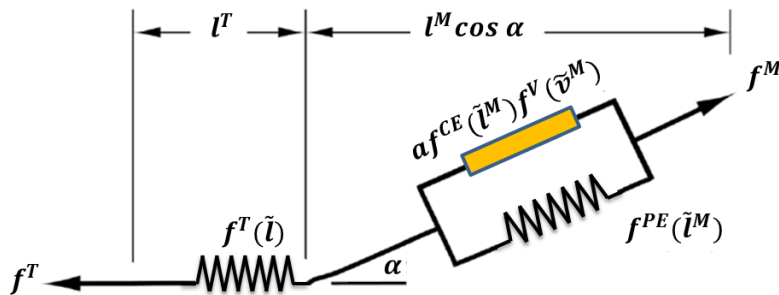


Figure 1-23: Hill-type musculotendon actuator. Each muscle fiber can be considered as a contractile element and a parallel passive spring, together in series with a nonlinear spring representing the tendon.

The force generated by the contractile element of a musculotendon actuator is a coupled function of muscle activation, its length, and its velocity, and in the Hill-type model is assumed to be a multiplication of separate functions of these parameters; therefore by adding the force of the

passive element of the muscle that is only a function of muscle length, the total muscle force can be calculated as:

$$f^M(a, l^M, v^M) = [a\tilde{f}^{CE}(\tilde{l}^M)\tilde{f}^V(\tilde{v}^M) + \tilde{f}^{PE}(\tilde{l}^M)]f_o^M \quad (1-1)$$

Where a and f_o^M are muscle activation and muscle maximum isometric force respectively; and $\tilde{f}^{CE}(\tilde{l}^M)$, $\tilde{f}^{PE}(\tilde{l}^M)$, and $\tilde{f}^V(\tilde{v}^M)$ are force multipliers that are read from the normalized force-length and force-velocity curves for muscles (Figure 1-24).

Typical normalized force-length and force-velocity curves of muscles are shown in Figure 1-24. These graphs are obtained by fitting curves to the experimental data taken from *in vitro/in vivo* testing on animal specimens. Millard *et al.* [92] used the cross-bridge-based theoretical force-length relation proposed by Gordon *et al.*[93], to fit 5th order Bezier curves to the results of the experimental studies by Gollapudi *et al.* [94] and Winters [95]. Those curves, which were given to us through courtesy of Millard *et al.* [92], are plotted in Figure 1-24.

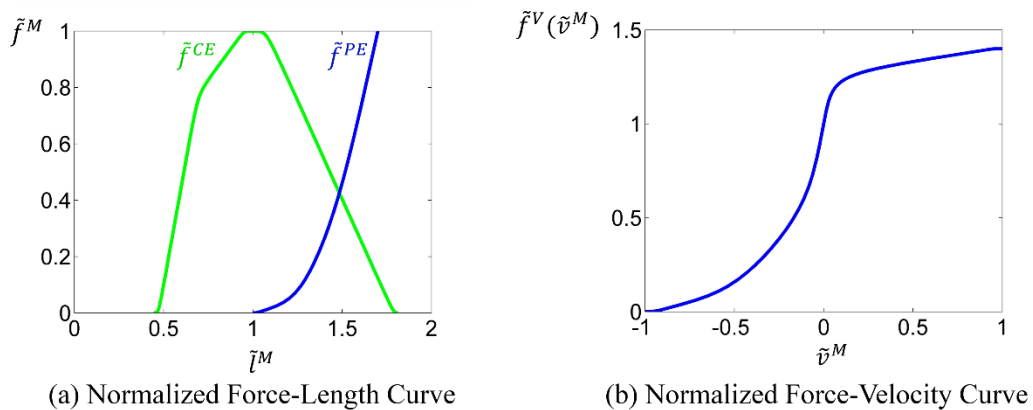


Figure 1-24: Muscle force-length and force-velocity curves. Data for plotting these figures is given to us through courtesy of Millard *et al.* [92].

Similarly, they used results of the experimental studies by Maganaris *et al.* [96] and Magnusson [97] on tendons, to obtain a normalized force-length relationship for tendons, which is plotted in Figure 1-25.

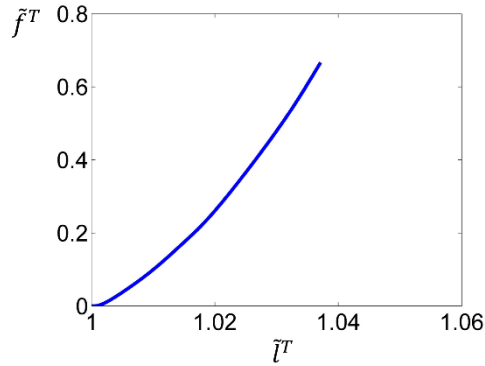


Figure 1-25: Normalized force-length curve for Tendon. Data for plotting this figure is given to us through courtesy of Millard *et al.* [92].

Since in some muscles, the muscle fibers are inserted on tendon at an oblique angle (α), known as pennation angle, the equilibrium condition along the line of action of the musculotendon actuator necessitates that:

$$f^M \cos \alpha - f^T = [a \tilde{f}^L(\tilde{l}^M) \tilde{f}^V(\tilde{v}^M)] f_o^M \cos \alpha - f^T = 0 \quad (1-2)$$

This equation is shown in form of a block diagrams in Figure 1-26. Note that the inputs to the diagram are length and velocity of the musculotendon (l^{MT} and v^{MT}), and not muscle length and velocity; therefore an internal differentiator is needed for calculation of muscle length and velocity. Some software packages, including ArtiSynth, do not implement that differentiator; rather, tendons are assumed to be rigid, thereby having constant lengths over the time.

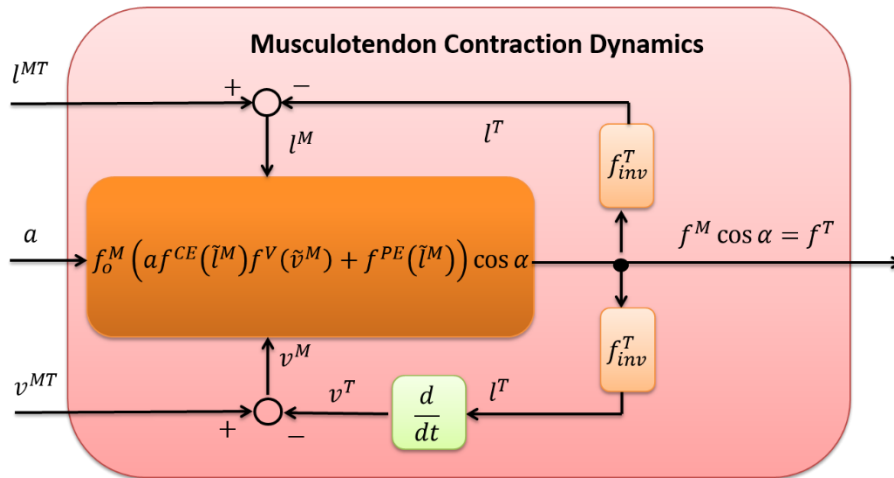


Figure 1-26: Musculotendon contraction dynamics.

1.5.1.3 Muscle Parameters

In order to use the normalized force-length and force-velocity curves for calculation of passive and active force within a muscle fascicle at each state, we need to know the optimal fiber length l_o^F and maximum isometric force f_o^M of that muscle fascicle. These values are not directly measured; instead are calculated from a few other muscle parameters that are directly measured from cadavers. Those parameters include sarcomere length l^S , fiber length l^F , musculotendon length l^{MT} , pennation angle α , and physiological cross sectional area (PCSA). Figure 1-27a demonstrates schematically a muscle fascicle that is attached via its tendon to bony elements A and B; and Figure 1-27b is merely a rearrangement of Figure 1-27a for better demonstration of aforementioned lengths.

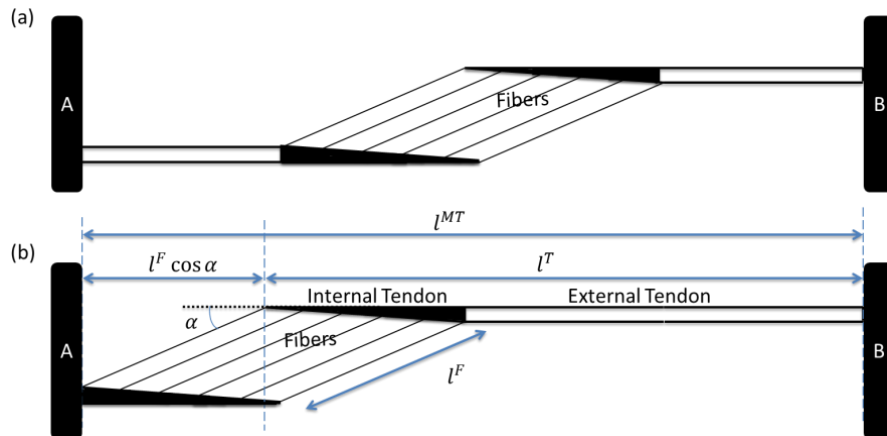


Figure 1-27: Muscle parameters including the pennation angle α , musculotendon length l^{MT} , and fiber length l^F . For better demonstration of muscle parameters, (b) is merely a rearrangement of (a).

○ **Optimal fiber length**

Optimal fiber length l_o^F is the length of fiber at which the muscle is at rest, i.e. under no tension. It is also the length at which the muscle can produce the maximum isometric force when fully activated. Optimal fiber length can be calculated by normalizing the fascicle and sarcomere lengths measured from cadavers against the optimal sarcomere length in the following manner:

$$l_o^F = l^F \times \frac{l_o^S}{l^S} \quad (1-3)$$

where l^F and l^S are the fiber and sarcomere lengths measured from fixed cadavers, and l_o^S is the optimal sarcomere length that for human muscle is considered to be between 2.7 to 2.8 μm [98][99]. While the fascicle (also fiber) length can be simply measured with a caliper, laser diffraction technique is used for measurement of the sarcomere length [99][100][101].

○ ***Maximum isometric force***

The maximum force that a fully activated muscle fiber can generate when remaining at its optimal length is called maximum isometric force f_o^M . This value can be calculated for each muscle fascicle through the following formula:

$$f_o^M = K \times PCSA \quad (1-4)$$

where PCSA is the physiological cross sectional area of that muscle fascicle and K is the muscle strength factor that is a constant, usually assumed to be equal for all the muscles in a model. PCSA is defined as the volume of a muscle fascicle divided by its optimal fiber length, whereas the muscle strength factor is an unknown and typically ranges between 10 to $100 \frac{N}{m^2}$ [12][102]. Since with current techniques, direct *in vivo* measurement of forces are not feasible, one way to assign a reasonable value for this parameter in models is to set it in a way so that the maximum producible moment by the model around a certain joint is the same as the maximum moment produced by subjects of some *in vivo* experiments. For instance, McNeill *et al.* [103] did an experiment in which they asked subjects of their study to make their maximum effort to resist against an increasing horizontal force applied anteriorly to the harness around their chests. McNeill *et al.* [103] reported the average of the maximum force born by their subjects and its corresponding moment around L5-S1 level to be 550 N and 200 Nm, respectively. Bogduk *et al.* [104] divided that 200 Nm by the maximum extension moment their model could produce around L5-S1 and obtained a value of 46.6 N/cm^2 for muscle strength factor.

○ **Normalized fiber length**

Besides optimal fiber length l_o^F and maximum isometric force f_o^M , one more parameter is needed to read the force from normalized force-length curve; that parameter is normalized fiber length \tilde{l}^F , which is defined as length of fiber over optimal fiber length:

$$\tilde{l}^F = \frac{l^F}{l_o^F}$$

1.5.2 Solution Methods for Determining Muscle Forces

After all components of a geometrical model are modeled, the relation between all forces applied on body segments and corresponding motions of the body segments can be written as:

$$\mathbf{M}(\mathbf{q})\ddot{\mathbf{q}} + \mathbf{C}(\mathbf{q}, \dot{\mathbf{q}}) + \mathbf{G}(\mathbf{q}) + \mathbf{R}(\mathbf{q})\mathbf{F}^{MT}(\mathbf{a}, \mathbf{q}, \dot{\mathbf{q}}) + \mathbf{E}(\mathbf{q}, \dot{\mathbf{q}}) = 0 \quad (1-5)$$

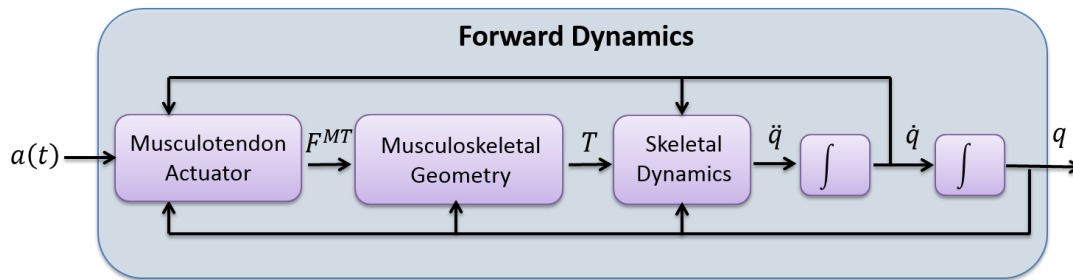
where \mathbf{q} , $\dot{\mathbf{q}}$, and $\ddot{\mathbf{q}}$ are the generalized coordinates, velocities, and accelerations; $\mathbf{M}(\mathbf{q})$ denotes the mass matrix of the system; $\mathbf{C}(\mathbf{q}, \dot{\mathbf{q}})$ represents centrifugal and Coriolis forces and torques; $\mathbf{G}(\mathbf{q})$ is the vector of forces and torques related to gravity; $\mathbf{R}(\mathbf{q})$ is the matrix of muscle moment arms; \mathbf{a} is the vector of muscle activations; $\mathbf{F}^{MT}(\mathbf{a}, \mathbf{q}, \dot{\mathbf{q}})$ is the vector of musculotendon forces; and lastly external forces and torques are represented by $\mathbf{E}(\mathbf{q}, \dot{\mathbf{q}})$.

1.5.2.1 Forward Dynamics versus Inverse Dynamics

In order to solve equation (1-5), either the generalized coordinates \mathbf{q} or the muscle activations \mathbf{a} must be fully known. As schematically shown in Figure 1-28, when muscle activations are known and fed into the model, musculotendon forces and consequently muscular moments can

be calculated and added to other forces and torques of the system. This way the right hand side of equation (1-6), which is obtained by rearrangement of equation (1-5), will be only a function of \mathbf{q} and $\dot{\mathbf{q}}$; and therefore, equation (1-6) can be integrated in a forward dynamics manner to solve for generalized coordinates \mathbf{q} .

$$\ddot{\mathbf{q}} = -\mathbf{M}(\mathbf{q})^{-1}[\mathbf{C}(\mathbf{q}, \dot{\mathbf{q}}) + \mathbf{G}(\mathbf{q}) + \mathbf{R}(\mathbf{q})\mathbf{F}^{MT}(\mathbf{a}, \mathbf{q}, \dot{\mathbf{q}}) + \mathbf{E}(\mathbf{q}, \dot{\mathbf{q}})] \quad (1-6)$$

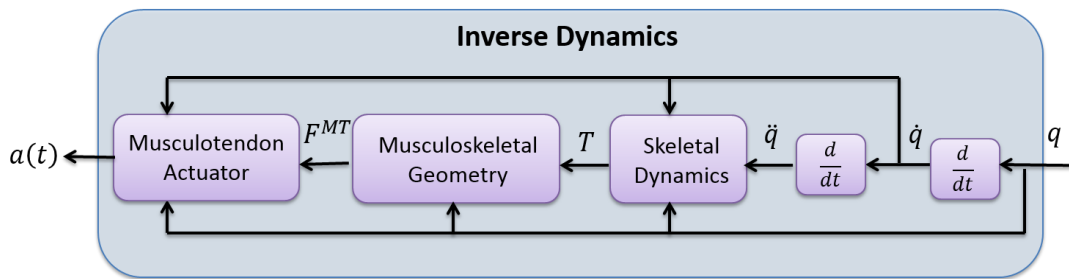


Adapted from Pandy *et al.* 2001

Figure 1-28: Forward Dynamics. When muscle activations are known and fed into the model, musculotendon forces and consequently muscular moments about the joints are calculated, which then with external forces are used in solving for kinematics of the body segments.

In inverse dynamics, the generalized coordinates \mathbf{q} , which are commonly obtained from gait data, are known, so is the right hand side of equation (1-7), which is obtained by rearrangement of equation (1-5). As also shown in Figure 1-29, once joint torques are calculated from equation (1-7), they are distributed between the muscles crossing each joint so that the forces and activations of each muscle are determined.

$$\mathbf{R}(\mathbf{q})\mathbf{F}^{MT}(\mathbf{a}, \mathbf{q}, \dot{\mathbf{q}}) = -[\mathbf{M}(\mathbf{q})\ddot{\mathbf{q}} + \mathbf{C}(\mathbf{q}, \dot{\mathbf{q}}) + \mathbf{G}(\mathbf{q}) + \mathbf{E}(\mathbf{q}, \dot{\mathbf{q}})] \quad (1-7)$$



Adapted from Pandy *et al.* 2001

Figure 1-29: Inverse Dynamics. In an inverse dynamics approach, the kinematic data are used for calculation of joint moments. By distribution of the joint moments between the muscles crossing each joint, the forces and activations of each muscle can be determined

Both inverse and forward dynamics have their own limitations. On one hand, for forward dynamics, obtaining activations of all muscles through electromyography is difficult and rare; on the other hand in inverse dynamics, since joint torques are directly calculated from gait kinematics, the calculated torques are very sensitive to kinematic errors. “The adoption of either an inverse or forward dynamics approach is typically dependent on the availability of the experimental data or the clinical/research question to be answered” [105].

1.5.2.2 Tackling Muscle Redundancy through Optimization

Irrespective of the method (inverse or forward dynamics) chosen for solving the problem, estimation of muscle forces requires optimization [106][105][107]. This is because in most of the musculoskeletal models the number of muscles is more than the DOFs of the system, meaning that different sets of muscle activations can produce the same kinematics. Therefore, optimization is needed to solve for a unique set of muscle activations.

It is assumed that the central nervous system recruits muscles in a way to minimize a cost function. That cost function varies in between studies, is dependent on solution method, and has been shown to depend on type of activities. However, almost all cost functions can be

categorized under the “Generalized Performance Criterion” proposed by Zajac and Winters [108] as:

$$J_c = k_k J_k + k_{nm} J_{nm} + k_{ld} J_{ld}$$

where the general performance criterion J_c consists of three subcriteria: J_k , J_{nm} , and J_{ld} , which are weighted by three scalar terms k_k , k_{nm} , and k_{ld} .

J_k represents kinematics-based performance criteria such as tracking a reference trajectory [109][110], minimizing jerk [111][112], reaching some extremum such as maximum jump [113], or highest velocity [114]. J_{nm} is the neuromuscular performance criterion, which can include minimizing muscle forces or muscle forces squared [115][116], muscle stresses, muscle stresses squared, muscle stresses cubed [117], muscle activations [118], muscular energy consumption [119], and so on. J_{ld} is the criterion related to loading along bones or on joints and can include minimizing joint forces [115], minimum joint moments [118], or maximum producible force, such as hand force along a given direction [120].

Among the studies that have investigated different powers of muscle forces and muscle stresses as cost functions, some studies found dependence of final results on cost functions [121], whereas the majority observed no significant difference [118][122][117]. However, according to the review article by Erdemir *et al.* [105], in general, for lower extremity, minimum sum of muscle stresses cubed seems to be broadly accepted whereas for upper extremity, minimum sum of muscle forces squared is more commonly used in the literature.

It is noteworthy that cost functions should be selected in accordance with a compatible optimization technique. For instance, in order to obtain a set of muscle forces in a model that

leads to maximum jump or minimum total muscle energy consumption, static optimization is not appropriate. Instead, dynamic optimization should be used.

- ***Static versus Dynamic Optimization***

The main difference between static and dynamic optimization is that in static optimization a cost function is minimized at each instant of time, whereas in dynamic optimization the cost function is optimized for a complete cycle of movement [106]. Dynamic optimization problems are usually solved in forward dynamics fashion and through optimal control strategies. One common strategy is to convert the dynamic optimization problem into a parameter optimization problem by parameterizing the input control variables (here muscle excitations. A set of nodal points through the history of each control input variables are identified and considered as optimization parameters) [123][106]. This provides a robust solution but increases the computation time. In a study by Anderson and Pandy 2001 [124] it was shown that for cases where both static and dynamic optimization techniques are applicable, both methods lead to similar results for joint forces and muscle activations. Therefore, given its substantially faster solution, static optimization is preferred over dynamic optimization. However, for occasions where no movement data is available or some special cost functions need to be used, dynamic optimization is the correct choice [105].

- ***Forward-Dynamics-Assisted Data Tracking***

Forward-dynamics-assisted data tracking is a method that uses kinematic data in a weaker fashion in comparison to inverse dynamics. In this method, at the beginning of each time step, a set of muscle activations are guessed and fed into a forward dynamics solver. The resulting kinematics of that time step are compared versus experimental kinematics. If they do not match,

the process of updating muscle activations continues until the set of muscle activations that best reproduce the experimental kinematics is obtained (Figure 1-30). The same procedure is performed at the beginning of next time steps.

The cost function in forward dynamics assisted data tracking is typically least squares fitting of experimental kinematics. However, for tackling muscle redundancy other cost functions, such as sum of muscle stresses cubed [125], joint torques [126], or ground reaction forces [127] can be added to that. Nonetheless, adding those cost functions may lead to increase in tracking error [125], whereas the extent of proper weighting between these cost functions is not yet known [105]. Since the optimization in this method is performed at each time step, as static optimization, this method is substantially faster in comparison to dynamic optimization [109]. Therefore sensitivity analysis between different cost functions can be easily done.

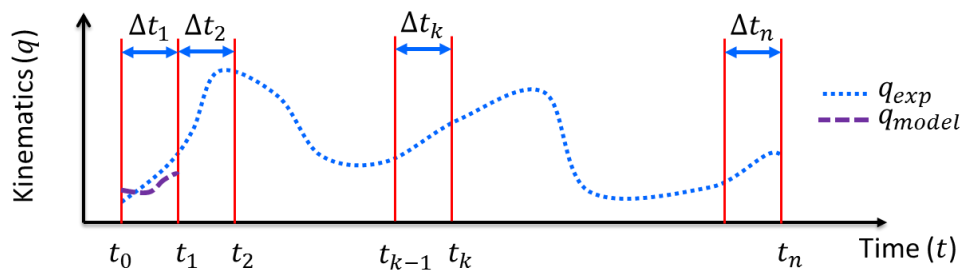


Figure 1-30: Forward-dynamics assisted data tracking. At the beginning of each time step, a set of muscle activations are guessed and fed into a forward dynamics solver. The resulting kinematics of that time step are compared versus experimental kinematics. If they do not match, the process of updating muscle activations continues until the set of muscle activations that best reproduce the experimental kinematics is obtained

1.5.3 Intra-Abdominal Pressure (IAP)

One parameter that should be considered in musculoskeletal modeling of the lumbar spine is intra-abdominal pressure (IAP). Increased IAP can unload the spine by applying an upward force on the thorax via the diaphragm. In fact, the abdomen can be considered as a pressurized barrel between the pelvis and the ribcage, with the diaphragm acting as its lid. As shown in Figure 1-31, the diaphragm has a parachute-like shape. Therefore, in order to calculate the resultant force of IAP on the diaphragm, one can multiply its top area by IAP [128].

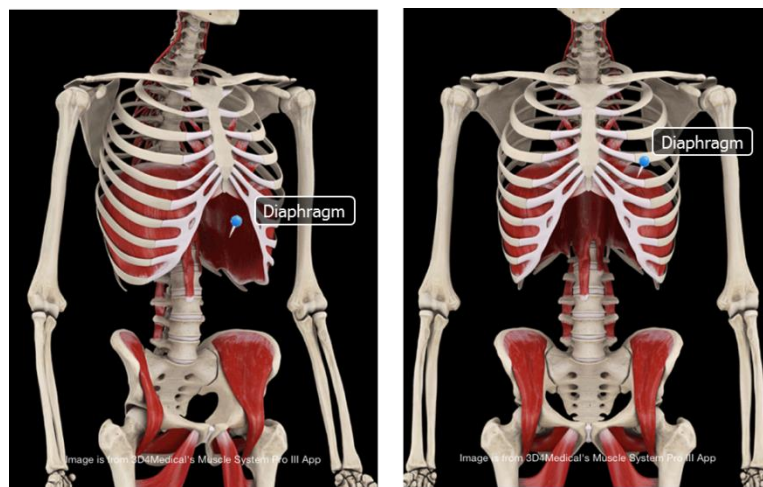


Figure 1-31: Parachute-like shape of the diaphragm. The intra-abdominal pressure can unload the spine by pushing the diaphragm upward. Reprinted from Muscle System Pro III app with permission from 3D4Medical company

It is well recognized in the literature that the abdomen behaves like a liquid-filled container; i.e. the abdominal pressure is hydrostatic [129][130]. In order to measure the IAP in daily activities, although direct methods are impractical, indirect methods such as measuring intravesical or intragastric pressure can be used. Currently, intravesical pressure is the clinical gold standard for IAP measurement. This method has been validated by Iberti *et al.* [131], who intraoperatively monitored intraperitoneal pressure (directly) and simultaneously measured intravesical pressure;

their results showed a linear relationship between the two pressures with correlation coefficient of 0.95. Intra-gastric pressure has also been validated in the studies by Collee *et al.* [132] and Surgue *et al.*[133], where it correlated well with intravesical pressure.

In order to study the normal range of IAP, Cobb and his colleagues [134] measured the intravesical pressure of 20 healthy subjects during different activities. Their results revealed that while the mean of normal standing IAP is 2.7 kPa (ranging between 2 to 3.6 kPa), it can reach to the maximum values of 14.5 and 22.8 kPa in coughing and jumping respectively. Daggfeldt *et al.* [12] studied the intra-gastric pressure of four male subjects during maximal back extension efforts. This value was maximum (19 kPa) when the subjects were fully flexed to 40 degrees and had its minimum value (12 kPa) when they were extended up to 20 degrees.

1.5.4 Musculoskeletal Models of the Lumbar Spine

To date various musculoskeletal models of the lumbar have been presented in the literature [135][136][137][138][139][1]. While spinal muscles are often simplified into one or a few muscle groups in some studies [140][141], recently, the anatomical complexity of the models has increased as it has been observed that even small variations in lines of action (5° - 15°) can substantially alter the spinal loading (>100 N) [142]. Further, it has been determined that inclusion of muscle force-length relationship is important for prediction of larger moment production in flexion than in extension which is observed in experimental studies [12][143]. These suggest the necessity of moving toward more physiological and anatomically detailed musculoskeletal models for correct estimation of spinal loads.

For calculation of muscle forces, EMG-assisted [135][136], optimization-based [138] [139] [1], and EMG-assisted optimization (EMGAO) techniques [144][145] have been used in the

literature. The EMG-assisted technique has the advantage of incorporating co-contraction of agonist and antagonist muscles (spinal and abdominal muscles); however, it has the limitation of not maintaining the joint moment at equilibrium [136]. While optimization methods satisfy joint moment equilibrium, they usually cannot predict antagonist muscle activations [146]. EMGAO was introduced to take advantage of both methods [144]. Cholewicki *et al.* [136] made a comparison between these three techniques and observed that while there was no significant difference between the results of the EMG-assisted and EMGAO methods, the activation patterns differed dramatically between the optimization and the other two methods; also optimization method estimated lower compressive forces (as low as 32% in extension and 43% in flexion).

Many biomechanical models solve for muscle forces by a single transverse cut across one of the lumbar levels (usually L4-L5 or L5-S1) [135] [136][147]. Regardless of whether EMG-assisted, EMGAO, or optimization is used, the muscle forces estimated from single level free body diagrams often violate the equilibrium at other levels of the spine [137][148][147]. It has been shown that the extent of violation could reach to 40% during flexion [148], which led to significantly different muscle activation patterns, though the compressive force did not change more than 9%. Therefore, the algorithms for solution methods should be designed so as to satisfy the equilibrium at all joint levels.

One advantage of multibody-dynamics based software packages such as AnyBody, OpenSim, and ArtiSynth for modeling redundant musculoskeletal systems is that the formulations for solving muscle forces in these software packages satisfies moment equilibrium at all joints. Moreover, with forward dynamics solvers that both ArtiSynth and OpenSim utilize, muscle physiology can be more easily incorporated into system equations [106]. Finally, in contrast to

most of the existing models in the literature that are hard coded, models that are developed using these software packages can be easily shared between research groups [139]. This saves substantial time for other researchers to improve existing models rather than constructing models from the ground up.

De Zee *et al.* [139] created a generic base model with 154 fascicles using AnyBody. They validated their model by comparing their model's maximum extension moment in upright standing to the experimental data. Their model was able to produce 238 Nm about L5-S1 which led to axial and shear forces of 4520 N and 639 N at that joint, respectively. Using the same software, Han *et al.* 2011 [149] extended that model by adding 56 short segmental muscles along with lumbar spine ligaments, intervertebral disc stiffness, and intra-abdominal pressure (IAP). They extended the validation of their model by comparing their results to the experimental studies by Rohlmann *et al.* [150], where *in vivo* spinal loads on vertebral body replacements were measured through telemetry. They also compared their results to Wilke *et al.*'s [151] *in vivo* measurement of intradiscal pressure. Han *et al.* 2011 [149] did not report on absolute values of spinal forces, rather normalized the spinal forces to standing and compared the ratios with normalized experimental loads measured in Rohlmann *et al.* [150] and Wilke *et al.*'s studies [151].

Using OpenSim, Christophy *et al.* [1] made their model closest in similarity to de Zee *et al.* [139], but added more muscles, including newer data on quadratus lumborum and multifidus, increasing the number of muscle fascicles to 238. In contrast to the other two models, Christophy's model can be downloaded for free due to open source nature of OpenSim. Furthermore, muscle parameters needed for a full Hill-type musculotendon model including the tendon ratio and the pennation angle are incorporated in Christophy *et al.*'s model, rendering it

as currently the model of the lumbar spine with the most physiologically detailed lumbar spinal muscles[152].

Christophy *et al.* [1] compared the moment arms of their model to anatomical data in the literature but did not compare the spinal loads of their model to other studies.

We intend to make our geometrical model similar to Christophy *et al.*'s model [1], but using ArtiSynth. ArtiSynth is an open source java-based biomechanical toolkit developed at UBC. The main superiority of ArtiSynth over the other two software packages is that this software combines and solves multibody dynamics and FEM in a fast and convenient fashion. This feature, that has been previously used for modeling jaw-tongue-hyoid complex [153], can be applied to modeling of the spine. Some part of interest of the spine (e.g. L4-L5 intervertebral disc) can be modeled with FEM while the other parts are modeled as multibody dynamics, resulting in a model that can be solved considerably faster than when all parts are modeled as FEM. Using this feature of ArtiSynth is not the focus of this study, but is a great potential for future studies, motivating us to use this software for developing our base model.

1.6 Objectives

Based on animal studies, overloading of the intervertebral disc accelerates disc degeneration and may be the reason for abnormal progression of disc degeneration adjacent to a spinal fusion. Overloading of the adjacent disc may happen if patients attempt to replicate their preoperative total lumbar ROM; this is because the mobile adjacent segments have to compensate for motion loss of fused vertebrae. Iatrogenic muscle damage can also postoperatively result in a different muscle activation pattern and lead to altered loading at the adjacent level. To provide insight on

possible contribution of each of these two factors on loading of the adjacent level and consequently its degeneration, the objectives of my thesis are:

- 1- To do a systematic review of *in vivo* studies on kinematics of the segment adjacent to a lumbar spine fusion to find evidence for adjacent segment hypermobility and whether it is a common occurrence so as to be linked with ASD.
- 2- To develop a musculoskeletal model of the lumbar spine to investigate the role of iatrogenic muscle damage on loading at the adjacent level.

The overall goal of this research is to investigate the biomechanical changes at the adjacent level so as to shed light on possible contributors to development of ASD. Investigating the impact of surgical parameters such as the number of fusion levels and the stiffness of fixations on loading at the adjacent levels are of interest, but not the objectives of current study. The following sections consist of two manuscripts (chapters 2 and 3), followed by an integrated discussion (chapter 4). A version of the first manuscript (chapter 2), which is a systematic analysis of the literature on *in vivo* kinematics of the segments adjacent to spinal implants, was submitted to the European Spine Journal. The second manuscript (chapter 3), which is on the role of iatrogenic muscle damage on loading at the adjacent level, is in preparation for submission to a biomechanical related journal.

1.7 Scope

The project presented in this thesis is a combination of two studies on biomechanics of the segment adjacent to a spinal fusion. In the first study, the literature of *in vivo* studies on kinematics of the segment adjacent to spinal fusion was critically analyzed and reviewed to search for evidence on altered mobility at the adjacent level. In the second study, a

musculoskeletal model of the lumbar spine was developed for investigation of role of iatrogenic muscle damage on loading at the adjacent levels.

For the first study, a systematic search was performed in the PubMed database (from 1970 to 2013) using the keywords, “adjacent” and “lumbar” in combination with each of the keywords: “range(s) of motion”, “kinematic”, “kinematics”, “instability”, “mobility”, “hypermobility”, or “angulation”. The search was limited to English literature. The title, abstract, and if necessary the full text of the identified articles were reviewed to select those studies that had investigated the range of motion of the segment adjacent to any types of spinal implants. Only those studies that had investigated absolute values for range of motion were considered and the studies reporting on relative values for range of motion were excluded.

For the second study, a musculoskeletal model of the lumbar spine was made using ArtiSynth software package. The geometrical model for the bones and muscles were taken from the study by Christophy *et al.* [1]. Instead of precisely modeling each of the ligaments, intervertebral discs, and ligaments, the functional spinal unit was modeled as a general spring with stiffness along each of the six degrees of freedom. Therefore the spring forces and moments represented the forces and moments at each intervertebral level and therefore, their distribution between anterior and posterior elements could not be calculated. Hill-type muscle model was used for modeling the muscles, and iatrogenic muscle damage was modeled by detaching those muscles that are resected from posterior elements of operated levels during the surgery. Although the model was developed for dynamic analysis, since the solution method for estimation of muscle forces was based on patients’ gait data as the input to the model and such data was not available, only static conditions were considered for all analyses. The results of the current study are not anticipated to

be used for determining what surgical treatments or approaches to be used, rather to shed light on factors that can affect the loading at the adjacent level.

Chapter 2 Do *in vivo* Kinematic Studies Provide Insight into Adjacent Segment Degeneration? – A Qualitative Systematic Literature Review

2.1 Introduction

Degeneration of the mobile intervertebral levels adjacent to a spinal fusion is a clinically common occurrence that does not consistently lead to symptoms or the need for further surgical treatment. While numerous clinical studies have identified a variety of risk factors associated with adjacent segment degeneration (ASD), the actual risk factors and pathogenesis remains unclear [75][49]. While some consider ASD to be a manifestation of the normal process of spinal degeneration [72][70], others believe it is accelerated by altered biomechanics at the levels immediately adjacent to the fusion level [49][51][74].

Adjacent segment degeneration may be manifest as either osteophytes and disc collapse that may diminish motion or as listhesis, which may increase intersegmental spinal mobility. Either of these two patterns of ASD may lead to clinical symptoms and neural element compression. The degree to which altered biomechanics at these adjacent segments contributes to the development of either of these patterns of ASD is not clearly understood.

Many *in vitro* studies have been performed in human cadaveric specimens to help identify a potential biomechanical explanation of ASD. These studies reported many changes at the adjacent levels, including increased range of motion [154][155][156][157], abnormal facet joint loading [156], and increased intradiscal pressure [157][158]. The detection of hypermobility in these *in vitro* studies is absolutely dependent on the experimental testing protocol [75]. Displacement-controlled protocols are based on the assumption that, post-operatively, patients replicate the same preoperative total range of motion (ROM). Load-controlled protocols assume

that patients will yield to postoperative activity restrictions and apply the same loads to their spine as pre-operatively [159]. Whether clinically observed scenarios represent the first or second of these experimental approaches or an intricate and dynamic blend of the two remains unknown. Moreover, while the posture of the spine and its movement are controlled by muscles attached to and between each individual vertebra, the majority of experimental studies only apply loading to the uppermost level of the spine. These and the limitations of *in vitro* experimental studies, which are reviewed thoroughly in the review article by Volkheimer *et al.* [159], necessitates a review of the reported *in vivo* changes after spinal surgery.

To shed light on the degree to which biomechanical mobility changes at the adjacent intervertebral level occur in patients, a series of biomechanical measurements have been made in clinical studies. The vast majority of these measurements are kinematic, i.e. relate to intervertebral motion. The purpose of this review article is to summarize and critically analyze the results from these clinical studies examining the kinematics of the adjacent segment and of the entire lumbar spine. The review includes studies of vertebral fusion and those with total disc replacement and various dynamic stabilization devices, in the lumbar spine.

2.2 Methodology

A comprehensive search of the PubMed database was conducted using the keywords “adjacent” and “lumbar” in combination with one of the following keywords: “range(s) of motion”, “kinematic”, “kinematics”, “instability”, “mobility”, “hypermobility”, or “angulation”. The search was limited to the English literature and performed from 1970 to 2013 and generated 697 articles. Each title and abstract and, when necessary, the full text were reviewed to select the studies that addressed the ROM of the segment adjacent to spinal implants or non-instrumented fusion in the lumbar spine of living human subjects. Thirty-five articles met the inclusion criteria. An additional four studies were found following a manual search of the references cited in these chosen articles. Subject matter experts were consulted to determine if additional articles existed. This search yielded a total of 39 articles for review. The included studies were divided into three surgical procedure groups: fusion (with or without instrumentation), total disc replacement (TDR), and dynamic stabilization. A summary of the articles is presented in Table 2-1, Table 2-2, and Table 2-3.

Kinematic Terminology

There are many kinematic parameters that may be used to describe the relative movements between vertebrae. These include range of motion (ROM), neutral zone (NZ), and instantaneous axis of rotation (IAR); precise definitions of these parameters can be found elsewhere [8]. In this review, the focus is on ROM, as that parameter has been reported most reliably in studies of *in vivo* kinematics.

ROM is defined as “the difference between the two points of physiologic extent of movement”[8] and it can be reported for either angular or translational motion. Clinical studies

investigating ROM mostly refer to angular changes between vertebrae or/and antero-posterior vertebral translation which in some cases is referred to as olisthesis: anterolisthesis or retrolisthesis.

There exist many definitions of spinal instability and it is often linked to certain kinematic parameters. For this review, instability in the clinical realm means excessive ROM beyond a pre-determined threshold, which for sagittal plane motion ranges between 3-4.5 mm for translation [160][161] and 8-15 degrees for angular change[160][57].

Kinematic Measuring Methods

The position of the vertebrae and the resultant kinematics of the spine in human subjects is typically recorded using skin-mounted markers or with medical imaging. The imaging techniques include standard planar radiography, biplanar stereophotogrammetry, videofluoroscopy, and less frequently computed tomography and magnetic resonance imaging (MRI).

The use of markers attached to the skin is the safest way for tracking the spine motion since ionizing radiation is not required. However, there are some well-recognized experimental limitations, including the relative movement between the markers and the skin and the absence of direct correlation between the skin motion and that of the underlying vertebral column. Therefore, the true kinematics of the vertebrae cannot be accurately defined by this method [162].

For this reason, most clinical researchers use radiography or x-ray techniques to examine ROM, as these more clearly delineate the borders and this motion of the vertebrae. The kinematics can

be recorded in three-dimensions using biplanar radiography in a technique called stereophotogrammetry which requires the insertion of small tantalum beads in the vertebrae but provides high kinematic accuracy of less than 0.02 mm [162]. Another approach is to use videofluoroscopy where continuous patterns of vertebral motion in two or three dimensions can be captured. Clearly, for all of these investigations there exists a trade-off between the duration of patients' activity (i.e. time of radiation exposure) and level of kinematic accuracy (i.e. intensity of radiation). Computed tomography has also been used to measure vertebral kinematics as a research tool [163][164]. The excellent visualization of the vertebrae in three dimensions is its main advantage, but the limited ability for subjects to move within the scanner and the high radiation dose are major limitations.

MRI has also been used as an alternative to the radiographic methods with the main advantage of no radiation exposure. However, the imaging time is much longer [48] and bone is more difficult to distinguish in MRI, which makes it less suitable for tracking motion in dynamic activities.

Among the 39 articles included for review, two articles studied dynamic motion of the spine through videofluoroscopy, three studies used MRI, and three studies performed static radiostereometric analysis (RSA). The remaining 31 studies used static radiographs.

Kinematic Study Designs

There are several types of study designs included in the literature where kinematics of the adjacent level and the entire lumbar spine were reported. These include the Case Control design, in which the post-operative kinematics is compared to a non-operative control group. Several different control groups have been used in the literature, including non-fusion back pain patients [165], patients with conservative treatment for back pain [71], asymptomatic volunteers

[166][44], and normal values from the literature [71][167]. Another study design is a Longitudinal Case Series where the post-operative kinematics was compared to the same patients before the fusion procedure. Randomized Controlled Trials (RCT) provide the highest level of evidence and are more commonly used to evaluate the effect of a treatment by randomly selecting the eligible participants for either the treatment group or the control group and comparing the outcomes. These different study designs, where appropriate, are recorded in the summary tables presented.

A fourth study design for reporting kinematic differences post-surgery is a cross sectional radiographic analysis whereby the authors defined a magnitude of motion that they deemed to reflect an unstable vertebral level. They then compared the number of patients with adjacent segment motion above this certain magnitude, thereby providing an indication of substantial kinematic changes post-surgery.

The vast majority of the reviewed studies reported two-dimensional motion and most of that was in the sagittal plane (i.e. flexion-extension). In our analysis, we included any studies that reported absolute kinematic data in any direction. Some studies on this subject reported relative kinematic changes and we believe this approach does not adequately reflect the actual changes that occur at a particular vertebral level and thus we did not include these data in this review. This topic is included in the Discussion section.

Within these studies, there exists a wide range of potentially important parameters such as age of the patients, initial diagnosis, type of surgery, and length of fixation that could influence the kinematic findings at the adjacent segment. However, there do not exist sufficient numbers of

subjects to tease out the effects of these parameters. They are included in the tabulated results, however.

2.3 Results

Fusion

Twenty-nine articles were identified in the fusion group; with seventeen studying only fusion while twelve included comparisons with either total disc replacement (TDR) or a dynamic implant (see Tables 1, 2, and 3).

For the segment immediately rostral to the fusion, twelve studies observed no changes in the average flexion-extension ROM, nine studies found an increase (or larger value), and three studies noted a significant decrease (see Table 2-4). None of the studies that examined the second, third or fourth rostral segments reported any significant increase in flexion-extension ROM [167][168][169].

For the first segment immediately caudal to the fusion, seven studies reported no change in flexion-extension ROM and three studies observed a decrease (see Table 2-1 and Table 2-4).

Among the studies that looked at ROM of the entire lumbar spine, one study saw no change [170], and five reported a decrease after fusion [165][166][168][171][172].

For lateral bending, three studies investigated the adjacent segment ROM [162][48][173], but only one of them found a significant change, which was a reduction in ROM [48]. Axial rotation ROM was reported in one study [162], but no comparison to the preoperative ROM was made.

Table 2-1: Summary of the clinical articles addressing kinematics of the segments adjacent to a spinal fusion

Author	Study Type	Study Design	No. of Patients	Diagnosis	Type of Surgery	Age (year)	Length of FU (month)	Length of Fixation		Index Levels	Imaging Method	Absolute values for sagittal ROM*		
								single-level	multi-level			Total Lumbar	Rostral AS	Caudal AS
Frymoyer <i>et al.</i> 1979 [165]	Retro	Case control (control group: nonfusion)	132	Residual back pain, nerve root symptoms and functional impairment	96 Fusion (disc excision + posterior midline fusion)	38	164	9	87	9 L5-S1, 81 L4-S1, 6 L3-S1	Biplanar orthogonal radiographs Flexion-Extension (without pelvic restraint)	Smaller	Larger	Not applicable
					36 Nonfusion (laminectomy + disc excision)	42	-	-	Not specified					
Luk <i>et al.</i> 1995 [166]	Retro	Case control (control group: asymptomatic volunteers)	52	Degenerative disc disease	52 ALIF	37	> 60	32	20	32 L4-L5 20 L4-S1	Radiographs Flexion-Extension (with patients lying on one side and wrapping their arms around their knees to assist flexion)	Smaller	Smaller (single-level)	Smaller
					30 asymptomatic volunteers									No change (multi-level)
Seitsalo <i>et al.</i> 1997 [71]	Retro	Case control (control groups: patients with conservative treatment; normal data from literature)	227	Symptomatic isthmic spondylolisthesis at L5	145 Fusion (87 posterior fusion, 55 posterolateral fusion, 3 anterior fusion) 82 conservative treatment	14 (8-19)	185 (60-360)	48	97	48 L5-S1 84 L4-S1 13 L3-S1	Radiographs Flexion-Extension (standing)	NI	No difference	Not applicable
Leferink <i>et al.</i> 2002 [167]	Pro	Case control (control group: normal data from literature)	82	Fracture of thoracolumbar spine	Fusion (with either Dick internal fixator or Universal Spine System; both were taken out after 9 months)	39	24	82	-	18 T12 42 L1 17 L2 5 L3	Radiographs Flexion-Extension (standing)	NI	Smaller	Smaller
kamioka & Yamamoto 1990 [168]	Retro	Case series	26	Spondylolytic or degenerative spondylolisthesis	Fusion (laminectomy + fusion + trapezoid shape plate and screws)	49 (12-67)	29 (7-56)	26	-	4 L3-L4, 17 L4-L5, 5 L5-S1	Radiographs Flexion-Extension	Decreased	Increased (lumbosacral fusion)	Mixed (floating fusion)
Axelsson <i>et al.</i> 1997 [174]	Pro	Case series	6	Back pain + spondylolysis-olsthesis Grade 1-2	Posterolateral fusion without fixation	37 (28-46)	12	6	-	L5-S1	RSA Supine-Sitting	NI	No change	Not applicable
Chou <i>et al.</i> 2002 [171]	Retro	Case series	32	degenerative spondylolisthesis or spinal stenosis	Fusion (posterior decompression + posterolateral fusion + Isola rods or VSP plates)	71 (61-83)	56 (48-66)	18	14	18 L4-L5 8 L3-L5 6 L2-L5	Radiographs Flexion-Extension	Decreased	No change	Decreased
Axelsson <i>et al.</i> 2007 [50]	Pro	Case series	9	painful degenerative disc disease at L4-L5 or/and L5-S1	6 Posterolateral fusion (3 with and 3 without fixation), 3 ALIF with threaded cages	45 (35-59)	60	6	3	2 L4-L5, 4 L5-S1 3 L4-S1	RSA Supine-Sitting	NI	No change	NI

Table 2-1: Summary of the clinical articles addressing kinematics of the segments adjacent to a spinal fusion (continued).

Author	Study Type	Study Design	No. of Patients	Diagnosis	Type of Surgery	Age (year)	Length of FU (month)	Length of Fixation			Imaging Method	Absolute values for sagittal ROM*		
								single-level	multi-level	Index Levels		Total Lumbar	Rostral AS	Caudal AS
Kim <i>et al.</i> 2009 [175]	Retro	Case series	28	Degenerative disc disease or Spondylolisthesis	14 Instrumented posterolateral fusion	45 (21-57)	24	28	-	L4-L5	Radiographs Flexion-Extension (Standing)	NI	Increased	No change
					14 Anterior fusion without instrumentation	43 (22-57)						NI	No change	No change
Ogawa <i>et al.</i> 2009 [176]	Pro	Case series	54	spinal canal stenosis + lumbar spine instability	27 Instrumented posterolateral fusion + conventional sublaminar stabilization at cephalad end site of fusion	67 (34-80)	40 (29-55)	-	54	Not specified	Radiographs Flexion-Extension	NI	Decreased	NI
					27 Instrumented posterolateral fusion without wiring							NI	Increased	NI
Kaito <i>et al.</i> 2010 [74]	Retro	Case series	85	L4 spondylolisthesis	Instrumented PLIF	64 (36-83)	39 (24-84)	85	-	L4-L5	Radiographs Flexion-Extension	NI	No change	NI
Aota <i>et al.</i> 1995 [57]	Retro	Cross sectional (checking for instability)	65	spinal canal stenosis, instability, disc herniation	laminectomy + lateral fusion + fixation	56 (36-78)	39 (24-65)	44	21	34 L4-L5, 10 L5-S1, 8 L3-L5, 9 L4-S1, 4 L3-S1	Radiographs Flexion-Extension (lateral decubitus position)	NI	NI	NI
Wimmer <i>et al.</i> 1997 [177]	Retro	Cross sectional (checking for instability)	120	painful spondylolisthesis (95 isthmic, 4 dysplastic, 21 degenerative)	combined anterior and posterior fusion + fixation (pedicle screws or laminar hooks)	40 (9-65)	36 (26-84)	46	74	11 L4-L5, 35 L5-S1, 45 L4-S1, 6 L3-L5, 18 L3-S1, 2 L2-L5, 3 L2-S1	Radiographs Flexion-Extension	NI	NI	NI
Nakai <i>et al.</i> 1999 [160]	Retro	Cross sectional (checking for instability)	48	degenerative spondylolisthesis, lumbar intervertebral disk herniation	PLIF	49 (22-73)	103 (60-180)	45	3	3 L3-L4, 37 L4-L5, 5 L5-S1, 2 L3-L5, 1 L4-S1	Radiographs Flexion-Extension (standing)	NI	NI	NI
Lai <i>et al.</i> 2004a [178]	Retro	Cross sectional (checking for instability)	60	degenerative or spondylolytic spondylolisthesis	Laminectomy + posterolateral fusion + instrumentation	60 (36-77)	72	60	-	5 L3-L4, 46 L4-L5, 9 L5-S1	Radiographs Flexion-Extension	NI	NI	NI
Lai <i>et al.</i> 2004b [179]	Retro	Cross sectional (checking for instability)	101	degenerative or spondylolytic spondylolisthesis	Laminectomy + posterolateral fusion + instrumentation	61 (36-78)	(72-84)	60	41	5 L3-L4, 46 L4-L5, 9 L5-S1, 16 L3-L5, 25 L4-S1	Radiographs Flexion-Extension	NI	NI	NI

Table 2-1: Summary of the clinical articles addressing kinematics of the segments adjacent to a spinal fusion (continued).

Author	Study Type	Study Design	No. of Patients	Diagnosis	Type of Surgery	Age (year)	Length of FU (month)	Length of Fixation			Imaging Method	Absolute values for sagittal ROM*		
								single-level	multi-level	Index Levels		Total Lumbar	Rostral AS	Caudal AS
Anderst <i>et al.</i> 2008 [162]	Pro	Case series	5	Not specified	4 Instrumented posterior fusion, 1 Anterior fusion with interbody cage	44	6	4	1	2 L5-S1, 2 L4-L5 1 L4-S1	Dynamic RSA Flexion-Extension, Lateral Bending, and Axial Rotation. (sitting)	NI	NI	NI

Abbreviations: ALIF, anterior lumbar interbody fusion; AS: adjacent segment, FU, follow-up; NI, not investigated; PLIF, posterior lumbar interbody fusion; Pro: prospective; RCT, randomized controlled trial; Retro: retrospective.

* Absolute values for ROM are considered as either "increased", "no change", or "decreased", if the comparison is made between pre- and postoperative values. If the postoperative ROM is contrasted versus a control group, the words "larger", "no difference", or "smaller" are used. The status is "NI" (not investigated) for studies that did not calculate or compare those values.

Table 2-2: Summary of the clinical articles addressing kinematics of the segments adjacent to a TDR

Author	Study Type	Study Design	No. of Patients	Diagnosis	Type of Surgery	Age (year)	Length of FU (month)	Length of Fixation			Imaging Method	Absolute values for sagittal ROM*		
								single-level	multi-level	Index Levels		TL	Rostral AS	Caudal AS
Auerbach <i>et al.</i> 2007 [44]	Pro	Case control (control group: asymptomatic volunteers)	13	Degenerative disc disease	8 ProDisc-L	45	(6-14)	5	3	5 L4-L5 or L5-S1, 3 L4-S1	Videofluoroscopy (standing)	NI	Mixed	NI
					5 Circumferential fusion	36		3	2	3 L4-L5 or L5-S1, 2 L4-S1		NI	Increased	NI
					4 asymptomatic Volunteers	25		-	-	-				
Delamarter <i>et al.</i> 2003 [169]	Pro	RCT	53	Degenerative disc disease	35 ProDisc-II	40	6	19	16	9 L4-L5, 10 L5-S1, 1 L3-L5, 14 L4-S1	Radiographs Flexion-Extension	NI	No change	NI
					18 Circumferential fusion	42 (26-59)		8	10	1 L3-L4, 4 L4-L5, 3 L5-S1, 10 L4-S1		NI	No change	NI
Cunningham <i>et al.</i> 2008 [180]	Pro	RCT	93	Symptomatic degenerative disc disease	61 CHARITE	40	24	61	-	L4-L5	Radiographs Flexion-Extension	NI	No change	No change
					31 ALIF with BAK threaded cages	40		32	-			NI	No change	No change
Guyer <i>et al.</i> 2009 [181]	Pro	RCT	133	Degenerative disc disease	90 CHARITE	40	60	90	-	26 L4-L5, 64 L5-S1	Radiographs Flexion-Extension	NI	No change	No change
					43 ALIF with BAK threaded cages	39 (25-55)	60	43	-	10 L4-L5, 33 L5-S1		NI	No change	No change
Auerbach <i>et al.</i> 2009 [170]	Pro	RCT	200	Degenerative disc disease	155 ProDisc-L	39	24	155	-	51 L4-L5, 104 L5-S1	Radiographs Flexion-Extension	Mixed	NI	NI
					45 Circumferential fusion	40		45	-	15 L4-L5, 30 L5-S1		No change	NI	NI
Berg <i>et al.</i> 2011 [182]	Pro	RCT	152	Symptomatic degenerative disc disease	80 ProDisc, CHARITE, or Maverick	40	24	Not specified	Not specified	Not specified	Radiographs (DCRA) Flexion-Extension (lying down)	NI	Mixed	No change
					72 Fusion (44 Posterolateral fusion and 28 PLIF)							NI	Increased	No change
Zigler <i>et al.</i> 2012 [161]	Pro	RCT	166	Degenerative disc disease	123 ProDisc-L	38	60	123	-	3 L3-L4, 45 L4-L5, 75 L5-S1	Radiographs Flexion-Extension	NI	No change	Increased
					43 Circumferential fusion	41		43	-	1 L3-L4, 12 L4-L5, 30 L5-S1		NI	No change	No change

Table 2-2: Summary of the clinical articles addressing kinematics of the segments adjacent to a TDR (continued).

Abbreviations: ALIF, anterior lumbar interbody fusion; AS: adjacent segment, FU, follow-up; NI, not investigated; PLIF, posterior lumbar interbody fusion; Pro: prospective; RCT, randomized controlled trial; Retro: retrospective.
* Absolute values for ROM are considered as either “increased”, “no change”, or “decreased”, if the comparison is made between pre- and postoperative values. If the postoperative ROM is contrasted versus a control group, the words “larger”, “no difference”, or “smaller” are used. The status is “NI” (not investigated), for studies that did not calculate or compare those values.

Table 2-3: Summary of the clinical articles addressing kinematics of the segments adjacent to a dynamic implant															
Author	Study Type	Study Design	No. of Patients	Diagnosis	Type of Surgery	Age (year)	Length of FU (month)	Length of Fixation			Index Levels	Imaging Method	Absolute values for sagittal ROM*		
								single-level	multi-level				TL	Rostral AS	Caudal AS
Beastall <i>et al.</i> , 2007 [48]	Pro	Case series	24	Dominant low back pain	Dynesys (with/without nerve root decompression)	44 (25-59)	9	8	16	Mixed	MRI Flexion-Extension (sitting) Lateral flexion (standing)	Decreased	No change	No change	
Lee <i>et al.</i> , 2008 [183]	Pro	Case series	19	Spinal stenosis with degenerative spondylolisthesis, ASD after fusion, disc herniation	Dynesys (decompression)	61 (46-70)	27 (16-35)	9	10	Mixed	Radiographs Flexion-Extension (standing)	No change	No change	No change	
Hu <i>et al.</i> , 2011 [173]	Retro	Case series	32	Lumbar intervertebral disc protrusion, degenerative stenosis, degenerative isthmic spondylolisthesis	Dynesys (posterior laminectomy)	58 (43-78)	16 (6-23)	23	9	1 L2-L3, 2 L3-L4, 12 L4-L5, 8 L5-S1 2 L2-L4, 3 L3-L5, 4 L4-S1	Radiographs Flexion-Extension + Lateral bending (standing)	NI	No change	No change	
Kim <i>et al.</i> , 2011 [52]	Retro	Case series	21	Degenerative spinal stenosis + spondylolisthesis grade I and/or dynamic instability	Dynesys (decompression)	61	29 (4-50)	7	14	Mixed	Radiographs Flexion-Extension	No change	Increased	No change	
Cakir <i>et al.</i> , 2009 [172]	Retro	Case series	26	Back pain+claudication due to degenerative instability+spinal stenosis	11 Dynesys (decompression)	57	37 (24-56)	11	-	L4-L5	Radiographs Flexion-Extension	No change	No change	No change	
					15 Fusion (decompression + fusion + fixation)	58	45 (30-72)	15	-		Decreased	No change	No change		
Yu <i>et al.</i> , 2012 [184]	Pro	RCT	53	Spinal stenosis + severe instability	27 Dynesys	52	36	27	-	L4-L5	Radiographs Flexion-Extension	NI	NI	NI	
					26 Instrumented PLIF	56		26	-		NI	NI	NI		
Champain <i>et al.</i> , 2007 [185]	Retro	Case control (Control group: asymptomatic volunteers)	49	Back pain+ disc herniation	Twinflex (discectomy + posterolateral lumbosacral fusion + Twinflex)	47 (29-73)	60 (24-120)	11	38	12 L3-S1, 26 L4-s1, 11 L5-S1	Radiographs Flexion-Extension	NI	Mixed	Mixed	

Table 2-3: Summary of the clinical articles addressing kinematics of the segments adjacent to a dynamic implant (continued).

Author	Study Type	Study Design	No. of Patients	Diagnosis	Type of Surgery	Age (year)	Length of FU (month)	Length of Fixation			Index Levels	Imaging Method	Absolute values for sagittal ROM*		
								single-level	multi-level				TL	Rostral AS	Caudal AS
Park <i>et al.</i> 2009 [186]	Retro	Case series	27	Chronic degenerative herniated lumbar disc +stenosis, flexion instability, degenerative/spondylolytic spondylolisthesis	Bioflex (decompressive laminectomy with/without discectomy + bioflex without fusion)	59 (47-80)	12	3	24	Not specified	Radiographs Flexion-Extension	Decreased	No change	No change	
Siddiqui <i>et al.</i> , 2006 [187]	Pro	Case series	26	Lumbar Spinal Stenosis + neurogenic intermittent claudication	X-Stop	71 (57-93)	6	15	11	1 L2-L3, 3 L3-L4, 11 L4-L5, 10 L3-L5, 1 L4-S1	MRI Flexion-Extension (supine, sitting, standing)	No change	No change	No change	
Nandakumar <i>et al.</i> 2010 [188]	Pro	Case series	38	Symptomatic spinal Stenosis	X-Stop	>50	24	22	16 (double-level)	not mentioned	MRI Flexion-Extension (sitting)	No change	single-level: Increased	No change	
JIA & SUN 2012 [189]	Retro	Case series	19	Lumbar degenerative disease	Wallis (decompression)	61 (46-70)	27 (16-35)	Not specified	Not specified	Not specified	Radiographs Flexion-Extension	No change	No change	No change	
Ha <i>et al.</i> 2013 [190]	Pro	Case series	31	Degenerative lumbar stenosis + neurogenic claudication + pain	DIAM (decompressive laminotomy)	63 (46-72)	31 (24-56)	31	-	1 L2-L3, 4 L3-L4, 26 L4-L5	Radiographs Flexion-Extension (standing)	NI	No change	No change	
Kong <i>et al.</i> 2007 [191]	Retro	Case series	42	Degenerative Spinal Stenosis with segmental instability	18 Coflex (decompression with laminotomy)	62 (40-71)	12	18	-	L4-L5	Radiographs Flexion-Extension	NI	No change	No change	
					24 PLIF	56 (38-78)	12	24	-		NI	Increased	No change		
LIU <i>et al.</i> 2012 [192]	Retro	Case series	67	Lumbar intervertebral disc herniation or spinal stenosis	25 PLIF + Wallis or Coflex (discectomy + interbody fusion + fixation + Wallis or Coflex)	45 (21-64)	24 (12-40)	25	-	L5-S1	Radiographs Flexion-Extension	NI	Mixed	Not applicable	
					42 PLIF (discectomy + interbody fusion + fixation)	42 (15-76)	23 (12-38)	42	-		NI	Increased	Not applicable		

Table 2-3: Summary of the clinical articles addressing kinematics of the segments adjacent to a dynamic implant (continued).

Author	Study Type	Study Design	No. of Patients	Diagnosis	Type of Surgery	Age (year)	Length of FU (month)	Length of Fixation			Index Levels	Imaging Method	Absolute values for sagittal ROM*		
								single-level	multi-level				TL	Rostral AS	Caudal AS
Korovessis et al. 2009 [51]	Pro	RCT	45	Symptomatic spinal stenosis or spondylolisthesis	24 Fusion + Wallis (decompression + posterior rigid fixation + fusion + Wallis)	65 (32-72)	54	-	45	not specified	Radiographs Flexion-Extension (sitting)	NI	No change	NI	
					21 Fusion (decompression + posterior rigid fixation + fusion)	64 (33-71)					NI	Increased	NI		

Abbreviations: ALIF, anterior lumbar interbody fusion; AS: adjacent segment, FU, follow-up; NI, not investigated; PLIF, posterior lumbar interbody fusion; Pro: prospective; RCT, randomized controlled trial; Retro: retrospective.
 * Absolute values for ROM are considered as either “increased”, “no change”, or “decreased”, if the comparison is made between pre- and postoperative values. If the postoperative ROM is contrasted versus a control group, the words “larger”, “no difference”, or “smaller” are used. The status is “NI” (not investigated), for studies that did not calculate or compare those values.

Table 2-4: How do the absolute values for sagittal ROM change after a spinal fusion?									
	Total Lumbar Spine			Rostral AS			Caudal AS		
	Increase	No Change	Decrease	Increase	No Change	Decrease	Increase	No Change	Decrease
RCT	Auerbach 2009			Korovessis 2009 Berg 2011	Delamarter 2003 Cunningham 2008 Guyer 2009 Zigler 2012		Cunningham 2008 Guyer 2009 Berg 2011 Zigler 2012		
CS			Kamioka 1990 Chou 2002 Cakir 2009	Kamioka 1990 Kong 2007 Ogawa 2009 Kim 2009 LIU 2012	Axelsson 1997 Chou 2002 Axelsson 2007 Kim 2009 Cakir 2009 Kaito 2010		Kong 2007 Kim 2009 Cakir 2009		Chou 2002
CC			Frymoyer 1979 Luk 1995	Frymoyer 1979 Auerbach 2007	Luk 1995 Seitsalo 1997	Luk 1995 Leferink 2002			Luk 1995 Leferink 2002
Abbreviations: RCT: randomized controlled trial; CS: case series; CC: case control									

Table 2-5: How do the absolute values for sagittal ROM change after a TDR?									
	Total Lumbar Spine			Rostral AS			Caudal AS		
	Increase	No Change	Decrease	Increase	No Change	Decrease	Increase	No Change	Decrease
	Auerbach 2009	Auerbach 2009		Auerbach 2007 Berg 2011	Delamarter 2003 Auerbach 2007 Cunningham 2008 Guyer 2009 Berg 2011 Zigler 2012		Zigler 2012	Cunningham 2008 Guyer 2009 Berg 2011	

Table 2-6: How do the absolute values for sagittal ROM change after a dynamic implant?

	Total Lumbar Spine			Rostral AS			Caudal AS		
	Increase	No Change	Decrease	Increase	No Change	Decrease	Increase	No Change	Decrease
PSDS		Lee 2008 Kim 2011 Cakir 2009	Beastall 2007 Park 2009	Kim 2011	Beastall 2007 Lee 2008 Cakir 2009 Park 2009 Hu 2011			Beastall 2007 Lee 2008 Cakir 2009 Park 2009 Hu 2011 Kim 2011	
ISDD		Siddiqui 2006 Nandakumar 2010 JIA and SUN 2012		Nandakumar 2010	Siddiqui 2006 Kong 2007 Korovessis 2009 Nandakumar 2010 JIA and SUN 2012 LIU 2012 Ha 2013	LIU 2012		Siddiqui 2006 Kong 2007 Nandakumar 2010 JIA and SUN 2012 Ha 2013	
Abbreviations: ISDD: interspinous distraction devices; PSDS: pedicle-screw-based dynamic stabilizers.									

Table 2-7: Incidence of instability after a spinal fusion

	Rostral		Caudal	
	Study	Instability incidence	Study	Instability incidence
Translational	Nakai 1999	1/48 = 2%	Nakai 1999	0/48 = 0%
	Zigler 2012	2/43 = 5%	Zigler 2012	0/43 = 0%
	Wimmer 1997	13/120 = 11%		
	Ogawa 2009	4/27 = 15%		
	Chou 2002	6/32 = 19%		
	Seitsalo 1997	32/145 = 22%		
	Auerbach 2007	4/5 = 80%		
Angular	Nakai 1999	0/48 = 0%	Nakai 1999	0/48 = 0%
Mixed	Lai 2004a	10/60 = 17%	Aota 1995	1/61 = 2%
	Lai 2004b	19/101 = 19%	Lai 2004b	3/101 = 3%
	Aota 1995	14/61 = 23%	Yu 2012	1/26 = 4%
	Yu 2012	6/26 = 23%	Lai 2004a	3/60 = 5%
Instability incidence = $\frac{\text{Number of the patients with instability}}{\text{Total number of the patients}}$				

Three studies defined sub-groups of subjects for further analysis. Kaito *et al.* [74] identified three groups: no ASD, radiographic but asymptomatic ASD and symptomatic ASD. They observed that while preoperatively there was no difference between the groups regarding adjacent segment kinematics, postoperatively, both the group with symptomatic ASD and the group with radiographic ASD manifested a significantly larger ROM in comparison to the group with no ASD. Kong *et al.* [191] observed that 33% of the patients experienced an increase of more than five degrees of rotation between preoperative and postoperative ROM at the rostral adjacent segment, 46% showed an increase of less than five degrees and 21% had a decreased ROM. With comparable analyses, similar trends were observed in studies by Kamioka and Yamamoto [168].

Eleven studies investigated the “instability” of the adjacent segment, where “instability” was defined as per our Methodology description above (see Table 2-7). Six of the studies only analyzed translational instability; of the remaining five studies, one study separated the incidence of translational instability from angular instability, but the other four studies analyzed them together. While observed instability at the caudal adjacent segment was rare (between 0-5%), the majority of studies observed that rostral adjacent segment instability occurred more commonly, among 10-30% of the patients.

Total Disc Replacement (TDR)

For TDR, many studies investigated the kinematics of the operated levels [193-203], but only six studies addressed absolute values for the adjacent segment ROM (see Table 2-2). Four of the articles found no change in ROM for the immediately rostral adjacent segment. The results for the other two studies indicated differences that appeared dependent on the anatomical level of the TDR surgery. Berg *et al.* [182] saw no change when the TDR was L5-S1, but did find an

increase when the surgical level was L4-L5. Auerbach *et al.* [44] observed an increase in extension ROM when the index level was L5-S1 and no change when the surgical level was L4-L5 (see Table 2-5).

For the caudal adjacent segment, three studies found no change [182][180][181] and only one study noted an increase in motion [161].

One study reported that if the surgical level was L4-L5, there was an observed increase in range of motion of the entire lumbar spine, however, when L5-S1 was the surgical level, there was no such observed change [170].

No rostral nor caudal adjacent segment instability was observed in the two studies that investigated this parameter [161][44].

Dynamic implants

Fifteen studies reported on kinematic changes following surgery with dynamic implants and these can be divided into two subgroups: eight studies that used pedicle-screw-based systems such as Dynesys, Twinflex, BioFlex, etc., and seven studies that used Interspinous Distraction Devices (ISDD) such as the X-Stop spacer, Coflex, DIAM and Wallis implants. Only two of the 15 studies demonstrated significant increase in the flexion-extension ROM at either the rostral or the caudal adjacent segments. Kim *et al.* [52] reported an increase in ROM at the rostral adjacent segment and Nandakumar *et al.* [188] reported an increase in motion at the caudal segment (see Table 2-6).

Total lumbar ROM decreased in two studies [172][186], and did not change in any of the other studies that investigated this parameter [172][183][187][189][52][188].

Rostral adjacent segment instability was examined in two studies, and found to affect 29% of patients in one study [52], but only 4% in the other [184]. Neither of these two studies noted any instability at the caudal adjacent segment.

2.4 Discussion

The primary objective of this study was to review all of the *in vivo* kinematic data on this topic, to determine the evidence, if any, for kinematic changes adjacent to a spinal fusion, TDR, or a dynamic implant in the lumbar spine. A secondary objective was to examine the nature, magnitude and interrelationship of these kinematic changes.

While the studies included were somewhat heterogeneous and the data available inconsistent, some summary observations can be made. Adjacent to a spinal fusion, the majority of studies do not demonstrate any predictable change in vertebral kinematics. While some studies have reported an increase in the ROM of the immediately rostral segment, no studies report an increase in kinematics caudal to a spinal fusion.

Despite the failure of these studies to observe any predictable change in adjacent segment kinematics, clinical experience is that some patients do experience both asymptomatic and symptomatic increases in intervertebral kinematics adjacent to a spinal fusion, with reported rates ranging from 10-30% [74][191][57][177].

Our review of the literature found fewer reported kinematic changes adjacent to a TDR or a flexible posterior device (see Table 2-4). However more studies and longer follow up periods are required before any firm conclusions can be made.

The overall motion of the entire lumbar spine appears to decrease after a spinal fusion, based on five of the six studies that measured this parameter. This is actually contrary to a fundamental assumption of many *in vitro* studies using displacement-control that presumed that overall spine motion after spinal fusion would be the same as pre-operatively. This includes the popular

Hybrid Method for assessing the adjacent segment as proposed by Panjabi [80]. Obviously, this is an important point for future investigations on this topic.

Challenges and Limitations of Studies

There are clearly many challenges to conducting in-vivo studies of ASD. We outline some of the challenges here and also describe some of the limitations in the existing literature. These include topics such as study design, patient selection, and analysis of kinematic data.

To study the kinematics of ASD, one needs a reasonably accurate method of measuring spinal motion. Three-dimensional dynamic measurement would be ideal but this capability, which has been used previously for various joints [204][205], has been used more recently for the spine [162]. The study by Anderst *et al.* [162] demonstrates the possibility of such measurement in the spine using dynamic RSA, with the main limitation of this technique being the invasiveness of the insertion of tantalum beads before the surgery. Nevertheless, it is an exciting methodology that promises to enhance our future understanding of this problem. Three-dimensional static motion of the spine after fusion has been used to study ASD using the RSA technique and these studies are extremely insightful since they represent highly accurate motion measurements [174][50]. The majority of studies summarized in this review used simple x-ray techniques to report two-dimensional, static kinematics of the spine after fusion. These studies are the lowest accuracy and simply report the relative positions of the vertebrae at their endpoints of motion, but they are a good start to help us understand the problem.

Possibly the most challenging element in measuring spinal kinematics with respect to ASD is obtaining reliable measurements in patients with low back pain by standardizing the techniques used to obtain radiographs. Various protocols were utilized for taking flexion-extension

radiographs. In most of the studies reporting on flexion-extension ROM, patients were asked to naturally flex and extend as much as they could while sitting [51][48][187][188] or standing [160][71][44][190][175]. In some cases patients were assisted by leaning against a table [71], wrapping their arms around their knees [166] or using support bars [48]. Four studies took the images with patients lying supine or prone [182][187][174][50], and in two studies flexion-extension radiographs were taken with patients in the lateral decubitus position [57][166]. However, there were many studies that did not clearly describe or even mention the protocol adopted by patients when measuring kinematics. Since spine posture and type of activity performed during imaging as well as the patient's level of comfort can all affect the range and the pattern of motion, investigators must standardize the techniques for these evaluations particularly when attempts are made to compare between studies. These technical issues may increase the variability in the data and thereby mask real differences if sufficient care is not taken.

Due to high inter-individual variability in spinal segmental alignment and consequently in kinematics, the comparison of post-operative with pre-operative kinematic data is ideal since the statistical comparisons are then done with each subject as their own control. Presence and absence of symptoms during evaluation will confound these measurements. Several studies compared post-operative results against asymptomatic controls or literature norms. However, this is fraught with challenges due to the wide variation between subjects. Both approaches remain feasible, but the former is certainly preferred.

For the analysis of kinematic data, most studies reported the absolute magnitude of segmental ROM. In contrast, some studies reported the relative contribution of that level to overall lumbar spine ROM [170][171][180][206][207]. In the context of understanding ASD, the former method

of comparing absolute motions is clearly optimal since the tissues at that intervertebral joint will be under the same stresses and strains only when the absolute kinematics are the same. The latter method of comparing relative motions is potentially misleading. For example, by comparing the percent contribution of each segment to the total lumbar spine ROM between a fusion and an asymptomatic group, Lin *et al.* [207] reported that a compensatory increased mobility occurred at the adjacent segments above the fusion; whereas, an increase in percent segmental ROM does not mean an increase in absolute values for ROM and thus it does not reflect increased stresses or strains in those tissues. In a study by Cunningham *et al.* [180], the fusion group experienced a significant increase in percentage of segmental ROM at both rostral and caudal levels but the corresponding absolute values did not change, which is due to the decrease in total lumbar ROM. Thus, it is hard to see how such a change in relative ROM could be suggested as a cause of ASD. We prepared a simple example to reflect this situation in Figure 2-1.

The majority of studies combine patients with different lengths and levels of fixation for analysis (see Table 2-1, Table 2-2, and Table 2-3), while there were studies that showed different length of fixation results in different kinematic behaviour of the adjacent segment. Luk *et al.* [166] observed that in comparison with asymptomatic volunteers, patients with single-level fusion had smaller ROM at the rostral level while patients with multi-level fusion showed no difference. In the study by Kim *et al.*[52], excessive translational ROM (more than 4 mm) was observed at the rostral adjacent segment only in the group with multiple levels of fixation. By investigating patients with different length and levels of fusion, Wimmer *et al.* [177] showed that instability correlated with the number of fused segments and that the instability occurred only in those who had lumbosacral fusion.

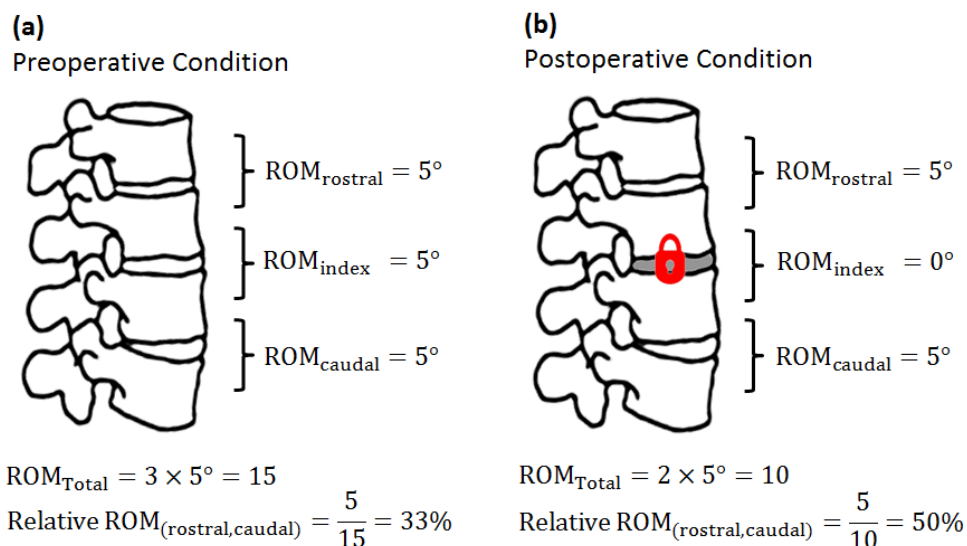


Figure 2-1: Schematic demonstration of the difference between absolute ROM and relative ROM. Assuming a preoperative ROM of five degrees for each segment (a) and considering the ROM to decrease to zero postoperatively only at the operated (index) level (b), then, although the relative ROM (i.e. $\frac{\text{Absolute ROM}}{\text{Total ROM}}$) for each adjacent segment increases from 33% to 50%, absolute ROM at the adjacent segments remains unchanged (5°). Therefore a change in relative ROM does not necessarily represent a change in absolute ROM.

Similarly, the surgical approach may influence the adjacent segment kinematics. Kim *et al.* [175] described two groups; one undergoing interbody fusion from anterior method alone (ALIF), and the other one undergoing instrumented posterolateral fusion. Two years post-surgery, only the group with instrumented posterolateral fusion experienced an increase at the rostral adjacent segment, which may be due to iatrogenic injury of posterior musculature in the posterolateral fusion group. Lai *et al.* [179] noted a significantly lower incidence of adjacent segment instability (6%) in patients whose supra- and interspinous ligaments were preserved by partial laminectomy in comparison with those that underwent total laminectomy (24%). These observations suggest that distinction between patients undergoing different surgery methods may affect the outcomes of the studies that analyzed the patients altogether irrespective of the surgical methods they received [71][177].

Future Considerations

To study the ASD phenomenon from a biomechanical perspective, more accurate measurement of spine motion and adjacent segment kinematics is needed. Accurate kinematic data can serve as inputs to computational models that would enable the calculation of intervertebral loading changes such as disc pressures or facet contact forces at different levels of the spine. Given the high stiffness of the spine, even small errors in kinematic inputs result in large errors in the predicted loads. Moreover, since the motion of the spine is coupled (e.g. between lateral bending and axial rotation [208][209]), capturing the kinematics in 2D may not be sufficient for a precise analysis of spinal biomechanics. Therefore, a movement toward more accurate 3D dynamic tracking of spine motion seems reasonable [162][44].

Chapter 3 Role of Iatrogenic Muscle Damage on Loading at the Level Adjacent to a Lumbar Spine Fusion – A Biomechanical Analysis

3.1 Introduction

The degeneration of the segment adjacent to a lumbar spine fusion is a common complication of fusion surgeries [49]. Prevention of adjacent segment degeneration (ASD) requires an understanding of its etiology. While some believe this phenomenon is natural [70][50][71], many believe ASD is an abnormal accelerated degeneration that has roots in biomechanics [49][51][74][45]. It has been shown in animal studies that increased loading accelerates disc degeneration [76][20][77][78][79]; therefore, any factor that changes normal loading at the adjacent levels may have an influence on development of ASD.

Posterior fusion surgeries are associated with gross damage of spinal muscles [102]. In these surgeries, paraspinal muscles are resected from the posterior elements of the spine to provide exposure to the bony surfaces either for performing laminectomy/facetectomy or placement of the bone grafts [210]. The resected muscles are then sutured and left there to heal, but will not reattach to the vertebrae. Therefore, they will not be able to directly apply any load on the operated segments. Retraction of paraspinal muscles to the side, which is done for keeping the operation area open during the surgery, can also damage the muscles [81][83][84]. Spinal muscle damage after posterior fusion surgeries has been manifest in forms of loss of cross sectional area (CSA) [85], atrophy [86][87], altered muscle activations [88][89], and reduced muscle strength [90][91][81][86]. These consequences of iatrogenic muscle damage can lead to alterations in spinal loading after surgery, especially at the adjacent levels, and may affect or contribute to degeneration of the adjacent segment.

To the author's knowledge, the effect of iatrogenic muscle damage on spinal loading has not been investigated in the literature. Bresnahan *et al.* [102] used the musculoskeletal model developed by de Zee *et al.* [139] and investigated the effect of the reduction of muscle cross sectional areas on muscle recruitment strategy and observed a substantial change in estimated muscle activation pattern. However, they did not report on spinal loading. Also the model that they used for their analysis did not include intervertebral disc stiffness, ligaments, and muscle force-length curves. The purpose of our study is to investigate the effect of iatrogenic muscle damage on spinal loading at the adjacent levels by developing and using a more physiological musculoskeletal model of the lumbar spine.

3.2 Methodology

For developing our model we used ArtiSynth. ArtiSynth is a biomechanical modeling toolkit for physical simulation of anatomical structures. It is an open source toolkit developed at UBC and has the potential of combining and solving multi-body dynamics and FEM in a fast and convenient fashion. The bone and muscle geometries were taken from the study by Christophy *et al.* [1]. Christophy *et al.*'s model incorporates muscle parameters needed for a full Hill-type musculotendon model including the tendon ratios and the pennation angles, and to the best of our knowledge has currently the most physiologically detailed model of the lumbar spinal muscles [152].

3.2.1 Geometrical Model

3.2.1.1 Bone

With their stiff behaviour, bones can be fairly considered as rigid bodies. Since the focus of our study is on the lumbar spine, we are only considering the five lumbar vertebrae to be dynamic; i.e. the thoracic vertebrae and ribcage will be combined as a single rigid body and fixed to L1 vertebra, whereas the sacrum and pelvis are fixed to the ground.

We used the bones from the model developed by Christophy *et al.* [1]. The bony geometries used in their model are those that were digitized from a 170 cm tall male subject and have been used in the generic model developed by Delp *et al.* [211] (the geometry files can be downloaded from OpenSim website²). Christophy *et al.* [1] translated and rotated each vertebra of Delp *et al.*'s model so that the posture and lordosis of their lumbar spine model matched with *in vivo* MRI measurements of Meakin *et al.* [212] and the mean posture of the cadavers used by Cholewicki

² https://simtk.org/project/xml/downloads.xml?group_id=567#package_id1101

et al. [213]. It is noteworthy that the geometric dimensions of the vertebrae compared well with the studies by Gilad and Nissan [214][215] and the study by Panjabi *et al.*[216].

The masses and moments of inertia for each vertebral level (including all surrounding soft tissues and the abdominal organs) were taken from the study by Pearsall *et al.* [217], who used pixel intensity/density relationship to calculate these values from CT images of four adults with average height and weight of 171 cm and 71 kg (Table 3-1). Their study, however, was only on the trunk. We calculated the masses of the head, neck, and upper extremities by multiplying the average mass of the subjects in Pearsall *et al.*'s study by the body mass percentiles reported by Dempster *et al.* [218]. This led to masses of 5.76 kg for the head-neck complex and 6.78 kg for upper extremities. While we modeled the mass of the head-neck complex as a point mass, we distributed the mass of the upper extremities over the volume of the humeri. Both humeri and the weight of the head and neck were fixed to the lumped thorax.

Table 3-1: Masses and mass moments of inertia of the thorax, pelvis and sacrum, and transverse slices of the body at each lumbar vertebral level taken from Pearsall *et al.*'s study [217]

Body parts	Mass (kg)	Body Mass (%)	Moments of Inertia (kg/cm ²)		
			I_{xx}	I_{yy}	I_{zz}
Thorax	13.15	18.5	1250.0	1650.0	1500.0
L1	1.68	2.4	64.0	111.3	175.3
L2	1.69	2.4	59.1	109.1	168.2
L3	1.67	2.3	54.1	106.6	160.8
L4	1.80	2.6	52.0	112.3	164.3
L5	1.82	2.6	54.6	121.9	176.5
Pelvis and Sacrum	7.49	10.7	300	750.0	800.0

3.2.1.2 Functional Spinal Unit (FSU)

Instead of precisely modeling each of the ligaments, facet joints, and the intervertebral disc, one may consider modeling the functional spinal unit as the building block of the lumbar spine. The functional spinal unit (FSU) is defined as “a pair of adjacent vertebrae and the connecting disc and ligaments, but devoid of musculature”[8]. Since the upper vertebra has six degrees of freedom with respect to the lower one, the stiffness of such unit, in the most general case, can be fully described by a 6×6 stiffness matrix. Similarly, a 6×6 damping matrix can be used to represent the viscoelastic behavior of the unit.

Panjabi pioneered this concept for obtaining the stiffness matrix of thoracic spine FSUs [219]. Considering sagittal plane symmetry and infinitesimal rotations, the number of independent terms of the stiffness matrix can be reduced to 12. Gardner-Morse and Stokes obtained these 12 terms for human lumbar spine under 0, 250, and 500 N compressive preloads [220]. They observed that the stiffness along all six degrees of freedom of human spine FSUs increased by increasing the preload. This observation has also been reported in other studies [221][222]. Therefore, we will use the stiffness that they obtained for 500 N preload, as 500N is the closest to *in vivo* spinal loads during upright standing reported in the literature [150].

One crucial consideration in using the stiffness matrix of the study by Gardner-Morse *et al.* [220] (and other similar studies) is that since in their study the load cells for measurement of the forces and moments were located at the centers of the vertebral bodies, in modeling, the mechanical element simulating the FSU stiffness must apply the restoring forces and moments at the same points (i.e. the centers of the vertebral bodies). Otherwise, the estimated forces and moments by the model will be substantially erroneous.

Let us analyze the aforementioned point in more detail. Current multi-body dynamics/musculoskeletal modeling software such as ADAMS, LifeMOD, SIMM, OpenSim, and ArtiSynth use bushing elements for modeling joints with stiffness along all their six DOF [223]. A bushing element consists of two frames (coordinate systems), the distance between origins of which are multiplied by the bushing element stiffness to calculate the restoring forces that will be applied at each frame's origin. Similarly, the angles between the axes of two frames are used for calculation of restoring moments. Therefore, origins and axes of two frames must coincide for the bushing element to be at rest. This means, when modeling the intervertebral joints, origins of the bushing element frames cannot be put at centers of the vertebral bodies, as this will cause an initial preload on both vertebrae. Alternatively, if both frames are put at the middle of the FSU (center of the intervertebral disc), as vertebrae move, moment artifacts will be generated about the centers of vertebral bodies. This is explained in the following example.

As illustrated in Figure 3-1, assume in order to obtain the stiffness of the L3-L4 FSU experimentally, L3 is translated horizontally to an amount δ , while L4 is fixed. Also assume the load cell, which is located at the center of L3, measures the horizontal force to be equal to F and for other forces and moments to be zero. This way the stiffness would be $K = \frac{F}{\delta}$.

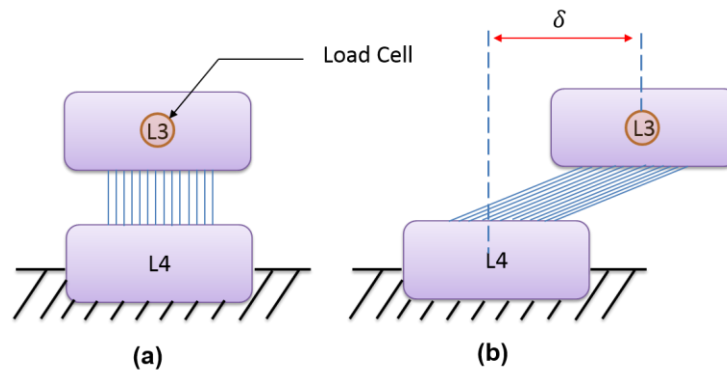


Figure 3-1: Schematic representation of an experiment for obtaining the stiffness of the FSU with the load cell located at the center of the upper segment. Starting from the rest position (a), and deforming the FSU horizontally to an amount δ (b), where the horizontal force is measured to be equal to F and the other forces and moments are zero, the translational stiffness of the FSU is obtained as $K = \frac{F}{\delta}$.

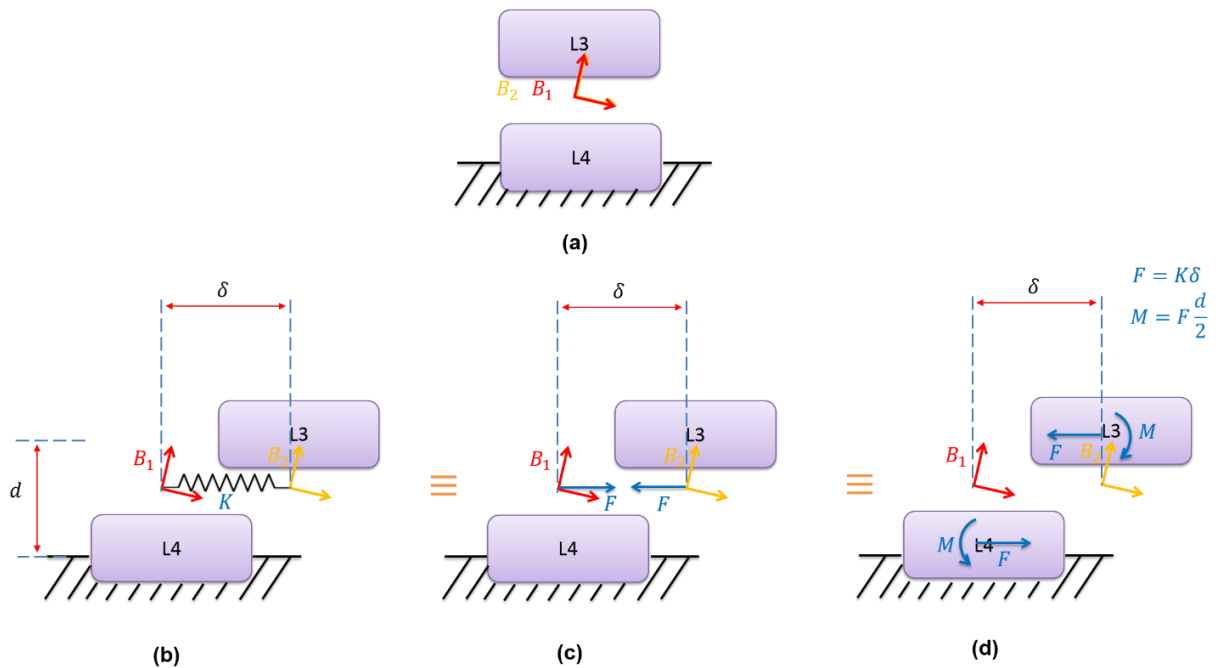


Figure 3-2: Limitation of the bushing element for modeling the FSU. If the FSU is modeled by a bushing element which is initially at rest (a), by displacing the upper segment of the FSU to the amount δ (b), the reaction forces at the origins of the frames (c) create artifact moments of $M = F \frac{d}{2}$ at the centers of the two segments (d), which are not consistent with the moments that the load cell had measured in the experiment illustrated in Figure 3-1 (i.e. $M = 0$).

Now let us simulate this experiment by a bushing element whose two frames are initially coincident in between L3 and L4 (Figure 3-2a). When a translation of δ is applied, the bushing element acts as a spring with stiffness k (Figure 3-2b) whose restoring forces would be applied at origins of $B1$ and $B2$, which are fixed to L3 and L4, respectively (Figure 3-2c). This is equivalent to applying force $F = K\delta$ and moment $M = F \frac{d}{2}$ at centers of the vertebral bodies (Figure 3-2d), which is not consistent with what the load cell had measured in the experiment, i.e. $F = K\delta$ and $M = 0$.

This limitation of bushing elements for modeling FSUs was first noted by Christophy *et al.*[223]. We developed a new type of spring in ArtiSynth, called “OffsetFrameSpring”, which addresses and resolves this limitation (see section A.6).

Although with OffsetFrameSprings a full stiffness matrix can be modeled in ArtiSynth, we decided to only model the diagonal terms, due to lack of experimental data in the literature. We only used the terms corresponding to translational stiffness from Gardner-Morse *et al.*'s study[220], as the rotational displacements for determining the stiffness were very small in their study (1 degree for flexion and 1.5 degrees for lateral bending). For rotational load-displacement relationship we used the data presented in the study by Heuer *et al.* [224]. In their study, Heuer *et al.* [224] applied 1, 2.5, 5, 7.5 and 10 Nm moments on intact FSUs along all directions, i.e. flexion, extension, lateral bending, and axial rotation, and measured the corresponding rotational displacements. By fitting curves to their data assuming the curves pass from the origin, we obtained load-displacement relationships for all rotations, which are presented in Table 3-2. The curves are plotted in Figure 3-4, where for the sake of comparison we have also included flexion moment-rotation relationship of the study by Gardner-Morse *et al.* [220]. Note that all the

equations and loads reported in this document are according to the coordinate system shown in Figure 3-3.

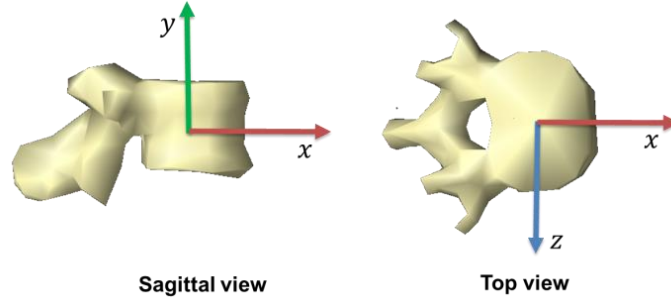


Figure 3-3: The coordinate system used for the results of current study.

Table 3-2: Correlation between the moments and rotations of the FSU. The correlations are obtained by fitting curves to the data of the study by Heuer *et al.* [224].

	Angle (<i>degrees</i>)	Moments (<i>N.m</i>)
Flexion	For $\theta_z < 0$	$\tau_z = (0.0312 \theta_z ^2 - 0.1818 \theta_z + 1.1181)\theta_z$
Extension	For $\theta_z > 0$	$\tau_z = 0.0288 \theta_z^3 + 0.0192 \theta_z^2 + 1.248 \theta_z$
Lateral Bending	For all θ_x	$\tau_x = (0.0081 \theta_x ^2 + 0.1417 \theta_x + 0.4741)\theta_x$
Axial Rotation	For all θ_y	$\tau_y = (0.0291 \theta_y ^2 - 0.0044 \theta_y + 2.5695)\theta_y$

All lumbar FSUs in our spine model are currently using HeuerOffsetFrameSpring, which is an OffsetFrameSpring that for rotations uses the equations of Table 3-2, while for translations uses the following stiffness constants taken from Gardner-Morse *et al.*'s study ($K_{axial} = 2420000$ N/m, $K_{Anterior-Posterior} = 435000$ N/m, and $K_{lateral\ translation} = 523000$ N/m) [220]. We verified the performance of HeuerOffsetFrameSpring by an example that is provided in section A.7.

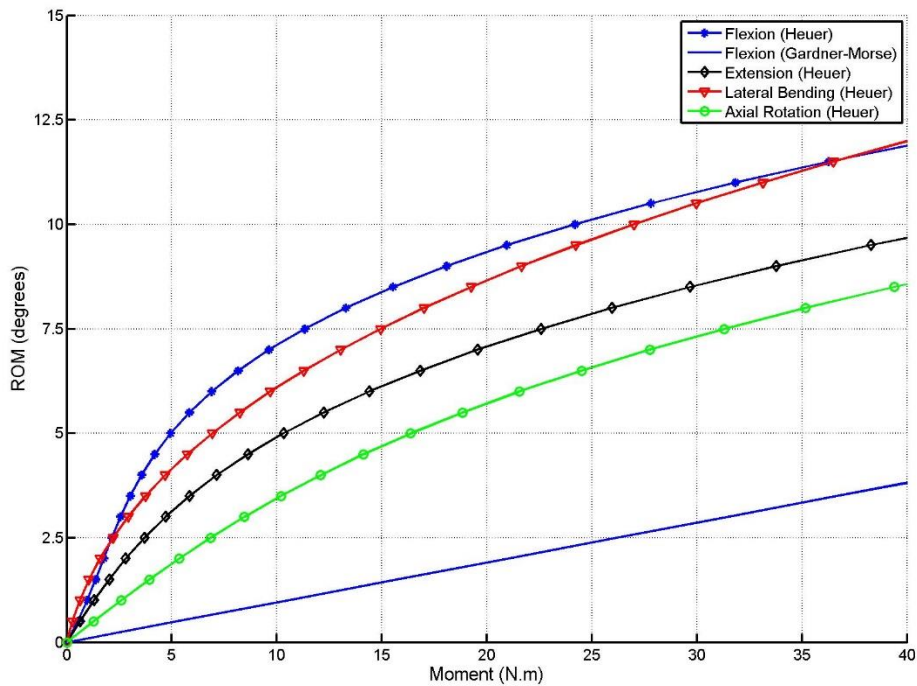


Figure 3-4: Moment-rotation relation for the flexion, extension, lateral bending, and the axial rotation of the FSU. The curves are fitted to the experimental data provided by Heuer *et al.* [224].

3.2.1.3 Muscles

For the scope of the current study, we only focused on modeling the muscle groups that influence the loading at the lumbar spine. These include the erector spinae, multifidus, psoas major, quadratus lumborum, internal oblique, external oblique, and rectus abdominis.

- *Fascicular Anatomy of the Lumbar Spine Musculature*

Although anatomy books provide invaluable qualitative description of muscles, what people in modelling world need is a set of quantitative information of muscles. This includes origin/insertion points of muscles for construction of the geometrical model, in addition to

muscle fiber-length, its physiological cross sectional area (PCSA), its sarcomere length, and the length of the tendon it is attached to for calculation of muscle mechanical properties

For the purpose of determining origin/insertion points, since spinal muscles are wide, fleshy, and connected to multiple points, they need to be quantified in terms of fascicles. Macintosh and Bogduk, who have done extensive studies on spinal muscle architecture, defined the muscle fascicle as “a group of muscle fibres that shared a common, discrete area of attachment on the vertebral column that was discontinuous from other areas of attachment, and which differed from other areas in terms of the vertebra or parts of the vertebra to which it was attached”[225]. With this definition, they studied several cadavers and provided detailed description of mean attachment sites of erector spinae [226][227] and multifidus [228][229], which was later put together by Bogduk *et al.* [104] to build a universal model of the lumbar spine. Our model contains the same fascicles and attachment sites as does their model.

Erector Spinae

According to Bogduk *et al.* [104], lumbar erector spinae consists of four components: iliocostalis lumborum pars thoracis (ILpT), iliocostalis lumborum pars lumborum (ILpL), longissimus thoracis pars thoracis (LTpT), and longissimus thoracis pars lumborum (LTpL).

Eight fascicles comprise ILpT that originate from ribs and serially insert on the iliac crest (Figure 3-5c). Four fascicles represent ILpL, which arise from the tips of the transverse processes of the L1 to L4 vertebrae and insert into the iliac crest (Figure 3-5b). LTpL consists of five fascicles that arise from the medial site of the transverse process of each lumbar vertebra and insert into the posterior superior end of the iliac crest (Figure 3-6b). For LTpT, while approximately half of the fascicles arise from the transverse processes of thoracic vertebrae, the

rest originate from lower ribs and all insert into either the lumbar spinous processes or sacrum and ilium (Figure 3-6c).

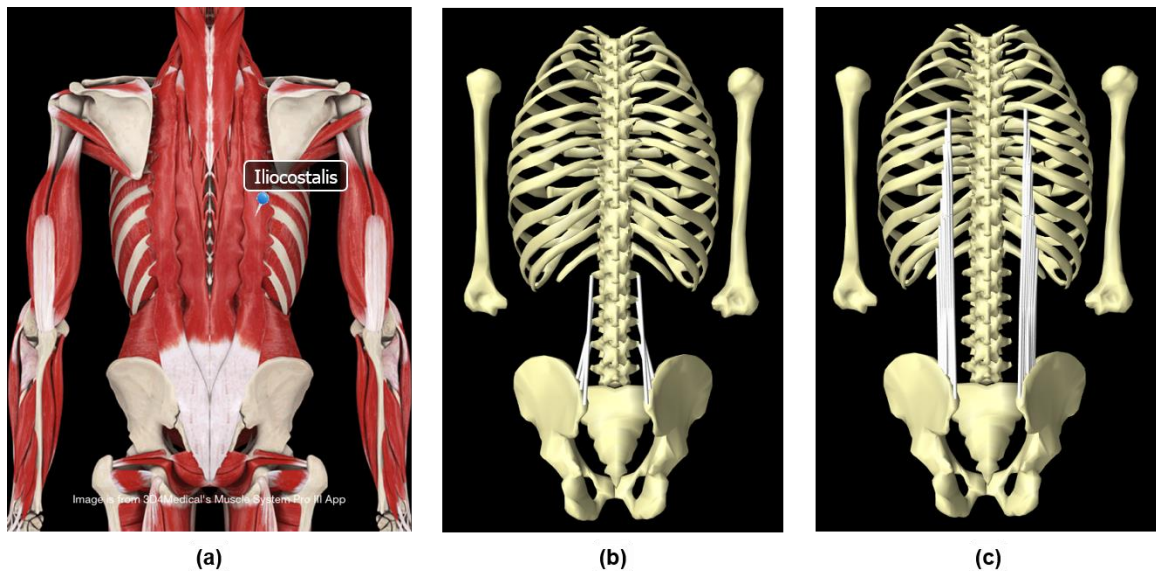


Figure 3-5: Iliocostalis lumbarum anatomy and its incorporation in our model. (a) Anatomy of the iliocostalis lumbarum reprinted from Muscle System Pro III app with permission from 3D4Medical company. (b) Incorporation of iliocostalis lumbarum pars lumbarum and (c) iliocostalis lumbarum pars thoracis in our model.

Multifidus

The main fascicles of the multifidus arise from the lateral site of the spinous processes and are caudally connected to the mamillary processes of the inferior vertebrae or on certain areas of the posterior site of the iliac crest and the sacrum [229]. Implementation of these muscles is shown in Figure 3-7

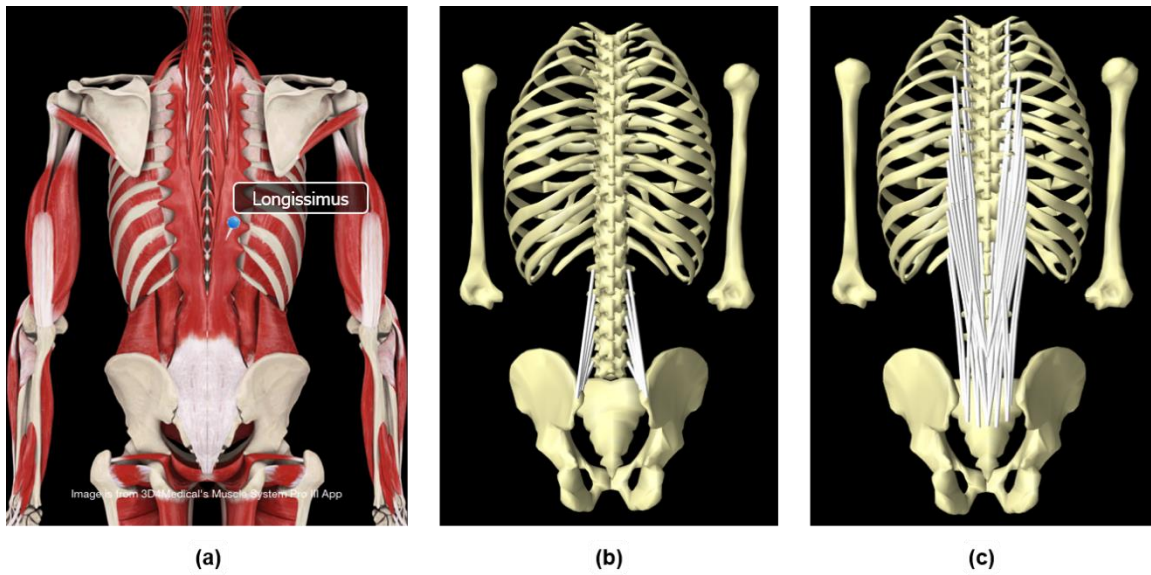


Figure 3-6: Longissimus thoracis anatomy and its incorporation in our model. (a) Anatomy of the longissimus thoracis. Reprinted from Muscle System Pro III app with permission from 3D4Medical company. (b) Incorporation of the longissimus thoracis pars lumborum and (c) longissimus thoracis pars thoracis in our model.

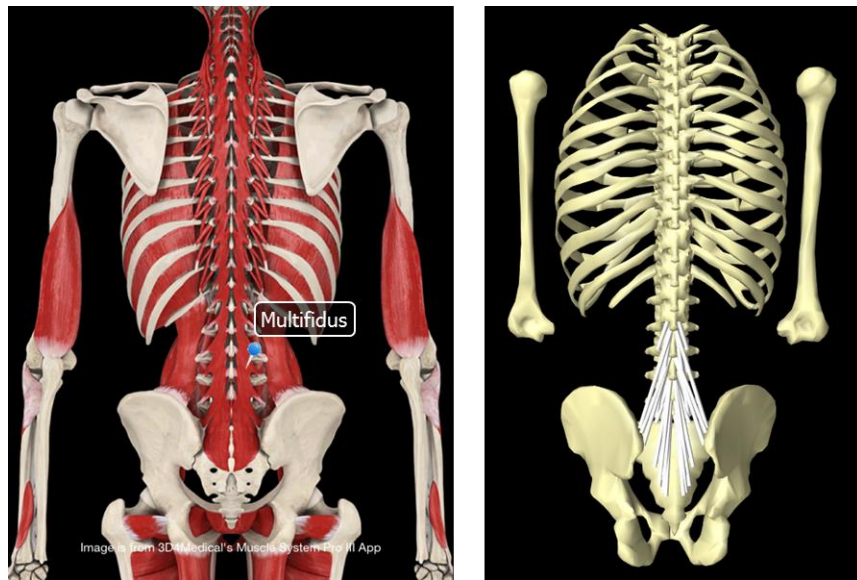


Figure 3-7: Multifidus anatomy and its incorporation in our model. Adapted from Muscle System Pro III app with permission from 3D4Medical company.

Quadratus Lumborum and Psoas Major

Although not categorized as spinal muscles in Gray's or Moore's anatomy books [11][10], quadratus lumborum and psoas major are two muscle groups that both are attached to the lumbar vertebrae and therefore can influence the loading at the lumbar spine.

The fascicles of quadratus lumborum arise from the iliac crest and insert into the lower anterior surface of the twelfth rib, either directly or by passing from transverse processes of the lumbar vertebrae. This muscle consists of anterior, middle, and posterior layers, which can be distinguished by their different fiber arrangements. The fascicular information of each of these layers was presented by Phillips *et al.* [230] and is implemented in our model of the quadratus lumborum. In fact, in their study of four cadavers, they found large variability in the number and size of the fascicles of quadratus lumborum and therefore they only included the fascicles that were repeated in at least half of the specimens. Figure 3-8 is a demonstration of how this muscle is incorporated in our model.

Psoas major is regarded as a hip flexor but since its fascicles arise from lumbar vertebrae, when the lower limb is fixed it can also act as a lumbar spine flexor. According to Bogduk *et al.* [225] psoas major consists of 11 fascicles that all insert into a common site on the femur: five fascicles originate from the lateral side of T12-L1 to L4-L5 intervertebral discs, five fascicles originate from the anterior surface of the transverse processes of each of lumbar vertebrae, and finally one singular fascicle arises from L1 vertebral body as depicted in Figure 3-9.

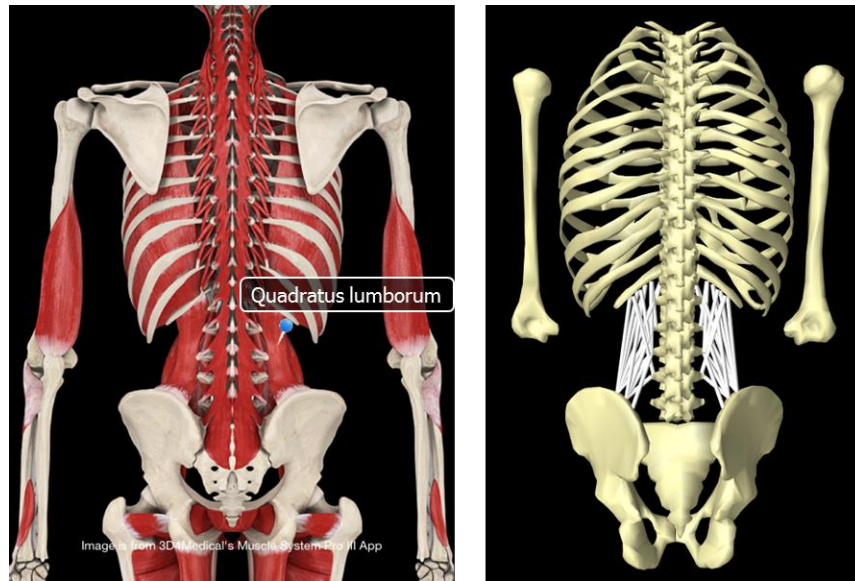


Figure 3-8: Quadratus Lumborum anatomy and its incorporation in our model. Reprinted from Muscle System Pro III app with permission from 3D4Medical company.

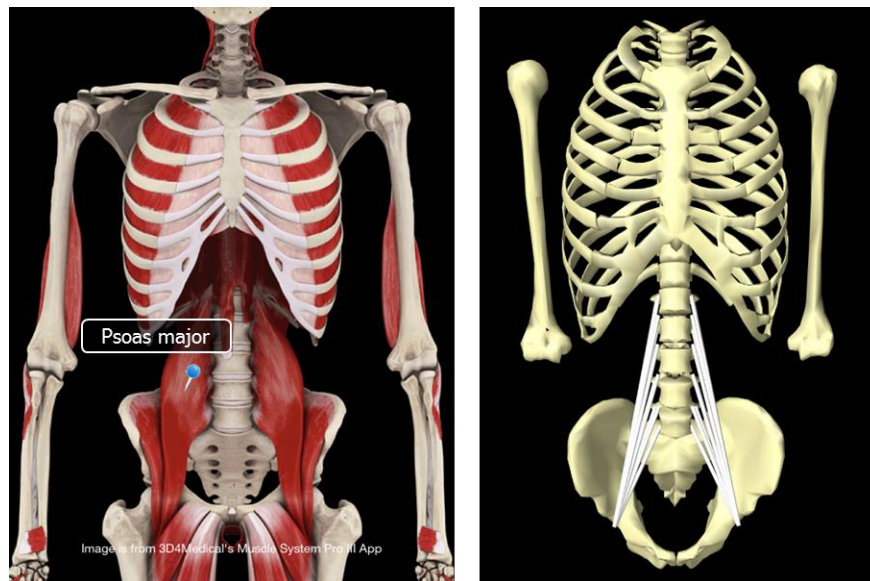


Figure 3-9: Psoas major anatomy and its incorporation in our model. Reprinted from Muscle System Pro III app with permission from 3D4Medical company.

Abdominal Muscles

Abdominal muscles consist of four main muscle groups: external oblique, internal oblique, transversus abdominis, and rectus abdominis. As described by Stokes and Gardner-Morse [231] “the abdominal muscles are layered curved sheets of muscle which have very long and curved attachments, and diverging fiber directions, making the centroid method unsuitable for these muscles”. Therefore they examined two cadavers and used transverse photographic images of the subjects of the Visible Human Project (National Library of Medicine, Bethesda, MD) in order to obtain a fascicular model of internal and external obliques. They eventually modeled each of these muscles with six fascicles, whose directions were representative of the dominant fibers of each division of the muscle (Figure 3-10 and Figure 3-11). Those fascicles whose ends are not attached to either the iliac crest or the ribcage, are connected to the rectus sheath, which is a tendinous tissue in the middle that encapsulates the rectus abdominis. The transversus abdominis was ignored by Stokes and Gardner-Morse [231] as it is the smallest abdominal muscle, does not have an anterior connection to the ribcage, and has a very curved line of action. Rectus abdominis was modeled as two fascicles arising from the pubic symphysis and attaching to the cartilage of the fifth to seventh ribs (Figure 3-12).

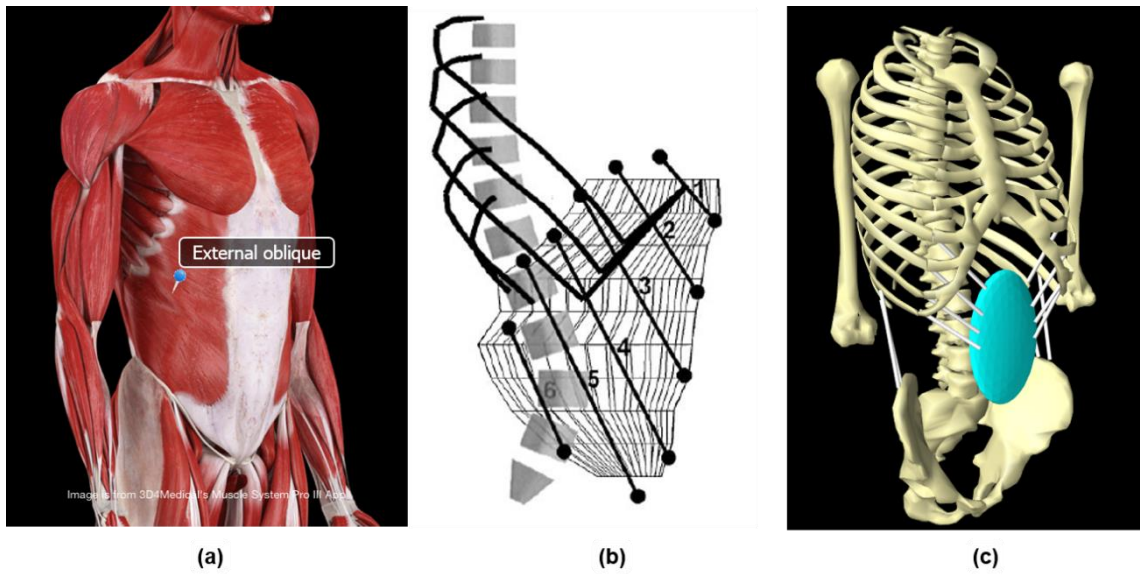


Figure 3-10: External oblique anatomy and its incorporation in our model. (a) External oblique anatomy. Reprinted from Muscle System Pro III app with permission from 3D4Medical company. (b) Representation of the curved fibers of the external oblique by six straight fascicles. Reprinted from Stokes and Gardner-Morse [231] with permission from Elsevier. (c) Incorporation of the external oblique in our model.

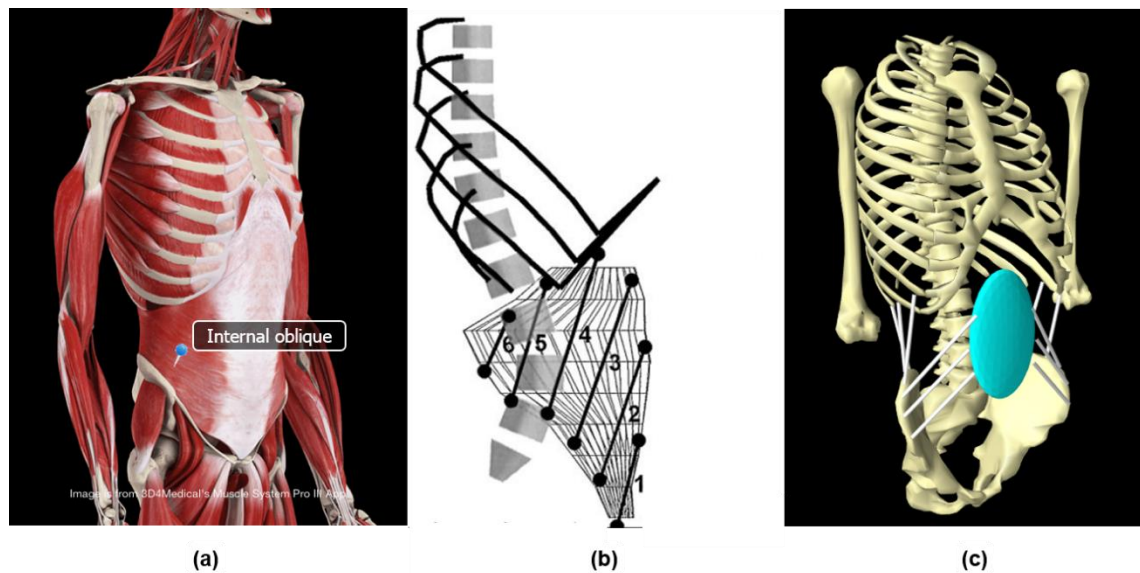


Figure 3-11: Internal oblique anatomy and its incorporation in our model. (a) Internal oblique anatomy. Reprinted from Muscle System Pro III app with permission from 3D4Medical company. (b) Representation of the curved fibers of the internal oblique by six straight fascicles. Reprinted from Stokes and Gardner-Morse [231] with permission from Elsevier. (c) Incorporation of the internal oblique in our model.

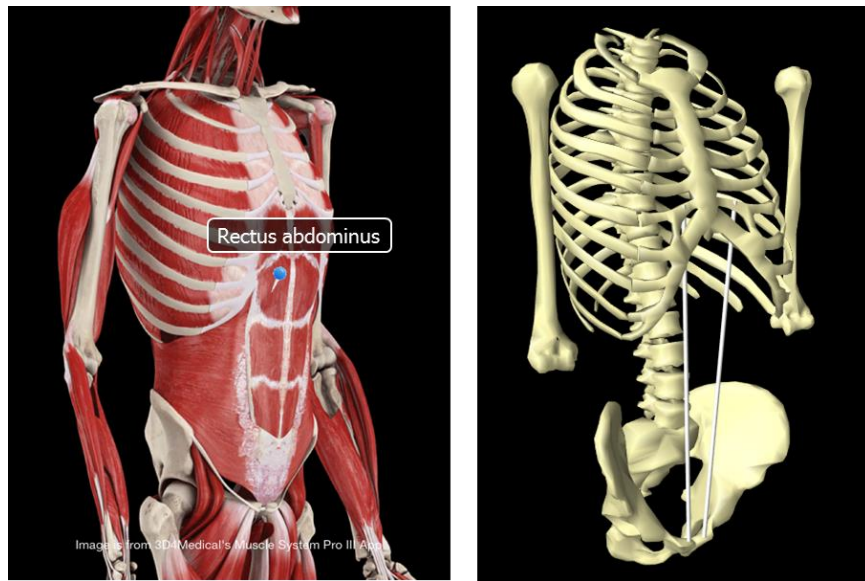


Figure 3-12: Rectus abdominis anatomy and its incorporation in our model. Reprinted from Muscle System Pro III app with permission from 3D4Medical company.

Muscle fascicles are modeled in ArtiSynth using classes “Muscle” or “MultiPointMuscle”. Figure 3-13 demonstrates a fascicle (LTpT_R6) that is attached to several points using “MultiPointMuscle”, and therefore follows the curvature of spine.

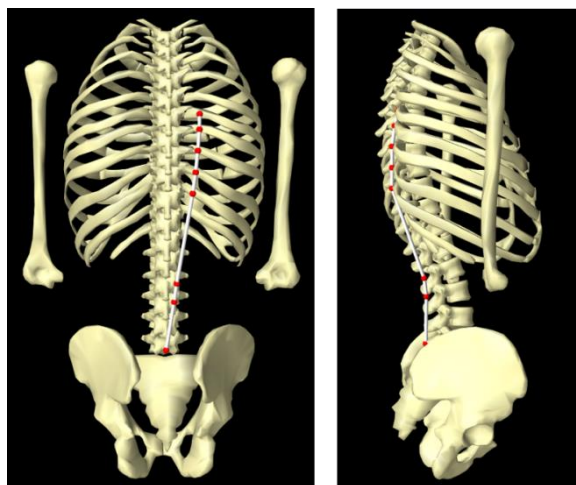


Figure 3-13: Modeling of a multi segmental muscle with seven attachment sites using MultiPointMuscle in ArtiSynth.

Rectus sheath

We modeled rectus sheath as a rigid body that is connected to the sacrum through a revolute joint (Figure 3-14). To simulate rectus sheath movement when the body moves, we applied a constraint on the joint, so that the rotation of the rectus sheath about the joint is a linear function of the total lumbar spine rotation (Figure 3-14). Note that the only role of rectus sheath in our model is to serve as an attachment site for abdominal muscles. Therefore, its dynamic behaviour is not considered in system equations.

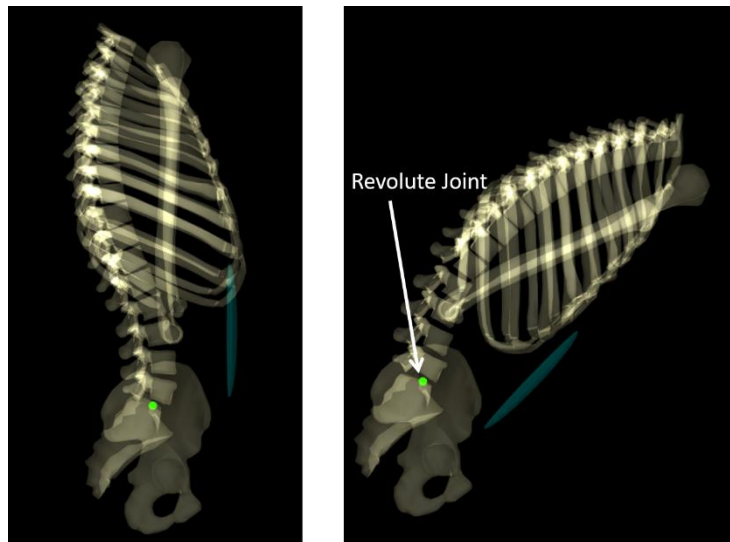


Figure 3-14: Rectus sheath modeled as a massless rigid body connected to the sacrum through a revolute joint. Rotation of the rectus sheath about the joint was constrained by a linear function of the total lumbar spine rotation.

○ **Muscle Parameters**

Translation of muscle parameters measured from cadavers into models, and thereafter, correct formulation of \tilde{l}^F in models requires some considerations, which are discussed in Appendix B.

Here we only present the final formula used in our model for \tilde{l}^F , which is:

$$\begin{aligned} & \tilde{l}_{model}^F \\ = & \frac{l_{model,t=t_0}^{MT} - l_{model,t=t_0}^{MT} \left(1 - \frac{l_{cad}^F \cos \alpha_{cad}}{l_{cad}^{MT}} \right)}{l_{model,t=0}^{MT} \times \frac{l_{cad}^F}{l_{cad}^{MT}} \times \frac{l_o^S}{l_{cad}^S} \times \sqrt{\left(l_{model}^{MT} - l_{rigid}^T \right)^2 + \left(\frac{l_{model}^{MT}}{l_{cad}^{MT}} l_{cad}^F \sin \alpha_{cad} \right)^2}} \end{aligned} \quad (3-1)$$

where subscript “cad” for each parameter means that parameter is taken from cadaveric studies.

In equation (3-1) only l_{model}^{MT} varies with time and the rest of the parameters are constants that are all taken or calculated from the data in the literature. With this formulation, minimum three

muscle parameters are required from the literature: $\frac{l_{cad}^F}{l_{cad}^{MT}}$, l_{cad}^S , and α_{cad} . These parameters for the

muscle fascicles included in our model are presented in Table 3-3.

Table 3-3: Muscle parameters for the abdominal and spinal muscles. The source of the data for each muscle parameter is given at the top of each muscle group column. This table is adapted from the study by Christophy *et al.*[1])

Muscle	Name	Measured From Cadavers				Model	
		l^S (μm)	l^F / l^{MT}	α (degrees)	$PCSA$ (mm^2)	l_0^M (m)	f_0^M (N)
Ps		[W]	est. [G]	[Ar]	[B-Ps]		
	Ps_L1_VB	3.11	0.8	10.7	211	0.184	211
	Ps_L1_TP	3.11	0.8	10.7	61	0.182	61
	Ps_L2_TP	3.11	0.8	10.7	211	0.160	211
	Ps_L3_TP	3.11	0.8	10.7	101	0.139	101
	Ps_L4_TP	3.11	0.8	10.7	161	0.120	161
	Ps_L5_TP	3.11	0.8	10.7	173	0.103	173
	Ps_L5_VB	3.11	0.8	10.7	191	0.090	191
	Ps_L1_L2_IVD	3.11	0.8	10.7	120	0.169	120
	Ps_L2_L3_IVD	3.11	0.8	10.7	119	0.146	119
	Ps_L3_L4_IVD	3.11	0.8	10.7	36	0.124	36
	Ps_L4_L5_IVD	3.11	0.8	10.7	79	0.102	79
RA		[D]	[D]	[D]	[S]		
	rect_abd	2.83	0.788	0	567	0.299	567
ES		[D]	[D],[M]	[D]	[B1]		
ILpL	IL_L4	2.37	0.274	13.8	189	0.016	189
	IL_L3	2.37	0.274	13.8	182	0.023	182
	IL_L2	2.37	0.274	13.8	154	0.037	154
	IL_L1	2.37	0.274	13.8	108	0.051	108
ILpT	IL_R5	2.37	0.381	13.8	23	0.161	23
	IL_R6	2.37	0.417	13.8	31	0.156	31
	IL_R7	2.37	0.452	13.8	39	0.155	39
	IL_R8	2.37	0.462	13.8	34	0.140	34
	IL_R9	2.37	0.6	13.8	50	0.155	50
	IL_R10	2.37	0.6	13.8	100	0.131	100
	IL_R11	2.37	0.64	13.8	123	0.116	123
	IL_R12	2.37	0.64	13.8	147	0.089	147
LTpL	LTpL_L1	2.31	0.419	12.6	79	0.081	79
	LTpL_L2	2.31	0.433	12.6	91	0.068	91
	LTpL_L3	2.31	0.436	12.6	103	0.053	103
	LTpL_L4	2.31	0.438	12.6	110	0.039	110
	LTpL_L5	2.31	1	12.6	116	0.052	116
LTpT	LTpT_T1	2.31	0.26	12.6	29	0.101	29
	LTpT_T2	2.31	0.257	12.6	57	0.105	57
	LTpT_T3	2.31	0.257	12.6	56	0.106	56
	LTpT_T4	2.31	0.257	12.6	23	0.107	23
	LTpT_T5	2.31	0.257	12.6	22	0.105	22

Table 3-3: Muscle parameters for the abdominal and spinal muscles. The source of the data for each muscle parameter is given at the top of each muscle group column. This table is adapted from the study by Christophy *et al.*[1]) (continued).

Muscle	Name	Measured From Cadavers				Model	
		l^S (μm)	l^F / l^{MT}	α (degrees)	$PCSA$ (mm^2)	l_0^M (m)	f_0^M (N)
	LTpT_T6	2.31	0.267	12.6	32	0.104	32
	LTpT_T7	2.31	0.306	12.6	39	0.120	39
	LTpT_T8	2.31	0.346	12.6	63	0.128	63
	LTpT_T9	2.31	0.33	12.6	73	0.126	73
	LTpT_T10	2.31	0.33	12.6	80	0.114	80
	LTpT_T11	2.31	0.33	12.6	84	0.099	84
	LTpT_T12	2.31	0.33	12.6	69	0.079	69
	LTpT_R4	2.31	0.33	12.6	23	0.136	23
	LTpT_R5	2.31	0.33	12.6	22	0.127	22
	LTpT_R6	2.31	0.353	12.6	32	0.136	32
	LTpT_R7	2.31	0.333	12.6	39	0.136	39
	LTpT_R8	2.31	0.29	12.6	63	0.107	63
	LTpT_R9	2.31	0.254	12.6	73	0.093	73
	LTpT_R10	2.31	0.327	12.6	80	0.109	80
	LTpT_R11	2.31	0.37	12.6	84	0.107	84
	LTpT_R12	2.31	0.3	12.6	69	0.068	69
QL		[D]	[D]	[D]	[P]		
	QL_post_I.1-L3	2.38	0.505	7.4	40	0.038	40
	QL_post_I.2-L4	2.38	0.505	7.4	53	0.022	53
	QL_post_I.2-L3	2.38	0.505	7.4	31	0.035	31
	QL_post_I.2-L2	2.38	0.505	7.4	19	0.050	19
	QL_post_I.3-L1	2.38	0.505	7.4	28	0.069	28
	QL_post_I.3-L2	2.38	0.505	7.4	30	0.050	30
	QL_post_I.3-L3	2.38	0.505	7.4	50	0.036	50
	QL_mid_L3-12.3	2.38	0.624	7.4	13	0.055	13
	QL_mid_L3-12.2	2.38	0.624	7.4	14	0.058	14
	QL_mid_L3-12.1	2.38	0.624	7.4	24	0.063	24
	QL_mid_L2-12.1	2.38	0.624	7.4	20	0.041	20
	QL_mid_L4-12.3	2.38	0.624	7.4	12	0.073	12
	QL_ant_I.2-T12	2.38	0.624	7.4	15	0.105	15
	QL_ant_I.3-T12	2.38	0.624	7.4	29	0.103	29
	QL_ant_I.2-12.1	2.38	0.624	7.4	10	0.100	10
	QL_ant_I.3-12.1	2.38	0.624	7.4	19	0.099	19
	QL_ant_I.3-12.2	2.38	0.624	7.4	13	0.093	13
	QL_ant_I.3-12.3	2.38	0.624	7.4	15	0.087	15
MF		[W-MF]	[R]	[An]	[B1]		
	MF_m1s	2.27	0.661	0	40	0.047	40

Table 3-3: Muscle parameters for the abdominal and spinal muscles. The source of the data for each muscle parameter is given at the top of each muscle group column. This table is adapted from the study by Christophy *et al.*[1]) (continued).

Muscle	Name	Measured From Cadavers				Model	
		l^S (μm)	l^F / l^{MT}	α (degrees)	$PCSA$ (mm^2)	l_0^M (m)	f_0^M (N)
	MF_m1t.1	2.27	0.73	0	42	0.075	42
	MF_m1t.2	2.27	0.73	0	36	0.094	36
	MF_m1t.3	2.27	0.73	0	60	0.103	60
	MF_m2s	2.27	0.677	0	39	0.045	39
	MF_m2t.1	2.27	0.727	0	39	0.064	39
	MF_m2t.2	2.27	0.727	0	99	0.081	99
	MF_m2t.3	2.27	0.727	0	99	0.092	99
	MF_m3s	2.27	0.661	0	54	0.040	54
	MF_m3t.1	2.27	0.709	0	52	0.103	52
	MF_m3t.2	2.27	0.709	0	52	0.085	52
	MF_m3t.3	2.27	0.709	0	52	0.085	52
	MF_m4s	2.27	0.562	0	47	0.037	47
	MF_m4t.1	2.27	0.667	0	47	0.055	47
	MF_m4t.2	2.27	0.667	0	47	0.073	47
	MF_m4t.3	2.27	0.667	0	47	0.085	47
	MF_m5s	2.27	0.562	0	23	0.015	23
	MF_m5t.1	2.27	0.667	0	23	0.076	23
	MF_m5t.2	2.27	0.667	0	23	0.057	23
	MF_m5t.3	2.27	0.667	0	23	0.041	23
					[R]		
	MF_m1.laminar	2.27	0.681	0	19	0.031	19
	MF_m2.laminar	2.27	0.681	0	22	0.027	22
	MF_m3.laminar	2.27	0.681	0	23	0.026	23
	MF_m4.laminar	2.27	0.681	0	17	0.029	17
	MF_m5.laminar	2.27	0.681	0	36	0.026	36
EO		[D]	est.[G]	[D]	[S]		
	EO1	2.83	0.389	0	196	0.036	196
	EO2	2.83	0.41	0	232	0.038	232
	EO3	2.83	0.455	0	243	0.038	243
	EO4	2.83	0.47	0	234	0.040	234
	EO5	2.83	0.48	0	273	0.054	273
	EO6	2.83	0.5	0	397	0.049	397
IO		[D]	est. [G]	[D]	[S]		
	IO1	2.83	0.4	0	185	0.042	185
	IO2	2.83	0.4	0	224	0.044	224
	IO3	2.83	0.4	0	226	0.052	226
	IO4	2.83	0.6	0	268	0.070	268

Table 3-3: Muscle parameters for the abdominal and spinal muscles. The source of the data for each muscle parameter is given at the top of each muscle group column. This table is adapted from the study by Christophy *et al.*[1]) (continued).

Muscle	Name	Measured From Cadavers				Model	
		l^S (μm)	l^F / l^{MT}	α (degrees)	$PCSA$ (mm^2)	l_0^M (m)	f_0^M (N)
	IO5	2.83	0.6	0	235	0.057	235
	IO6	2.83	0.6	0	207	0.054	207

Key: [Ar]:Arnold *et al.* [232]; [An]:Anderson *et al.* [233]; [B1]:Bogduk *et al.* [104]; [B-LD]:Bogduk *et al.* [234]; [B-Ps]:Bogduk *et al.* [225]; [D]:Delp *et al.* [99]; [G]:Gray [11]; [M]:Macintosh and Bogduk [226]; [P]:Phillips *et al.* [230]; [R]:Rosatelli *et al.* [235]; [S]: Stokes and Gardner-Morse [231]; [W]:Ward *et al.* [98]; and [W-MF]:Ward *et al.* [236].

3.2.1.4 Intra-abdominal Pressure (IAP)

We modeled the mechanical effect of the IAP as an upward force fixed to the thorax (so that moving with it) and applied at 5 cm anterior to T12, in a way to be consistent with the lever arms measured for IAP at different levels of the lumbar spine in the study by Daggfeldt *et al.* [12] (Figure 3-15).

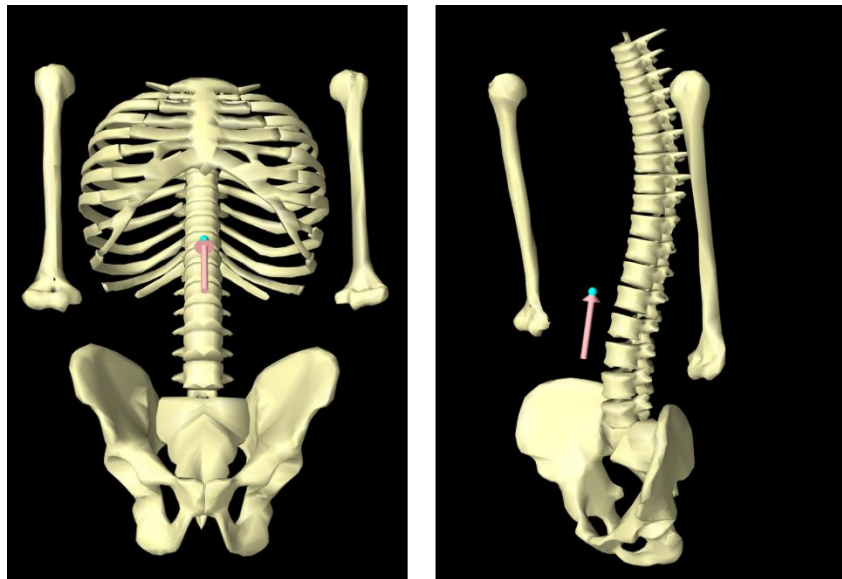


Figure 3-15: The mechanical effect of the intra-abdominal pressure modeled as an upward force applied on the thorax.

Daggfeldt *et al.* [12] measured cross sectional area of the abdomen of their subjects from their transverse MR images. The average of this value when subjects were at 10° flexion and 10° extension was 200 and 210 cm^2 , respectively. We assumed 205 cm^2 to be closest to standing. Multiplying that by 2.7 kPa , which is the value measured by Cobb *et al.* [134], we estimated the upward force applied by IAP to the thorax during normal standing to be about 60N.

3.2.2 Solution Method

In ArtiSynth, forward-dynamics assisted data tracking is implemented in a way that a set of weighted cost functions, which are all expressed in quadratic forms, are combined as a total cost function and minimized per each time step through quadratic programming (equation (3-2)).

$$\phi_{total} = w_1\phi_1(\mathbf{a}) + w_2\phi_2(\mathbf{a}) + w_3\phi_3(\mathbf{a}) \quad (3-2)$$

$$0 \leq \mathbf{a}_j \leq 1 \quad \text{for } j = 1, 2, \dots, N \quad N = \text{number of exciters}$$

In equation (3-2), w_1 , w_2 , and w_3 are weighting terms, while ϕ_1 , ϕ_2 , and ϕ_3 are the cost functions defined as:

$$\begin{aligned} \phi_1 &= \frac{1}{2} \left\| \frac{\mathbf{q}^{k+1}_{desired} - \mathbf{q}^k_{model}}{\Delta t} - \frac{\mathbf{q}^{k+1}_{model}(\mathbf{a}) - \mathbf{q}^k_{model}}{\Delta t} \right\|^2 \\ &= \frac{1}{2} \left\| \mathbf{v}_{desired} - \mathbf{v}_{model}(\mathbf{a}) \right\|^2 \end{aligned} \quad (3-3)$$

$$\phi_2 = \frac{1}{2} \left\| \mathbf{a}^k \right\|^2 \quad (3-4)$$

$$\phi_3 = \frac{1}{2} \left\| \mathbf{a}^k - \mathbf{a}^{k-1} \right\|^2 \quad (3-5)$$

where Δt is the time step and \mathbf{a}^k is the activation vector at time step k , which contains the activations of all exciters (muscle fascicles) of the model. In equation (3-3) \mathbf{q} denotes the position vector of a point in the model to be tracked; \mathbf{q}^k_{model} is the current position of that point,

$\mathbf{q}_{desired}^{k+1}$ is the position where the point is desired to be at the next time step, and \mathbf{q}_{model}^{k+1} is the position where with current muscle activations (\mathbf{a}) of the model, the point will end up being at the next time step. This way the desired velocity can be defined as the velocity that will take the point from its current position to the desired position, which can be obtained as:

$$\mathbf{v}_{desired} = \frac{\mathbf{q}_{desired}^{k+1} - \mathbf{q}_{model}^k}{\Delta t} \quad (3-6)$$

Therefore, by minimizing ϕ_1 , the model-generated velocity $\mathbf{v}_{model}(\mathbf{a})$ that is closest to the desired velocity will be obtained. While ϕ_1 is associated with data tracking, the other two cost functions, ϕ_2 and ϕ_3 , are included for tackling muscle redundancy of the model. ϕ_2 is a l_2 regularization term, which is half of the sum of muscle activations squared and ϕ_3 is a damping term, which is the difference between activations of current and previous time steps. Smaller ϕ_2 results in smaller muscle forces and minimizing ϕ_3 leads to smoother muscle activation over the time [110]. In this study, we used the aforementioned cost functions as they were already implemented in the solver of the software. Moreover, the study by Arjmand and Shirazi-Adl [117] revealed that the differences in predicted axial and shear forces by the eight different cost functions that they investigated were less than 14% and 20%, respectively. The investigated cost functions in their study were sum of muscle stresses, muscle stresses squared, muscle stresses cubed, muscle forces, muscle forces squared, muscle fatigue, maximum muscle intensity, and axial compression on the spine. Note that muscle activations are proportional to both muscle forces and stresses. Therefore, I felt it appropriate to use the existing cost functions.

In ArtiSynth, forward-dynamics-assisted data tracking is coded in a way so that the trajectories of multiple points can be tracked. Those trajectories can be even weighted based on their

importance. We specified two target points in our model, whose locations are symmetric with respect to the sagittal plane and both belong to the ribcage (Figure 3-16). Their weights were set to be equal.

Finally, to get the solver to work, a set of exciters must be specified. Although each muscle fascicle can be assigned an individual exciter, in order to alleviate the redundancy by reducing the number of variables, one can assign one exciter for a group of muscle fascicles. Assuming symmetric activations of muscles for within sagittal plane movements, we specified one exciter for each symmetric pair of fascicles in all muscle groups, except in ILpT, LTpL, and rectus abdominis. Each fascicle of these three muscle groups had an independent exciter so as to enable the model to have out of plane movements. This way our model with 210 muscle fascicles had 119 exciters.

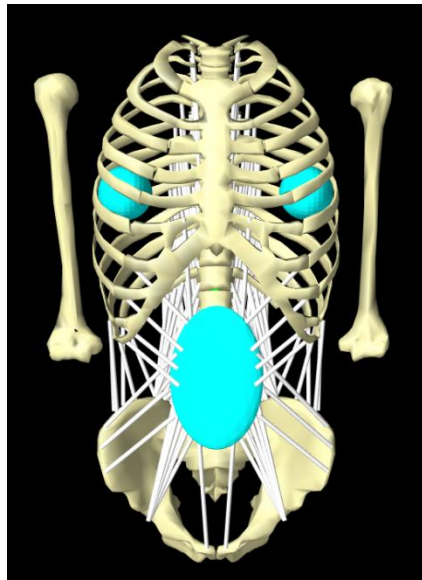


Figure 3-16: Symmetric target points specified for tracking the motion of the thorax.

3.2.3 Validation

For validation of our model, we compared our results with two *in vivo* studies in the literature: one conducted by Daggfeldt *et al.* [12] and the other by Wilke *et al.* [151].

In the study by Daggfeldt *et al.* [12], maximal voluntary back-extension strength of four male subjects was measured in terms of maximum torque produced by the spinal muscles about the L5-S1 joint. In their experiment, subjects were lying down on their right side with their legs and pelvises fixed to a vertical board, while their torso was attached to another board mounted on a swivel table. The subjects were positioned on tables so that their L5-S1 level would be located over the center of rotation of the swivel table; this way the angle between the boards represented the amount of flexion-extension of the body about the L5-S1 joint (Figure 3-17). The torques about the L5-S1 joint were calculated through multiplication of the force measured by a force transducer on the wire fixating the swivel table and its known lever arm about the center of rotation of the swivel table.

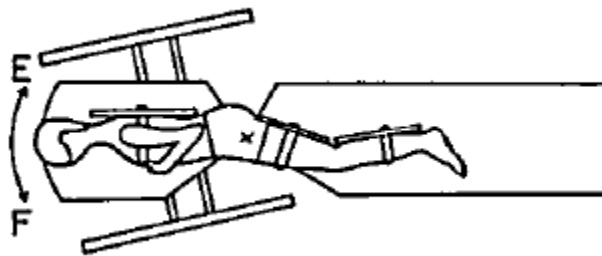


Figure 3-17: The position of the subjects of Daggfeldt *et al.*'s study for measurement of the maximum extension moment about the L5-S1 joint. Reprinted from [143] with permission from Lippincott Williams & Wilkins.

All subjects performed maximal voluntary back-extension tests for five different angles between the boards: -45° , -30° , -10° , 10° , and 20° , where the negative sign denotes flexion. Simultaneously the intragastric pressure of the subjects was recorded by a transducer inserted

through the esophagus into the stomach. Moreover, MRI images were obtained, so that the effective area for IAP and its lever arm about all lumbar joints could be determined. The results of their study are summarized in Table 3-4.

Table 3-4: Average of the maximum extension moment, IAP, and diaphragm area at different positions for subjects of the of Daggfeldt *et al.*'s study. The negative sign for extension angles represents flexion.

Extension angle (°)	Torque (Nm)	IAP (kPa)	Diaphragm Area (cm ²)	$F_{IAP} = IAP \times Area$ (N)
20	110 (90-130)	12	190 (150-230)	228
10	180 (150-210)	16	200 (160-240)	320
-10	240 (210-270)	18	210 (180-240)	378
-30	290 (240-340)	18	240 (220-260)	432
-45	300 (250-350)	19	240 (220-260)	456

In our model, we simulated the reaction force of the swivel table board on the subjects' backs with a horizontal force applied at T3 COM, whose lever arm about L5-S1 joint was 0.39 m. Therefore, dividing the measured torques about the L5-S1 joint by 0.39 gave the equivalent force at T3 COM (Table 3-5). Since for all cases of our study design the spine was in upright standing (see section 03.2.4), only the data for -10 and 10 angles were used for validation of the model, as they are closest to the upright standing.

Table 3-5: Maximum extension moment and the equivalent maximum horizontal force measured for 10° extension and 10° flexion in the study by Daggfeldt *et al.* [12].

Extension angle (°)	Torque (Nm)	Equivalent Force (N)	F_{IAP} (N)
10	180	461	320
-10	240	615	378

In the study by Wilke *et al.* [151], a pressure transducer was inserted in the nucleus pulposus of the L4-L5 disc of a male subject for measurement of intradiscal pressure during daily activities. Three of the activities dealt with the subject standing statically in neutral posture: once standing

normally, once standing while holding a crate of weight 190 N close to the chest, and once holding that crate far from the chest (Figure 3-18). The height and weight of the subject were 1.73 m and 73 kg, respectively, and its area of L4-L5 disc, which was measured through MRI, amounted to 18 cm².

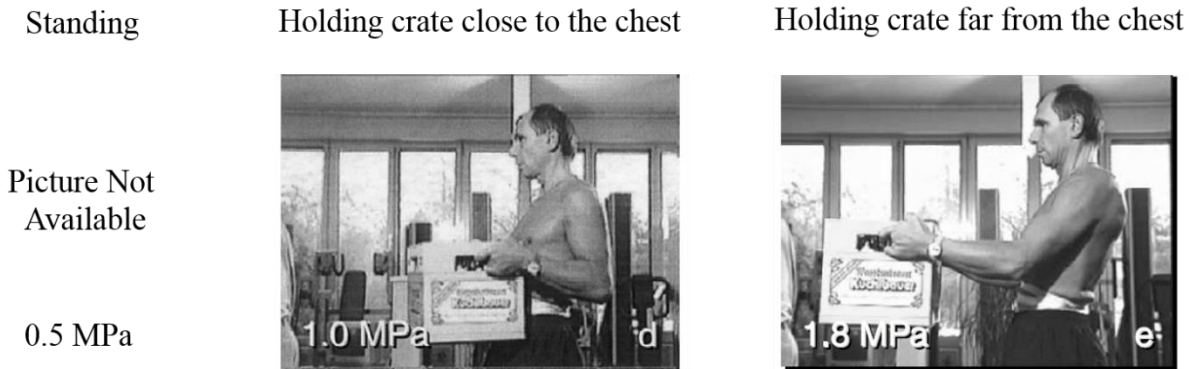


Figure 3-18: *In vivo* measured intradiscal pressure for three activities of Wilke *et al.*'s study. Reprinted from [151] with permission from Elsevier.

3.2.3.1 Calibration Procedure

Four unknown parameters in our model were left to be determined during the calibration procedure. One parameter was muscle strength factor K , and the other three parameters were the weighting terms for optimization cost functions. Among those three weighting terms, the dominant term was w_1 (which is the one related to minimization of tracking errors). Therefore by keeping the other two terms constant ($w_2 = 0.025$ and $w_3 = 0.005$), we only treated w_1 as a variable. It is noteworthy that the ratios of weighting terms are important, not their absolute values.

Through trial-and-error method, we eventually found $w_1 = 2.5$ and $K = 100$ to best match the aforementioned two experiments. In order to provide a sense of how these parameters were

found, we first go through the process of finding proper w_1 for when $K = 100$. Table 3-4 presents the minimum error the model could achieve for 5 different values of w_1 . It can be noted that by increasing w_1 from 0.5 to 2.5 smaller errors can be achieved, whereas by going beyond that, e.g. $w_1 = 3.5$ the solver cannot find a stable solution. Moreover, it was observed that whenever an external load was to be carried or resisted by the model which required larger contribution of muscles, the minimum achievable accuracy would increase. For instance, for $w_1 = 2.5$, when holding a crate far from the chest, the model could not stay closer to the target than 1 cm, whereas when holding nothing an accuracy of 0.2 mm could be achieved.

Table 3-6: Minimum achievable errors for different optimization terms (w_1) when simulating neutral standing and holding crate far from the chest.

Activity	Minimum Achievable Errors (mm)				
	$w_1 = 0.5$	$w_1 = 1$	$w_1 = 2.5$	$w_1 = 3.5$	$w_1 = 5$
Neutral Standing	7	1.6	0.2	Unstable	Unstable
Holding Crate Far From Chest	-	30	10	5	Unstable

By selecting $w_1 = 2.5$, we tried simulating the study by Daggfeldt *et al.* [12] for three muscle strength factors of 46.4, 70, and 100. Given that with $w_1 = 2.5$, minimum error of 1 cm could be achieved (Table 3-6), we increased the horizontal force until the error could not be less than 1 cm. That force was considered as the maximum force that the model could voluntarily resist. However, we also continued increasing the horizontal force until minimum achievable error would rise to 2 cm and included that force in Table 3-7. It can be noted that the forces corresponding to 1 cm and 2 cm error do not differ much from each other (see Table 3-7); moreover, the results for $k=100$ (420 N at 10° extension and 600 N at 10° flexion) are in good agreement with the experimental results (461 N at 10° extension and 615 N at 10° flexion).

Table 3-7: Maximum resistible forces at 10° flexion ($\theta = -10^\circ$) and 10° extension ($\theta = 10^\circ$) for different muscle strength factors. Values are reported for minimum achievable errors of 1 cm and 2 cm.

	1 cm error		2 cm error	
	$\theta = -10^\circ$	$\theta = 10^\circ$	$\theta = -10^\circ$	$\theta = 10^\circ$
K =100	420 N	600 N	495 N	625 N
K = 70	300 N	455 N	379 N	485 N
K= 46.6	-	330 N	-	365 N

Therefore we believe $K = 100$ and $w_1 = 2.5$ were appropriate for the solution method that we utilized. With these parameters our model was able to predict axial forces at L4-L5 that had the same ratio between them as had the three measured IDPs in the study by Wilke *et al.* [151] (see Table 3-8).

The forces predicted by our model were similar in magnitudes to multiplication of the measured *in vivo* IDP and intervertebral disc area of the subject of the study by Wilke *et al.* [151]; however, since the nucleus only constitutes a portion of the disc, multiplication of the entire disc area by the measured intradiscal pressure (IDP) overestimates the force on the disc. The results of a detailed FEA analysis by Dreischarf *et al.* [237], suggests a correction factor of 0.66 when estimating axial disc forces from intradiscal pressure. Therefore, we calculated the axial forces on L4/L5 disc of the subject in Wilke *et al.*'s study as $F_{axial} = IDP \times Disc\ Area \times 0.66$ (see Table 3-8). It should be noted that while this relation only gives the axial force on the intervertebral discs, the estimated forces in our model represent the force born by the FSUs, which include the forces born by posterior elements of the spine.

Table 3-8: Comparison between the axial forces predicted by the model and the *in vivo* intradiscal pressure (IDP) measured in Wilke *et al.*'s study.

	Experimental data				Predicted by the Model	
	IDP (MPa)	Normalized IDP (vs. Standing)	IDP×Disc Area (N)	IDP×Disc Area×0.66 (N)	Axial Forces (N)	Normalized Axial Forces (against standing)
Standing	0.5	1	900	594	984	1
Holding crate close to chest	1.0	2	1800	1188	2050	2.1
Holding crate far from chest	1.8	3.6	3240	2138	3770	3.8

3.2.4 Study Design

As mentioned in chapter 1, in posterior lumbar fusion surgeries, those muscles that are connected to the posterior elements of the vertebrae receiving instrumentations are detached from their bony attachment sites. This detachment renders those muscles unable to apply any force on the instrumented vertebrae. To study the effect of this change in spinal muscle architecture on spinal loading, we designed two model scenarios.

The first scenario (scenario 1) consisted of two models: one model representing the spine of a healthy subject with intact muscles, while the other characterizing the spine of that subject after a sham surgery, in which the muscles were detached from L2 to L5 (Figure 3-19). Both models were asked to stay upright by prescribing the same target positions. The resulting forces at the intervertebral joints of the models were contrasted.

The second scenario was similar to scenario 1, with a difference that both models of scenario 2 had instrumentation: one model represented the spine of a patient receiving minimally invasive fusion surgery with percutaneous pedicle screw fixation, where posterior muscles are kept intact,

and the other typified a patient undergoing open fusion surgery, where muscles were detached from the instrumented vertebrae (Figure 3-20).

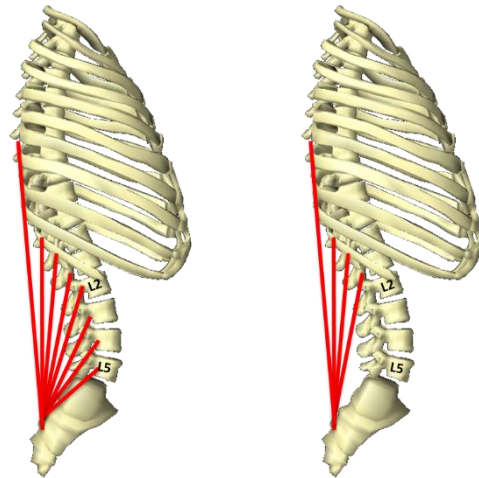


Figure 3-19: Scenario 1 of the study design: comparing the spinal loads between a healthy subject and a patient undergoing sham surgery.

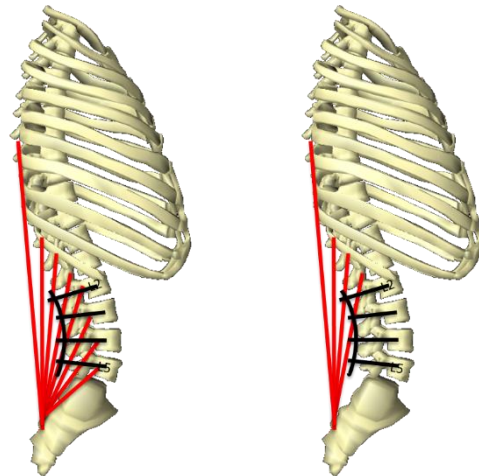


Figure 3-20: Scenario 2 of the study design: comparing the spinal loads between a patient receiving percutaneous pedicle screw fixation and a patient undergoing open fusion surgery.

Note that in order to simulate muscle damage, we treated muscle fascicles of our model in two ways. If a fascicle had only two attachment points and at least one of them was on the injured levels, that fascicle was removed from the model. But if a fascicle had multiple attachment points, only the points that were located at the injury levels were removed and the remaining points were connected together again to form that fascicle (Figure 3-21).

Also note that instead of modeling flexible screws and rods, we assumed that the fusion is complete and therefore we treated the instrumented vertebrae (here L2 to L5) as one rigid body by fixing them together using Solid Joints in ArtiSynth.

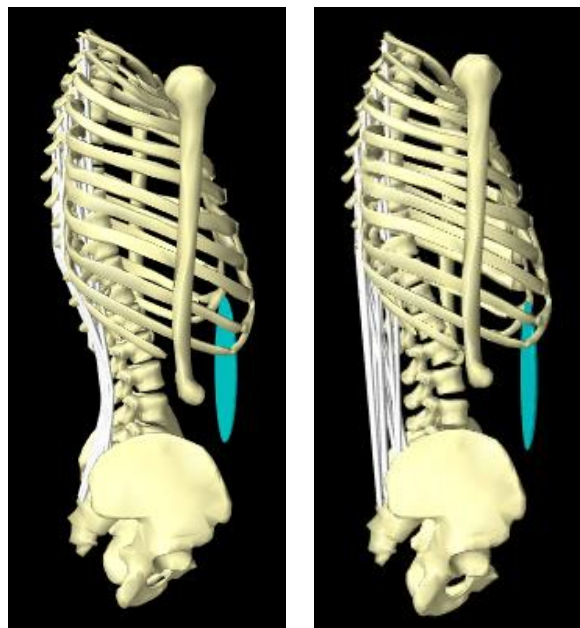


Figure 3-21: Simulation of iatrogenic muscle damage to the longissimus thoracis pars thoracis. For fascicles with multiple attachment points, the points that were located at injury levels were removed and the remaining points were reconnected together to again form that fascicle.

3.3 Results

3.3.1 Results for Scenarios of the Study Design

For scenario 1, the loads at the adjacent vertebral levels (i.e. L1-L2 and L5-S1) are presented in Figure 3-22. The results showed that when muscles were injured the axial and shear forces at both L1-L2 and L5-S1 levels increased. Interestingly, the increase in the axial force was larger at the L1-L2 than L5-S1 (483 N vs. 307 N), while the increase in the shear force was more pronounced at L5-S1. The magnitude of flexion-extension moments applied on adjacent levels, however, were small. The negative sign for flexion moments denotes that the segment is in extension.

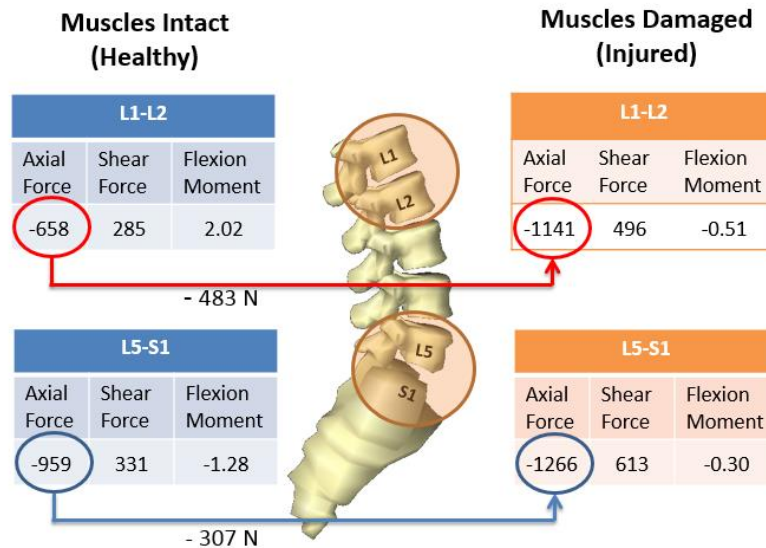


Figure 3-22: Predicted spinal loads at the adjacent levels for scenario 1. Forces are in N and moments are in Nm.

The same trend was observed for scenario 2, i.e. both the axial and shear forces increased at the adjacent levels when muscles were removed: the increase in the axial force at the rostral adjacent level was larger than caudal one, whereas for the shear force the increase at the caudal adjacent level was larger (Figure 3-23).

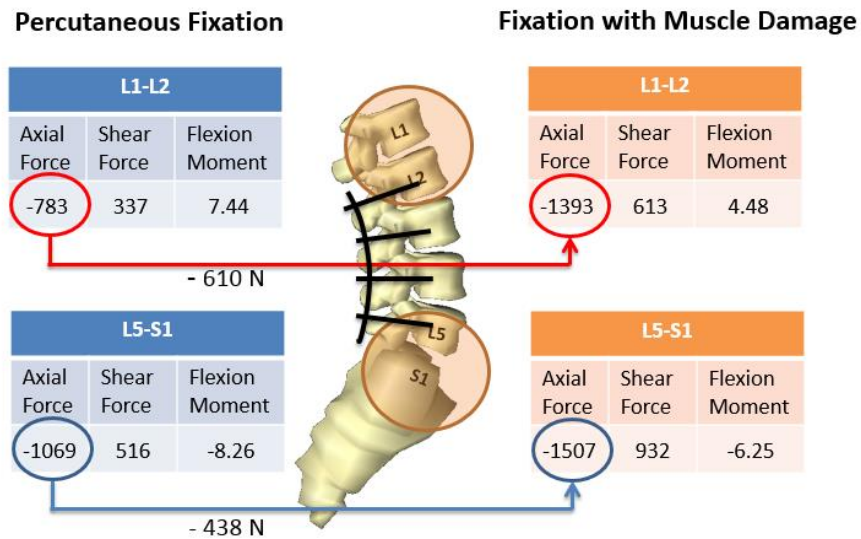


Figure 3-23: Predicted spinal loads at the adjacent levels for scenario 2. Forces are in N and moments are in Nm.

3.3.2 Further Results for scenario 1

We did further analysis to determine the reason for a larger increase in the axial force at the rostral adjacent level in comparison to the caudal one. Since the trends of the results were similar in both scenarios, we only explored scenario 1 in more detail. We prepared Figure 3-25, which presents the loads at each intervertebral level, and Figure 3-26 and Figure 3-27, which provide information regarding the physiological cross sectional area (PCSA) and forces of each muscle group crossing L1-L2 and L3-L4 levels, respectively. Each level (e.g. level L3-L4) was defined by a transverse plane passing through the midpoint of the line connecting the centroids of the two vertebrae adjacent to that plane (here L3 and L4. See Figure 3-24). Only those fascicles whose end points were at two sides of the plane were considered to cross that level. Therefore, the method was effective only for levels L1-L2, L2-L3, and L3-L4, and could not be used for L4-L5 and L5-S1; as for those levels the transverse plane cuts through the pelvis, thereby the cross sectional area of the fascicles whose origins are on top of the pelvis crest (above the plane) ends up not being considered while they should.

When comparing the PCSAs of the muscle groups between the healthy and the injured models we observed that while at the L1-L2, the injury only reduced the PCSAs of QL and LTpT (QL: 163 mm^2 and LTpT: 369 mm^2), at the L3-L4, it led to substantial reduction of PCSA of MF, ILpL, and LTpL in addition to QL and LTpT (MF: 750 mm^2 , ILpL: 665 mm^2 , LTpL: 381 mm^2 , QL: 358 mm^2 , and LTpT: 411 mm^2).

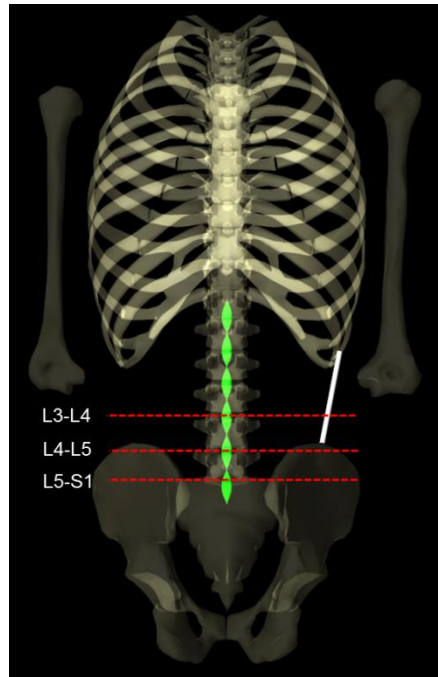


Figure 3-24: Limitation of our method for calculation of muscle cross sectional areas at L4-L5 and L5-S1 levels.

Healthy				Injured			
	Axial Force	Shear Force	Flexion Moment		Axial Force	Shear Force	Flexion Moment
L1-L2	-659	285	2.02	L1-L2	-1141	496	-0.50
L2-L3	-796	272	0.24	L2-L3	-1268	326	-0.59
L3-L4	-893	228	-0.87	L3-L4	-1324	179	-0.42
L4-L5	-985	44	-1.40	L4-L5	-1365	135	-0.35
L5-S1	-959	331	-1.20	L5-S1	-1265	614	-0.29

The Amount of Increase in Loads After Injury			
	Axial Force	Shear Force	Flexion Moment
L1-L2	-482	211	-2.52
L2-L3	-472	54	-0.83
L3-L4	-431	-49	0.45
L4-L5	-380	91	1.05
L5-S1	-306	283	0.91

Figure 3-25: Predicted spinal loads at all lumbar intervertebral levels for scenario 1. Forces are in N and moments are in Nm.

Healthy			Injured		
	PCSA	Force (N)		PCSA	Force (N)
EO	3111	2	EO	3111	119
IO	2656	178	IO	2656	402
RA	1129	0	RA	1129	2
Ps	733	29	Ps	773	61
MF	0	0	MF	0	0
QL	419	4	QL	256	6
ILpL	215	34	ILpL	215	52
ILpT	1086	56	ILpT	1086	90
LTpL	155	9	LTpL	155	14
LTpT	2193	156	LTpT	1824	267

Difference		
	PCSA	Force (N)
EO	0	117
IO	0	224
RA	0	2
Ps	0	32
MF	0	0
QL	-163	2
ILpL	0	18
ILpT	0	34
LTpL	0	5
LTpT	-369	111

Figure 3-26: Physiological cross sectional area (PCSA) and force of each muscle group crossing L1-L2 level for scenario 1. PCSA is in mm^2 .

As depicted in Figure 3-27, the change in PCSAs led to different muscle force distribution. To better understand the change in muscle force distribution, we can consider the muscle groups as three major groups: IO and EO as abdominal muscles; LTpT and ILpL as global muscles (which span the entire lumbar spine and are inserted on thoracic region); and finally MF, LTpL, and ILpL as local muscles (which are attached to different levels of the lumbar spine). Our results showed that after injury, the sum of forces in IO and EO increased by 341 N at both L1-L2 and L3-L4 levels. Similarly the sum of forces in LTpT and ILpT (global muscles) increased at both levels (145 N for L1-L2 and 148 N for L3-L4). However, while the sum of forces in MF, LTpL, and ILpL (local muscles) decreased at L3-L4 by 105 N, it increased at L1-L2 by 23 N. That the increase in abdominal muscles and thoracic muscles affects both L1-L2 and L3-L4 almost

equally is because those muscles are attached to the thorax and therefore their forces will affect all lumbar vertebral levels, whereas for the lumbar muscles this is not true.

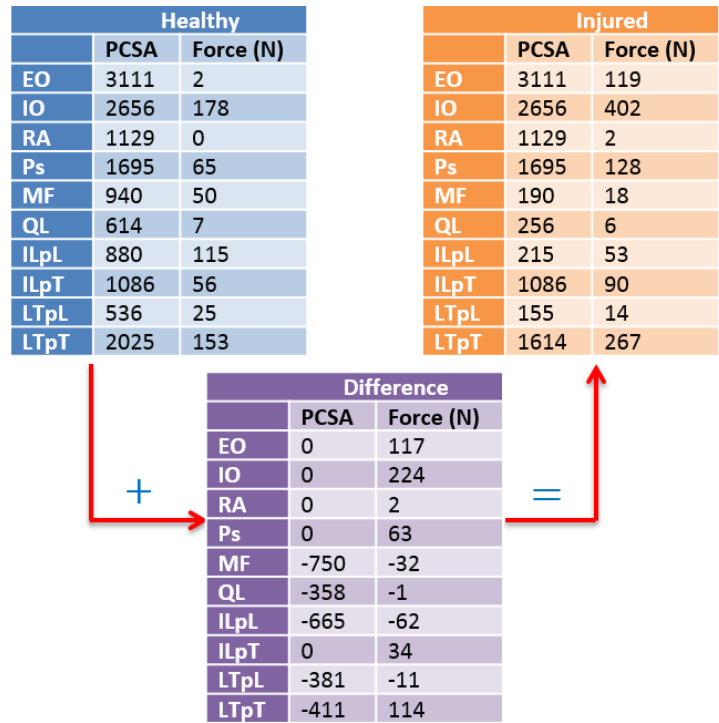


Figure 3-27: Physiological cross sectional area (PCSA) and force of each muscle group crossing L3-L4 level for scenario 1. PCSA is in mm^2 .

A deeper look into the distribution of the loads between muscle fascicles of both EO and IO revealed that the increase in both muscle groups forces is caused by the fascicles that directly originate from the iliac crests and attach to the ribcage. The forces in other fascicles, which are attached to the rectus sheath, were all zero (Figure 3-28 and Figure 3-29). This can also be noted in Figure 3-30, which graphically demonstrates the excitation of each muscle fascicle as gradient of red color (the higher the excitation, the greater its red color).

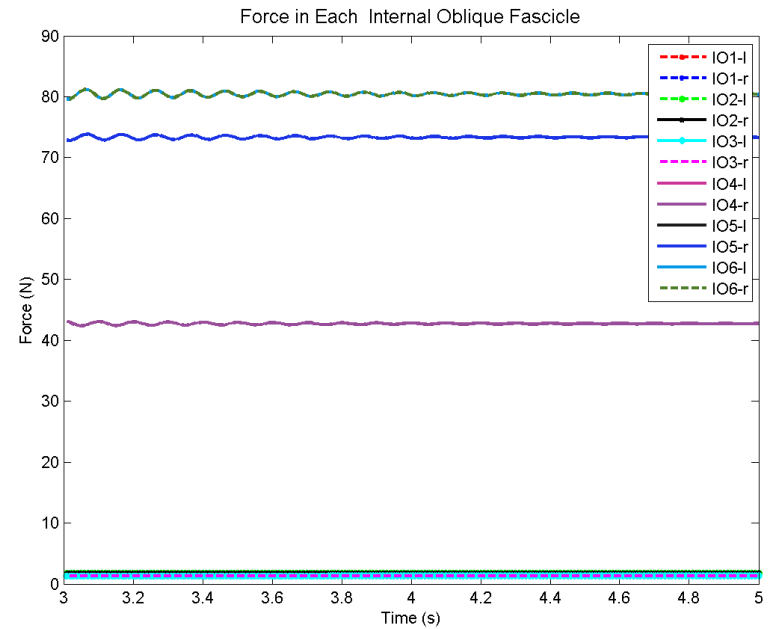
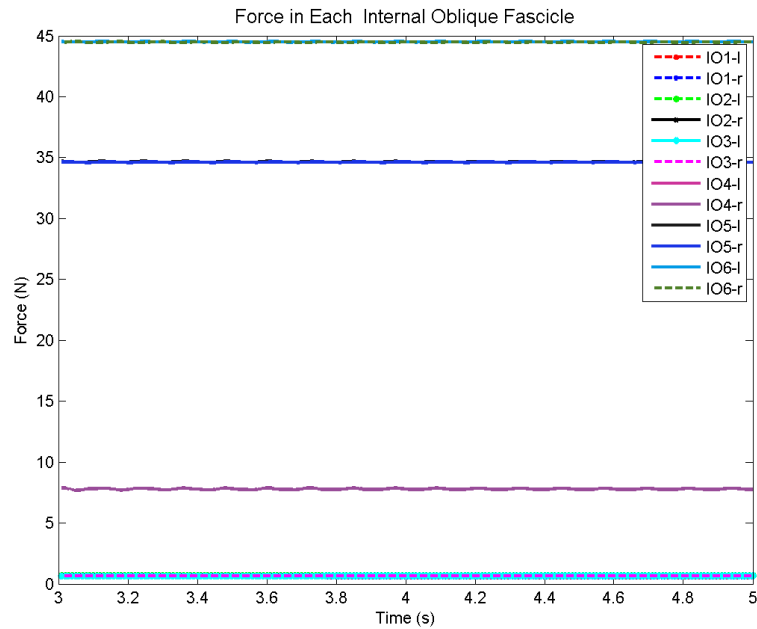


Figure 3-28: Force in each internal oblique fascicle for scenario 1. Among the six pairs of internal oblique fascicles, IO1, IO2, and IO3 are attached to the rectus sheath, while IO4, IO5, and IO6 are directly connected to the ribcage. Those fascicles that are attached to the rectus sheath are not activated neither for the healthy model (the figure on the left side) nor for the injured model (the right figure). After muscle damage, the forces in these fascicles that are directly attached to the ribcage increase.

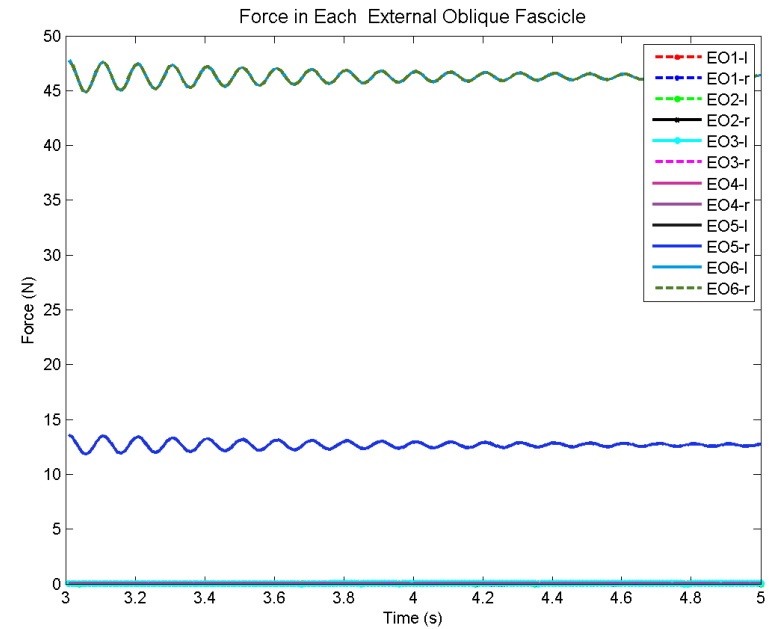
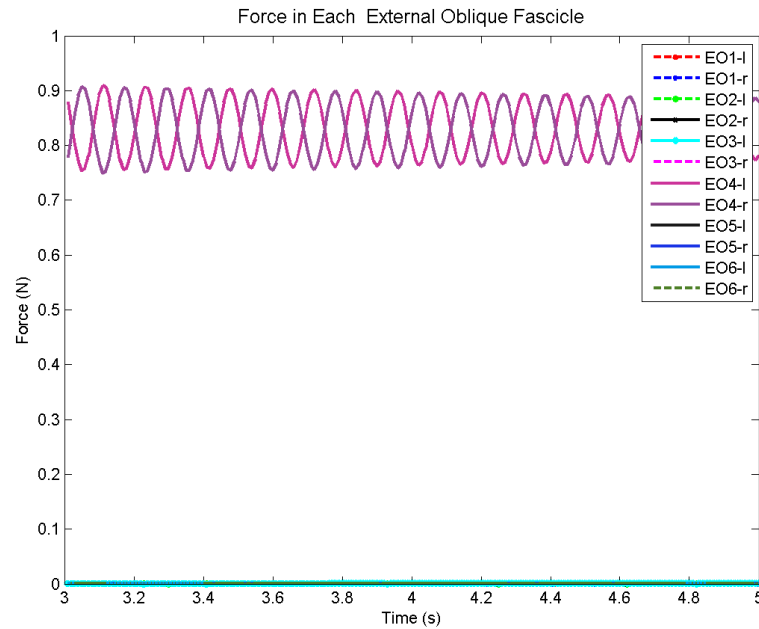


Figure 3-29: Force in each external oblique fascicle for scenario 1. Among the six pairs of external oblique fascicles, EO1, EO2, EO3, and EO4 are attached to the rectus sheath, while EO5, and EO6 are directly connected to the ribcage. Those fascicles that are attached to the rectus sheath are not activated neither for the healthy model (the figure on right side) nor for the injured model (the left figure). After muscle damage, the forces in these fascicles that are attached to the ribcage increase.

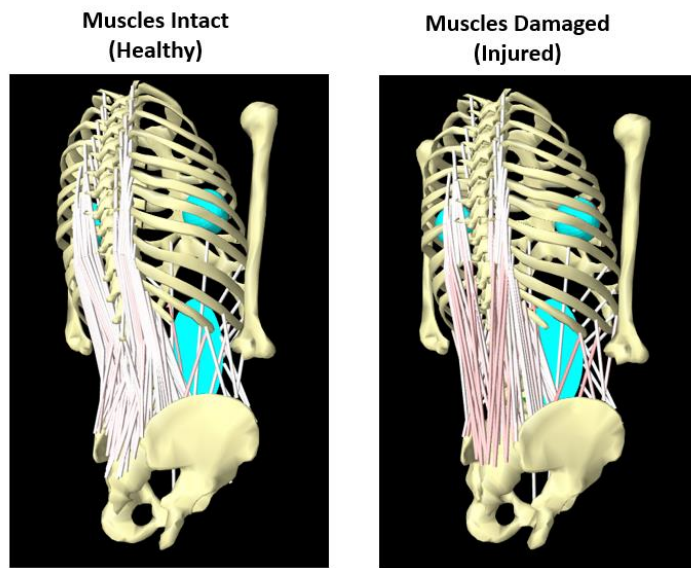


Figure 3-30: Muscle excitations during upright standing. The greater red color of the global muscles in the injured model represents higher excitation of those muscles after muscle damage.

3.4 Discussion

In order to study the effect of iatrogenic muscle damage on spinal loading, specifically at the adjacent levels, a musculoskeletal model of the lumbar spine was developed. Iatrogenic muscle damage was simulated by detaching the muscle fascicles that are resected from the vertebrae during the surgery. This was done in two scenarios: once with and once in the absence of rigid fixation. Both scenarios led to increased loading at both adjacent levels during neutral standing, indicating the possible role of muscle damage in altered loading and accelerated degeneration of the disc adjacent to the lumbar spinal fusion.

Our results demonstrated larger increase in axial forces at the rostral adjacent level (78% in presence of fixation and 73% without fixation) in comparison to the caudal level (41% in presence of fixation and 32% without fixation). This is very interesting as both radiographic and symptomatic ASD are reported in clinical studies to mostly occur at the rostral level, thereby supporting our results and the role of muscle damage on disc degeneration [238][239] [171] [51][5].

In order to further investigate the reason for a larger increase in axial force at the rostral adjacent level, we provided the following example that analytically predicts similar results. Consider the entire spine as a rigid bar that is hinged to the sacrum at the L5-S1 joint. If a force W representing the body weight is applied at the tip of the bar, in order to keep the bar at equilibrium, a force representing the resultant of muscle forces should be applied in a way to cancel out the moment caused by the force W about the revolute joint (Figure 3-31).

To study the effect of removal of lumbar muscles on spinal loads, we consider two cases, where in case 1 the force representing the resultant of local muscles (attached to the lumbar spine) is

applied at the middle of the bar (Figure 3-31b), while in case 2 the force representing the global muscles (attached to the thoracic spine) is applied at the tip of the bar (Figure 3-31c). We also assume the direction of the forces is such that they meet at point P in a way that $\overline{OM} = \overline{PM} = \overline{MT}$ so that $\theta_1 = 2\theta_2$ (see Figure 3-31a).

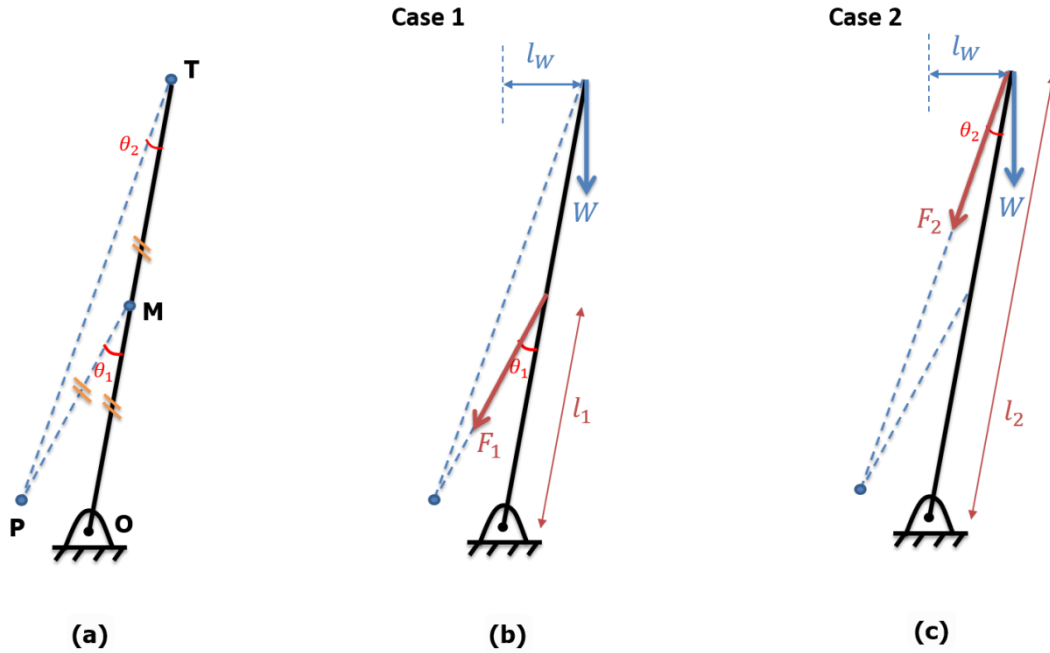


Figure 3-31: A simple mathematical model of the spine. (a) The spine is modeled as a rigid bar hinged at L5-S1 joint (point O). (b) Case 1 represents a spine maintained at equilibrium by the resultant of local muscles, while in case 2 (c), the resultant of the global muscles is keeping the spine upright.

By writing the equilibrium equations for both cases we obtain:

$$F_1 l_1 \sin \theta_1 - W l_W = 0 \quad (3-7)$$

$$F_2 l_2 \sin \theta_2 - W l_W = 0$$

from which the muscle forces can be written as:

$$F_1 = \frac{W l_W}{l_1 \sin \theta_1} \quad \text{and} \quad F_2 = \frac{W l_W}{l_2 \sin \theta_2} \quad (3-8)$$

and the ratio of forces between two cases could be easily obtained as:

$$\frac{F_2}{F_1} = \frac{l_1 \sin \theta_1}{l_2 \sin \theta_2} = \frac{l_1 (2 \sin \theta_2 \cos \theta_2)}{l_2 \sin \theta_2} = \cos \theta_2 \quad (3-9)$$

Considering the projection of forces along bar direction (\overline{OT}) as axial component of those forces, we obtained the ratio between axial forces as:

$$\begin{aligned} \frac{(F_2)_{axial}}{(F_1)_{axial}} &= \frac{F_2 \cos \theta_2}{F_1 \cos \theta_1} = \frac{l_1 \tan \theta_1}{l_2 \tan \theta_2} = \frac{1 \tan 2\theta_2}{2 \tan \theta_2} = \frac{1}{2} \frac{2 \tan \theta_2}{(1 - (\tan \theta_2)^2) \tan \theta_2} \\ &= \frac{1}{1 - (\tan \theta_2)^2} \end{aligned} \quad (3-10)$$

Note that both ratios in equations (3-9) and (3-10) are only functions of θ_2 and do not depend on the angle the bar makes with horizontal line. Moreover, as depicted in Figure 3-32, the location of point P can be anywhere on the circle with radius \overline{OM} whose center is at M.

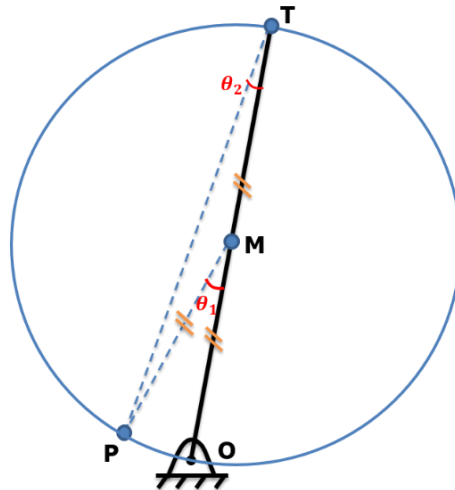


Figure 3-32: Importance of the position of point P to the analytical solution. As long as the point P is located on the blue circle, both equations (3-9) and (3-10) are valid.

The ratios between the axial forces and forces themselves are plotted in Figure 3-33 as θ_2 varies between 0 to 40 degrees. It can be observed that for small angles ($\theta_2 < 20^\circ$) the ratio between the axial forces is almost one (less than 1.15)(Table 3-9). This means that for small angles, whether F_1 (representing local muscles) or F_2 (representing global muscles) is maintaining the balance of the bar, the axial force at L5-S1 (point o in Figure 3-31a) will not be very different. This links with the small increase (32%) observed at the caudal adjacent segment when lumbar muscles were damaged.

However, the difference between case 1 and case 2 is that in case 1, the axial force ($F_2 \cos \theta_2$) is applied all over the bar whereas in case 1, the axial force ($F_1 \cos \theta_1$) starts from the middle of the bar. Therefore with L1-L2 being located above the middle point, in case 1 there is no axial force on L1-L2, whereas in case 2, the axial force by F_2 is applied on L1-L2. This explains the observed larger axial force at the rostral adjacent level (73%).

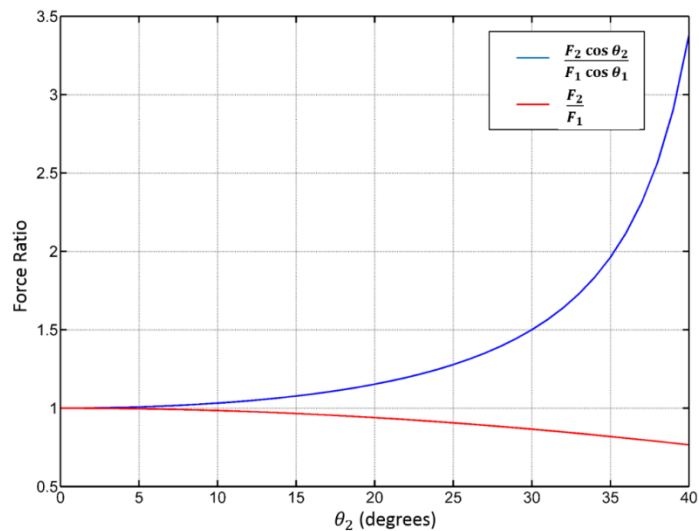


Figure 3-33: The ratios of muscle forces and their axial components between case 1 and case 2 as a function of θ_2 .

Table 3-9: The ratios of muscle forces and their axial components between case 1 and case 2 for three different values of θ_2 .

	$\theta_2 = 10^\circ$	$\theta_2 = 20^\circ$	$\theta_2 = 30^\circ$
$\frac{(F_2)_{axial}}{(F_1)_{axial}}$	1.03	1.15	1.5
$\frac{F_2}{F_1}$	0.98	0.94	0.86

To the best of my knowledge, the effect of muscle damage on spinal loading has not been investigated previously. One study investigated the effect of muscle damage on muscle activations pattern, but did not report on spinal loading [102]. In that study, Bresnahan *et al.* [102] used the model developed by de Zee *et al.* [139] and simulated the muscle damage by successively reducing the CSA of the damaged muscles at L3-L5 by 10%, 30%, and 40% from all posterior muscles (multifidus, LTpL, ILpL, LTpT, ILpT). They observed that accordingly, the activation of erector spinae muscle changed in flexion-extension and lateral bending, but the change was largest in axial rotation. However, they did not measure the spinal loads; and intervertebral disc stiffness, ligaments, and muscle force-length and force-velocity curves were not incorporated in their model.

Muscle force-length curves and nonlinear stiffness of the FSU were implemented in our model. Also, the motions of the lumbar vertebrae were not predefined as a function/fraction of the total lumbar spine motion, which was done in the studies by de Zee *et al.* [139], Han *et al.* [149], and Christophy *et al.* [1]. This feature allowed each vertebra to move independently and was necessary for modeling the rigid fixation, which would alter the motion function. Finally, in contrast to Bresnahan [102], in our model muscle damage was simulated by detaching the injured fascicles rather than uniformly reducing the CSAs of all posterior muscles. Detaching muscles led to nonuniform reduction in CSAs of posterior muscles and varied between levels

(see Figure 3-27). Despite these strengths, our model had some limitations that are needed to be improved in future.

3.4.1 Limitations

3.4.1.1 Solution Method

One major limitation of our model was high sensitivity of the spinal forces to kinematic inputs. The solution method was based on following the trajectories of two target points. Due to high stiffness of the spine along the axial direction (y axis), even 1 mm change in input trajectories of the target points could lead to substantial changes in spinal forces. For example, for normal standing, the axial force at L4-L5 would change from 984 N to 1285 N or 1630 N, if y component of the target position was specified 1 or 2 mm lower than its original position, respectively. However, 1 mm change in x or z coordinates of the target position did not result in more than 15 N changes in axial forces. This implies that sub-millimeter accuracy in kinematic inputs, especially for y component, is needed for this method to correctly calculate spinal forces.

Non-invasive *in vivo* kinematic data with such an (sub-millimeter) accuracy has been measured for other joints of the body including knee [240], shoulder [204], and cervical spine [241], but is very challenging to be obtained for the lumbar spine due to the large amount of paraspinal soft tissues [242]. Even if such accurate kinematic data is provided, patient specific models are required to utilize that, as translation of the kinematic data to a generic model like ours would again add errors. For the purpose of current study we manually assigned input target positions. However, the issue of high sensitivity of the solution method to the y component of target positions should be solved in future studies, which can be done by modifying the solution

method to only track the angular motion of the vertebrae, instead of tracking the position of target points.

Another issue with the current solution method was that even in static analysis, the position where the model ended up staying at time step k (\mathbf{q}_{model}^k) was different from the prescribed (desired) position at that time step ($\mathbf{q}_{desired}^k$). See section 3.2.2 for details about \mathbf{q}_{model}^k and $\mathbf{q}_{desired}^k$. Also, the difference between the two positions $|\mathbf{q}_{model}^k - \mathbf{q}_{desired}^k|$, which we define as “kinematic error”, would increase whenever more contribution of muscles was needed. For example, when the model was standing without holding any weight, the kinematic error was less than 0.2, whereas when the model was holding the 190 N crate, which required larger muscle forces, the kinematic error of less than 1 cm could not be achieved. This appears to have root in the way the optimization solver is set in ArtiSynth.

As described in section 3.2.2, at each time step the solver minimizes the total cost function ϕ , rather than each of the cost functions ϕ_1 , ϕ_2 , and ϕ_3 . For static analyses, ϕ_3 easily becomes zero, as the difference between activations of two consecutive time steps would be zero in convergence. The other two cost functions, however, do not become zero. While ϕ_1 has the potential of getting to zero, ϕ_2 does not, as it is the sum of squared muscle activations and zero muscle activations equals falling down of the model. Since the solver does not minimize each of these cost functions separately, there is always a balance between ϕ_1 and ϕ_2 , and hence a bit of kinematic error when ϕ_1 is not zero. For cases of heavy tasks (such as holding a heavy crate), where larger muscle activations are needed, in favor of finding smaller set of activations to minimize ϕ_2 , the solver compromises ϕ_1 and hence the kinematic inaccuracy increases. This explains why for when holding a crate of 190 N, less than 1 cm accuracy could not be achieved.

Improving the kinematic accuracy could be obtained by giving more weighting (w_1) to ϕ_1 in cases of heavy tasks, but such manipulation is not desired (i.e. it is not desired that the user of the model constantly changes the weighting terms for different loading scenarios).

An ideal solution method would be to first find (filter) those sets of muscle activations that make ϕ_1 equal to zero, and among them find the set of muscle activations that has minimum sum of squared muscle activations. This might slow down the solution method, but tackles the current issue.

Those models that use inverse dynamics [138] do not face this issue as in those models the kinematics are not affected by the calculated forces, rather are used for calculation of joint torques. The joint torques are then distributed between the muscles through optimization. Therefore, optimization has no influence on kinematics; whereas in models using forward dynamics solvers, the muscle forces calculated from the optimization are fed to the solver and kinematics are produced as results (Figure 1-28), therefore the optimization influences the kinematics.

Our study design was set out so that the results were not affected by the two aforementioned issues. First of all, we only considered static conditions. Secondly, in each scenario, we prescribed the same target position for the healthy and the injured models. Not only the prescribed positions ($q_{desired}^k$) were the same, but also, the final positions of the targets (q_{model}^k) were not any different than 0.06 mm along z and y directions and 0.1 mm along x direction from each other. Such a difference could hardly result in more than 25 N errors in spinal forces. This way, we made sure that the results were not affected by the input target positions and hence the observed changes in loadings at the adjacent levels can only be attributed to removal of the

muscles. Note that we did not study the effect of adding fixation on loading, since adding a fixation would change the geometry of the model. Therefore, assigning the same target positions for the models with and without the fixation, would not necessarily reflect the effect of adding fixation, rather, the input positions could play a role.

Although our model was able to produce spinal loads with similar ratios to the study by Wilke *et al.* [151], those ratios were dependent on the target positions. This means we could have set the input positions of the targets one millimeter lower and obtain larger forces than what was reported. Therefore, a comprehensive validation of the model could not be performed before solving the current issues we experience with the solver. In future studies, once the issues are solved, extensive validation of the model is expected, which can be in form of making comparisons between the estimated muscle forces and activation pattern with other studies and/or EMG data. Nonetheless, it should be noted that the purpose of current study was not to estimate the exact spinal loads, rather the focus was on studying the possible effect that iatrogenic muscle damage, as a surgical parameter, can have on spinal loading.

3.4.1.2 Geometrical Model /Mechanical Properties

As in other musculoskeletal models, there were some assumptions and limitations in construction of our geometrical model. Muscles were modeled as straight lines between their attachment points. Although for multi-segmental muscles, use of MultiPointMuscles enabled following the curvature of the lumbar spine, simulation of muscle damage by removing one of the attachment points and connecting the remaining points deviated those muscles from the curvature of the lumbar spine (Figure 3-21). This affects the moment arms of those muscles and can influence the spinal loads [243][142]. Using wrapping surfaces could help solve this issue, but unfortunately

they are not currently available in ArtiSynth. Other software packages such as OpenSim use wrapping surfaces to ensure physiological lines of action. However, wrapping surfaces have some limitations. They are mathematically involved and hence increase computational expenses [244]. Also, in some cases the muscles have been reported to jump off the wrapping surfaces leading to sudden drastic changes in muscle moment arms and consequently muscle forces [244].

Tendons were assumed to be rigid in our model; however, this may not influence the results much. The study of Millard *et al.* [92] on a benchmark problem revealed that the amount of error in normalized muscle force associated with rigid-tendon assumption depended on the ratio of tendon slack length to muscle optimal fiber length ($\frac{l_s^T}{l_M^T}$). While for $\frac{l_s^T}{l_M^T} < 2$ the error was less than 10%, it could reach to values of about 20% and 40% for ratios of 5 and 10, respectively. The ratio for the majority of muscle fascicles in our study was less than 2. Less than 10 muscle fascicles (mainly in ILpL and LTpT muscle groups) had ratios of about 3. Therefore the overall error due to rigid tendon assumption should not exceed 10% in our model.

For the stiffness of the FSU, only diagonal terms of the FSU stiffness matrix were implemented in our model. We selected the rotational stiffness terms from the study by Heuer *et al.* [224]; as they had not measured the translational stiffness, we used the translational stiffness terms of the stiffness matrix proposed by Gardner-Morse *et al.* [220]. Such a combination is not ideal and was due to the scarcity of the literature on the lumbar spine stiffness matrix. We did not use the rotational stiffness from Gardner-Morse's study, as in their experiment the displacements for measurement of the stiffness were very small. Moreover, the rotational stiffness terms in their study were too large. For example, based on the stiffness term of their study, 2.5° flexion of the

FSU requires 25 Nm flexion moment, whereas 2.5 Nm is enough for such a rotation according to the stiffness reported by Heuer *et al.* [224] or other cadaveric studies [222][245] (see Figure 3-4).

Christophy *et al.* [1] studied the effect of neglecting the off-diagonal terms of the stiffness matrix on muscle forces. They created two simple models, each having four muscle fascicles: two rectus abdominis (flexors) and two erector spinae (extensor) fascicles. One model only used the diagonal terms, while the other used the full stiffness matrix of Gardner-Morse *et al.*'s study [220]. They observed that for a sinusoidal motion of 10° flexion-extension, the muscle forces were dramatically different between the two models. While this signifies the importance of considering off diagonal terms, such a dramatic change, however, can be due to the very large terms of the stiffness matrix that they have used, and might have not been observed if a more reasonable stiffness matrix was used. As mentioned, the data on lumbar spine stiffness matrix is rare and therefore true effect of off-diagonal terms on muscle forces and consequently spinal loading remains to be further investigated in future.

3.4.1.3 Study Design

The current study only simulated the muscle damage at three vertebral levels (L2-L5). Also, the fusion and fixation were assumed to be rigid. Investigation of the effects of other lengths and levels of muscle damage and also the effect of fixations with different stiffness are of high interest to the clinicians and will be the focus of our future studies.

Chapter 4 Discussion and Conclusion

The etiology of adjacent segment degeneration (ASD) after spinal surgery is clearly complex and likely multifactorial. It is a challenging topic with some questioning the existence of ASD, alternatively suggesting that any observed degenerative changes adjacent to a spinal fusion are merely the natural history of that intervertebral segment independent of any surgical intervention [75][72][70]. The absence of consensus on this point makes studying its etiology very challenging. However, given the preponderance of literature on the topic and the frequent presentation of symptomatic adjacent segment disease, it seems likely that ASD does exist to some degree.

With respect to its etiology, the predominant hypothesis is that ASD is due, at least in part, to biomechanical changes within the instrumented segments and at the adjacent vertebral levels. It certainly seems reasonable that a spinal fusion would alter the loading patterns and/or the manner in which the spine moves and that some form of degenerative changes might result. However, interestingly, this has never been proven conclusively. There is a vast body of *in vitro* literature that describes adjacent segment changes at the remaining unfused lumbar spinal motion segments. As the review by Volkheimer *et al.* [159] demonstrates however, these studies are based upon assumptions that are either false or unproven.

The requirement for fusion of a segment of the lumbar spine for degeneration is of itself an indication of the extent of the degenerative process that affects most or all lumbar segments in that individual. It is unknown how the biomechanical alterations associated with an adjacent fusion may influence the degenerative process within the unfused segments; either by accelerating disc collapse, or by inducing hypermobility orolisthesis at these adjacent levels.

In an endeavor to shed more light on etiology of ASD, the objective of this thesis was to biomechanically analyze a mechanism and a factor that can alter the loading at the adjacent level and result in accelerated degeneration: the mechanism was adjacent segment hypermobility and the factor is iatrogenic muscle damage.

4.1 Summary of Thesis Results

A systematic review and critical analysis of all *in vivo* studies that investigated kinematics of the segment adjacent to a lumbar spine fusion was conducted to search for evidence of hypermobility at the adjacent levels. While none of the studies observed any hypermobility at the caudal adjacent level, increased ROM for the rostral adjacent segment was reported in 10-30% of the patients. To investigate the role of iatrogenic muscle damage on loading at the adjacent levels, a 3D musculoskeletal model of the lumbar spine with detailed muscle architecture was developed. Iatrogenic muscle damage was simulated by removal of certain fascicles that are intraoperatively resected from the posterior elements. By removal of those muscles from the model, the axial intervertebral forces were predicted to increase at both adjacent levels during neutral standing, with larger increases at the rostral level (73% for the rostral and 32% for the caudal adjacent segment); the effects of removal of muscles were even more pronounced in the presence of a rigid fixation (78% for the rostral and 41% for caudal adjacent segments). The results of both studies implying higher susceptibility of the rostral adjacent level to disc degeneration is in harmony with clinical prevalence of ASD occurring in 70 to 100% of the cases at the rostral level [238][239] [171] [51][5].

4.2 Evidence for Association of ASD and Iatrogenic Muscle Damage: Comparison between the Outcomes of Different Surgical Approaches

4.2.1 Minimally Invasive (MI) surgeries

In non-comparative studies a lower incidence of ASD is reported for minimally invasive (MI) surgeries. In a prospective investigation of 304 patients undergoing MI TLIF (12 at two levels and the rest at one level), only 6 patients (2%) required reoperation for development of ASD. In a retrospective study of 63 patients receiving single-level fusion through MI ALIF followed by percutaneous pedicle screw fixation (PPSF) progression of ASD was observed in 6 patients (9.5%) at five years follow-up, but was symptomatic only in two (3.2%) of them. Similarly, nine out of 103 (8.7%) of the patients of the retrospective study by Bae *et al.* [246], who were treated either by ALIF or TLIF followed by PPSF, developed radiographic ASD at three years follow up, of which 1.9% (2/103) were symptomatic. The rates of ASD for DLIF were a bit higher. Two studies investigated development of ASD in patients who underwent DLIF. In the prospective study by Pimenta *et al.* [247], 30 patients with DDD were treated through DLIF at L4-L5. After three years, four out of total 30 patients (13%) needed reoperation due to ASD. Rodgers *et al.* [248] also prospectively followed 283 patients who underwent DLIF (206 one-level, 56 two-level, 19 three-level, and two four-level). At two years follow up, 22 patients (7.8%) required reoperation due to ASD.

Although lower incidence of ASD is reported for MI surgeries, it must be noted that the definition of ASD, especially the radiographic ASD, varies to a great deal between studies, which is probably one of the reasons for the wide range of 5.2-100% reported for incidence of radiographic ASD in the literature. Different definitions for ASD can mask the results and lead to incorrect conclusions when comparing studies. Therefore, comparative studies, where the

patients with different treatments are assessed by one observer, are necessary to better investigate the effect of iatrogenic muscle damage or any other biomechanical factors on development of ASD.

4.2.2 Open vs. MI Surgeries

To date only two studies, which both are retrospective, have compared the incidence of ASD between open TLIF and MI TLIF; neither found a significant difference between two groups with respect to symptomatic ASD. In the study by Seng *et al.* [249] 80 patients with single level fusion (40 with open TLIF and 40 with MI TLIF) were paired matched for their age, sex, BMI, and the levels of fusion. After five years, the incidence of symptomatic ASD in both groups was 10% (four patients in each group). In the study by Yee *et al.*[5], 52 patients underwent MI TLIF and 16 had open TLIF. All patients received single-level fusion with L4-L5 being the most common fusion level. With minimum follow up of six months (while 75% had longer than 16 months follow-up), seven patients (10%) developed symptomatic ASD: four patients from open TLIF and three from MI TLIF group.

In a recent study by Radcliff *et al.* 2014 [250], 53 patients underwent single or double level ALIF, with 23 patients instrumented by PPSF and 30 patients receiving posterior instrumentation through open surgery. The rate of reoperation for ASD in both groups was 30% (9/30 in open and 7/23 in MI ALIF group).

Although symptomatic ASD was reported to be the same between MI and open surgeries, none of the studies investigated the rate of radiographic ASD. More comparative studies are required to investigate the effectiveness of MI surgeries with regard to both symptomatic and radiographic ASD.

4.2.3 ALIF vs. PLIF

As in ALIF, in contrast to PLIF, posterior muscles are intact a comparison between the two approaches can be related to role of muscles. We found only one comparative study between ALIF and PLIF regarding incidence of ASD in the literature. Min *et al.* [239], retrospectively studied 48 patients with preoperative spondylolisthesis and minimal ASD, who received fusion at L4-L5: 25 through ALIF with PPSF and 23 through instrumented PLIF. Although only two patients in PLIF group needed reoperation due to symptomatic ASD, the rate of radiographic ASD was high in both groups and was substantially (two-times) more in PLIF than ALIF group: 44% (11/25) in ALIF and 82.6% (19/23) in PLIF. This implies sparing of posterior muscles in ALIF method may have been the reason. However, lower rate of ASD in ALIF can also be attributed to the role of laminectomy that was performed in PLIF and not in ALIF. Liu *et al.* [251] observed that among the patients receiving fusion at L4-L5 the rate of radiographic ASD was significantly higher in patients with full laminectomy than those who had similar surgery with semi-laminectomy or only facetectomy. Therefore, possible role of other iatrogenic soft and hard tissue damages should be considered when contrasting surgical approaches for determining the role of iatrogenic muscle damage in degeneration of adjacent segment.

4.3 Evidence for Association of ASD and Adjacent Segment Kinematics: Comparison between Fusion and Motion Preserving Implants

4.3.1 Fusion vs. TDR

Among the seven comparative studies between fusion and TDR on kinematics of the adjacent segment, only one study investigated prevalence of radiographic ASD. In a prospective RCT study by Zigler *et al.* [161], 123 patients receiving single-level Pro-disc L and 43 patients with single-level circumferential fusion were included. Loss of disc height, end plate sclerosis,

osteophytes, and spondylolisthesis were included for definition of Radiographic ASD in a way that each of these parameters was assigned grades based on their severity, and their average was used to determine the overall grade of radiographic ASD. After five years follow up, 9.2% of TDR patients and 28.6% of fusion patients developed radiographic ASD. The incidence of radiographic ASD in patients that had not pre-existing degeneration was 6.7% and 23.8% for TDR and fusion groups, respectively. Interestingly, neither translational nor rotational ROM had changed at the proximal level for either of the groups after five years follow-up. This indicates that the degeneration may not be related to kinematics of the adjacent segment. Instead, other characteristics of TDR including its surgical approach may associate with its lower degeneration rate. In contrast to a circumferential fusion, TDR is inserted from an anterior approach, through which integrity of posterior elements and spinal muscles are not disrupted. It is noteworthy that incidence of symptomatic ASD, however, was low and not different between the two groups (1.9% in TDR and 4% in fusion patients).

In addition to Zigler *et al.* [161], one more group investigated symptomatic ASD between TDR and fusion groups. Similarly, in their study the rates were low and not much different between TDR and fusion (1.1% for TDR and 4.6% in fusion).

4.3.2 Fusion vs. Dynamic Implants

Among the studies that reported kinematics of the segment adjacent to a dynamic implant, only one study investigated ASD, which was a comparative study. In the study by Liu *et al.* [192], 67 patients received PLIF at L5-S1, 25 of whom received an additional ISDD (either Coflex or Wallis) at the adjacent level. With mean follow up of 24 month, neither radiographic nor symptomatic ASD was observed in any of the groups. However, the ROM increased in fusion

group, whereas it did not change in flexion and even decreased in extension for the group with an additional ISDD.

Although the studies comparing fusion versus motion-preserving implants are very few and more studies are needed to make a conclusive remark, with current evidence, it appears that adjacent segment hypermobility may not be the driving factor in development of radiographic ASD, or at least it does not show an association with it.

4.4 Fusion and Loss of Disc Height

Loss of disc height is one of the most frequently criteria used for assessment of disc degeneration [45]. A recent study of four European RCTs that compared fusion versus non-operative care of patients with chronic low back pain revealed interesting results on loss of disc height [45]. The study involved 369 patients (272 fusion and 97 conservative treatment) with mean follow up of 13.1 years (7-22 years). The surgical treatment for 52% of the patients was instrumented posterior fusion, 16% posterior fusion with no instrumentation, 25% circumferential fusion (ALIF/TLIF), and 7% received dynamic stabilization devices.

In both fusion and conservative treatment groups the disc heights of the rostral adjacent segment and the two IVDs above it decreased significantly at long term follow-up. Interestingly, the reduction in disc heights of the adjacent disc and one level above was significantly more in fusion group than the conservative treatment group. However, the difference in disc height was not associated with patients' back pain or disability. Moreover, they found that loss of disc height was correlated with the number of fusion levels, while it had no correlation with the type of fusion.

That the significant difference in loss of disc height between the fusion and conservative treatment groups was not associated with any difference in level of pain or disability implies that the effects of biomechanical factors on ASD may be better manifest in rates of radiographic rather than symptomatic ASD. For example, in order to find clinical evidence for whether iatrogenic muscle damage increases the loading at the adjacent level and accelerate the degeneration, rates of radiographic rather than symptomatic ASD should be compared between open and MI surgeries. This explains why almost all comparative studies between MI and open surgeries found similar rates for symptomatic ASD [5][249][250]. Unfortunately, none of them investigated radiographic ASD. Radiographic ASD was studied only in one comparative study between ALIF and PLIF [239], which showed two times higher rate of radiographic ASD for PLIF group supporting our findings that muscle-sparing approaches may result in less alteration of loading at the adjacent level and hence, lower rate of radiographic ASD.

Among the studies that investigated kinematics of the segment adjacent to a fusion, loss of disc height was not associated with adjacent segment hypermobility. In the study by Seitsalo *et al.* [71], 22% of patients developed retrolisthesis and 31% had more than 50% loss of height after an average follow-up of 15 years (minimum 6 years); only 2% of them had both retrolisthesis and more than 50% loss of disc height. Similar observation was noted in the study by Nakai *et al.* [160]. In a prospective study, while the patients with instrumented fusion showed increased ROM at the rostral adjacent segment, the height of adjacent disc remained unchanged [176]. Similar observation was reported by Berg *et al.* [182]. Kaito *et al.* [74], divided the patients who had all received instrumented PLIF into two groups: one group with either radiographic or symptomatic ASD, and the other group with no ASD. Postoperatively, while the ROM did not differ between two groups, the group with ASD had significantly smaller disc height at the

adjacent level. This is while preoperatively there was no difference in disc height or ROM between the two groups. These results suggest that there seems not to be a firm association between increased ROM and loss of disc height.

4.5 Study Strengths and Limitations

4.5.1 Strengths

The focus of the current study was to provide insight into two biomechanical factors that may be associated with ASD. Considering the limitations of *in vitro* studies for studying adjacent level effects, we searched for *in vivo* evidence of kinematic changes at the adjacent level in the literature. In an attempt to be as inclusive as possible, a systematic search with various keywords were conducted to find any study that had addressed kinematics of the segment adjacent to a lumbar spine fusion or any types of spinal implants. The abstract and if necessary the full text of the 697 identified articles were inspected to find the relevant studies. Care was taken not to include studies that had only investigated the relative ROM as changes in relative ROM does not necessarily correlate with changes in absolute ROM and hence altered spinal loading to be linked with ASD. To find possible risk factors for adjacent segment kinematic changes, age, type of surgery, levels of fusion, length of fixation, initial diagnosis, and length of follow up of all the studies were provided and summarized in Table 2-1 to Table 2-3, though due to too much heterogeneity of the studies and not enough number of the studies a firm conclusion with regard to the risk factors could not be made.

The effect of iatrogenic muscle damage on spinal loading was studied using a musculoskeletal model of the lumbar spine. To the author's knowledge, this has not been previously investigated in the literature. A physiologically and anatomically detailed musculoskeletal model of the

lumbar spine was developed using ArtiSynth. Muscle parameters necessary for a full Hill type musculotendon actuator including the pennation angle and tendon length along with muscle force-length relation were incorporated in this model. Our model was validated by reproducing similar maximal extension moments to those produced by the subjects of the study by Daggfeldt *et al.* [12]. In their study, subjects' average maximum extension moments about L5-S1 joint were 180 Nm in 10° extension and 240 Nm for 10° flexion, respectively. Similarly, our model predicted smaller maximal extension moment in 10° extension (164 Nm) than 10° flexion (246 Nm). The difference in maximum extension moment between the flexion and extension postures is due to muscle force-length relation [12]. Models that do not include the muscle force-length relation predict higher moments in extension than flexion [252]. The reason is that the spinal muscle moment arms are larger in extension [12][252]. Therefore, higher maximum extension moment should be expected in extension than flexion when force-length relation is not considered.

The limitation of bushing elements for modeling the stiffness of the FSU was considered and tackled in our model by defining a new type of element we named OffsetFrameSpring. With OffsetFrameSpring, full stiffness matrix of the FSU measured from the experimental studies could be modeled, which is necessary for modeling the coupled motion of the spine.

Current lumbar spine models in AnyBody and OpenSim distribute the total lumbar spine motion between the lumbar vertebrae by a predetermined function. In our model each lumbar vertebra can move independently. This enables studying the effect of different motion patterns and kinematic changes of the adjacent segment on spinal loading in addition to easier simulation of fusion and fixation. Finally, with ArtiSynth being able to solve FEM and multibody dynamics together, our base model has the potential of being extended to a combined FEM and multibody

dynamic model for further biomechanical investigations such as assessing the intervertebral disc pressure, stresses, or strains.

4.5.2 Limitations

4.5.2.1 Review Study

While translational ROM links with spinal shear loads, the angular ROM is related to applied moments on the spine. In our review of adjacent segment kinematics we did not separately analyze the studies that reported on translational versus angular ROM. On the other hand, the kinematics measured in most of the studies were 2D, taken through static planar radiographs, and at the end of a motion; while studies that captured continuous motion of the vertebrae through videofluoroscopy, observed both out-of-plane and nonlinear motion pattern of the adjacent segment [162]. Such kinematic data, especially when used as input to spine musculoskeletal models, may provide insight on changes in loading pattern at the adjacent levels. Therefore, a move toward more accurate 3D kinematics of the adjacent segments would be helpful in shedding more light on our understanding of adjacent segment kinematics and other biomechanical changes at that level.

The threshold for instability differed between studies and ranged between 3-4.5 mm for translation [160][161] and 8-15 degrees for angular change[160][57]. In most of the studies reporting on flexion-extension ROM, patients were asked to naturally flex and extend as much as they could while sitting [51][48][187][188] or standing [160][71][44][190][175]. In some cases patients were assisted by leaning against a table [71], wrapping their arms around their knees [166] or using support bars [48]. Also in some cases patients were lying supine or prone [182][187][174][50] or in the lateral decubitus position [57][166]. These in addition to

differences in patients such as initial diagnosis, type of surgery, and length of fixation add to the heterogeneity of the studies, making the comparison between studies and identifying potential parameters influencing the kinematic changes at the adjacent levels difficult.

The number of studies comparing the association of ASD and adjacent segment kinematics are very few. Such studies are necessary to assess whether development of ASD is due to hypermobility of the adjacent segments to justify the use of motion preserving implants instead of fusion. With respect to the effectiveness of dynamic implants and TDR in prevention of adjacent segment kinematics and/or ASD, the data in the literature is rare and more RCT studies and longer follow ups are required.

4.5.2.2 Musculoskeletal Modeling

The limitations of musculoskeletal modeling consist of general challenges for *in vivo* load measurements and some limitations that are specific to models. *In vivo* loads needed for validation of the models are difficult to obtain. Recently, telemetrized spinal fixation [253] or vertebral body replacement [150] have provided invaluable information on *in vivo* spinal loads. However, these devices are inserted in patients who undergo invasive surgeries, where substantial morbidity are caused to both their hard and soft tissues. More importantly, these devices only measure some portions of the spinal loads [254]. In fact, the load sharing between these devices and posterior/anterior elements of the spine has been shown to vary at different postures and motions [255]. Similar limitations exist with intradiscal pressure [245]. Lastly, *in vivo* measurement of muscle forces are not feasible. Muscle activations, which are recorded through electromyography, does not necessarily correlate linearly with muscle forces [256]. Moreover, despite complex anatomy of the lumbar spine, electromyography is usually recorded

for a few superficial muscles, whereas even within the same muscle, deep fibers are activated differently than superficial ones [257]. These limitations keep modeling and validation of the lumbar spine models challenging to date.

There are some limitations specific to our model. The solution method for estimation of the muscle forces in our model was based on tracking the trajectories of two target points. Due to spine's high stiffness, especially along the axial direction, even a millimeter change in target trajectories could substantially affect the predicted spinal forces by our model. Also with the current optimization method utilized in ArtiSynth, the final position of our model differed from the desired prescribed target position and the difference between these two positions was dependent on the amount of muscle activations. These issues limited both the study design and validation of our model. Our model was able to produce the same ratios as those between the *in vivo* measured intradiscal pressure of the study by Wilke *et al.* [151]; however, the ratios could change in our model by changing the target positions. Our study design was also affected by the solution method limitations. We could not investigate the effect of adding fixation on spinal loading independently, as adding a fixation would change the geometry of the model. Therefore, assigning the same target positions for the models with and without the fixation, would not necessarily reflect the effect of adding fixation, rather, the input positions could play a role.

Once the aforementioned issues are solved, accurate *in vivo* kinematic data are still required for correct estimation of spinal loads. Skin-mounted reflective markers cannot accurately measure the lumbar spine motion [162], rather medical imaging should be used. However, due to the large amount of the surrounding soft tissues, obtaining the dynamic motion of the lumbar spine would be limited by the trade-off between the duration of patients' activity (i.e. time of radiation exposure) and level of kinematic accuracy (i.e. intensity of radiation).

Muscle activations pattern estimated by our model were not contrasted against any experimental EMG data. The EMG patterns differ between individuals and between different trials [136]. Therefore it would be ideal to simultaneously record EMG activations of spinal muscles during measurement of kinematics through medical imaging. The kinematic data can serve as the input to the model and the EMG data could be used for validation of the optimization solver in prediction of muscle forces for that experiment. However, to our knowledge such a data is not provided in the literature.

The effect of muscle damage on spinal loading at the adjacent levels was studied in our model only for when three vertebral levels were treated (L2-L5). We did not explore the effect of other lengths and extent of muscle damage on spinal loads. Also, only the effect of iatrogenic detachment of muscles, which is evident right after the surgery was investigated. Muscle atrophy or reduction of muscle cross sectional areas, which are observed at long term follow ups were not simulated. The effect of muscle damage on spinal loads at the adjacent levels was more pronounced in the presence of a rigid spinal fixation. This implies that low-stiffness spinal fixation may lead to lower forces at the adjacent levels; however, such an effect was not investigated in our study.

The stiffness of the FSU for all vertebral levels was assumed in our model to be equal, whereas it differs between the vertebral levels. For instance, most terms of the stiffness matrix were significantly different between the L2-L3 and the L5-S1 FSU in the study by Gardner-Morse *et al.* [220]. Also in their study the stiffness terms were dependent on the compressive preload and increased by that, while in our model we assumed constant stiffness for all compressive forces. Finally, due to the scarcity of *in vitro* studies on the stiffness of the FSU, we were not able to include the off-diagonal terms of the FSU stiffness matrix in our model. We did not use those

terms from Gardner-Morse *et al.*'s study [220], as the angular displacement in their study for measurement of spinal stiffness were too small. This way the coupled motion of the lumbar spine was not considered in our model.

4.6 Future Work and Conclusions

4.6.1 Future Work

Considering that the mobility of the adjacent segment has been reported to depend on length of fixation [52][166], type of surgery [175][179], and patient factors, stricter inclusion criteria for more homogenous patient population is needed for future studies to be able to identify the involved parameters in increased ROM of the adjacent segment. Also given that between 10-30% of the patients experience increased ROM at the rostral level, future studies should be focused on that portion rather than the average of the population, to investigate their susceptibility to development of ASD.

Future work for improvement of the model should be focused on addressing its current limitations. The first priority is to modify the solution method so as to circumvent the model's high sensitivity to target trajectory. This can be achieved by tracking only the angular motion of each vertebra instead of following a target point trajectory. Also a modification of the optimization method is desired so that the difference between the final position of the model from the prescribed target position is not dependent on the amount of muscle activations. Once the aforementioned limitations are solved, an extensive validation of the model is expected. Recently, *in vivo* data measured from telemetrized spinal fixation and vertebral body replacement are collected for various activities [258][259][260]. The data from these studies could be used for extending the validation of the model to body postures other than upright

standing and even dynamic activities. Such validation paves the way for investigating the effect of muscle damage and other surgical parameters such as length of fixation and implant stiffness on spinal loading during various daily tasks.

4.6.2 Conclusions

With reference to the objectives of this thesis, it can be concluded that:

- 1a) The majority of *in vivo* studies do not see an average change for the rostral adjacent segment ROM after fusion;
- 1b) The rostral adjacent segment ROM increases above a pre-determined benchmark for 10-30% of the patients after fusion;
- 1c) No change was observed in the ROM at the caudal adjacent segment after fusion;
- 1d) ROM of the total lumbar spine appears to decrease after fusion;
- 1e) There appear to be fewer adjacent segment changes after non-fusion implants than after fusion, but more data and longer follow-up is needed.
- 2a) Iatrogenic damage to spinal muscles, which is common in open posterior fusion surgeries, increases the axial force at both adjacent levels, more substantially at the rostral level.
- 2b) The effect of iatrogenic muscle damage on loading at the adjacent levels is amplified in the presence of rigid fixation.

The long term goal of this research is to understand the possible biomechanical factors that can accelerate degeneration of the adjacent disc. Once significance of those factors is identified, they can be used for optimized surgical planning regarding the type of implants, surgical approaches,

and other surgical parameters such as stiffness and length of fixation to minimize the likelihood of ASD.

Bibliography

- [1] M. Christophy, N. A. Faruk Senan, J. C. Lotz, and O. M. O'Reilly, "A musculoskeletal model for the lumbar spine.," *Biomech. Model. Mechanobiol.*, vol. 11, no. 1–2, pp. 19–34, Jan. 2012.
- [2] S. S. Rajaei, H. W. Bae, L. E. A. Kanim, and R. B. Delamarter, "Spinal fusion in the United States: analysis of trends from 1998 to 2008," *Spine (Phila. Pa. 1976)*, vol. 37, no. 1, pp. 67–76, 2012.
- [3] D. Y. Lee, S.-H. Lee, and D. H. Maeng, "Two-level anterior lumbar interbody fusion with percutaneous pedicle screw fixation: a minimum 3-year follow-up study," *Neurol. Med. Chir. (Tokyo)*, vol. 50, no. 8, pp. 645–650, 2010.
- [4] G. Cheh, K. H. Bridwell, L. G. Lenke, J. M. Buchowski, M. D. Daubs, Y. Kim, and C. Baldus, "Adjacent segment disease following lumbar/thoracolumbar fusion with pedicle screw instrumentation: a minimum 5-year follow-up," *Spine (Phila. Pa. 1976)*, vol. 32, no. 20, pp. 2253–2257, 2007.
- [5] T. J. Yee, S. W. Terman, F. La Marca, and P. Park, "Comparison of adjacent segment disease after minimally invasive or open transforaminal lumbar interbody fusion.," *J. Clin. Neurosci. Off. J. Neurosurg. Soc. Australas.*, 2014.
- [6] N. Miyakoshi, E. Abe, Y. Shimada, K. Okuyama, T. Suzuki, and K. Sato, "Outcome of one-level posterior lumbar interbody fusion for spondylolisthesis and postoperative intervertebral disc degeneration adjacent to the fusion," *Spine (Phila. Pa. 1976)*, vol. 25, no. 14, pp. 1837–1842, 2000.
- [7] F. H. Netter, *Atlas of human anatomy*. Elsevier Health Sciences, 2010.
- [8] A. A. White and M. M. Panjabi, *Clinical biomechanics of the spine*, vol. 446. Lippincott Philadelphia, 1990.
- [9] N. Bogduk, *Clinical anatomy of the lumbar spine and sacrum*. Elsevier Health Sciences, 2005.
- [10] K. L. Moore, A. F. Dalley, and A. M. R. Agur, *Clinically oriented anatomy*. Lippincott Williams & Wilkins, 2013.
- [11] S. Standring, H. Ellis, J. C. Healy, D. Jhonson, A. Williams, and P. Collins, "Gray's anatomy: the anatomical basis of clinical practice," *Am. J. Neuroradiol.*, vol. 26, no. 10, p. 2703, 2005.

- [12] K. Daggfeldt and A. Thorstensson, "The mechanics of back-extensor torque production about the lumbar spine," *J. Biomech.*, vol. 36, no. 6, pp. 815–825, Jun. 2003.
- [13] G. B. J. Andersson, "Epidemiological features of chronic low-back pain," *Lancet*, vol. 354, no. 9178, pp. 581–585, 1999.
- [14] J. N. Katz, "Lumbar disc disorders and low-back pain: socioeconomic factors and consequences," *J. Bone Jt. Surg.*, vol. 88, no. suppl_2, pp. 21–24, 2006.
- [15] F. M. Phillips, P. J. Slosar, J. A. Youssef, G. Andersson, and F. Papatheofanis, "Lumbar spine fusion for chronic low back pain due to degenerative disc disease: a systematic review," *Spine (Phila. Pa. 1976)*, vol. 38, no. 7, pp. E409–E422, 2013.
- [16] S. H. Ahn, H. W. Park, W. M. Byun, M. W. Ahn, J.-H. Bae, S.-H. Jang, and Y. K. Kim, "Comparison of clinical outcomes and natural morphologic changes between sequestered and large central extruded disc herniations," *Yonsei Med. J.*, vol. 43, no. 3, pp. 283–290, 2002.
- [17] E. I. T. de Schepper, J. Damen, J. B. J. van Meurs, A. Z. Ginai, M. Popham, A. Hofman, B. W. Koes, and S. M. Bierma-Zeinstra, "The association between lumbar disc degeneration and low back pain: the influence of age, gender, and individual radiographic features," *Spine (Phila. Pa. 1976)*, vol. 35, no. 5, pp. 531–536, 2010.
- [18] J. W. Kallewaard, M. A. M. B. Terheggen, G. J. Groen, M. E. Sluijter, R. Derby, L. Kapural, N. Mekhail, and M. Van Kleef, "15. Discogenic low back pain," *Pain Pract.*, vol. 10, no. 6, pp. 560–579, 2010.
- [19] M. C. Battié, T. Videman, and E. Parent, "Lumbar disc degeneration: epidemiology and genetic influences," *Spine (Phila. Pa. 1976)*, vol. 29, no. 23, pp. 2679–2690, 2004.
- [20] I. A. F. Stokes and J. C. Iatridis, "Mechanical conditions that accelerate intervertebral disc degeneration: overload versus immobilization," *Spine (Phila. Pa. 1976)*, vol. 29, no. 23, pp. 2724–2732, 2004.
- [21] H. J. Wilke, P. Neef, M. Caimi, T. Hoogland, and L. E. Claes, "New *in vivo* measurements of pressures in the intervertebral disc in daily life.," *Spine (Phila. Pa. 1976)*, vol. 24, no. 8, pp. 755–62, Apr. 1999.
- [22] S. M. Kurtz and A. Edidin, *Spine technology handbook*. Academic Press, 2006.
- [23] J. R. Meakin, T. W. Redpath, and D. W. L. Hukins, "The effect of partial removal of the nucleus pulposus from the intervertebral disc on the response of the human annulus fibrosus to compression," *Clin. Biomech.*, vol. 16, no. 2, pp. 121–128, 2001.
- [24] J. C. Iatridis and I. ap Gwynn, "Mechanisms for mechanical damage in the intervertebral disc annulus fibrosus," *J. Biomech.*, vol. 37, no. 8, pp. 1165–1175, 2004.

- [25] M. A. Adams and P. J. Roughley, "What is intervertebral disc degeneration, and what causes it?," *Spine (Phila. Pa. 1976)*, vol. 31, no. 18, pp. 2151–2161, 2006.
- [26] S. J. Ferguson and T. Steffen, "Biomechanics of the aging spine," *Eur. Spine J.*, vol. 12, no. 2, pp. S97–S103, 2003.
- [27] M. A. Adams, N. Bogduk, K. Burton, and P. Dolan, *The biomechanics of back pain*. Churchill Livingstone, 2003.
- [28] V. Haughton, "Medical imaging of intervertebral disc degeneration: current status of imaging," *Spine (Phila. Pa. 1976)*, vol. 29, no. 23, pp. 2751–2756, 2004.
- [29] R. A. Deyo, D. T. Gray, W. Kreuter, S. Mirza, and B. I. Martin, "United States trends in lumbar fusion surgery for degenerative conditions," *Spine (Phila. Pa. 1976)*, vol. 30, no. 12, pp. 1441–1445, 2005.
- [30] W. C. Pannell, D. D. Savin, T. P. Scott, J. C. Wang, and M. D. Daubs, "Trends in the surgical treatment of lumbar spine disease in the United States," *Spine J.*, 2013.
- [31] N. M. Raizman, J. R. O'Brien, K. L. Poehling-Monaghan, and D. Y. Warren, "Pseudarthrosis of the spine," *J. Am. Acad. Orthop. Surg.*, vol. 17, no. 8, pp. 494–503, 2009.
- [32] R. J. Mobbs, A. Loganathan, V. Yeung, and P. J. Rao, "Indications for Anterior Lumbar Interbody Fusion," *Orthop. Surg.*, vol. 5, no. 3, pp. 153–163, 2013.
- [33] T. Kaner and A. F. Ozer, "Dynamic stabilization for challenging lumbar degenerative diseases of the spine: a review of the literature," *Adv. Orthop.*, vol. 2013, 2013.
- [34] R. E. Wiltfong, C. M. Bono, W. M. S. C. Malveaux, and A. D. Sharan, "Lumbar interbody fusion: review of history, complications, and outcome comparisons among methods," *Curr. Orthop. Pract.*, vol. 23, no. 3, pp. 193–202, 2012.
- [35] B. B. K. Tay and S. Berven, "Indications, techniques, and complications of lumbar interbody fusion," in *Seminars in neurology*, 2002, vol. 22, no. 02, pp. 221–230.
- [36] J. D. Schwender, L. T. Holly, D. P. Rouben, and K. T. Foley, "Minimally invasive transforaminal lumbar interbody fusion (TLIF): technical feasibility and initial results," *J. Spinal Disord. Tech.*, vol. 18, pp. S1–S6, 2005.
- [37] K. T. Foley and S. K. Gupta, "Percutaneous pedicle screw fixation of the lumbar spine: preliminary clinical results," *J. Neurosurg. Spine*, vol. 97, no. 1, pp. 7–12, 2002.
- [38] M. Payer, "'Minimally invasive' lumbar spine surgery: a critical review," *Acta Neurochir. (Wien)*, vol. 153, no. 7, pp. 1455–1459, 2011.

- [39] H. M. Mayer, "The ALIF concept," *Eur. Spine J.*, vol. 9, no. 1, pp. S035–S043, 2000.
- [40] R. C. Sasso, J. K. Burkus, and J.-C. LeHuec, "Retrograde ejaculation after anterior lumbar interbody fusion: transperitoneal versus retroperitoneal exposure," *Spine (Phila. Pa. 1976)*, vol. 28, no. 10, pp. 1023–1026, 2003.
- [41] S. A. Brau, "Mini-open approach to the spine for anterior lumbar interbody fusion: description of the procedure, results and complications," *spine J.*, vol. 2, no. 3, pp. 216–223, 2002.
- [42] B. M. Ozgur, H. E. Aryan, L. Pimenta, and W. R. Taylor, "Extreme Lateral Interbody Fusion (XLIF): a novel surgical technique for anterior lumbar interbody fusion," *Spine J.*, vol. 6, no. 4, pp. 435–443, 2006.
- [43] J. Inamasu and B. H. Guiot, "Laparoscopic anterior lumbar interbody fusion: a review of outcome studies," *min-Minimally Invasive Neurosurg.*, vol. 48, no. 06, pp. 340–347, 2005.
- [44] J. D. Auerbach, B. P. D. Wills, T. C. McIntosh, and R. a Balderston, "Evaluation of spinal kinematics following lumbar total disc replacement and circumferential fusion using *in vivo* fluoroscopy.," *Spine (Phila. Pa. 1976)*, vol. 32, no. 5, pp. 527–36, Mar. 2007.
- [45] A. F. Mannion, G. Leivseth, J.-I. Brox, P. Fritzell, O. Hägg, and J. C. Fairbank, "Long-Term Follow Up Suggests Spinal Fusion is Associated With Increased Adjacent Segment Disc Degeneration but Without Influence on Clinical Outcome: Results of a Combined Follow-Up from 4 RCTs.," *Spine (Phila. Pa. 1976)*, 2014.
- [46] J.-P. Lemaire, H. Carrier, E.-H. S. Ali, W. Skalli, and F. Lavaste, "Clinical and radiological outcomes with the CHARITÉ™ Artificial Disc: a 10-year minimum follow-up," *J. Spinal Disord. Tech.*, vol. 18, no. 4, pp. 353–359, 2005.
- [47] K. D. van den Eerenbeemt, R. W. Ostelo, B. J. van Royen, W. C. Peul, and M. W. van Tulder, "Total disc replacement surgery for symptomatic degenerative lumbar disc disease: a systematic review of the literature," *Eur. Spine J.*, vol. 19, no. 8, pp. 1262–1280, 2010.
- [48] J. Beastall, E. Karadimas, M. Siddiqui, M. Nicol, J. Hughes, F. Smith, and D. Wardlaw, "The Dynesys lumbar spinal stabilization system: a preliminary report on positional magnetic resonance imaging findings," *Spine (Phila. Pa. 1976)*, vol. 32, no. 6, pp. 685–690, 2007.
- [49] P. Park, H. J. Garton, V. C. Gala, J. T. Hoff, and J. E. McGillicuddy, "Adjacent segment disease after lumbar or lumbosacral fusion: review of the literature.," *Spine (Phila. Pa. 1976)*, vol. 29, no. 17, pp. 1938–44, Sep. 2004.
- [50] P. Axelsson, R. Johnsson, and B. Strömquist, "Adjacent segment hypermobility after lumbar spine fusion after surgery," *Acta Orthop.*, vol. 78, no. 6, pp. 834–839, Dec. 2007.

- [51] P. Korovessis, T. Repantis, S. Zacharatos, and A. Zafiropoulos, “Does Wallis implant reduce adjacent segment degeneration above lumbosacral instrumented fusion?,” pp. 830–840, 2009.
- [52] C. H. Kim, C. K. Chung, and T. Jahng, “Comparisons of Outcomes After Single or Multilevel Dynamic Stabilization :,” vol. 24, no. 1, pp. 60–67, 2011.
- [53] J. D. Auerbach, R. J. Davis, and W. Sears, “Interlaminar Stabilization Maintains a More Normal Segmental Contribution to Total Lumbar Range of Motion Compared With Fusion at 2 Years,” 2011.
- [54] W. R. Sears, I. G. Sergides, N. Kazemi, M. Smith, G. J. White, and B. Osburg, “Incidence and prevalence of surgery at segments adjacent to a previous posterior lumbar arthrodesis,” *Spine J.*, vol. 11, no. 1, pp. 11–20, 2011.
- [55] K. Yamashita, K. Ohzono, and K. Hiroshima, “Five-year outcomes of surgical treatment for degenerative lumbar spinal stenosis: a prospective observational study of symptom severity at standard intervals after surgery,” *Spine (Phila. Pa. 1976).*, vol. 31, no. 13, pp. 1484–1490, 2006.
- [56] S. Etebar and D. W. Cahill, “Risk factors for adjacent-segment failure following lumbar fixation with rigid instrumentation for degenerative instability.,” *J. Neurosurg.*, vol. 90, no. 2 Suppl, pp. 163–9, Apr. 1999.
- [57] Y. Aota, K. Kumano, and S. Hirabayashi, “Postfusion instability at the adjacent segments after rigid pedicle screw fixation for degenerative lumbar spinal disorders,” *J. Spinal Disord. Tech.*, vol. 8, no. 6, pp. 464–473, 1995.
- [58] M. D. Rahm and B. B. Hall, “Adjacent-segment degeneration after lumbar fusion with instrumentation: a retrospective study,” *J. Spinal Disord. Tech.*, vol. 9, no. 5, pp. 392–400, 1996.
- [59] J. S. Harrop, J. a Youssef, M. Maltenfort, P. Vorwald, P. Jabbour, C. M. Bono, N. Goldfarb, A. R. Vaccaro, and A. S. Hilibrand, “Lumbar adjacent segment degeneration and disease after arthrodesis and total disc arthroplasty.,” *Spine (Phila. Pa. 1976).*, vol. 33, no. 15, pp. 1701–7, Jul. 2008.
- [60] S. Okuda, M. Iwasaki, A. Miyauchi, H. Aono, M. Morita, and T. Yamamoto, “Risk factors for adjacent segment degeneration after PLIF,” *Spine (Phila. Pa. 1976).*, vol. 29, no. 14, pp. 1535–1540, 2004.
- [61] C. S. Lee, C. J. Hwang, S.-W. Lee, Y.-J. Ahn, Y.-T. Kim, D.-H. Lee, and M. Y. Lee, “Risk factors for adjacent segment disease after lumbar fusion,” *Eur. Spine J.*, vol. 18, no. 11, pp. 1637–1643, 2009.

- [62] G. Ghiselli, J. C. Wang, N. N. Bhatia, W. K. Hsu, and E. G. Dawson, "Adjacent segment degeneration in the lumbar spine.," *J. Bone Joint Surg. Am.*, vol. 86-A, no. 7, pp. 1497–503, Jul. 2004.
- [63] T. W. Throckmorton, A. S. Hilibrand, G. A. Mencio, A. Hodge, and D. M. Spengler, "The impact of adjacent level disc degeneration on health status outcomes following lumbar fusion," *Spine (Phila. Pa. 1976).*, vol. 28, no. 22, pp. 2546–2550, 2003.
- [64] J.-H. Min, J.-S. Jang, B. joo Jung, H. Y. Lee, W.-C. Choi, C. S. Shim, G. Choi, and S.-H. Lee, "The clinical characteristics and risk factors for the adjacent segment degeneration in instrumented lumbar fusion," *J. Spinal Disord. Tech.*, vol. 21, no. 5, pp. 305–309, 2008.
- [65] M. N. Kumar, A. Baklanov, and D. Chopin, "Correlation between sagittal plane changes and adjacent segment degeneration following lumbar spine fusion," *Eur. Spine J.*, vol. 10, no. 4, pp. 314–319, Aug. 2001.
- [66] J. D. Schlegel, J. A. Smith, and R. L. Schleusener, "Lumbar motion segment pathology Adjacent to thoracolumbar, Lumbar and Lumbosacral Fusions." *Spine*, pp. 970–981, 1996.
- [67] T. S. Whitecloud III, J. M. Davis, and P. M. Olive, "Operative treatment of the degenerated segment adjacent to a lumbar fusion," *Spine (Phila. Pa. 1976).*, vol. 19, no. 5, pp. 531–536, 1994.
- [68] L. L. Wiltse, S. E. Radecki, H. M. Biel, P. P. DiMartino, R. A. Oas, G. Farjalla, F. A. Ravessoud, and C. Wohletz, "Comparative study of the incidence and severity of degenerative change in the transition zones after instrumented versus noninstrumented fusions of the lumbar spine.," *J. Spinal Disord. Tech.*, vol. 12, no. 1, pp. 27–33, 1999.
- [69] J.-H. Kim, S.-S. Kim, and S.-I. Suk, "Incidence of proximal adjacent failure in adult lumbar deformity correction based on proximal fusion level," *Asian Spine J.*, vol. 1, no. 1, pp. 19–26, 2007.
- [70] E. K. Wai, E. R. G. Santos, R. A. Morcom, and R. D. Fraser, "Magnetic resonance imaging 20 years after anterior lumbar interbody fusion," *Spine (Phila. Pa. 1976).*, vol. 31, no. 17, pp. 1952–1956, 2006.
- [71] S. Seitsalo and D. Schlenzka, "Disc degeneration in young patients with isthmic spondylolisthesis treated operatively or conservatively: a long-term follow-up," *Eur. Spine J.*, pp. 393–397, 1997.
- [72] M. Penta, A. Sandhu, and R. D. Fraser, "Magnetic resonance imaging assessment of disc degeneration 10 years after anterior lumbar interbody fusion," *Spine (Phila. Pa. 1976).*, vol. 20, no. 6, pp. 743–747, 1995.

- [73] K. E. Radcliff, C. K. Kepler, A. Jakoi, G. S. Sidhu, J. Rihn, A. R. Vaccaro, T. J. Albert, and A. S. Hilibrand, "Adjacent segment disease in the lumbar spine following different treatment interventions," *Spine J.*, vol. 13, no. 10, pp. 1339–1349, 2013.
- [74] T. Kaito, N. Hosono, Y. Mukai, T. Makino, T. Fuji, and K. Yonenobu, "Induction of early degeneration of the adjacent segment after posterior lumbar interbody fusion by excessive distraction of lumbar disc space.," *J. Neurosurg. Spine*, vol. 12, no. 6, pp. 671–9, Jun. 2010.
- [75] T. Lund and T. R. Oxland, "Adjacent level disk disease--is it really a fusion disease?," *Orthop. Clin. North Am.*, vol. 42, no. 4, pp. 529–41, viii, Oct. 2011.
- [76] J. C. Lotz and J. R. Chin, "Intervertebral disc cell death is dependent on the magnitude and duration of spinal loading," *Spine (Phila. Pa. 1976)*, vol. 25, no. 12, pp. 1477–1483, 2000.
- [77] B. A. Walter, C. L. Korecki, D. Purmessur, P. J. Roughley, A. J. Michalek, and J. C. Iatridis, "Complex loading affects intervertebral disc mechanics and biology," *Osteoarthr. Cartil.*, vol. 19, no. 8, pp. 1011–1018, 2011.
- [78] S. C. W. Chan, S. J. Ferguson, and B. Gantenbein-Ritter, "The effects of dynamic loading on the intervertebral disc," *Eur. spine J.*, vol. 20, no. 11, pp. 1796–1812, 2011.
- [79] J. Kim, S.-J. Yang, H. Kim, Y. Kim, J. B. Park, C. DuBose, and T.-H. Lim, "Effect of shear force on intervertebral disc (IVD) degeneration: an *in vivo* rat study," *Ann. Biomed. Eng.*, vol. 40, no. 9, pp. 1996–2004, 2012.
- [80] M. M. Panjabi, "Hybrid multidirectional test method to evaluate spinal adjacent-level effects.," *Clin. Biomech. (Bristol, Avon)*, vol. 22, no. 3, pp. 257–65, Mar. 2007.
- [81] R. Gejo, H. Matsui, Y. Kawaguchi, H. Ishihara, and H. Tsuji, "Serial changes in trunk muscle performance after posterior lumbar surgery.," *Spine (Phila. Pa. 1976)*, vol. 24, no. 10, pp. 1023–8, May 1999.
- [82] Y. Kawaguchi, H. Matsui, and H. Tsuji, "Back muscle injury after posterior lumbar spine surgery: part 2: histologic and histochemical analyses in humans," *Spine (Phila. Pa. 1976)*, vol. 19, no. 22, pp. 2598–2602, 1994.
- [83] Y. Kawaguchi, H. Matsui, R. Gejo, and H. Tsuji, "Preventive measures of back muscle injury after posterior lumbar spine surgery in rats," *Spine (Phila. Pa. 1976)*, vol. 23, no. 21, pp. 2282–2287, 1998.
- [84] Y. Kawaguchi, H. Matsui, and H. Tsuji, "Back muscle injury after posterior lumbar spine surgery: a histologic and enzymatic analysis," *Spine (Phila. Pa. 1976)*, vol. 21, no. 8, pp. 941–944, 1996.

- [85] D. T. Cawley, M. Alexander, and S. Morris, "Multifidus innervation and muscle assessment post-spinal surgery," *Eur. spine J.*, vol. 23, no. 2, pp. 320–327, 2014.
- [86] A. Keller, R. Gunderson, O. Reikerås, and J. I. Brox, "Reliability of computed tomography measurements of paraspinal muscle cross-sectional area and density in patients with chronic low back pain.," *Spine (Phila. Pa. 1976)*, vol. 28, no. 13, pp. 1455–60, Jul. 2003.
- [87] A. Keller, J. I. Brox, R. Gunderson, I. Holm, A. Friis, and O. Reikerås, "Trunk muscle strength, cross-sectional area, and density in patients with chronic low back pain randomized to lumbar fusion or cognitive intervention and exercises," *Spine (Phila. Pa. 1976)*, vol. 29, no. 1, pp. 3–8, 2003.
- [88] H.-L. Wang, F.-Z. Lu, J.-Y. Jiang, X. Ma, X.-L. Xia, and L.-X. Wang, "Minimally invasive lumbar interbody fusion via MAST Quadrant retractor versus open surgery: a prospective randomized clinical trial," *Chinese Med. Journal-Beijing*, vol. 124, no. 23, p. 3868, 2011.
- [89] M. Kramer, P. Katzmaier, R. Eisele, V. Ebert, L. Kinzl, and E. Hartwig, "Surface electromyography-verified muscular damage associated with the open dorsal approach to the lumbar spine," *Eur. Spine J.*, vol. 10, no. 5, pp. 414–420, 2001.
- [90] D.-Y. Kim, S.-H. Lee, S. K. Chung, and H.-Y. Lee, "Comparison of multifidus muscle atrophy and trunk extension muscle strength: percutaneous versus open pedicle screw fixation," *Spine (Phila. Pa. 1976)*, vol. 30, no. 1, pp. 123–129, 2004.
- [91] T. omg Mayer, H. Vanharanta, R. J. Gatchel, V. Mooney, D. Barnes, L. Judge, S. Smith, and A. Terry, "Comparison of CT scan muscle measurements and isokinetic trunk strength in postoperative patients," *Spine (Phila. Pa. 1976)*, vol. 14, no. 1, pp. 33–36, 1989.
- [92] M. Millard, T. Uchida, A. Seth, and S. L. Delp, "Flexing computational muscle: Modeling and simulation of musculotendon dynamics," *J. Biomech. Eng.*, vol. 135, no. 2, p. 21005, 2013.
- [93] A. M. Gordon, A. F. Huxley, and F. J. Julian, "The variation in isometric tension with sarcomere length in vertebrate muscle fibres," *J. Physiol.*, vol. 184, no. 1, pp. 170–192, 1966.
- [94] S. K. Gollapudi and D. C. Lin, "Experimental determination of sarcomere force–length relationship in type-I human skeletal muscle fibers," *J. Biomech.*, vol. 42, no. 13, pp. 2011–2016, 2009.
- [95] T. M. Winters, M. Takahashi, R. L. Lieber, and S. R. Ward, "Whole muscle length-tension relationships are accurately modeled as scaled sarcomeres in rabbit hindlimb muscles," *J. Biomech.*, vol. 44, no. 1, pp. 109–115, 2011.

- [96] C. N. Maganaris and J. P. Paul, "Tensile properties of the *in vivo* human gastrocnemius tendon," *J. Biomech.*, vol. 35, no. 12, pp. 1639–1646, 2002.
- [97] S. P. Magnusson, P. Aagaard, S. Rosager, P. Dyhre-Poulsen, and M. Kjaer, "Load–displacement properties of the human triceps surae aponeurosis *in vivo*," *J. Physiol.*, vol. 531, no. 1, pp. 277–288, 2001.
- [98] S. R. Ward, C. M. Eng, L. H. Smallwood, and R. L. Lieber, "Are current measurements of lower extremity muscle architecture accurate?," *Clin. Orthop. Relat. Res.*, vol. 467, no. 4, pp. 1074–1082, 2009.
- [99] S. L. Delp, S. Suryanarayanan, W. M. Murray, J. Uhler, and R. J. Triolo, "Architecture of the rectus abdominis, quadratus lumborum, and erector spinae," *J. Biomech.*, vol. 34, no. 3, pp. 371–375, 2001.
- [100] W. M. Murray, T. S. Buchanan, and S. L. Delp, "The isometric functional capacity of muscles that cross the elbow," *J. Biomech.*, vol. 33, no. 8, pp. 943–952, 2000.
- [101] R. L. Lieber, B. M. Fazeli, and M. J. Botte, "Architecture of selected wrist flexor and extensor muscles," *J. Hand Surg. Am.*, vol. 15, no. 2, pp. 244–250, 1990.
- [102] L. Bresnahan, R. G. Fessler, and R. N. Natarajan, "Evaluation of change in muscle activity as a result of posterior lumbar spine surgery using a dynamic modeling system.," *Spine (Phila. Pa. 1976)*, vol. 35, no. 16, pp. E761–7, Jul. 2010.
- [103] T. McNeill, D. Warwick, G. Andersson, and A. Schultz, "Trunk strengths in attempted flexion, extension, and lateral bending in healthy subjects and patients with low-back disorders," *Spine (Phila. Pa. 1976)*, vol. 5, no. 6, pp. 529–538, 1980.
- [104] N. Bogduk, J. E. Macintosh, and M. J. Pearcy, "A universal model of the lumbar back muscles in the upright position.," *Spine (Phila. Pa. 1976)*, vol. 17, no. 8, pp. 897–913, Aug. 1992.
- [105] A. Erdemir, S. McLean, W. Herzog, and A. J. van den Bogert, "Model-based estimation of muscle forces exerted during movements.," *Clin. Biomech. (Bristol, Avon)*, vol. 22, no. 2, pp. 131–54, Feb. 2007.
- [106] M. G. Pandy, "Computer modeling and simulation of human movement," *Annu. Rev. Biomed. Eng.*, vol. 3, no. 1, pp. 245–273, 2001.
- [107] D. Tsirakos, V. Baltzopoulos, and R. Bartlett, "Inverse optimization: functional and physiological considerations related to the force-sharing problem," *Crit. Rev. Biomed. Eng.*, vol. 25, no. 4–5, 1997.

- [108] F. E. Zajac and J. M. Winters, "Modeling musculoskeletal movement systems: joint and body segmental dynamics, musculoskeletal actuation, and neuromuscular control," in *Multiple muscle systems*, Springer, 1990, pp. 121–148.
- [109] D. G. Thelen, "Adjustment of Muscle Mechanics Model Parameters to Simulate Dynamic Contractions in Older Adults," *J. Biomech. Eng.*, vol. 125, no. 1, p. 70, 2003.
- [110] I. K. Stavness, "Byte Your Tongue," no. December, 2010.
- [111] M. G. Pandy, B. A. Garner, and F. C. Anderson, "Optimal control of non-ballistic muscular movements: a constraint-based performance criterion for rising from a chair," *J. Biomech. Eng.*, vol. 117, no. 1, pp. 15–26, 1995.
- [112] L. L. Menegaldo, A. de T. Fleury, and H. I. Weber, "Biomechanical modeling and optimal control of human posture," *J. Biomech.*, vol. 36, no. 11, pp. 1701–1712, 2003.
- [113] M. G. Pandy, F. E. Zajac, E. Sim, and W. S. Levine, "An optimal control model for maximum-height human jumping," *J. Biomech.*, vol. 23, no. 12, pp. 1185–1198, 1990.
- [114] C. C. Raasch, F. E. Zajac, B. Ma, and W. S. Levine, "Muscle coordination of maximum-speed pedaling," *J. Biomech.*, vol. 30, no. 6, pp. 595–602, 1997.
- [115] P. G. S. Trainor, K. R. McLachlan, and W. D. McCall, "Modelling of forces in the human masticatory system with optimization of the angulations of the joint loads," *J. Biomech.*, vol. 28, no. 7, pp. 829–843, 1995.
- [116] R. Happee, "Inverse dynamic optimization including muscular dynamics, a new simulation method applied to goal directed movements," *J. Biomech.*, vol. 27, no. 7, pp. 953–960, 1994.
- [117] N. Arjmand and a Shirazi-Adl, "Sensitivity of kinematics-based model predictions to optimization criteria in static lifting tasks," *Med. Eng. Phys.*, vol. 28, no. 6, pp. 504–14, Jul. 2006.
- [118] G. Li, K. R. Kaufman, E. Y. S. Chao, and H. E. Rubash, "Prediction of antagonistic muscle forces using inverse dynamic optimization during flexion/extension of the knee," *J. Biomech. Eng.*, vol. 121, no. 3, pp. 316–322, 1999.
- [119] R. Happee and F. C. T. Van der Helm, "The control of shoulder muscles during goal directed movements, an inverse dynamic analysis," *J. Biomech.*, vol. 28, no. 10, pp. 1179–1191, 1995.
- [120] R. E. Hughes, M. G. Rock, and K.-N. An, "Identification of optimal strategies for increasing whole arm strength using Karush–Kuhn–Tucker multipliers," *Clin. Biomech.*, vol. 14, no. 9, pp. 628–634, 1999.

- [121] R. E. Hughes, D. B. Chaffin, S. A. Lavender, and G. B. J. Andersson, "Evaluation of muscle force prediction models of the lumbar trunk using surface electromyography," *J. Orthop. Res.*, vol. 12, no. 5, pp. 689–698, 1994.
- [122] J. J. Collins, "The redundant nature of locomotor optimization laws," *J. Biomech.*, vol. 28, no. 3, pp. 251–267, 1995.
- [123] M. G. Pandy, F. C. Anderson, and D. G. Hull, "A parameter optimization approach for the optimal control of large-scale musculoskeletal systems.," *J. Biomech. Eng.*, vol. 114, no. 4, pp. 450–60, Nov. 1992.
- [124] F. C. Anderson and M. G. Pandy, "Static and dynamic optimization solutions for gait are practically equivalent.," *J. Biomech.*, vol. 34, no. 2, pp. 153–61, Feb. 2001.
- [125] G. T. Yamaguchi and F. E. Zajac, "Restoring unassisted natural gait to paraplegics via functional neuromuscular stimulation: a computer simulation study," *Biomed. Eng. IEEE Trans.*, vol. 37, no. 9, pp. 886–902, 1990.
- [126] R. R. Neptune, S. A. Kautz, and F. E. Zajac, "Contributions of the individual ankle plantar flexors to support, forward progression and swing initiation during walking," *J. Biomech.*, vol. 34, no. 11, pp. 1387–1398, 2001.
- [127] S. G. McLean, A. Su, and A. J. van den Bogert, "Development and validation of a 3-D model to predict knee joint loading during dynamic movement," *J. Biomech. Eng.*, vol. 125, no. 6, pp. 864–874, 2003.
- [128] I. a F. Stokes, M. G. Gardner-Morse, and S. M. Henry, "Intra-abdominal pressure and abdominal wall muscular function: Spinal unloading mechanism.," *Clin. Biomech. (Bristol, Avon)*, vol. 25, no. 9, pp. 859–66, Nov. 2010.
- [129] S. H. Loring, K. Yoshino, W. R. Kimball, and G. M. Barnas, "Gravitational and shear-associated pressure gradients in the abdomen," *J. Appl. Physiol.*, vol. 77, no. 3, pp. 1375–1382, 1994.
- [130] B. L. De Keulenaer, J. J. De Waele, B. Powell, and M. Malbrain, "What is normal intra-abdominal pressure and how is it affected by positioning, body mass and positive end-expiratory pressure?," in *Applied Physiology in Intensive Care Medicine 2*, Springer, 2012, pp. 219–226.
- [131] T. J. Iberti, C. E. Lieber, and E. Benjamin, "Determination of intra-abdominal pressure using a transurethral bladder catheter: clinical validation of the technique," *Anesthesiology*, vol. 70, no. 1, pp. 47–50, 1989.
- [132] G. G. Collee, D. M. Lomax, C. Ferguson, and G. C. Hanson, "Bedside measurement of intra-abdominal pressure (IAP) via an indwelling naso-gastric tube: clinical validation of the technique," *Intensive Care Med.*, vol. 19, no. 8, pp. 478–480, 1993.

- [133] M. Sugrue, M. D. Buist, A. Lee, D. J. Sanchez, and K. M. Hillman, "Intra-abdominal pressure measurement using a modified nasogastric tube: description and validation of a new technique," *Intensive Care Med.*, vol. 20, no. 8, pp. 588–590, 1994.
- [134] W. S. Cobb, J. M. Burns, K. W. Kercher, B. D. Matthews, H. James Norton, and B. Todd Heniford, "Normal intraabdominal pressure in healthy adults," *J. Surg. Res.*, vol. 129, no. 2, pp. 231–235, 2005.
- [135] S. M. McGill and R. W. Norman, "Partitioning of the L4-L5 dynamic moment into disc, ligamentous, and muscular components during lifting.," *Spine (Phila. Pa. 1976)*, vol. 11, no. 7, pp. 666–78, Sep. 1986.
- [136] J. Cholewicki, S. M. McGill, and R. W. Norman, "Comparison of muscle forces and joint load from an optimization and EMG assisted lumbar spine model: towards development of a hybrid approach," *J. Biomech.*, vol. 28, no. 3, pp. 321–331, 1995.
- [137] I. A. F. Stokes and M. Gardner-Morse, "Lumbar spine maximum efforts and muscle recruitment patterns predicted by a model with multijoint muscles and joints with stiffness," *J. Biomech.*, vol. 28, no. 2, pp. 173–186, 1995.
- [138] N. Arjmand and a Shirazi-Adl, "Model and *in vivo* studies on human trunk load partitioning and stability in isometric forward flexions.," *J. Biomech.*, vol. 39, no. 3, pp. 510–21, Jan. 2006.
- [139] M. de Zee, L. Hansen, C. Wong, J. Rasmussen, and E. B. Simonsen, "A generic detailed rigid-body lumbar spine model.," *J. Biomech.*, vol. 40, no. 6, pp. 1219–27, Jan. 2007.
- [140] F. Ezquerro, "Combination of finite element modeling and optimization for the study of lumbar spine biomechanics considering the 3D thorax–pelvis orientation," *Med. Eng. Phys.*, vol. 26, no. 1, pp. 11–22, Jan. 2004.
- [141] K. T. Huynh, I. Gibson, W. F. Lu, and B. N. Jagdish, "Simulating dynamics of thoracolumbar spine derived from LifeMOD under haptic forces," *World Acad. Sci. Eng. Technol.*, vol. 64, pp. 278–285, 2010.
- [142] M. A. Nussbaum, D. B. Chaffin, and C. J. Rechten, "Muscle lines-of-action affect predicted forces in optimization-based spine muscle modeling," *J. Biomech.*, vol. 28, no. 4, pp. 401–409, 1995.
- [143] E. Andersson, L. Swärd, and A. Thorstensson, "Trunk muscle strength in athletes.," *Med. Sci. Sports Exerc.*, vol. 20, no. 6, pp. 587–593, 1988.
- [144] J. Cholewicki and S. M. McGill, "EMG assisted optimization: a hybrid approach for estimating muscle forces in an indeterminate biomechanical model," *J. Biomech.*, vol. 27, no. 10, pp. 1287–1289, 1994.

- [145] D. Gagnon, C. Larivière, and P. Loisel, “Comparative ability of EMG, optimization, and hybrid modelling approaches to predict trunk muscle forces and lumbar spine loading during dynamic sagittal plane lifting.,” *Clin. Biomech. (Bristol, Avon)*, vol. 16, no. 5, pp. 359–72, Jun. 2001.
- [146] R. E. Hughes, J. C. Bean, and D. B. Chaffin, “Evaluating the effect of co-contraction in optimization models,” *J. Biomech.*, vol. 28, no. 7, pp. 875–878, 1995.
- [147] N. Arjmand, D. Gagnon, a Plamondon, a Shirazi-Adl, and C. Larivière, “A comparative study of two trunk biomechanical models under symmetric and asymmetric loadings.,” *J. Biomech.*, vol. 43, no. 3, pp. 485–91, Feb. 2010.
- [148] N. Arjmand, a Shirazi-Adl, and M. Parnianpour, “Trunk biomechanical models based on equilibrium at a single-level violate equilibrium at other levels.,” *Eur. Spine J.*, vol. 16, no. 5, pp. 701–9, May 2007.
- [149] K.-S. Han, T. Zander, W. R. Taylor, and A. Rohlmann, “An enhanced and validated generic thoraco-lumbar spine model for prediction of muscle forces.,” *Med. Eng. Phys.*, vol. 34, no. 6, pp. 709–16, Jul. 2012.
- [150] A. Rohlmann, F. Graichen, A. Bender, R. Kayser, and G. Bergmann, “Loads on a telemeterized vertebral body replacement measured in three patients within the first postoperative month,” *Clin. Biomech.*, vol. 23, no. 2, pp. 147–158, 2008.
- [151] H.-J. Wilke, P. Neef, B. Hinz, H. Seidel, and L. Claes, “Intradiscal pressure together with anthropometric data—a data set for the validation of models,” *Clin. Biomech.*, vol. 16, pp. S111–S126, 2001.
- [152] T. T. Dao, P. Pouletaut, F. Charleux, Á. Lazáry, P. Eltes, P. P. Varga, and M. C. H. B. Tho, “Estimation of Patient Specific Lumbar Spine Muscle Forces Using Multi-physical Musculoskeletal Model and Dynamic MRI,” in *Knowledge and Systems Engineering*, Springer, 2014, pp. 411–422.
- [153] I. Stavness, J. E. Lloyd, Y. Payan, and S. Fels, “Coupled hard–soft tissue simulation with contact and constraints applied to jaw–tongue–hyoid dynamics,” *Int. j. numer. method. biomed. eng.*, vol. 27, no. 3, pp. 367–390, 2011.
- [154] M. Panjabi, G. Malcolmson, E. Teng, Y. Tominaga, G. Henderson, and H. Serhan, “Hybrid testing of lumbar CHARITE discs versus fusions,” *Spine (Phila. Pa. 1976)*, vol. 32, no. 9, pp. 959–966, 2007.
- [155] P. Strube, S. Tohtz, E. Hoff, C. Gross, C. Perka, and M. Putzier, “Dynamic stabilization adjacent to single-level fusion: Part I. Biomechanical effects on lumbar spinal motion,” *Eur. Spine J.*, vol. 19, no. 12, pp. 2171–2180, 2010.

- [156] H. Nagata, M. J. Schendel, E. E. Transfeldt, and J. L. Lewis, “The effects of immobilization of long segments of the spine on the adjacent and distal facet force and lumbosacral motion,” *Spine (Phila. Pa. 1976)*, vol. 18, no. 16, pp. 2471–2479, 1993.
- [157] F. J. Molz, J. I. Partin, and J. S. Kirkpatrick, “The acute effects of posterior fusion instrumentation on kinematics and intradiscal pressure of the human lumbar spine,” *J. Spinal Disord. Tech.*, vol. 16, no. 2, pp. 171–179, 2003.
- [158] S. L. Weinhoffer, R. D. Guyer, M. Herbert, and S. L. Griffith, “Intradiscal pressure measurements above an instrumented fusion: a cadaveric study,” *Spine (Phila. Pa. 1976)*, vol. 20, no. 5, pp. 526–531, 1995.
- [159] D. Volkheimer, M. Malakoutian, T. R. Oxland, and H.-J. Wilke, “Can biomechanics explain the degeneration of adjacent segments? Review of the current literature of *in vitro* experiments,” *Eur. J. Spine*, 2013.
- [160] S. Nakai, H. Yoshizawa, and S. Kobayashi, “Long-term follow-up study of posterior lumbar interbody fusion,” *J. Spinal Disord. Tech.*, vol. 12, no. 4, pp. 293–299, 1999.
- [161] J. Zigler, J. Glenn, and R. Delamarter, “Five-year adjacent-level degenerative changes in patients with single-level disease treated using lumbar total disc replacement with ProDisc-L versus circumferential,” *J. Neurosurg. Spine*, pp. 1–8, 2012.
- [162] W. J. Anderst, R. Vaidya, and S. Tashman, “A technique to measure three-dimensional *in vivo* rotation of fused and adjacent lumbar vertebrae,” *Spine J.*, vol. 8, no. 6, pp. 991–7, 2008.
- [163] S. Ohtori, M. Yamashita, G. Inoue, K. Yamauchi, T. Koshi, M. Suzuki, M. Takaso, S. Orita, Y. Eguchi, and N. Ochiai, “Rotational hypermobility of disc wedging using kinematic CT: preliminary study to investigate the instability of discs in degenerated scoliosis in the lumbar spine,” *Eur. Spine J.*, vol. 19, no. 6, pp. 989–994, 2010.
- [164] R. S. Ochia, N. Inoue, S. M. Renner, E. P. Lorenz, T.-H. Lim, G. B. J. Andersson, and H. S. An, “Three-dimensional *in vivo* measurement of lumbar spine segmental motion,” *Spine (Phila. Pa. 1976)*, vol. 31, no. 18, pp. 2073–2078, 2006.
- [165] J. W. Frymoyer, E. N. Hanley Jr, J. Howe, D. Kuhlmann, and R. E. Mattern, “A comparison of radiographic findings in fusion and nonfusion patients ten or more years following lumbar disc surgery,” *Spine (Phila. Pa. 1976)*, vol. 4, no. 5, pp. 435–440, 1979.
- [166] K. D. Luk, D. H. Chow, J. H. Evans, and J. C. Leong, “Lumbar spinal mobility after short anterior interbody fusion,” *Spine (Phila. Pa. 1976)*, vol. 20, no. 7, pp. 813–818, 1995.
- [167] V. J. M. Leferink, K. W. Zimmerman, J. Nijboer, E. Veldhuis, E. ten Vergert, and H. ten Duis, “Thoracolumbar spinal fractures: segmental range of motion after dorsal

- spondylodesis in 82 patients: a prospective study,” *Eur. Spine J.*, vol. 11, no. 1, pp. 2–7, 2002.
- [168] Y. Kamioka and H. Yamamoto, “Lumbar trapezoid plate for lumbar spondylolisthesis: a clinical study on preoperative and postoperative instability,” *Spine (Phila. Pa. 1976)*, vol. 15, no. 11, pp. 1198–1203, 1990.
- [169] R. B. Delamarter, D. M. Fribourg, L. E. a Kanim, and H. Bae, “ProDisc artificial total lumbar disc replacement: introduction and early results from the United States clinical trial,” *Spine (Phila. Pa. 1976)*, vol. 28, no. 20, pp. S167–75, Oct. 2003.
- [170] J. D. Auerbach, K. J. Jones, A. H. Milby, O. a Anakwenze, and R. a Balderston, “Segmental contribution toward total lumbar range of motion in disc replacement and fusions: a comparison of operative and adjacent levels,” *Spine (Phila. Pa. 1976)*, vol. 34, no. 23, pp. 2510–2517, Nov. 2009.
- [171] W.-Y. Chou, C.-J. Hsu, W.-N. Chang, and C.-Y. Wong, “Adjacent segment degeneration after lumbar spinal posterolateral fusion with instrumentation in elderly patients,” *Arch. Orthop. Trauma Surg.*, vol. 122, no. 1, pp. 39–43, Feb. 2002.
- [172] B. Cakir, C. Carazzo, R. Schmidt, T. Mattes, H. Reichel, and W. Käfer, “Adjacent segment mobility after rigid and semirigid instrumentation of the lumbar spine,” *Spine (Phila. Pa. 1976)*, vol. 34, no. 12, pp. 1287–91, May 2009.
- [173] Y. Hu, Y. Gu, R. Xu, L. Zhou, and W. Ma, “Short-term clinical observation of the Dynesys neutralization system for the treatment of degenerative disease of the lumbar vertebrae,” *Orthop. Surg.*, vol. 3, no. 3, pp. 167–75, Aug. 2011.
- [174] P. Axelsson, R. Johnsson, and B. Strömquist, “The spondylolytic vertebra and its adjacent segment: mobility measured before and after posterolateral fusion,” *Spine (Phila. Pa. 1976)*, vol. 22, no. 4, pp. 414–417, 1997.
- [175] H.-J. Kim, S.-H. Moon, H.-J. Chun, K.-T. Kang, H.-S. Kim, E.-S. Moon, J.-O. Park, B.-Y. Hwang, and H.-M. Lee, “Comparison of mechanical motion profiles following instrumented fusion and non-instrumented fusion at the L4-5 segment,” *Clin. Invest. Med.*, vol. 32, no. 1, pp. E64–9, Jan. 2009.
- [176] H. Ogawa, H. Hori, H. Oshita, A. Akaike, Y. Koyama, T. Shimizu, K. Yamada, and D. Ishimaru, “Sublaminar wiring stabilization to prevent adjacent segment degeneration after lumbar spinal fusion,” *Arch. Orthop. Trauma Surg.*, vol. 129, no. 7, pp. 873–8, Jul. 2009.
- [177] C. Wimmer, H. Gluch, M. Krismer, M. Ogon, and R. Jesenko, “AP-translation in the proximal disc adjacent to lumbar spine fusion: a retrospective comparison of mono- and polysegmental fusion in 120 patients,” *Acta Orthop.*, vol. 68, no. 3, pp. 269–272, 1997.

- [178] P.-L. Lai, L.-H. Chen, C.-C. Niu, and W.-J. Chen, "Effect of postoperative lumbar sagittal alignment on the development of adjacent instability.," *J. Spinal Disord. Tech.*, vol. 17, no. 5, pp. 353–357, Oct. 2004.
- [179] P. Lai, L. Chen, C. Niu, T. Fu, and W. Chen, "Relation Between Laminectomy and Development of Adjacent Segment Instability After Lumbar Fusion With Pedicle Fixation," vol. 29, no. 22, pp. 2527–2532, 2004.
- [180] B. W. Cunningham, P. C. McAfee, F. H. Geisler, G. Holsapple, K. Adams, S. L. Blumenthal, R. D. Guyer, A. Cappuccino, J. J. Regan, I. L. Fedder, and P. J. Tortolani, "Distribution of *in vivo* and *in vitro* range of motion following 1-level arthroplasty with the CHARITE artificial disc compared with fusion.," *J. Neurosurg. Spine*, vol. 8, no. 1, pp. 7–12, Jan. 2008.
- [181] R. D. Guyer, P. C. McAfee, R. J. Banco, F. D. Bitan, A. Cappuccino, F. H. Geisler, S. H. Hochschuler, R. T. Holt, L. G. Jenis, M. E. Majd, J. J. Regan, S. G. Tromanhauser, D. C. Wong, and S. L. Blumenthal, "Prospective, randomized, multicenter Food and Drug Administration investigational device exemption study of lumbar total disc replacement with the CHARITE artificial disc versus lumbar fusion: five-year follow-up," *Spine J.*, vol. 9, no. 5, pp. 374–386, 2009.
- [182] S. Berg, H. T. Tropp, and G. Leivseth, "Disc height and motion patterns in the lumbar spine in patients operated with total disc replacement or fusion for discogenic back pain. Results from a randomized controlled trial.," *Spine J.*, vol. 11, no. 11, pp. 991–8, Nov. 2011.
- [183] S. Lee and S. Park, "Clinical experience of the dynamic stabilization system for the degenerative spine disease," *J. Korean ...*, 2008.
- [184] S.-W. Yu, S.-C. Yang, C.-H. Ma, C.-H. Wu, C.-Y. Yen, and Y.-K. Tu, "Comparison of Dynesys posterior stabilization and posterior lumbar interbody fusion for spinal stenosis L4L5," *Acta Orthopædica Belgica*, vol. 78, pp. 230–239, 2012.
- [185] S. Champain, C. Mazel, A. Mitulescu, and W. Skalli, "Quantitative analysis in outcome assessment of instrumented lumbosacral arthrodesis.," *Eur. Spine J.*, vol. 16, no. 8, pp. 1241–9, Aug. 2007.
- [186] H. Park, H.-Y. Zhang, B. Y. Cho, and J. Y. Park, "Change of lumbar motion after multi-level posterior dynamic stabilization with bioflex system : 1 year follow up.," *J. Korean Neurosurg. Soc.*, vol. 46, no. 4, pp. 285–291, Oct. 2009.
- [187] M. Siddiqui and E. Karadimas, "Effects of X-STOP device on sagittal lumbar spine kinematics in spinal stenosis," *J. spinal ...*, vol. 19, no. 5, pp. 328–333, 2006.

- [188] A. Nandakumar, N. Clark, and J. Peehal, "The increase in dural sac area is maintained at 2 years after X-stop implantation for the treatment of spinal stenosis with no significant alteration in lumbar spine range," *Spine J.*, vol. 10, no. 9, pp. 762–768, 2010.
- [189] Y. JIA and P. SUN, "Preliminary evaluation of posterior dynamic lumbar stabilization in lumbar degenerative disease in Chinese patients," *Chin. Med. J. (Engl.)*, vol. 125, no. 2, pp. 253–256, 2012.
- [190] K.-Y. Ha, J.-Y. Seo, S.-E. Kwon, I.-N. Son, K.-W. Kim, and Y.-H. Kim, "Posterior dynamic stabilization in the treatment of degenerative lumbar stenosis: validity of its rationale: Clinical article," *J. Neurosurg. Spine*, vol. 18, no. January, pp. 24–31, 2013.
- [191] D. Kong, E. Kim, and W. Eoh, "One-year outcome evaluation after interspinous implantation for degenerative spinal stenosis with segmental instability," *J. Korean Med. ...*, no. January 2000, pp. 330–335, 2007.
- [192] H. Liu, J. Zhou, B. Wang, H. Wang, Z. Jin, Z. Zhu, and K. Miao, "Comparison of Topping-off and posterior lumbar interbody fusion surgery in lumbar degenerative disease: a retrospective study.," *Chin. Med. J. (Engl.)*, vol. 125, no. 22, pp. 3942–3946, 2012.
- [193] N. R. Ordway, A. H. Fayyazi, C. Abjornson, J. Calabrese, S.-A. Park, B. Fredrickson, K. Yonemura, and H. a. Yuan, "Twelve-Month Follow-up of Lumbar Spine Range of Motion Following Intervertebral Disc Replacement Using Radiostereometric Analysis," *SAS J.*, vol. 2, no. 1, pp. 9–15, Mar. 2008.
- [194] C. Tournier, S. Aunoble, J. C. Le Huec, J. P. Lemaire, P. Tropiano, V. Lafage, and W. Skalli, "Total disc arthroplasty: consequences for sagittal balance and lumbar spine movement.," *Eur. Spine J.*, vol. 16, no. 3, pp. 411–21, Mar. 2007.
- [195] C. J. Siepe, W. Hitzl, and P. Meschede, "Interdependence between disc space height, range of motion and clinical outcome in total lumbar disc replacement," *Spine (Phila. Pa. 1976)*, vol. 34, no. 9, pp. 904–916, 2009.
- [196] C. S. Shim, S. Lee, H. Shin, and H. S. Kang, "CHARITE Versus ProDisc A Comparative Study of a Minimum 3-Year Follow-up," vol. 32, no. 9, pp. 1012–1018, 2007.
- [197] E. SariAli, J. P. Lemaire, H. Pascal-Mousselard, H. Carrier, and W. Skalli, "In vivo study of the kinematics in axial rotation of the lumbar spine after total intervertebral disc replacement: long-term results: a 10-14 years follow up evaluation.," *Eur. Spine J.*, vol. 15, no. 10, pp. 1501–1510, Oct. 2006.
- [198] S.-A. Park, N. R. Ordway, A. H. Fayyazi, B. E. Fredrickson, and H. a Yuan, "Comparison of Cobb technique, quantitative motion analysis, and radiostereometric analysis in measurement of segmental range of motions after lumbar total disc arthroplasty.," *J. Spinal Disord. Tech.*, vol. 22, no. 8, pp. 602–9, Dec. 2009.

- [199] G. Leivseth, S. Braaten, W. Frobin, and P. Brinckmann, "Mobility of lumbar segments instrumented with a ProDisc II prosthesis: a two-year follow-up study," *Spine (Phila. Pa. 1976)*, vol. 31, no. 15, pp. 1726–1733, 2006.
- [200] R. C. Huang, F. P. Girardi, F. P. Cammisa Jr, P. Tropiano, and T. Marnay, "Long-term flexion-extension range of motion of the prodisc total disc replacement.," *J. Spinal Disord. Tech.*, vol. 16, no. 5, pp. 435–40, Oct. 2003.
- [201] R. C. Huang, F. P. Girardi, F. P. Cammisa, M. R. Lim, P. Tropiano, and T. Marnay, "Correlation between range of motion and outcome after lumbar total disc replacement: 8.6-year follow-up.," *Spine (Phila. Pa. 1976)*, vol. 30, no. 12, pp. 1407–1411, Jun. 2005.
- [202] R. C. Huang, P. Tropiano, T. Marnay, F. P. Girardi, M. R. Lim, and F. P. Cammisa, "Range of motion and adjacent level degeneration after lumbar total disc replacement.," *Spine J.*, vol. 6, no. 3, pp. 242–7, 2006.
- [203] S. S. Chung, C. S. Lee, C. S. Kang, and S. H. Kim, "The effect of lumbar total disc replacement on the spinopelvic alignment and range of motion of the lumbar spine.," *J. Spinal Disord. Tech.*, vol. 19, no. 5, pp. 307–11, Jul. 2006.
- [204] M. J. Bey, R. Zauel, S. K. Brock, and S. Tashman, "Validation of a new model-based tracking technique for measuring three-dimensional, *in vivo* glenohumeral joint kinematics," *J. Biomech. Eng.*, vol. 128, no. 4, p. 604, 2006.
- [205] S. Tashman and W. Anderst, "In-vivo measurement of dynamic joint motion using high speed biplane radiography and CT: application to canine ACL deficiency," *Trans. Soc. Mech. Eng. J. Biomech. Eng.*, vol. 125, no. 2, pp. 238–245, 2003.
- [206] Y. Morishita, H. Ohta, M. Naito, Y. Matsumoto, G. Huang, M. Tatsumi, Y. Takemitsu, and H. Kida, "Kinematic evaluation of the adjacent segments after lumbar instrumented surgery: a comparison between rigid fusion and dynamic non-fusion stabilization.," *Eur. Spine J.*, vol. 20, no. 9, pp. 1480–5, Sep. 2011.
- [207] S.-C. Lin, W.-C. Tsai, S.-S. Wu, and P.-Q. Chen, "Radiological and Mathematical Studies Regarding the Effects of Spinal Fixation on Kinematics and Mechanics at the Parafixed Segments," *J. Mech.*, vol. 26, no. 03, pp. 413–422, May 2011.
- [208] J.-H. Shin, S. Wang, Q. Yao, K. B. Wood, and G. Li, "Investigation of coupled bending of the lumbar spine during dynamic axial rotation of the body," *Eur. Spine J.*, pp. 1–7, 2013.
- [209] G. Li, S. Wang, P. Passias, Q. Xia, G. Li, and K. Wood, "Segmental *in vivo* vertebral motion during functional human lumbar spine activities.," *Eur. Spine J.*, vol. 18, no. 7, pp. 1013–21, Jul. 2009.
- [210] S. T. Canale and J. H. Beaty, *Campbell's Operative Orthopaedics: Expert Consult Premium Edition-Enhanced Online Features*. Elsevier Health Sciences, 2012.

- [211] S. L. Delp, J. P. Loan, M. G. Hoy, F. E. Zajac, E. L. Topp, and J. M. Rosen, “An interactive graphics-based model of the lower extremity to study orthopaedic surgical procedures,” *Biomed. Eng. IEEE Trans.*, vol. 37, no. 8, pp. 757–767, 1990.
- [212] J. R. Meakin, J. S. Gregory, F. W. Smith, F. J. Gilbert, and R. M. Aspden, “Characterizing the shape of the lumbar spine using an active shape model: reliability and precision of the method,” *Spine (Phila. Pa. 1976)*, vol. 33, no. 7, pp. 807–13, Apr. 2008.
- [213] J. Cholewicki, J. J. Crisco, T. R. Oxland, I. Yamamoto, and M. M. Panjabi, “Effects of posture and structure on three-dimensional coupled rotations in the lumbar spine. A biomechanical analysis,” *Spine (Phila. Pa. 1976)*, vol. 21, no. 21, pp. 2421–8, Nov. 1996.
- [214] I. Gilad and M. Nissan, “A study of vertebra and disc geometric relations of the human cervical and lumbar spine,” *Spine (Phila. Pa. 1976)*, vol. 11, no. 2, pp. 154–157, 1986.
- [215] I. Gilad and M. Nissan, “Sagittal evaluation of elemental geometrical dimensions of human vertebrae,” *J. Anat.*, vol. 143, p. 115, 1985.
- [216] M. M. Panjabi, V. Goel, T. Oxland, K. Takata, J. Duranceau, M. Krag, and M. Price, “Human lumbar vertebrae: quantitative three-dimensional anatomy,” *Spine (Phila. Pa. 1976)*, vol. 17, no. 3, pp. 299–306, 1992.
- [217] D. J. Pearsall, J. G. Reid, and L. a Livingston, “Segmental inertial parameters of the human trunk as determined from computed tomography,” *Ann. Biomed. Eng.*, vol. 24, no. 2, pp. 198–210, 1996.
- [218] W. T. Dempster and G. R. L. Gaughran, “Properties of body segments based on size and weight,” *Am. J. Anat.*, vol. 120, no. 1, pp. 33–54, 1967.
- [219] M. M. Panjabi, R. A. Brand Jr, and A. A. White III, “Three-dimensional flexibility and stiffness properties of the human thoracic spine,” *J. Biomech.*, vol. 9, no. 4, pp. 185–192, 1976.
- [220] M. G. Gardner-Morse and I. a. F. Stokes, “Structural behavior of human lumbar spinal motion segments,” *J. Biomech.*, vol. 37, no. 2, pp. 205–212, Feb. 2004.
- [221] W. Tawackoli, R. Marco, and M. A. K. Liebschner, “The effect of compressive axial preload on the flexibility of the thoracolumbar spine,” *Spine (Phila. Pa. 1976)*, vol. 29, no. 9, pp. 988–993, 2004.
- [222] A. G. Patwardhan, R. M. Havey, G. Carandang, J. Simonds, L. I. Voronov, A. J. Ghanayem, K. P. Meade, T. M. Gavin, and O. Paxinos, “Effect of compressive follower preload on the flexion–extension response of the human lumbar spine,” *J. Orthop. Res.*, vol. 21, no. 3, pp. 540–546, 2003.

- [223] M. Christophy, M. Curtin, N. A. F. Senan, J. C. Lotz, and O. M. O'Reilly, "On the modeling of the intervertebral joint in multibody models for the spine," *Multibody Syst. Dyn.*, vol. 30, no. 4, pp. 413–432, 2013.
- [224] F. Heuer, H. Schmidt, Z. Klezl, L. Claes, and H.-J. Wilke, "Stepwise reduction of functional spinal structures increase range of motion and change lordosis angle," *J. Biomech.*, vol. 40, no. 2, pp. 271–280, 2007.
- [225] N. Bogduk, M. Pearcy, and G. Hadfield, "Anatomy and biomechanics of psoas major," *Clin. Biomech.*, vol. 7, no. 2, pp. 109–119, 1992.
- [226] J. Macintosh and N. Bogduk, "1987 Volvo Award in Basic Science: The Morphology of the Lumbar Erector Spinae," *Spine (Phila. Pa. 1976)*, vol. 12, no. 7, pp. 658–668, 1987.
- [227] J. Macintosh and N. Bogduk, "The attachments of the lumbar erector spinae," *Spine (Phila. Pa. 1976)*, vol. 16, no. 7, pp. 783–792, 1991.
- [228] J. E. Macintosh, F. Valencia, N. Bogduk, and R. R. Munro, "The morphology of the human lumbar multifidus," *Clin. Biomech.*, vol. 1, no. 4, pp. 196–204, 1986.
- [229] J. E. Macintosh and N. Bogduk, "The biomechanics of the lumbar multifidus," *Clin. Biomech.*, vol. 1, no. 4, pp. 205–213, 1986.
- [230] S. Phillips, S. Mercer, and N. Bogduk, "Anatomy and biomechanics of quadratus lumborum," *Proc. Inst. Mech. Eng. Part H J. Eng. Med.*, vol. 222, no. 2, pp. 151–159, Feb. 2008.
- [231] I. a Stokes and M. Gardner-Morse, "Quantitative anatomy of the lumbar musculature," *J. Biomech.*, vol. 32, no. 3, pp. 311–6, Mar. 1999.
- [232] E. M. Arnold, S. R. Ward, R. L. Lieber, and S. L. Delp, "A model of the lower limb for analysis of human movement," *Ann. Biomed. Eng.*, vol. 38, no. 2, pp. 269–279, 2010.
- [233] J. S. Anderson, A. W. Hsu, and A. N. Vasavada, "Morphology, architecture, and biomechanics of human cervical multifidus," *Spine (Phila. Pa. 1976)*, vol. 30, no. 4, pp. E86–E91, 2005.
- [234] N. Bogduk, G. Johnson, and D. Spalding, "The morphology and biomechanics of latissimus dorsi," *Clin. Biomech.*, vol. 13, no. 6, pp. 377–385, 1998.
- [235] A. L. Rosatelli, K. Ravichandiran, and A. M. Agur, "Three- dimensional study of the musculotendinous architecture of lumbar multifidus and its functional implications," *Clin. Anat.*, vol. 21, no. 6, pp. 539–546, 2008.
- [236] S. R. Ward, C. W. Kim, C. M. Eng, L. J. GottschalkIV, A. Tomiya, S. R. Garfin, and R. L. Lieber, "Architectural analysis and intraoperative measurements demonstrate the unique

- design of the multifidus muscle for lumbar spine stability,” *J. Bone Jt. Surg.*, vol. 91, no. 1, pp. 176–185, 2009.
- [237] M. Dreischarf, A. Rohlmann, R. Zhu, H. Schmidt, and T. Zander, “Is it possible to estimate the compressive force in the lumbar spine from intradiscal pressure measurements? A finite element evaluation,” *Med. Eng. Phys.*, vol. 35, no. 9, pp. 1385–1390, 2013.
- [238] S.-Y. Poh, W.-M. Yue, J. L.-T. Chen, C.-M. Guo, W. Yeo, and S.-B. Tan, “Two-year outcomes of transforaminal lumbar interbody fusion,” *J. Orthop. Surg.*, vol. 19, no. 2, 2011.
- [239] J.-H. Min, J.-S. Jang, and S.-H. Lee, “Comparison of anterior-and posterior-approach instrumented lumbar interbody fusion for spondylolisthesis,” 2007.
- [240] W. Anderst, R. Zael, J. Bishop, E. Demps, and S. Tashman, “Validation of three-dimensional model-based tibio-femoral tracking during running,” *Med. Eng. Phys.*, vol. 31, no. 1, pp. 10–16, 2009.
- [241] W. J. Anderst, E. Baillargeon, W. F. Donaldson III, J. Y. Lee, and J. D. Kang, “Validation of a Non-Invasive Technique to Precisely Measure *In vivo* Three-Dimensional Cervical Spine Movement,” *Spine (Phila. Pa. 1976)*, vol. 36, no. 6, p. E393, 2011.
- [242] A. K. Aiyangar, L. Zheng, S. Tashman, W. J. Anderst, and X. Zhang, “Capturing Three-Dimensional *In vivo* Lumbar Intervertebral Joint Kinematics Using Dynamic Stereo-X-Ray Imaging,” *J. Biomech. Eng.*, vol. 136, no. 1, p. 11004, 2014.
- [243] N. Arjmand, a Shirazi-Adl, and B. Bazrgari, “Wrapping of trunk thoracic extensor muscles influences muscle forces and spinal loads in lifting tasks,” *Clin. Biomech. (Bristol, Avon)*, vol. 21, no. 7, pp. 668–75, Aug. 2006.
- [244] M. Christophy, “A Detailed Open-Source Musculoskeletal Model of the Human Lumbar Spine by,” 2010.
- [245] a Rohlmann, S. Neller, L. Claes, G. Bergmann, and H. J. Wilke, “Influence of a follower load on intradiscal pressure and intersegmental rotation of the lumbar spine,” *Spine (Phila. Pa. 1976)*, vol. 26, no. 24, pp. E557–61, Dec. 2001.
- [246] J. S. Bae, S.-H. Lee, J.-S. Kim, B. Jung, and G. Choi, “Adjacent segment degeneration after lumbar interbody fusion with percutaneous pedicle screw fixation for adult low-grade isthmic spondylolisthesis: minimum 3 years of follow-up,” *Neurosurgery*, vol. 67, no. 6, pp. 1600–1608, 2010.
- [247] L. Pimenta, L. Marchi, L. Oliveira, E. Coutinho, and R. Amaral, “A prospective, randomized, controlled trial comparing radiographic and clinical outcomes between stand-

- alone lateral Interbody lumbar fusion with either silicate calcium phosphate or rh-BMP2,” *J. Neurol. Surg. Part A Cent. Eur. Neurosurg.*, vol. 74, no. 06, pp. 343–350, 2013.
- [248] J. Rodgers, E. Gerber, J. Lehmen, and B. Rodgers, “Clinical and Radiographic Outcome in Less Invasive Lumbar Fusion: XLIF at Two Year Follow-Up,” *J. Spine Neurosurg.*, 2013.
- [249] C. Seng, M. A. Siddiqui, K. P. L. Wong, K. Zhang, W. Yeo, S. B. Tan, and W.-M. Yue, “Five-year outcomes of minimally invasive versus open transforaminal lumbar interbody fusion: a matched-pair comparison study,” *Spine (Phila. Pa. 1976)*, vol. 38, no. 23, pp. 2049–2055, 2013.
- [250] K. E. Radcliff, C. K. Kepler, M. Maaieh, D. G. Anderson, J. Rihn, T. Albert, A. Vaccaro, and A. Hilibrand, “What is the Rate of Lumbar Adjacent Segment Disease after Percutaneous versus Open Fusion?,” *Orthop. Surg.*, vol. 6, no. 2, pp. 118–120, 2014.
- [251] H. Liu, W. Wu, Y. Li, J. Liu, K. Yang, and Y. Chen, “Protective effects of preserving the posterior complex on the development of adjacent-segment degeneration after lumbar fusion: Clinical article,” *J. Neurosurg. Spine*, vol. 19, no. 2, pp. 201–206, 2013.
- [252] J. E. Macintosh, N. Bogduk, and M. J. Pearcy, “The effects of flexion on the geometry and actions of the lumbar erector spinae,” *Spine (Phila. Pa. 1976)*, vol. 18, no. 7, pp. 884–893, 1993.
- [253] A. Rohlmann, F. Graichen, U. Weber, and G. Bergmann, “Monitoring *in vivo* implant loads with a telemeterized internal spinal fixation device,” *Spine (Phila. Pa. 1976)*, vol. 25, no. 23, pp. 2981–2986, 2000.
- [254] A. Rohlmann, L. H. Riley III, G. Bergmann, and F. Graichen, “*In vitro* load measurement using an instrumented spinal fixation device,” *Med. Eng. Phys.*, vol. 18, no. 6, pp. 485–488, 1996.
- [255] a Rohlmann, G. Bergmann, F. Graichen, and U. Weber, “Comparison of loads on internal spinal fixation devices measured *in vitro* and *in vivo*,” *Med. Eng. Phys.*, vol. 19, no. 6, pp. 539–46, Sep. 1997.
- [256] B. A. Alkner, P. A. Tesch, and H. E. Berg, “Quadriceps EMG/force relationship in knee extension and leg press,” *Med. Sci. Sports Exerc.*, vol. 32, no. 2, pp. 459–463, 2000.
- [257] G. L. Moseley, P. W. Hodges, and S. C. Gandevia, “Deep and superficial fibers of the lumbar multifidus muscle are differentially active during voluntary arm movements,” *Spine (Phila. Pa. 1976)*, vol. 27, no. 2, pp. E29–E36, 2002.
- [258] A. Rohlmann, R. Petersen, V. Schwachmeyer, F. Graichen, and G. Bergmann, “Spinal loads during position changes,” *Clin. Biomech.*, vol. 27, no. 8, pp. 754–758, 2012.

- [259] A. Rohlmann, T. Zander, F. Graichen, M. Dreischarf, and G. Bergmann, "Measured loads on a vertebral body replacement during sitting," *Spine J.*, vol. 11, no. 9, pp. 870–875, 2011.
- [260] A. Rohlmann, H. Schmidt, U. Gast, I. Kutzner, P. Damm, and G. Bergmann, "In vivo measurements of the effect of whole body vibration on spinal loads," *Eur. Spine J.*, vol. 23, no. 3, pp. 666–672, 2014.
- [261] M. D. Shuster, "A survey of attitude representations," *Navigation*, vol. 8, no. 9, 1993.
- [262] F. E. Zajac, "Muscle and Tendon: Properties, Models, Scaling, and Application to Biomechanics and Motor Control." *Critical reviews in biomedical engineering* 17.4 (1989): 359-411,1989.
- [263] J. C. Iatridis, L. A. Setton, R. J. Foster, B. A. Rawlins, M. Weidenbaum, V. C. Mow. "Degeneration affects the anisotropic and nonlinear behaviors of human annulus fibrosus in compression." *Journal of biomechanics*, vol. 31, no. 6, pp 535-544, 1998.
- [264] E. N. Marieb, "Essential of human anatomy & physiology." *Pearson Education Inc*, 8th ed., p.350, 2006.

Appendix A Introduction to Mathematical Background in ArtiSynth

A.1 Frames

In ArtiSynth each rigid body has its own body frame whose configuration with respect to the world (global) frame can be described by a transformation matrix X_{1W} :

$$X_{1W} = \begin{pmatrix} R_{1W} & {}^W p_{1W} \\ 0 & 1 \end{pmatrix} \quad (\text{A-1})$$

Where R_{1W} is the rotation matrix that transforms the representation of a 3D vector in frame 1 to its representation in world frame W and p_{1W} is the vector connecting the origin of frame W to that of the frame 1. Note that the leading W superscript in ${}^W p_{1W}$ denotes world coordinate representation of the vector p_{1W} .

To be transformed by X_{1W} , all vectors are extended to 4D vectors with either 0 or 1 as their last entry, depending on the type of the vector they are representing. If ${}^1 r$ is the position vector of a point expressed in frame 1, its world coordinate representation will be obtained as:

$${}^W r = R_{1W} {}^1 r + {}^W p_{1W} \quad (\text{A-2})$$

whereas if ${}^1 f$ is the expression of a force vector in frame 1, then its representation in world coordinate does not need adding the term ${}^W p_{1W}$, i.e.:

$${}^W f = R_{1W} {}^1 f \quad (\text{A-3})$$

If we extend the position vector to $\tilde{r} = \begin{pmatrix} r \\ 1 \end{pmatrix}$ and the force vector to $\tilde{f} = \begin{pmatrix} f \\ 0 \end{pmatrix}$, both vectors can be transformed by X_{1W} as:

$${}^W\tilde{r} = X_{1W} {}^1\tilde{r} \quad \text{and} \quad {}^W\tilde{f} = X_{1W} {}^1\tilde{f} \quad (\text{A-4})$$

In fact, between any two frames, e.g. frame 2 and 1, we can define the transformation matrix X_{21} as:

$$X_{21} = \begin{pmatrix} R_{21} & {}^1p_{21} \\ 0 & 1 \end{pmatrix} \quad (\text{A-5})$$

which transforms the representation of vectors in 2 to that in frame 1. One feature of this transformation matrix is that its inverse, X_{21}^{-1} , is equal to X_{12} :

$$X_{21}^{-1} = \begin{pmatrix} R_{21}^{-1} & -R_{21}^{-1} {}^1p_{21} \\ 0 & 1 \end{pmatrix} = \begin{pmatrix} R_{12} & -R_{12} {}^1p_{21} \\ 0 & 1 \end{pmatrix} = \begin{pmatrix} R_{12} & {}^2p_{12} \\ 0 & 1 \end{pmatrix} = X_{12} \quad (\text{A-6})$$

Also when dealing with multiple frames, we can easily use the chain rule. For instance, for the frames shown in Figure A-1, knowing the transformation from frame 1 to frame A, X_{1A} , and from frame A to W, X_{AW} , we can obtain for X_{1W} to be:

$$X_{1W} = X_{AW}X_{1A} \quad (\text{A-7})$$

Knowing that $X_{2W} = X_{BW}X_{2B}$, we can obtain for X_{21} to be:

$$X_{21} = X_{W1}X_{2W} = X_{1W}^{-1}X_{2W} \quad (\text{A-8})$$

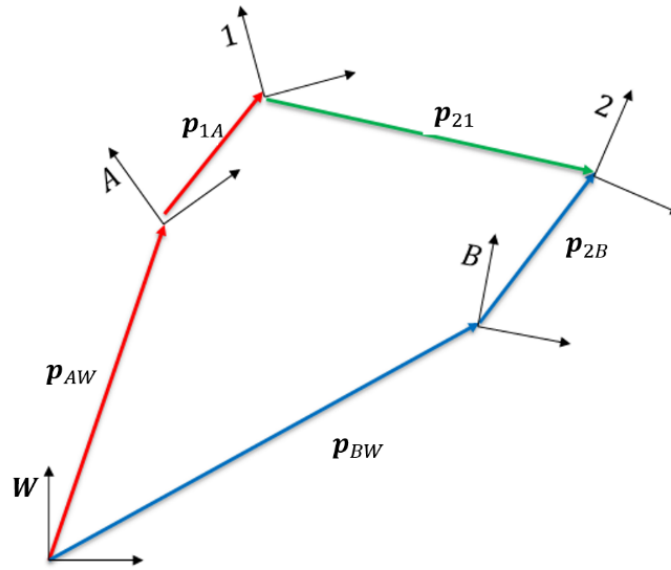


Figure A-1. Use of chain rule for obtaining the transformation matrix between two arbitrary frames. In order to obtain the transformation matrix from frame 2 to frame 1 X_{21} , knowing X_{2B} , X_{BW} , X_{WA} , X_{A1} one can use the chain rule as $X_{21} = X_{A1}X_{WA}X_{BW}X_{2B}$.

A.2 Variation of Rotation Matrix

The orthonormal bases of any two frames can always be related to each other by a rotation matrix [261]. Using the chain rule in part 1.1, we can relate the rotations between three frames 1, 2, and 2' in Figure A-2 through the formula:

$$R_{2'1} = R_{21}R_{2'2} \quad (\text{A-9})$$

In Figure A-2, 2' is the configuration of frame 2 after an infinitesimal time Δt ; θ_{21} and $\theta_{2'2}$ each represents the angle of rotations between frame 2 to 1 and 2' to 2, respectively. As one of the results of Euler theorem [261], each rotation matrix, e.g. R_{21} in here, can be described by an angle θ_{21} about a rotation vector \hat{n} as:

$$R_{21} = I + \sin \theta_{21} [\hat{n}] + (1 - \cos \theta_{21}) [\hat{n}]^2 \quad (\text{A-10})$$

where:

$$[\hat{n}] = \begin{pmatrix} 0 & -\hat{n}_z & \hat{n}_y \\ \hat{n}_z & 0 & -\hat{n}_x \\ -\hat{n}_y & \hat{n}_x & 0 \end{pmatrix} \quad (\text{A-11})$$

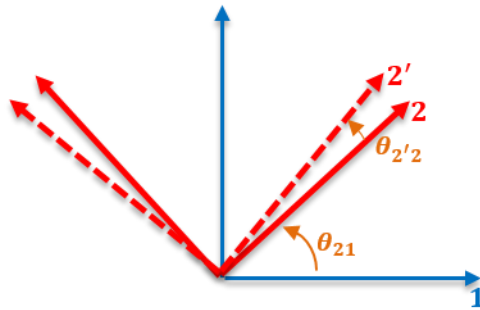


Figure A-2. Variation in frame configuration represented by an infinitesimal rotation angle.

For obtaining the variation of a rotation matrix, in order to better understand its concept, we start by taking time derivative of the rotation matrix:

$$\begin{aligned}
\frac{d}{dt}(R_{21}) &= \lim_{\Delta t \rightarrow 0} \frac{R_{2'1} - R_{21}}{\Delta t} = \lim_{\Delta t \rightarrow 0} \frac{R_{21}R_{2'2} - R_{21}}{\Delta t} = \lim_{\Delta t \rightarrow 0} \frac{R_{21}(R_{2'2} - I)}{\Delta t} \\
&= \lim_{\Delta t \rightarrow 0} \frac{R_{21}(I + \sin \theta_{2'2} [\hat{n}] + (1 - \cos \theta_{2'2})[\hat{n} \times]^2 - I)}{\Delta t} \\
&= \lim_{\Delta t \rightarrow 0} \frac{R_{21}(\theta_{2'2}[\hat{n}])}{\Delta t} = R_{21} [{}^2\omega_{21}] = [{}^1\omega_{21}]R_{21}
\end{aligned} \tag{A-12}$$

where ω_{21} is defined as:

$$[{}^2\omega_{21}] = \lim_{\Delta t \rightarrow 0} \frac{\theta_{2'2} [{}^2\hat{n}]}{\Delta t} \tag{A-13}$$

Therefore the variation of the rotation matrix R_{BA} can be expressed as:

$$\delta R_{21} = \frac{d}{dt}(R_{21}) dt = R_{21} [{}^2\omega_{21}] dt = R_{21} [{}^2\delta\theta_{21}] \tag{A-14}$$

Where ${}^2\delta\theta_{21}$ is defined as:

$${}^2\delta\theta_{21} = \theta_{2'2} [{}^2\hat{n}] \tag{A-15}$$

But this formulation is correct only for small angles for which $\sin \theta_{2'2} \approx \theta_{2'2}$.

A.3 Frame Springs

In ArtiSynth, one can attach springs and dampers between any two points on any two rigid bodies using the class “FrameSpring”, whose stiffness and damping can be defined through the class “FrameMaterial”. Each frame spring consists of two frames whose origins are located at the attachment points of the spring. Considering frame springs to be massless, the forces and moments on two ends of the frame springs are always equal and opposite so that:

$$f_2 = -f_1 \tag{A-16}$$

$$\tau_2 = -\tau_1$$

where f_1 and τ_1 are respectively the restoring force and torque generated by the frame spring and applied to the origin of frame 1. With the assumption that f_1 and τ_1 can be decomposed into separate functions of relative position and velocities between the two frames of the frame spring, f_1 and τ_1 can be written as:

$$f_1 = f_{1p}(p_{21}) + f_{1\theta}(\theta_{21}) + f_{1\dot{p}}(\dot{p}_{21}) + f_{1\omega}(\omega_{21}) \tag{A-17}$$

$$\tau_1 = \tau_{1p}(p_{21}) + \tau_{1\theta}(\theta_{21}) + \tau_{1\dot{p}}(\dot{p}_{21}) + \tau_{1\omega}(\omega_{21})$$

where p_{21} and \dot{p}_{21} are the displacement and relative velocity between the origins of the frames, while ω_{21} is the angular velocity of frame 2 with respect to frame 1, and θ_{21} is the rotation vector about which frame 1 could rotate so that its base vectors get mapped to the base vectors of frame 2.

Assuming that frame 1 is fixed and only frame 2 moves, in order to obtain the stiffness matrix of the frame spring, all we need to do is to calculate the variation of f_1 and τ_1 with respect to the variations in p_{21} , \dot{p}_{21} , ω_{21} and θ_{21} , when all vectors are represented in frame 1. Doing so we will have the following formulation:

$$\begin{Bmatrix} {}^1\delta f_1 \\ {}^1\delta \tau_1 \end{Bmatrix} = \begin{pmatrix} {}^1K_{fp} & {}^1K_{f\theta} \\ {}^1K_{\tau p} & {}^1K_{\tau\theta} \end{pmatrix} \begin{Bmatrix} {}^1\delta p_{21} \\ {}^1\delta \theta_{21} \end{Bmatrix} + \begin{pmatrix} {}^1D_{f\dot{p}} & {}^1D_{f\omega} \\ {}^1D_{\tau\dot{p}} & {}^1D_{\tau\omega} \end{pmatrix} \begin{Bmatrix} {}^1\delta v_{21} \\ {}^1\delta \omega_{21} \end{Bmatrix} \quad (\text{A-18})$$

in which ${}^1K_{fp}$ is the Jacobian of ${}^1f_{1p}$, usually depicted as:

$${}^1K_{fp} = \frac{\partial \left({}^1f_{1p_x}, {}^1f_{1p_y}, {}^1f_{1p_z} \right)}{\partial \left({}^1p_{21_x}, {}^1p_{21_y}, {}^1p_{21_z} \right)} \quad (\text{A-19})$$

where for instance ${}^1f_{1p_x}$ is the x component of the representation of f_{1p} in frame 1.

A.4 Calculation of Frame Spring Jacobians

This section can be skipped by users of current frame springs in ArtiSynth, because all they need to set is frame 1 representation of the stiffness and damping matrices in equation (A-18). However, those who want to define a custom frame spring may benefit from knowing the mathematics behind calculation of frame spring jacobians. In order to calculate the complete position and velocity jacobians for the frame spring, we need to write all variations in world coordinate. Assuming that both frames 1 and 2 are moving and knowing that ${}^1p_{21} = R_{W1}({}^Wp_{2W} - {}^Wp_{1W})$, we can take a time derivative to of ${}^1p_{21}$ to obtain:

$$\begin{aligned}
{}^1\dot{p}_{21} &= \dot{R}_{W1}({}^W p_{2W} - {}^W p_{1W}) + R_{W1}({}^W \dot{p}_{2W} - {}^W \dot{p}_{1W}) \\
&= R_{W1} [{}^W \omega_{W1}] ({}^W p_{2W} - {}^W p_{1W}) + R_{W1} ({}^W \dot{p}_{2W} - {}^W \dot{p}_{1W})
\end{aligned} \tag{A-20}$$

Multiplying equation (A-20) by dt yields:

$$\begin{aligned}
{}^1\delta p_{21} &= R_{W1} [{}^W \delta \theta_{W1}] ({}^W p_{2W} - {}^W p_{1W}) + R_{W1} ({}^W \delta p_{2W} - {}^W \delta p_{1W}) \\
&= R_{W1} \left([{}^W \delta \theta_{W1}] ({}^W p_{21}) + ({}^W \delta p_{2W} - {}^W \delta p_{1W}) \right) \\
&= R_{W1} \left([{}^W p_{21}] ({}^W \delta \theta_{1W}) + ({}^W \delta p_{2W} - {}^W \delta p_{1W}) \right)
\end{aligned} \tag{A-21}$$

where at the right hand side of the equation all terms are in world coordinates. Similarly, we can write for ${}^1\delta v_{21}$ and ${}^1\delta \omega_{21}$:

$$\begin{aligned}
{}^1\delta v_{21} &= R_{W1} \left([{}^W v_{21}] ({}^W \delta \theta_{1W}) + ({}^W \delta v_{2W} - {}^W \delta v_{1W}) \right) \\
{}^1\delta \omega_{21} &= R_{W1} \left([{}^W \omega_{21}] ({}^W \delta \theta_{1W}) + ({}^W \delta \omega_{2W} - {}^W \delta \omega_{1W}) \right)
\end{aligned} \tag{A-22}$$

Converting the force variations from frame 1 to World frame can be done through:

$$\begin{aligned}
{}^W \delta f_1 &= R_{1W} ({}^1\delta f_1 - [{}^1 f_1] \delta \theta_1) \\
{}^W \delta \tau_1 &= R_{1W} ({}^1\delta \tau_1 - [{}^1 \tau_1] \delta \theta_1)
\end{aligned} \tag{A-23}$$

Finally, based on the relation between angular velocities of frames that $[{}^1\omega_{21}] = R_{W1}([{}^W\omega_{2W}] - [{}^W\omega_{1W}])$, we can obtain for ${}^1\delta\theta_{21}$ to be:

$${}^1\delta\theta_{21} = R_{W1}({}^W\delta\theta_{2W} - {}^W\delta\theta_{1W}) \quad (\text{A-24})$$

Now by using equations (A-21), (A-22), (A-23), and (A-24), to substitute for ${}^1\delta f_1$, ${}^1\delta\tau_1$, ${}^1\delta p_{21}$, ${}^1\delta\theta_{21}$, ${}^1\delta v_{21}$, and ${}^1\delta\omega_{21}$ in equation (A-18), and dropping the preceding W superscript, we can summarize the relation between world representation of the variation of all vectors in the following equation:

$$\begin{aligned} \begin{pmatrix} \delta f_1 \\ \delta\tau_1 \\ \delta f_2 \\ \delta\tau_2 \end{pmatrix} &= J_K \begin{pmatrix} \delta x_{1W} \\ \delta\theta_{1W} \\ \delta p_{2W} \\ \delta\theta_{2W} \end{pmatrix} + J_D \begin{pmatrix} \delta v_{1W} \\ \delta\omega_{1W} \\ \delta v_{2W} \\ \delta\omega_{2W} \end{pmatrix} \\ &+ \left(\begin{pmatrix} -[f_1] \\ -[\tau_1] \\ [f_1] \\ [\tau_1] \end{pmatrix} - J_K \begin{pmatrix} [p_{21}] \\ 0 \\ 0 \\ 0 \end{pmatrix} - J_D \begin{pmatrix} [v_{21}] \\ [\omega_{21}] \\ 0 \\ 0 \end{pmatrix} \right) \delta\theta_{1W} \end{aligned} \quad (\text{A-25})$$

Where:

$$J_K = \begin{pmatrix} -K_{fx} & -K_{f\theta} & K_{fx} & K_{f\theta} \\ -K_{\tau x} & -K_{\tau\theta} & K_{\tau x} & K_{\tau\theta} \\ K_{fx} & K_{f\theta} & -K_{fx} & -K_{f\theta} \\ K_{\tau x} & K_{\tau\theta} & -K_{\tau x} & -K_{\tau\theta} \end{pmatrix} \quad (\text{A-26})$$

$$J_D = \begin{pmatrix} -D_{fv} & -D_{f\omega} & D_{fv} & D_{f\omega} \\ -D_{\tau v} & -D_{\tau\omega} & D_{\tau v} & D_{\tau\omega} \\ D_{fv} & D_{f\omega} & -D_{fv} & -D_{f\omega} \\ D_{\tau v} & D_{\tau\omega} & -D_{\tau v} & -D_{\tau\omega} \end{pmatrix}$$

Note that each term in J_K and J_D is in World coordinate. For instance K_{fx} is calculated from ${}^1K_{fx}$ as:

$${}^W K_{fx} = R_{1W} {}^1 K_{fx} R_{1W} \quad (\text{A-27})$$

A.5 Linear Frame Spring

In ArtiSynth, linear frame springs are frame springs whose generated restoring forces are linear functions of ${}^1p_{21}$, ${}^1v_{21}$, ${}^1\omega_{21}$, and ${}^1\hat{\theta}_{21}$, where $\hat{\theta}_{21}$ is the vector of small angle approximation of the rotation matrix between frame 2 and 1.

$$\begin{Bmatrix} {}^1f_1 \\ {}^1\tau_1 \end{Bmatrix} = \begin{pmatrix} {}^1K_{fp} & {}^1K_{f\hat{\theta}} \\ {}^1K_{\tau p} & {}^1K_{\tau\hat{\theta}} \end{pmatrix} \begin{Bmatrix} {}^1p_{21} \\ {}^1\hat{\theta}_{21} \end{Bmatrix} + \begin{pmatrix} {}^1D_{fp} & {}^1D_{f\omega} \\ {}^1D_{\tau p} & {}^1D_{\tau\omega} \end{pmatrix} \begin{Bmatrix} {}^1v_{21} \\ {}^1\omega_{21} \end{Bmatrix} \quad (\text{A-28})$$

In fact, while at each instant, ${}^1p_{21}$, ${}^1v_{21}$, and ${}^1\omega_{21}$ can be directly determined from the transformation matrices, $\hat{\theta}_{21}$ needs to get extracted from the rotation matrix R_{21} . Given that any rotation of a rigid body (or a frame) can be decomposed into three successive rotation about each of the body-fixed axes, also known as Euler axes (shuser), we can consider the rotation corresponding to R_{21} to be the result of a rotation about axis z (R_z), followed by a rotation about axis y (R_y) and then by a rotation about axis x (R_x), through the angles θ_z , θ_y , and θ_x , respectively. With this consideration we will obtain the following formulation for R_{21} :

$$\begin{aligned}
R_{21} = R_z R_y R_x &= \begin{pmatrix} c_z & -s_z & 0 \\ s_z & c_z & 0 \\ 0 & 0 & 1 \end{pmatrix} \begin{pmatrix} c_y & 0 & s_y \\ 0 & 1 & 0 \\ -s_y & 0 & c_y \end{pmatrix} \begin{pmatrix} 1 & 0 & 0 \\ 0 & c_x & -s_x \\ 0 & s_x & c_x \end{pmatrix} \\
&= \begin{pmatrix} c_z c_y & c_z s_y s_x - s_z c_x & c_z s_y c_x + s_z s_x \\ s_z c_y & s_z s_y s_x + c_z c_x & s_z s_y c_x - c_z s_x \\ -s_y & c_y s_x & c_y c_x \end{pmatrix}
\end{aligned} \tag{A-29}$$

Where $cx \equiv \cos \theta_x$, $cy \equiv \cos \theta_y$, $cz \equiv \cos \theta_z$, $sx \equiv \sin \theta_x$, $sy \equiv \sin \theta_y$, and $sz \equiv \sin \theta_z$. For small rotation angles we can approximate the angles as:

$$\hat{\theta}_x \approx s_x c_y = R_{21}(2,1), \hat{\theta}_y \approx s_x c_y = -R_{21}(2,0), \hat{\theta}_z \approx s_x c_y = R_{21}(1,0) \tag{A-30}$$

Where $R_{21}(2,1)$ is the entry at third row and second column of the rotation matrix R_{21} (this notation is utilized to be compatible with the software code, where the first and last entry of a matrix M is referenced as $M(0,0)$ and $M(2,2)$ respectively). In equation (A-30), we are as if defining $\hat{\theta}_{21}$ to be a function of R_{21} and therefore in order to calculate the variation of $\hat{\theta}_{21}$ we need to first calculate the variation of R_{21} :

$$\hat{\theta}_{21} = \begin{Bmatrix} \hat{\theta}_{21x} \\ \hat{\theta}_{21y} \\ \hat{\theta}_{21z} \end{Bmatrix} = \begin{Bmatrix} R_{21}(2,1) \\ -R_{21}(2,0) \\ R_{21}(1,0) \end{Bmatrix} \rightarrow \delta \hat{\theta}_{21} = \begin{Bmatrix} \delta \hat{\theta}_{21x} \\ \delta \hat{\theta}_{21y} \\ \delta \hat{\theta}_{21z} \end{Bmatrix} = \begin{Bmatrix} \delta R_{21}(2,1) \\ -\delta R_{21}(2,0) \\ \delta R_{21}(1,0) \end{Bmatrix} \tag{A-31}$$

Where from equation (A-12) we can easily see that:

$$\delta R_{21} = [{}^1\delta\theta_{21}]R_{21} \quad (\text{A-32})$$

By working out the equation (A-21) we obtain for $\delta\hat{\theta}_{21}$:

$$\begin{Bmatrix} \delta\hat{\theta}_{21x} \\ \delta\hat{\theta}_{21y} \\ \delta\hat{\theta}_{21z} \end{Bmatrix} = \begin{bmatrix} R_{21}(1,1) & -R_{21}(1,0) & 0 \\ -R_{21}(1,0) & R_{21}(0,0) & 0 \\ R_{21}(1,1) & 0 & R_{21}(0,0) \end{bmatrix} \begin{Bmatrix} {}^1\delta\theta_{21x} \\ {}^1\delta\theta_{21y} \\ {}^1\delta\theta_{21z} \end{Bmatrix} \quad (\text{A-33})$$

Therefore:

$${}^1K_{f\hat{\theta}} \delta\hat{\theta}_{21} = {}^1K_{f\hat{\theta}} \begin{bmatrix} R_{21}(1,1) & -R_{21}(1,0) & 0 \\ -R_{21}(1,0) & R_{21}(0,0) & 0 \\ R_{21}(1,1) & 0 & R_{21}(0,0) \end{bmatrix} \begin{Bmatrix} \delta\theta_{21x} \\ \delta\theta_{21y} \\ \delta\theta_{21z} \end{Bmatrix} \quad (\text{A-34})$$

Thus:

$${}^1K_{f\theta} = {}^1K_{f\hat{\theta}} \begin{bmatrix} R_{21}(1,1) & -R_{21}(1,0) & 0 \\ -R_{21}(1,0) & R_{21}(0,0) & 0 \\ R_{21}(1,1) & 0 & R_{21}(0,0) \end{bmatrix} \quad (\text{A-35})$$

Similarly:

$${}^1K_{\tau\theta} = {}^1K_{\tau\hat{\theta}} \begin{bmatrix} R_{21}(1,1) & -R_{21}(1,0) & 0 \\ -R_{21}(1,0) & R_{21}(0,0) & 0 \\ R_{21}(1,1) & 0 & R_{21}(0,0) \end{bmatrix} \quad (\text{A-36})$$

A.6 OffsetFrameSpring

For our special need for a frame spring whose resting length is not zero, we defined `OffsetFrameSpring`, whose restoring force is function of the displacement between origins of frames 1 and 2, and not the distance between them; i.e.:

$$\begin{Bmatrix} {}^1f_1 \\ {}^1\tau_1 \end{Bmatrix} = \begin{pmatrix} {}^1K_{fp} & {}^1K_{f\hat{\theta}} \\ {}^1K_{\tau p} & {}^1K_{\tau\hat{\theta}} \end{pmatrix} \begin{Bmatrix} ({}^1p_{21} - {}^1initialp_{21}) \\ {}^1\hat{\theta}_{21} \end{Bmatrix} + \begin{pmatrix} {}^1D_{fp} & {}^1D_{f\omega} \\ {}^1D_{\tau p} & {}^1D_{\tau\omega} \end{pmatrix} \begin{Bmatrix} {}^1v_{21} \\ {}^1\omega_{21} \end{Bmatrix} \quad (A-37)$$

where ${}^1initialp_{21}$ is the distance between origins of frames 1 and 2 at $t = 0$ seconds.

A.7 Verification of “HeuerOffsetFrameSpring”

`HeuerOffsetFrameSpring` is an `OffsetFrameSpring` whose stiffness terms are taken from the study by Heuer *et al.* [224]. In order to verify the performance of `HeuerOffsetFrameSpring`, we created a simple model consisting of two cubes of one Kg mass which were connected together by an `OffsetFrameSpring` whose two ends are located at centroids of the cubes. We set the translation stiffness as (435000 N/m, 2420000 N/m, 523000 N/m), while for the rotational load-displacement relationships we used the equations of Table 3-2. We fixed the lower cube to the ground and applied a horizontal force of f_x to the center of the upper cube:

$$f_x = 4350 \sin\left(\frac{\pi t}{10}\right) N \quad (A-38)$$

As shown in Figure A-3, the displacement of the upper cube along x (plotted in red) is 1 cm when the sinusoidal force reaches to 4350 N, which is consistent with the stiffness of the spring along x , i.e. 435000 N/m.

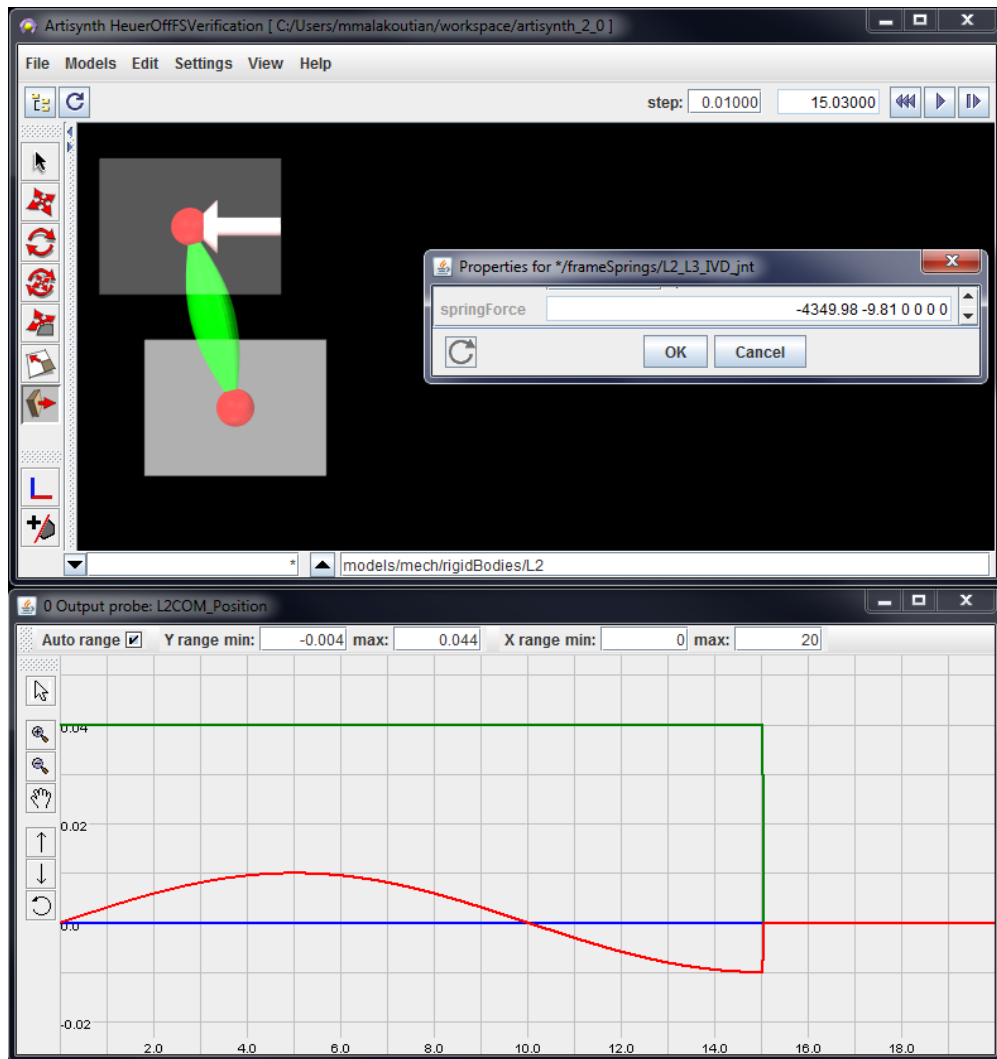


Figure A-3. Verification of the HeuerOffsetFrameSpring performance under a sinusoidal shear force. The x, y, and z coordinates of the position of the center of the upper cube are plotted in red, green, and blue, respectively. Since the global coordinate system is located at the center of the lower vertebra, the y component of the position of upper vertebra is equal to 4 cm over the time as that is the initial distance between the two cubes.

In order to test the rotational stiffness of the spring we applied two parallel but opposite forces that moved with body rotation as:

$$f = 300 \sin\left(\frac{\pi t}{10}\right) N \quad (\text{A-39})$$

With 4 centimeter distance between the two forces, the produced moment by the two forces was equal to $\tau_z = 12 \sin\left(\frac{\pi t}{10}\right) Nm$. As shown in Figure A-4, when applying 12 Nm in flexion, the upper segment flexes to 8° , while by application of the same moment in extension, it extends to 5.5° , which is consistent with the plots of the Figure 3-4.

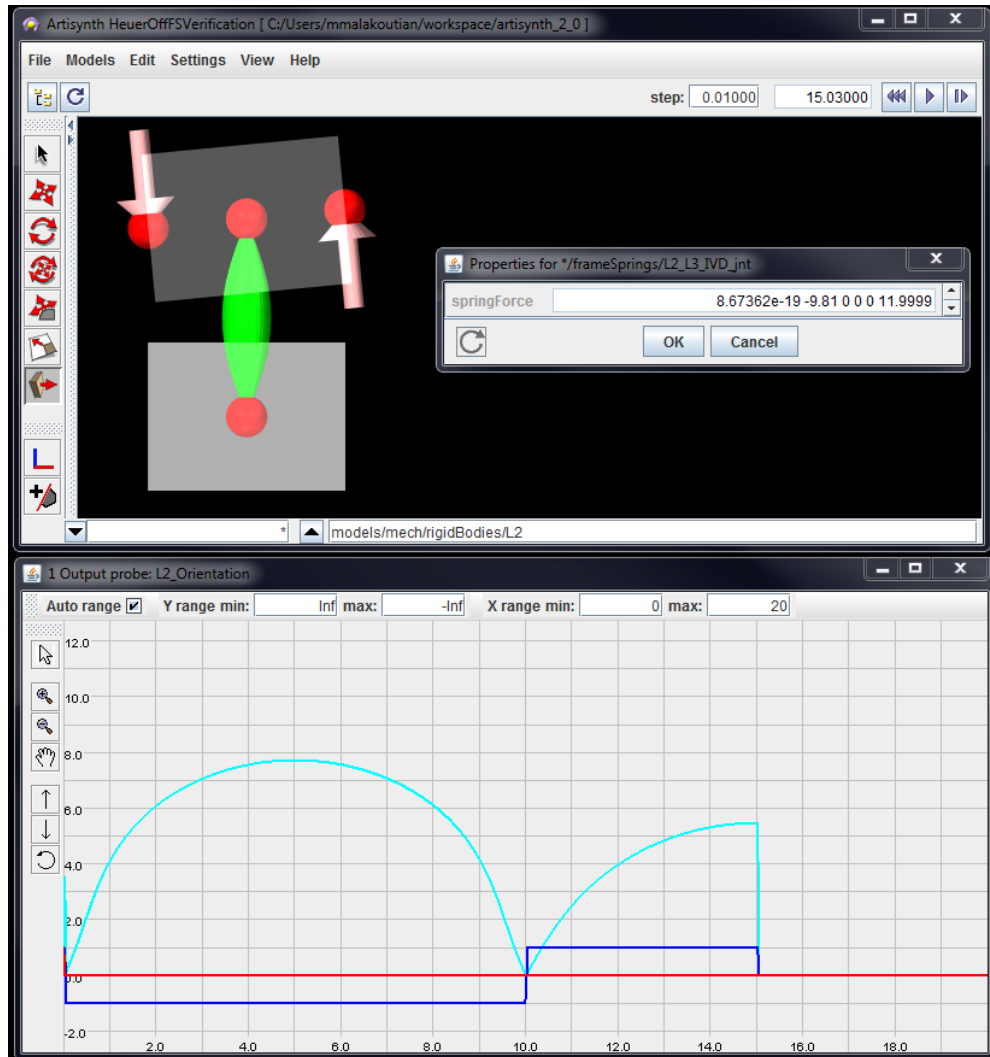


Figure A-4. Verification of the HeuerOffsetFrameSpring performance under a sinusoidal pure moment. The curve in cyan represents the amount of rotation of the upper cube with respect to the lower one. The blue line determines the direction of the rotation. The negative sign represents flexion.

Appendix B Formulation for \tilde{l}^F

In order to create muscles on a skeletal model, first the attachment sites of each muscle fascicle is identified on bony elements based on detailed description of anatomical studies. Then by connecting those attachment sites, muscle fascicles are formed. As shown in Figure 1-27, the resulting length of the connected points (the distance between A and B) is the length of the entire muscle tendon.

Since the size and distance between the bony elements of the model differs from cadavers used for measurement of muscle lengths, direct incorporation of cadaveric muscle parameters into the model is wrong; instead, they should get scaled by the ratio of the musculotendon length of the model l_{model}^{MT} to the musculotendon length of the cadaver l_{cad}^{MT} . For instance, the optimal fiber length of the model can be calculated as:

$$l_{o,model}^F = \frac{l_{model,t=t_0}^{MT}}{l_{cad}^{MT}} \times l_{o,cad}^F \quad (B-1)$$

where the subscript “cad” denotes the data taken from cadaveric studies. Using equation (3-3) for calculation of $l_{o,cad}^F$ in equation (B-1), we obtain:

$$\begin{aligned} l_{o,model}^F &= \frac{l_{model,t=t_0}^{MT}}{l_{cad}^{MT}} \times l_{o,cad}^F = \frac{l_{model,t=t_0}^{MT}}{l_{cad}^{MT}} \times l_{cad}^F \times \frac{l_o^S}{l_{cad}^S} \\ &= l_{model,t=t_0}^{MT} \times \frac{l_{cad}^F}{l_{cad}^{MT}} \times \frac{l_o^S}{l_{cad}^S} \end{aligned} \quad (B-2)$$

With rigid tendon assumption, the length of model tendon l_{model}^T will be constant over time and can be calculated as:

$$l_{model}^T = l_{model,t=t_0}^{MT} \left(1 - \frac{l_{cad}^F \cos \alpha_{cad}}{l_{cad}^{MT}}\right) \quad (B-3)$$

This way the fiber length of the model can be determined as a function of l_{model}^{MT} and $\cos \alpha$:

$$l_{model}^F = \frac{l_{model}^{MT} - l_{model}^T}{\cos \alpha} = \frac{l_{model}^{MT} - l_{model,t=t_0}^{MT} \left(1 - \frac{l_{cad}^F \cos \alpha_{cad}}{l_{cad}^{MT}}\right)}{\cos \alpha} \quad (B-4)$$

Note that as l_{model}^F changes by time, so does the pennation angle. With assumption of constant vertical distance between tendons at all instants [262], i.e. $l_{model}^F \sin \alpha = cte$, the cosine of the pennation angle at each instant can be calculated as:

$$\cos \alpha = \frac{l_{model}^{MT} - l_{model}^T}{\sqrt{(l_{model}^{MT} - l_{model}^T)^2 + \left(\frac{l_{model}^{MT}}{l_{cad}^{MT}} l_{cad}^F \sin \alpha_{cad}\right)^2}} \quad (B-5)$$

Substituting right hand side of equation (B-5) for $\cos \alpha$ in equation (B-4), and dividing them by the optimal fiber length of the model $l_{o,model}^F$, normalized fiber length of the model can be calculated as:

$$\begin{aligned}
\tilde{l}_{model}^F &= \frac{l_{model}^{MT} - l_{model,t=t_0}^{MT} \left(1 - \frac{l_{cad}^F \cos \alpha_{cad}}{l_{cad}^{MT}}\right)}{l_{o,model}^F \times \cos \alpha} \\
&= \frac{l_{model}^{MT} - l_{model,t=t_0}^{MT} \left(1 - \frac{l_{cad}^F \cos \alpha_{cad}}{l_{cad}^{MT}}\right)}{l_{model,t=t_0}^{MT} \times \frac{l_{cad}^F}{l_{cad}^{MT}} \times \frac{l_o^S}{l_{cad}^S} \times \sqrt{\left(l_{model}^{MT} - l_{rigid}^T\right)^2 + \left(\frac{l_{model}^{MT}}{l_{cad}^{MT}} l_{cad}^F \sin \alpha_{cad}\right)^2}}
\end{aligned} \tag{B-6}$$

Appendix C Spinal Loads and Muscle Forces During Upright Standing

C.1 Spinal Loads

Figure C-1, Figure C-2, and Figure C-3 respectively present the axial forces, shear forces, and flexion-extension moments at all vertebral levels when the model is standing upright. The smoothness of the curves represents the stability of the solution over the time.

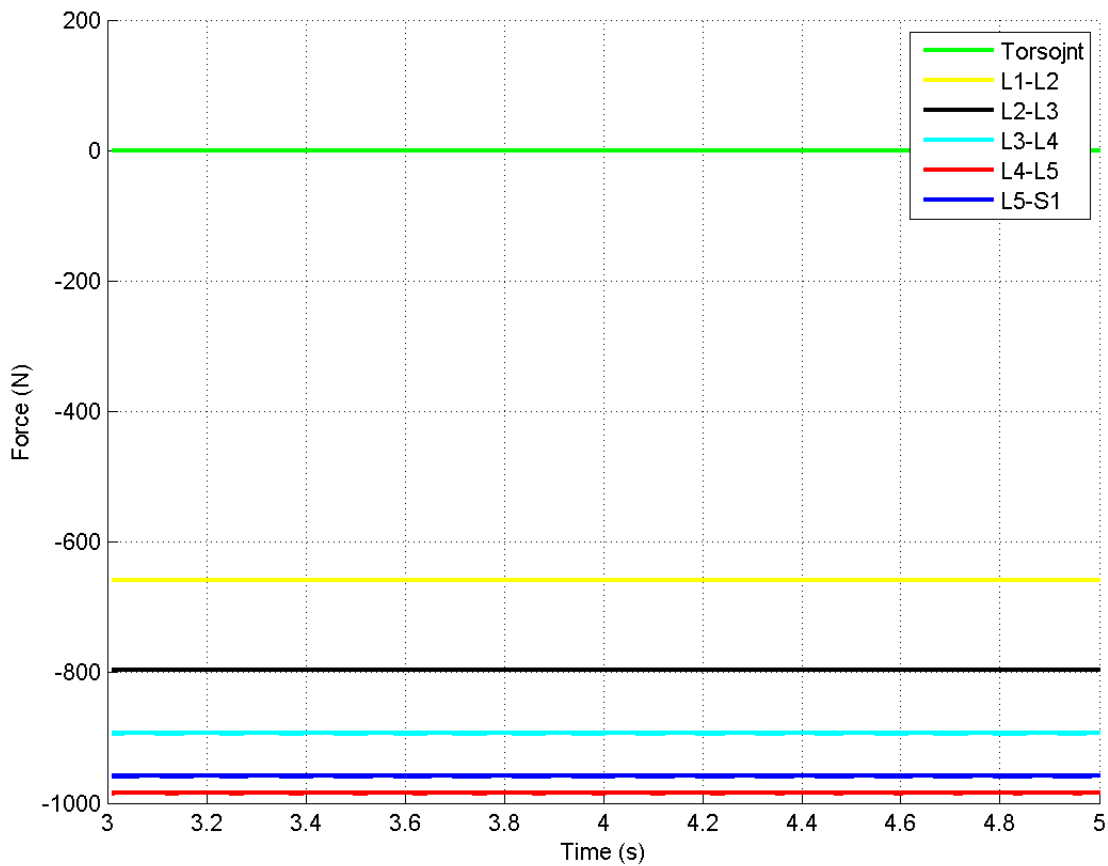


Figure C-1: Axial forces at all vertebral level during upright standing. The negative sign represents a compressive force.

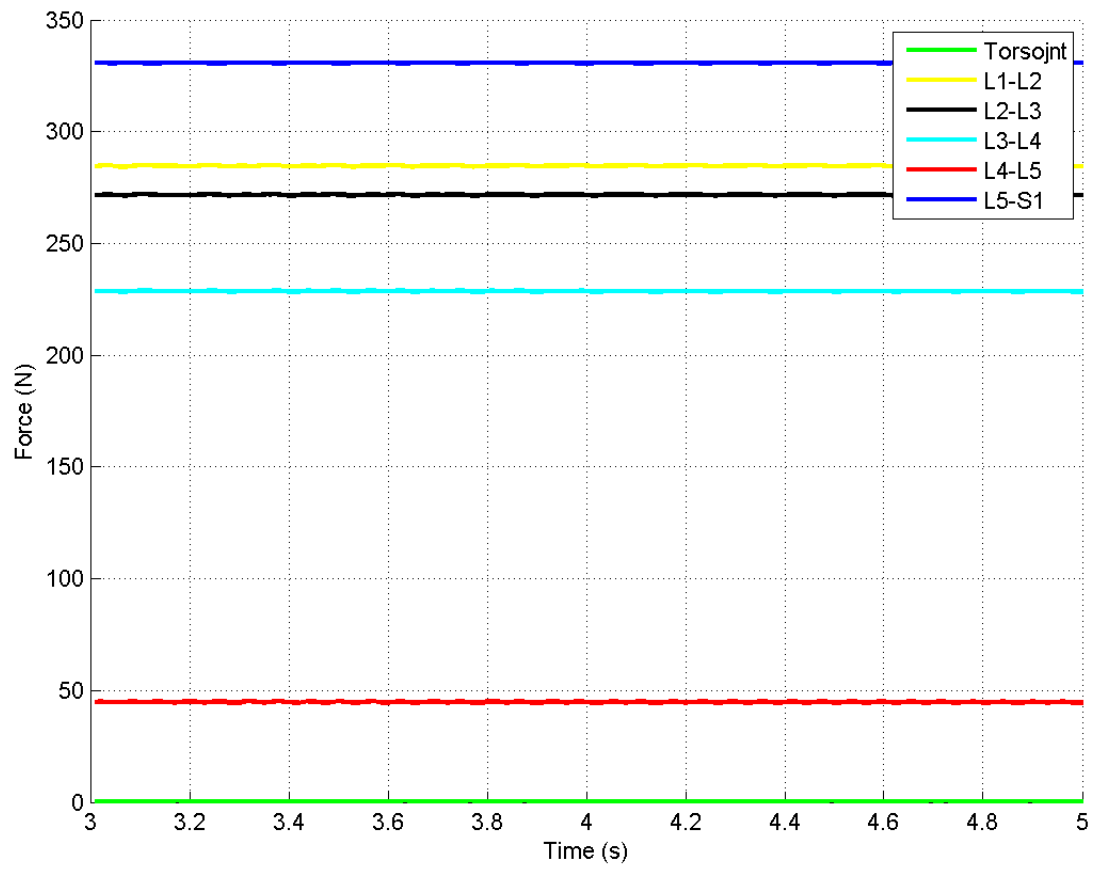


Figure C-2: Shear forces at all vertebral level during upright standing.

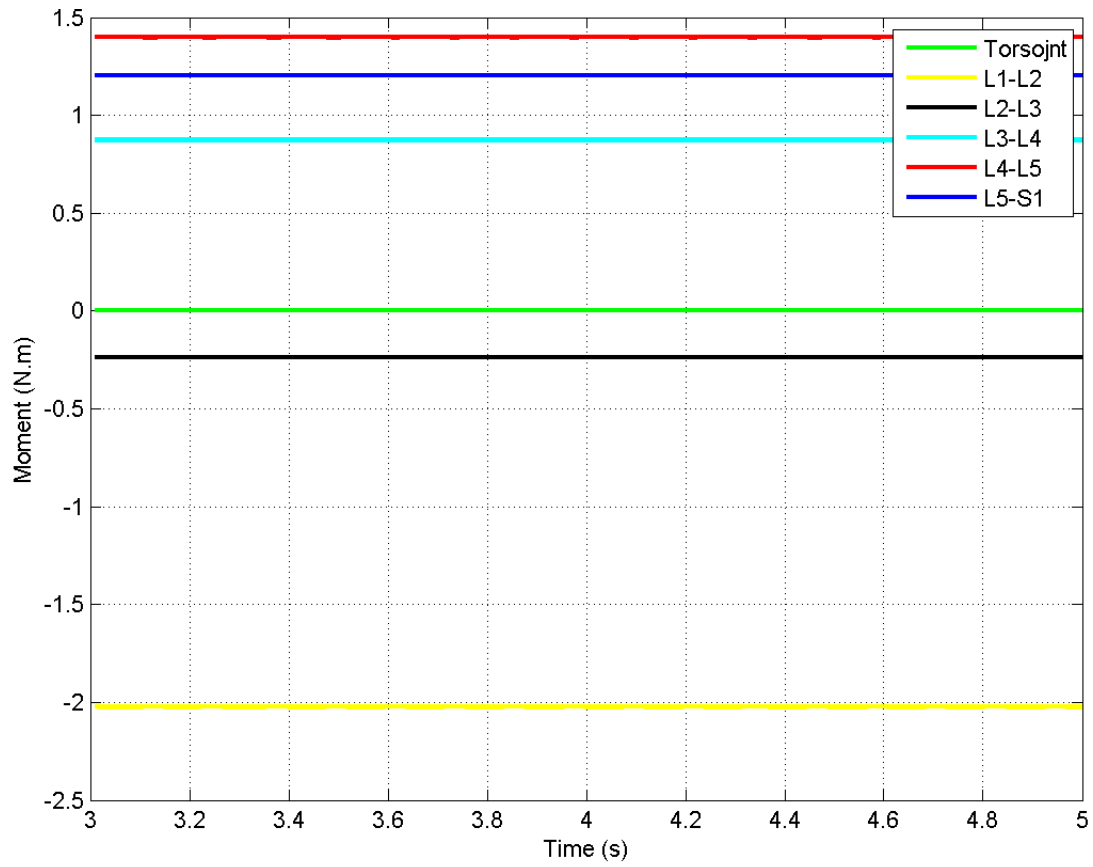


Figure C-3: Extension moments at all vertebral level during upright standing. The negative sign represents the flexion moment.

C.2 Muscle Forces

Figure C-4 presents the total forces in each muscle group for when the model is standing upright. Figure C-6 to Figure C-24 provide further detail on muscle forces by separating the active and passive components of muscle forces and showing the normalized lengths of fascicles of each muscle group.

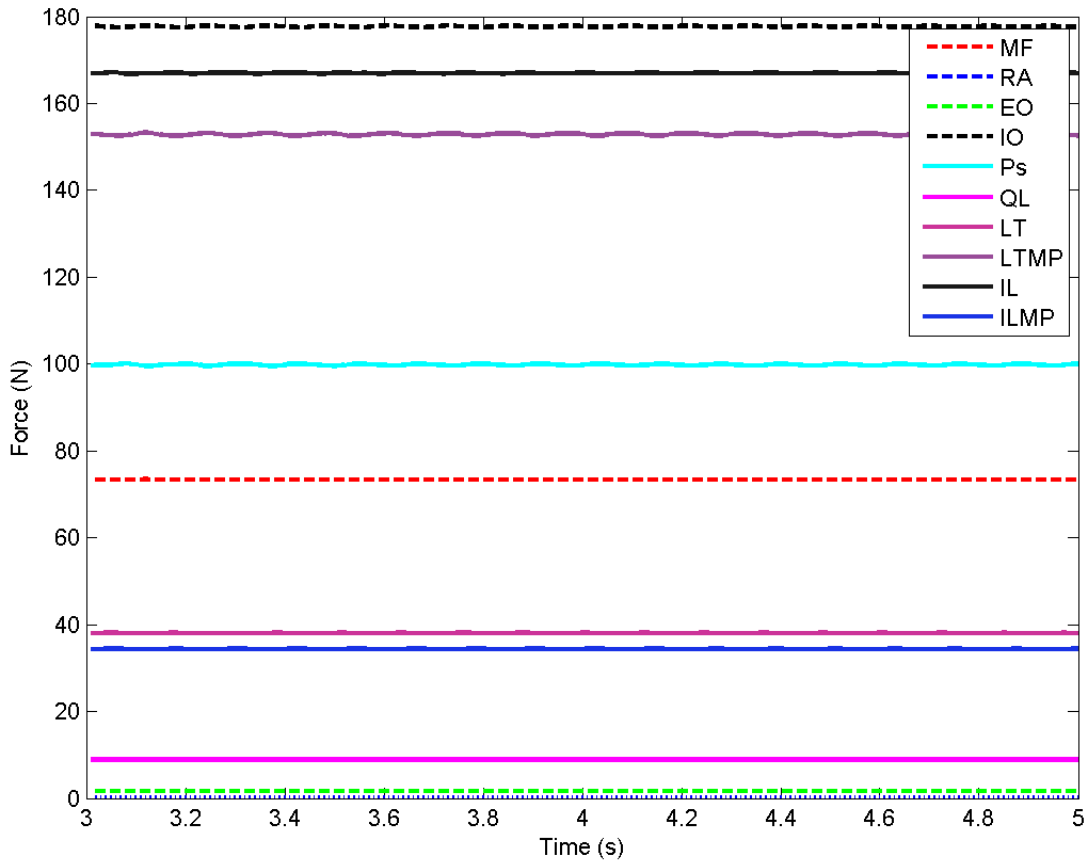


Figure C-4: Forces in each muscle group during upright standing. MF: multifidus; RA: rectus abdominis; EO: external oblique; IO: internal oblique; Ps: psoas major; QL: quadratus lumborum; LT: longissimus thoracis modeled with two-point fascicles; LTMP: longissimus thoracis modeled with multipoint fascicles; IL: iliocostalis lumborum modeled with two-point fascicles; ILMP: iliocostalis lumborum modeled with multipoint fascicles.

Since the graphs are plotted between $t = 3$ to $t = 5$ seconds, the initial length and final length in every other figure from Figure C-5 to Figure C-23 represent the length of fascicles at $t = 3$ and $t = 5$, while MaxLength and MinLength are maximum and minimum lengths of each fascicle between $t = 3$ to $t = 5$ seconds. It's noteworthy that for each muscle fascicle, all these points coincide, which is due to convergence of the solution.

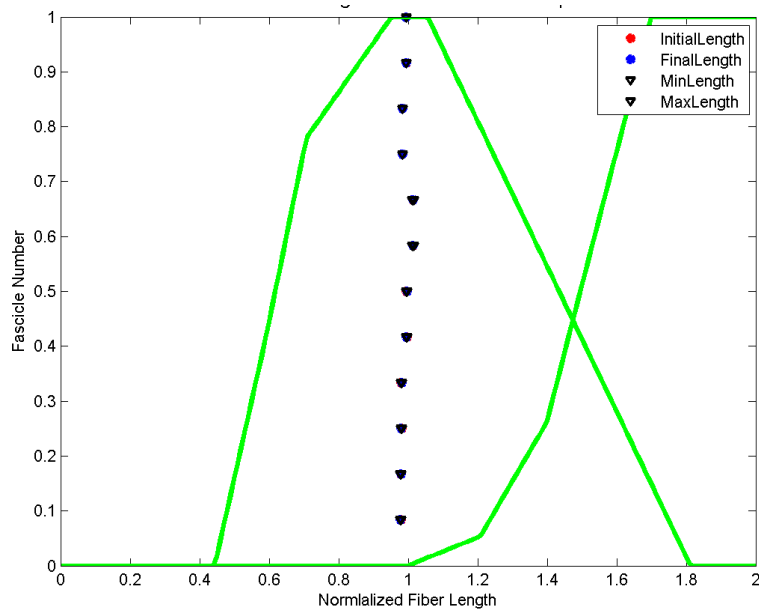


Figure C-5: Normalized fiber length of each external oblique fascicle during upright standing. The curves are the active and passive muscle force-length curves and each dot represents one fascicle.

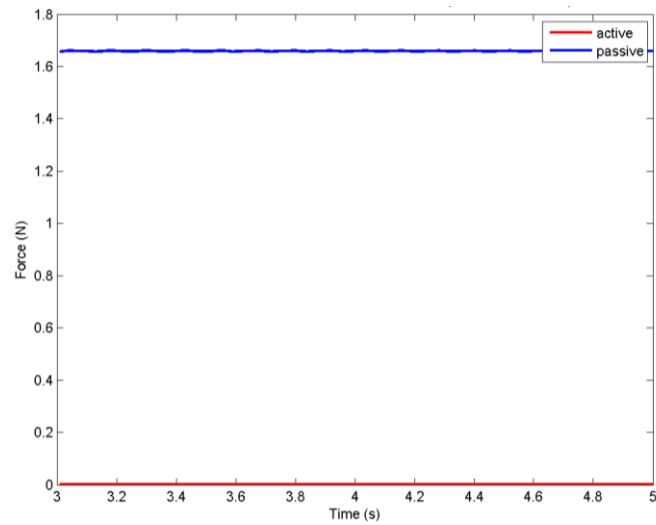


Figure C-6: Active and passive forces in external oblique muscle group during upright standing.

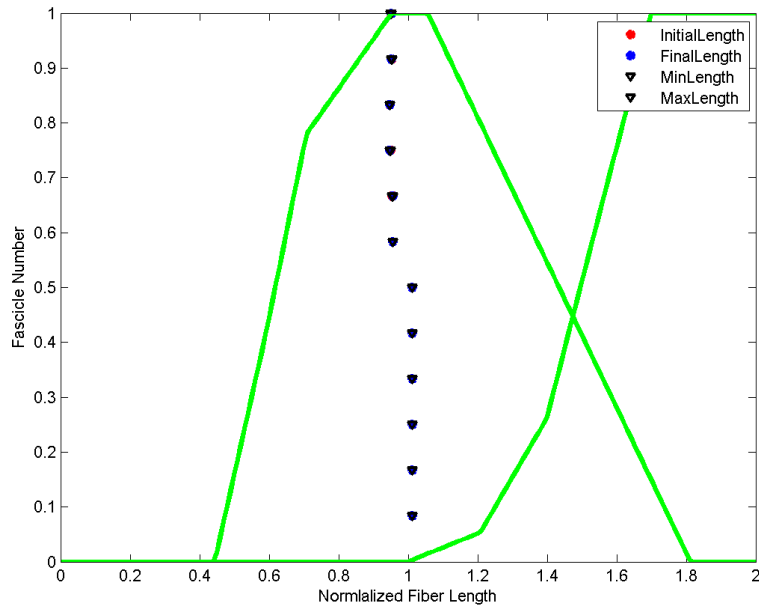


Figure C-7: Normalized fiber length of each internal oblique fascicle during upright standing. The curves are the active and passive muscle force-length curves and each dot represents one fascicle.

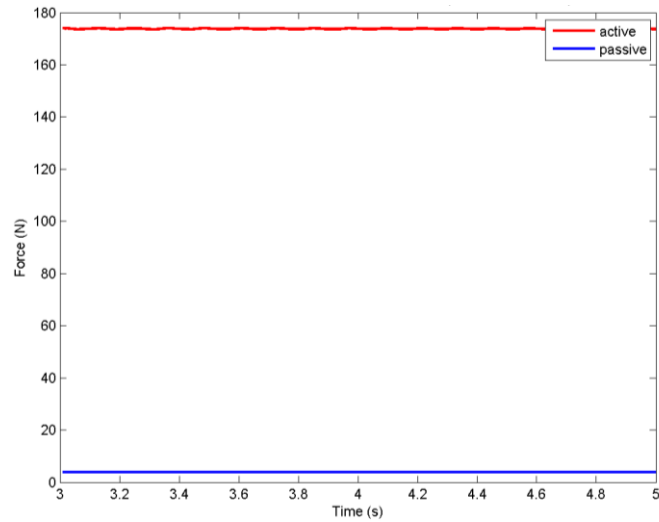


Figure C-8: Active and passive forces in internal oblique muscle group during upright standing.

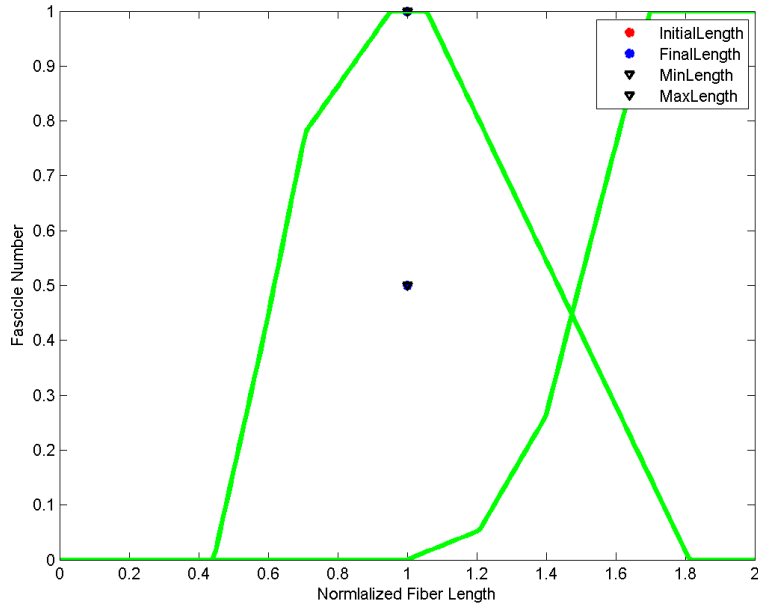


Figure C-9: Normalized fiber length of each rectus abdominis fascicle during upright standing. The curves are the active and passive muscle force-length curves and each dot represents one fascicle.

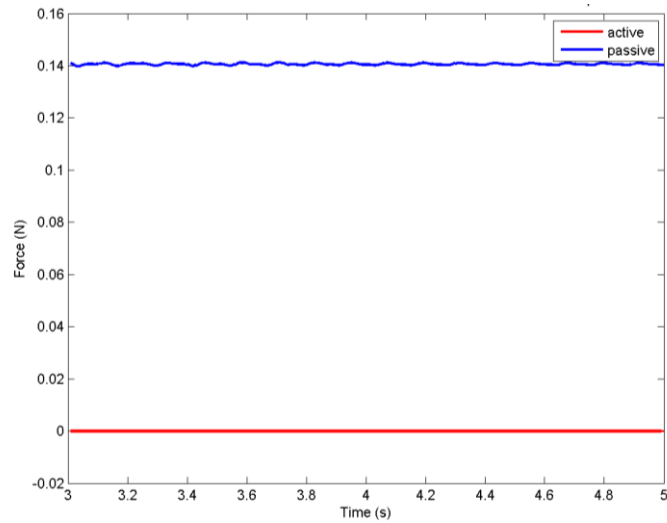


Figure C-10: Active and passive forces in rectus abdominis muscle group during upright standing.

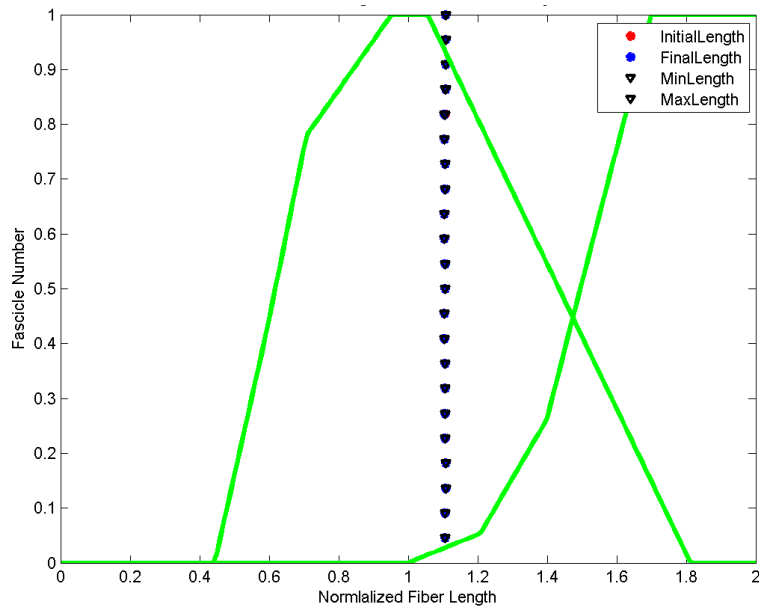


Figure C-11: Normalized fiber length of each psoas major fascicle during upright standing. The curves are the active and passive muscle force-length curves and each dot represents one fascicle.

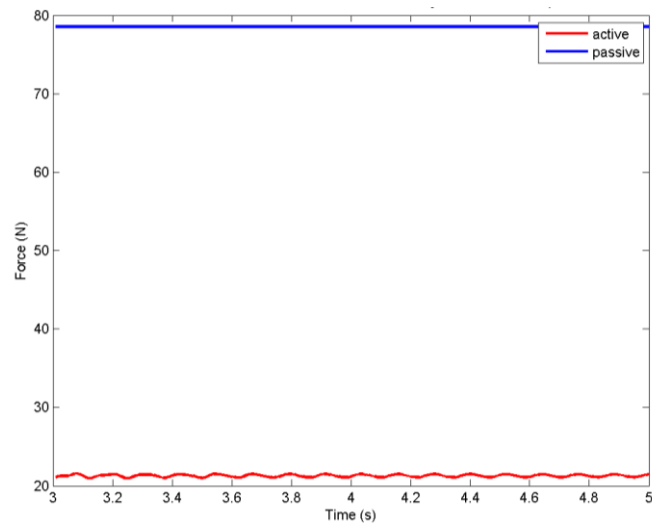


Figure C-12: Active and passive forces in psoas major muscle group during upright standing.

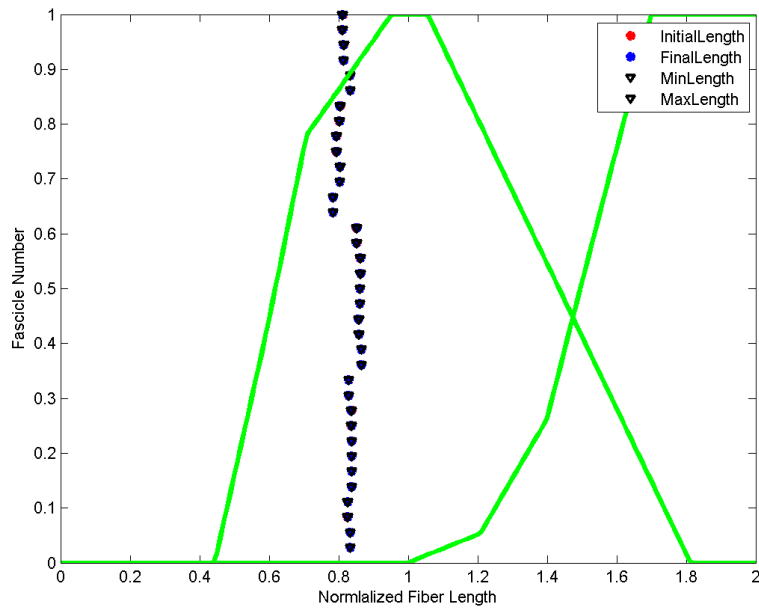


Figure C-13: Normalized fiber length of each quadratus lumborum fascicle during upright standing. The curves are the active and passive muscle force-length curves and each dot represents one fascicle.

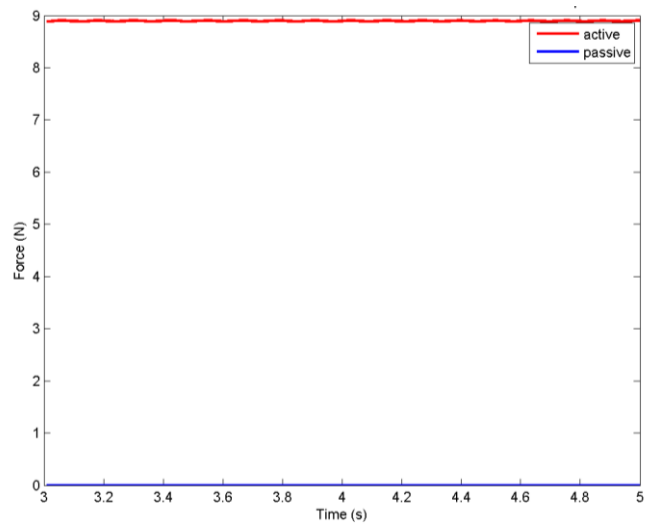


Figure C-14: Active and passive forces in quadratus lumborum muscle group during upright standing.

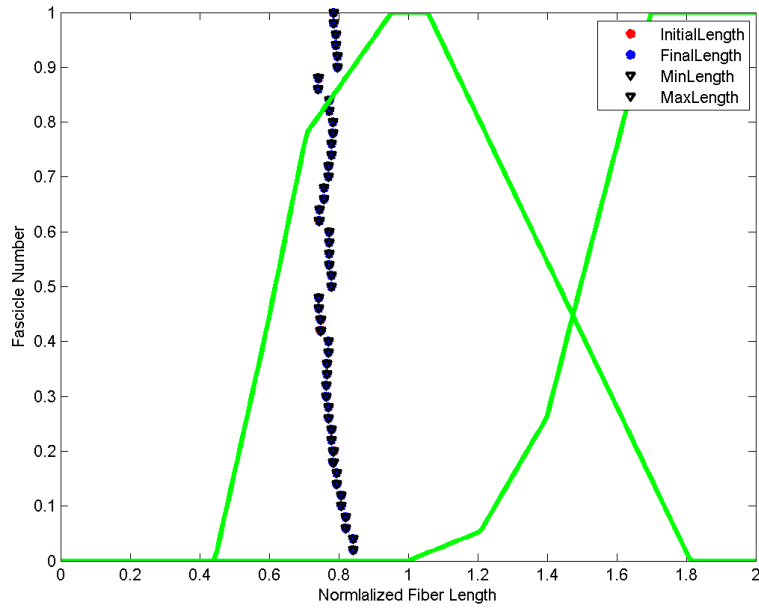


Figure C-15: Normalized fiber length of each multifidus fascicle during upright standing. The curves are the active and passive muscle force-length curves and each dot represents one fascicle.

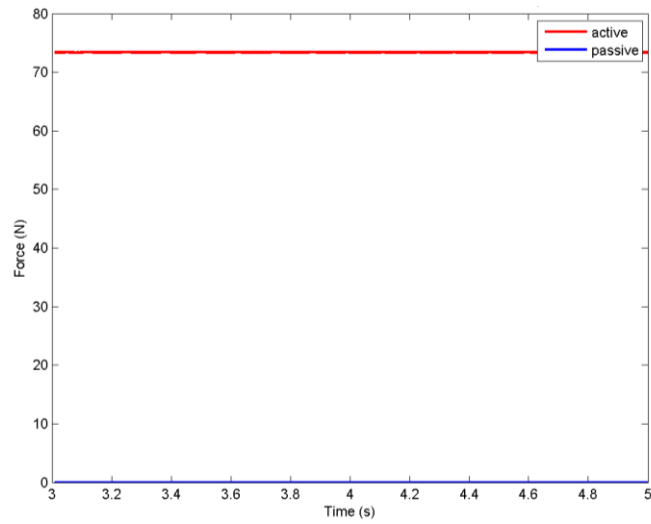


Figure C-16: Active and passive forces in multifidus muscle group during upright standing.

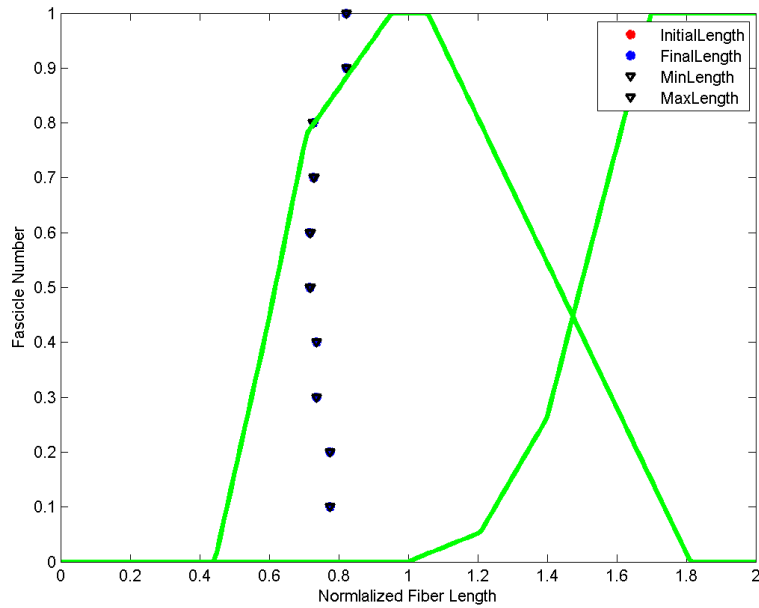


Figure C-17: Normalized fiber length of each two-point iliocostalis lumborum fascicle during upright standing. The curves are the active and passive muscle force-length curves and each dot represents one fascicle.

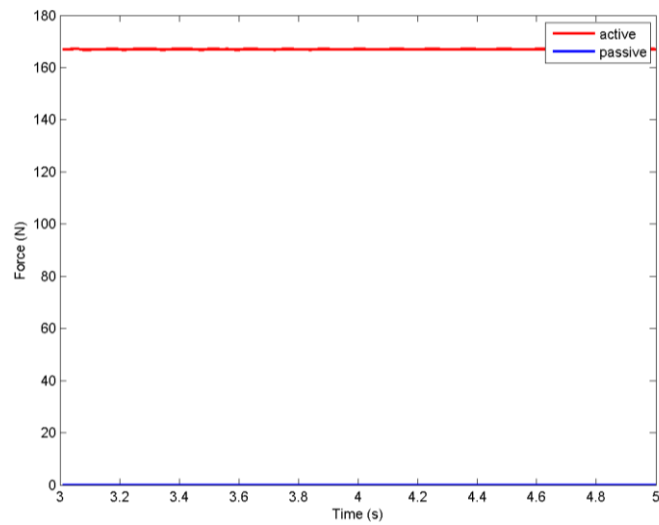


Figure C-18: Active and passive forces in two-point iliocostalis lumborum muscle group during upright standing.

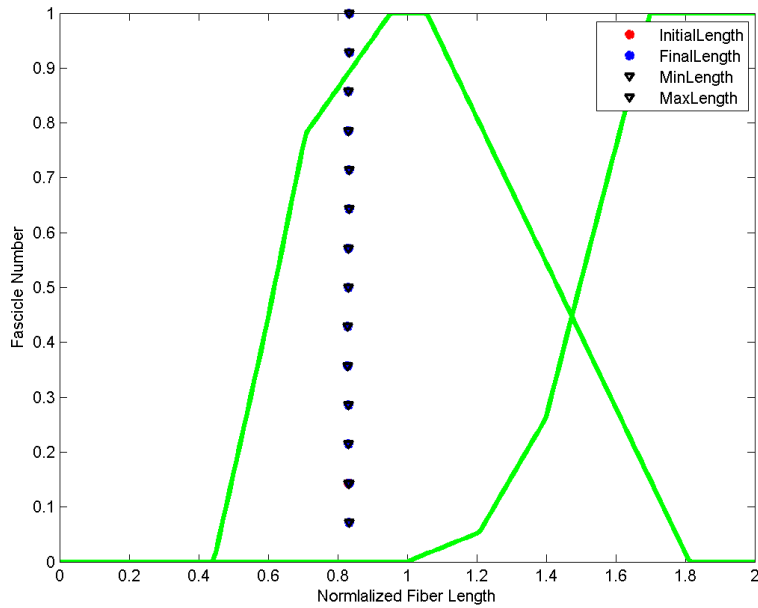


Figure C-19: Normalized fiber length of each multi-point iliocostalis lumborum fascicle during upright standing. The curves are the active and passive muscle force-length curves and each dot represents one fascicle.

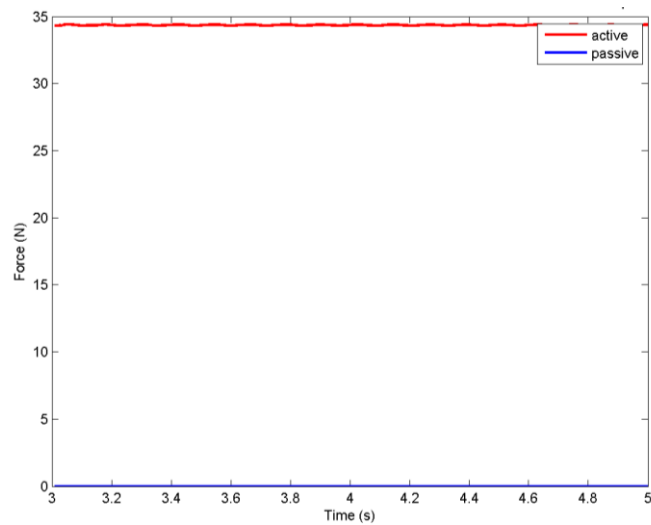


Figure C-20: Active and passive forces in multi-point iliocostalis lumborum muscle group during upright standing.

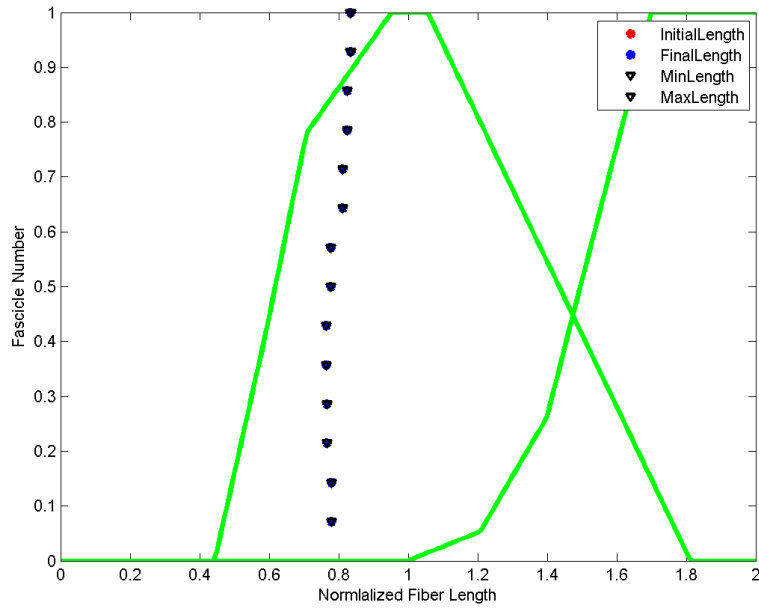


Figure C-21: Normalized fiber length of each two-point longissimus thoracis fascicle during upright standing. The curves are the active and passive muscle force-length curves and each dot represents one fascicle.

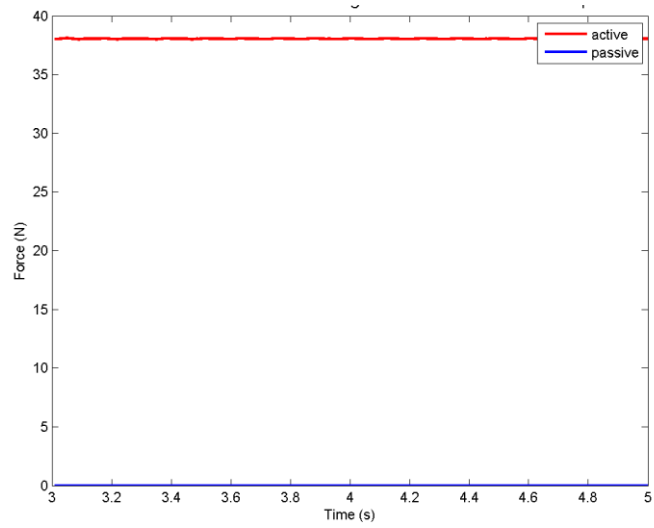


Figure C-22: Active and passive forces in two-point longissimus thoracis muscle group during upright standing.

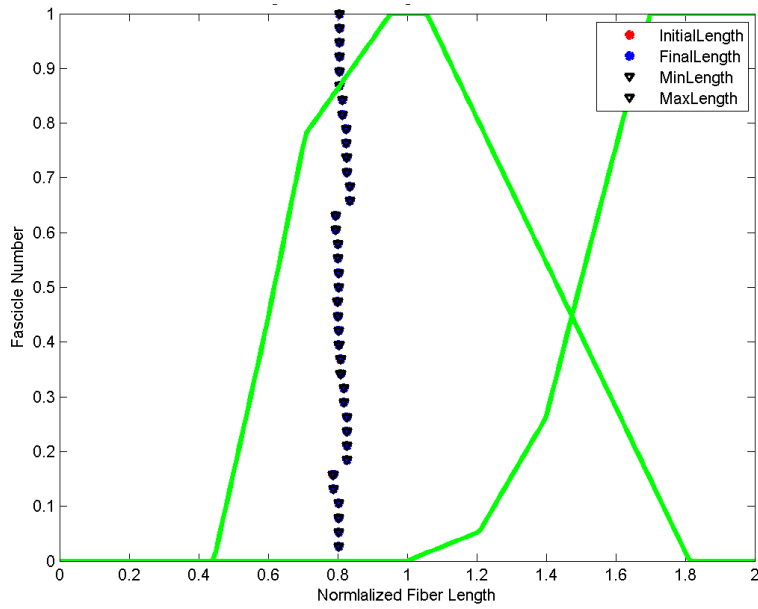


Figure C-23: Normalized fiber length of each multi-point longissimus thoracis fascicle during upright standing. The curves are the active and passive muscle force-length curves and each dot represents one fascicle.

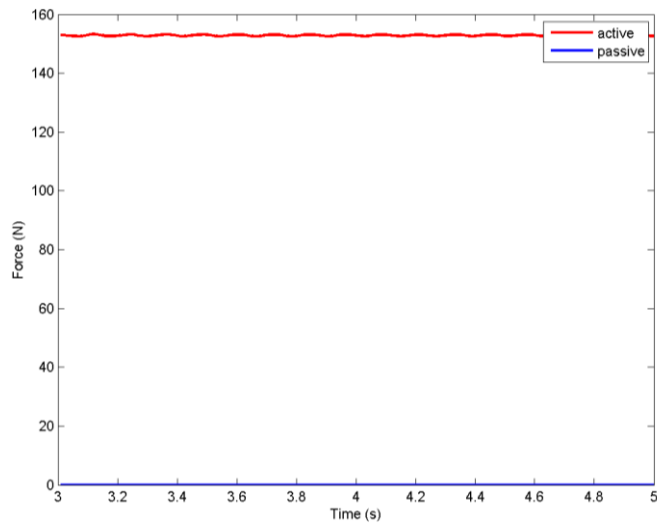


Figure C-24: Active and passive forces in multi-point longissimus thoracis muscle group during upright standing.